

The Eurasia Proceedings of Science, Technology, Engineering & Mathematics

EPSTEM

VOLUME 33 ICONTECH CONFERENCE

ISSN: 2602-3199

ISBN: 978-625-6959-70-5

ICONTECH 2025: 5th International Conference on Technology (IConTech)

May 01- 04, 2025 Trabzon, Türkiye

Edited by: Prof.Dr. Sabri KOCER - Necmettin Erbakan University, Türkiye

IConTECH 2025

International Conference on Technology (IConTech)

Proceedings Book

Editor

Sabri Kocer

Necmettin Erbakan University, Türkiye

ISBN: 978-625-6959-70-5

Copyright 2025

Published by the ISRES Publishing

Address: Askan Mah. Akinbey Sok. No: 5-A/Konya/TÜRKİYE

Web: www.isres.org

Contact: isrespublishing@gmail.com

Dates: May 01- 04, 2025

Location: Trabzon, Türkiye

<https://2025.icontechno.net>



This work is licensed under a [Creative Commons Attribution-NonCommercial-ShareAlike 4.0 International License](https://creativecommons.org/licenses/by-nc-sa/4.0/).

About Editor

Prof Dr. Sabri Kocer

Engineering Faculty, Department of Computer Engineering,
Division of Computer Software, Necmettin Erbakan University, Turkey

Email: skocer@erbakan.edu.tr

Language Editor

Lecturer Ceren Dogan

School of Foreign Languages, Necmettin Erbakan University, Türkiye

Email: cerendogan@erbakan.edu.tr

CONFERENCE PRESIDENT

Prof Dr. Sabri Kocer-Necmettin Erbakan University, Türkiye

SCIENTIFIC BOARD

Agata Mesjasz-Lech - Czestochowa University of Technology, Poland
Ahmad Manasrah - Al Zaytoonah University of Jordan, Jordan
Bogdan Patrut - Alexandru Ioan Cuza University, Romania
Dariusz Jacek Jakóbczak - Technical University of Koszalin, Poland
Ebba Ossiannilsson - Swedish Association for Distance Education, Swedish
Elena Raducan - Dunarea De Jos University, Romania
Eleonora Guseinoviene - Klaipeda University, Lithuania
Gabriel Delgado-Toral - Universidad Nacional Autónoma de México, Mexico
Isti Hidayah - Semarang State University, Indonesia
Jose Manuel Lopez Guede - University of Basque Country, Spain
Marija Stanić - University of Kragujevac, Serbia
M. Hanefi Calp - Karadeniz Technical University, Türkiye
Mohamed Ahmed - Mansoura University, Egypt
Nicu Bizon - Pitesti University, Romania
Ossi Autio - University of Helsinki, Finland
Pandian Vasant - Teknology Petronas University, Romania
Philipp Rosenberger - University of Applied Science, Austria
Rajnalkar Laxman - Gulbarga University, India
Yiyang Chen - Soochow University (CN), China
Yousef Jaradat - Al Zaytoonah University of Jordan, Jordan
Zairi Ismael Rizman - MARA University of Technology, Malaysia
Zipporah Pawat Duguryil - Federal College of Education, Nigeria

ORGANIZING COMMITTEE

Ahmad Manasrah - Al Zaytoonah University of Jordan, Jordan
Agata Mesjasz-Lech - Czestochowa University of Technology, Poland
Elena Raducan - Dunarea De Jos University, Romania
Hakan Yuksel - Isparta University of Applied Sciences, Türkiye
Mohammad Sarwar - Scialert, Dubai, United Arab Emirates
M. Hanefi Calp - Karadeniz Technical University, Türkiye
Mustafa Özhan Kalac - Manisa Celal Bayar University, Türkiye
Robert Beloiu - University of Pitesti, Romania
Ozgur Dunder - Necmettin Erbakan University, Türkiye
Selahattin Alan - Selcuk University, Türkiye
Yousef Jaradat - Al Zaytoonah University of Jordan, Jordan
Yusuf Uzun - Necmettin Erbakan University, Türkiye
Zairi Ismael Rizman - MARA University of Technology, Malaysia

Editorial Policies

ISRES Publishing follows the steps below in the proceedings book publishing process.

In the first stage, the papers sent to the conferences organized by ISRES are subject to editorial oversight. In the second stage, the papers that pass the first step are reviewed by at least two international field experts in the conference committee in terms of suitability for the content and subject area. In the third stage, it is reviewed by at least one member of the organizing committee for the suitability of references. In the fourth step, the language editor reviews the language for clarity.

Review Process

Abstracts and full-text reports uploaded to the conference system undergo a review procedure. Abstracts will be evaluated on the basis of abstracts/proposals. The conference system allows the full text to be sent if the abstract is accepted. Participants must wait for the evaluation results after uploading their article abstracts to the conference system. If their abstracts are accepted, they can upload their full texts to the conference system. The full texts are then sent to at least two reviewers for review. **The conference has a double-blind peer-review process.** Any paper submitted for the conference is reviewed by at least two international reviewers with expertise in the relevant subject area. Based on the reviewers' comments, papers are accepted, rejected or accepted with revision. If the comments are not addressed well in the improved paper, then the paper is sent back to the authors to make further revisions. The accepted papers are formatted by the conference for publication in the proceedings.

Aims & Scope

In the past, accessing information was tiring both financially and morally, but today, thanks to technology, it is easier and faster to access information. With this feature, technology not only makes daily life easier, but also accelerates the developments in science. Therefore, the focus of the conference is to share the studies on the developments in technology and the applications of technology in fields such as science and engineering by the participants. Studies in the fields of technology are accepted to the conference.

The aim of the conference is to bring together researchers and administrators from different countries, and to discuss theoretical and practical issues in the field of technology. At the same time, being aware of the applications of technology in different fields (such as engineering) is among the objectives of the conference.

Articles: 1- 16

CONTENTS

LMI-Based H-Infinity Controller Design for Missile Guidance Control / Pages:1-19

Oktay Malci , Meral Bayraktar , Hakan Yazici

A RAG-Based Automotive Sector AI Assistant for Enhanced Information Retrieval / Pages:20-27

Senda Yildirim , Ruya Samli

The Novelities by Using R Programming Language for Simulate Magnetic Hysteresis Loop /

Pages:28-35

Elena Raducan , Simona Moldovanu , Ciprian Vlad

Enhancing OCTA Image Classification Using Superpixel-Derived Geometric and Texture Features /

Pages:36-44

Stefan Miron , Mihaela Miron , Simona Moldovanu , Marian Barbu

Development and Evaluation of an Advanced Property Management System Using Unified OOAD for Optimizing Real Estate Operations / Pages:45-61

Riah Elcullada Encaranacion , Mary Rose Osorio Raz , Glaicel Anania Araneta

Implementation of Encryption Using Glushkov Product of Automata / Pages:62-72

Zhanat Saukhanova, Altynbek Sharipbay, Gulmira Shakhmetova, Alibek Barlybayev, Raykul Sayat, Khassenov Altay

Relay-Aided PDMA with Dynamic Power Control for Cell-Edge User Fairness / Pages:73-79

Rashed Alsakarnah , Mohammad Masoud , Shaher Slehat

Emerging Trends in Volatility Forecasting Using Machine Learning: A Bibliometric Analysis /

Pages:80-95

Beste Alpaslan

Enhancing Low-Resolution Facial Recognition in Classroom Environments Using YOLOv8 /

Pages:96-104

Gheri Febri Ananda , Hanung Adi Nugroho , Igi Ardiyanto

The Application of Big Data Algorithm in the Personalized Management of Students by College Counselors / Pages:105-113

Jing Gui , Jirawit Yanchinda

The Impact of Artificial Intelligence and Robotics on the Nursing Labor Market: Transformations, Opportunities, and Challenges / Pages:114-119

Rumyana Stoyanova

Fuzzy SVM Inverter-Based Field-Oriented Control of a DFIG used in a Wind Turbine / Pages:120-129

Azzedine Khati , Taieb Bessaad , Hamza Sahraoui

Influence of Different Behavior in Tension and Compression on Longitudinal Fracture of Inhomogeneous Beams Under Impact / Pages:130-139

Victor Rizov

The Advantages of Employing Transfer Learning in the Classification of Breast Cancer Histopathological Images / Pages:140-147

Classification of Industrial Wastewater Generated by Food and Beverage Industry / Pages:148-154
Slav Valchev , Nenko Nenov

Microhardness and Corrosion Resistance of AA1370 Aluminum Wire after Three ECAP-120° Passes /
Pages:155-160
Youcef Hadj - Ali, Fabienne Delaunois, Belkacem Koraichi, Djedjigua Benabdesselam, Nacer Zazi

The Eurasia Proceedings of Science, Technology, Engineering and Mathematics (EPSTEM), 2025

Volume 33, Pages 1-19

IConTech 2025: International Conference on Technology

LMI-Based H-Infinity Controller Design for Missile Guidance Control

Oktay Malci

Yıldız Technical University

Meral Bayraktar

Yıldız Technical University,

Hakan Yazici

Yıldız Technical University

Abstract: In this study, a state-space model of a representative missile was developed to analyze its dynamic behavior under various input conditions. Using MATLAB simulations, the system's responses to different control inputs were examined to understand the missile's natural dynamics and response characteristics. Subsequently, an LMI-based H-infinity controller was designed to enhance the stability and performance of the missile guidance system. The controller was developed by formulating an optimization problem within the Linear Matrix Inequalities (LMI) framework, ensuring maximum stability and disturbance attenuation. The control design also incorporated input saturation constraints and reference tracking by augmenting the system with integral action. The designed controller was implemented and tested in MATLAB, and its effectiveness was evaluated based on system stability, disturbance attenuation. The LMI-based design approach allowed the control gains to be optimally determined, considering external disturbances. Simulation results demonstrate that the LMI-based H-infinity controller provides superior stability and improved disturbance attenuation. This study highlights that LMI-based optimization techniques can be effectively applied to missile guidance systems, offering a powerful tool for managing dynamic uncertainties and external disturbances.

Keywords: Missile guidance, Linear matrix inequality, H-Infinity, Optimization, System dynamics

Introduction

Missile guidance and control systems play a critical role in ensuring precision engagement capabilities under dynamic and uncertain operational environments. These systems must cope with aerodynamic nonlinearities, external disturbances and rapid time-varying conditions, all while maintaining stability and accuracy. Over the past few decades, various control strategies have been developed to address these challenges, including classical PID controllers, optimal control techniques, and more recently, methods that ensure reliable performance under uncertain conditions.

Advanced control theory, particularly H_∞ control, has been extensively studied for aerospace applications due to its ability to attenuate the effect of worst-case disturbances and model uncertainties (Etkin, 1972; Etkin & Reid, 1996; Mackenroth, 2004). The H_∞ framework provides mathematical tools for shaping closed-loop performance through the minimization of the transfer function norm between disturbance inputs and performance outputs (Boyd et al., 1994). Linear Matrix Inequality (LMI) formulations have further facilitated the practical implementation of advanced control laws, enabling the inclusion of multiple design constraints within a convex optimization framework (Duan & Yu, 2013).

- This is an Open Access article distributed under the terms of the Creative Commons Attribution-Noncommercial 4.0 Unported License, permitting all non-commercial use, distribution, and reproduction in any medium, provided the original work is properly cited.

- Selection and peer-review under responsibility of the Organizing Committee of the Conference

© 2025 Published by ISRES Publishing: www.isres.org

In the context of missile guidance, various strategies have been explored in the literature, such as Proportional Navigation (PN), augmented PN, and Pure Pursuit guidance (Siouris, 2004; Yanushevsky, 2007). While these strategies provide intuitive and effective target engagement mechanisms, their integration with modern control theory remains an area of active research, (Nielsen, 1960; Zarchan, 2012). Furthermore, simplifying assumptions such as constant speed and small angle approximations are often adopted to linearize the inherently nonlinear missile dynamics, leading to decoupled longitudinal and lateral-directional state-space models suitable for control synthesis (Stevens et al., 2015).

In this study, a state-space missile model is constructed by applying linearization around an equilibrium condition under standard assumptions. The model incorporates aerodynamic forces and moments based on control surface inputs and flight conditions. A Pure Pursuit guidance law is employed to generate reference attitude commands, and H_∞ controller is designed via LMI optimization to ensure closed-loop stability and disturbance rejection. The proposed control approach is validated through MATLAB/Simulink simulations under both nominal and disturbed scenarios, demonstrating the effectiveness and reliability of the controller.

Conceptual Background

Guidance, navigation, and control systems constitute fundamental components of modern missile technologies. In these systems, ensuring accurate guidance towards the target and maintaining stability against external disturbances are of paramount importance. In this study, the missile model is based on the Skid-to-Turn (STT) principle. In STT-type missiles, directional control is achieved by applying lateral and vertical forces without altering the nose orientation of the airframe. This approach allows for a simpler and more efficient control structure.

The missile motion was modeled using six degrees of freedom (6-DOF) equations of motion, defined with respect to the Earth-Fixed Inertial Frame reference system. Force and moment equations were derived, aerodynamic coefficients were calculated using Athena Vortex Lattice (AVL) software, and the system was linearized separately for the longitudinal and lateral-directional planes. Previous studies have shown that linearized missile guidance models can yield highly accurate performance predictions under certain assumptions, making them a valid foundation for control design (Zarchan, 2012).

In this study, the Pure Pursuit guidance method is employed to generate the reference attitude commands for the missile. In the Pure Pursuit approach, the missile continuously points its nose directly toward the target by aligning its velocity vector with the line-of-sight vector to the target. This strategy provides a simple yet effective mechanism for target interception. The generated reference signals for the pitch and yaw angles guide the missile towards the target position during flight.

During the modeling process, several fundamental assumptions were adopted to simplify the system dynamics. First, the missile was treated as a rigid body, ignoring any structural deformation. The curvature of the Earth and Coriolis effects were also neglected, assuming a flat Earth model. Small angle approximations were applied during the linearization stage to facilitate analytical derivations. Finally, the missile was assumed to maintain a constant forward velocity throughout the flight. A basic guidance method was adopted to generate reference orientation angles for the missile, which will be detailed in subsequent sections. This method aligns with the objectives of achieving a simple and effective orientation control structure in this study.

Mathematical Modeling

Axis Systems

In order to accurately model the missile dynamics, it is necessary to define reference frames associated with both the Earth and the missile itself. In this study, two primary reference frames are used: the Earth-Fixed Inertial Frame and the Body-Fixed Frame as shown in Figure 1. The definitions and transformations between these coordinate systems are consistent with those described in modern aerospace dynamics literature 0.

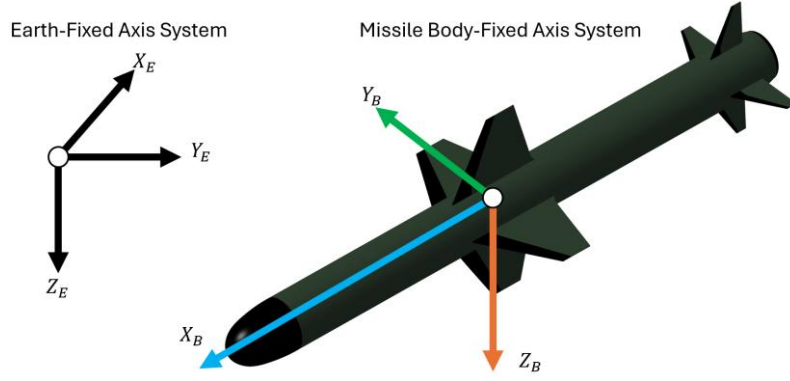


Figure 1. Missile body-fixed axis system and its orientation relative to the earth-fixed inertial frame

Earth-Fixed Inertial Frame

The Earth-Fixed Inertial Frame is a reference coordinate system assumed to be stationary relative to the Earth, and it is used to define the missile's position and velocity. In this frame, the X_E axis points east, the Y_E axis points north, and the Z_E axis is directed downward toward the center of the Earth. Here, the Flat Earth Assumption is adopted, neglecting the curvature and rotation of the Earth. Therefore, the Earth-Fixed Frame is considered inertial.

Body-Fixed Frame

The Body-Fixed Frame is a moving coordinate system attached to the missile. In this frame, the X_B axis points forward along the missile's nose, the Y_B axis points toward the right wing, and the Z_B axis is directed downward. The missile's body dynamics are expressed in terms of forces and moments defined with respect to this coordinate system.

Transformation Matrices

The transformation between the Earth-Fixed Inertial Frame and the Body-Fixed Frame is defined using Euler angles. In this transformation, Yaw (ψ) represents the rotation about the vertical Z_E axis, Pitch (θ) represents the rotation about the lateral Y_B axis, and Roll (ϕ) represents the rotation about the longitudinal X_B axis. Using these angles, the transformation matrix from the Body Frame to the Earth Frame is expressed as:

$$C_{B/E} = \begin{bmatrix} \cos\theta\cos\psi & \cos\theta\sin\psi & -\sin\theta \\ \sin\phi\sin\theta\cos\psi - \cos\phi\sin\psi & \sin\phi\sin\theta\sin\psi + \cos\phi\cos\psi & \sin\phi\cos\theta \\ \cos\phi\sin\theta\cos\psi + \sin\phi\sin\psi & \cos\phi\sin\theta\sin\psi - \sin\phi\cos\psi & \cos\phi\cos\theta \end{bmatrix} \quad (1)$$

where ϕ is the Roll angle, θ is the Pitch angle and ψ is the Yaw angle. This transformation matrix enables the conversion of vectors defined in the Body Frame into the Earth-Fixed Frame.

Force Equations

The forces acting on the missile consist of aerodynamic forces and gravitational forces. Since a constant forward velocity is assumed in this study, thrust force is not included in the model. The aerodynamic force components are defined with respect to the body-fixed frame as follows:

$$F_X = \frac{1}{2} \rho V_T^2 S C_X \quad (2)$$

$$F_Y = \frac{1}{2} \rho V_T^2 S C_Y \quad (3)$$

$$F_Z = \frac{1}{2} \rho V_T^2 S C_Z \quad (4)$$

Here, F_X represents the force acting along the missile's longitudinal axis (forward), F_Y represents the force acting along the lateral axis (side), and F_Z represents the force acting along the vertical axis (downward). ρ denotes the air density, V_T is the total velocity, and S is the reference surface area. The terms C_X , C_Y , and C_Z correspond to the aerodynamic force coefficients along the X, Y, and Z directions, respectively. The gravitational force is defined in the Earth-Fixed Inertial Frame and acts downward. It is transformed into the body-fixed frame using the transformation matrix $C_{B/E}$. The total force vector in the body frame is expressed as:

$$F_B = F_{aero} + C_{B/E} F_{gravity} \quad (5)$$

Moment Equations

The moments acting on the missile originate from aerodynamic effects. In this study, only aerodynamic moments are considered, and engine-generated moments or other external moments are neglected. The aerodynamic moment components are defined with respect to the body-fixed frame as follows:

$$M_X = \frac{1}{2} \rho V_T^2 S l C_L \quad (6)$$

$$M_Y = \frac{1}{2} \rho V_T^2 S l C_M \quad (7)$$

$$M_Z = \frac{1}{2} \rho V_T^2 S l C_N \quad (8)$$

Here, M_X represents the roll moment (rotation about the X-axis), M_Y represents the pitch moment (rotation about the Y-axis), and M_Z represents the yaw moment (rotation about the Z-axis). ρ denotes the air density, V_T is the total velocity, S is the reference surface area, and l is the reference length. The coefficients C_L , C_M , and C_N correspond to the roll, pitch, and yaw moments, respectively. The total aerodynamic moments are expressed with respect to the body-fixed frame and are associated with the changes in angular momentum in the dynamic equations.

Aerodynamic Coefficients and Derivatives

The aerodynamic forces and moments acting on the missile are modeled using specific aerodynamic coefficients. These coefficients are functions of the angle of attack (α), sideslip angle (β), control surface deflections, and angular rates. The aerodynamic force coefficients are defined as:

$$C_X = C_{X_0} + C_{X_\alpha} \alpha + C_{X_q} \frac{ql}{2V} + C_{X_{\delta_e}} \delta_e \quad (9)$$

$$C_Y = C_{Y_\beta} \beta + C_{Y_p} \frac{pl}{2V} + C_{Y_r} \frac{rl}{2V} + C_{Y_{\delta_a}} \delta_a + C_{Y_{\delta_r}} \delta_r \quad (10)$$

$$C_Z = C_{Z_0} + C_{Z_\alpha} \alpha + C_{Z_q} \frac{ql}{2V} + C_{Z_{\delta_e}} \delta_e \quad (11)$$

The aerodynamic moment coefficients are defined as:

$$C_L = C_{L_\beta} \beta + C_{L_p} \frac{pl}{2V} + C_{L_r} \frac{rl}{2V} + C_{L_{\delta_a}} \delta_a + C_{L_{\delta_r}} \delta_r \quad (12)$$

$$C_M = C_{M_0} + C_{M_\alpha} \alpha + C_{M_q} \frac{ql}{2V} + C_{M_{\delta_e}} \delta_e \quad (13)$$

$$C_N = C_{N_\beta} \beta + C_{N_p} \frac{pl}{2V} + C_{N_r} \frac{rl}{2V} + C_{N_{\delta_a}} \delta_a + C_{N_{\delta_r}} \delta_r \quad (14)$$

Here, α represents the angle of attack, β denotes the sideslip angle, p is the roll rate (angular velocity about the X-axis), q is the pitch rate (angular velocity about the Y-axis), and r is the yaw rate (angular velocity about the Z-axis). The terms δ_e , δ_a , and δ_r correspond to the elevator, aileron, and rudder control surface deflections, respectively. Additionally, l denotes the reference length, and V_T is the total velocity. The theoretical framework for aerodynamic coefficient modeling in this study aligns with classical missile aerodynamics formulations presented by Nielsen (1960). The aerodynamic stability and control derivatives used in this study were obtained using the AVL (Athena Vortex Lattice) software. The derivative values were computed based on nine different

combinations of angle of attack (α) and sideslip angle (β) values, each selected as -15° , 0° and 15° . These derivatives were directly integrated into the linearized missile dynamics model.

Table 1 summarizes the aerodynamic derivatives and their physical meanings.

Table 1. Aerodynamic derivatives and their physical meanings	
Symbol	Physical Meaning
C_{X_α}	X-force coefficient derivative with respect to angle of attack (α)
C_{X_q}	X-force coefficient derivative with respect to pitch rate (q)
$C_{X_{\delta_e}}$	X-force coefficient derivative with respect to elevator deflection (δ_e)
C_{Y_β}	Side force coefficient derivative with respect to sideslip angle (β)
C_{Y_p}	Side force coefficient derivative with respect to roll rate (p)
C_{Y_r}	Side force coefficient derivative with respect to yaw rate (r)
$C_{Y_{\delta_a}}$	Side force coefficient derivative with respect to aileron deflection (δ_a)
$C_{Y_{\delta_r}}$	Side force coefficient derivative with respect to rudder deflection (δ_r)
C_{l_β}	Roll moment coefficient derivative with respect to sideslip angle (β)
C_{l_p}	Roll moment coefficient derivative with respect to roll rate (p)
C_{l_r}	Roll moment coefficient derivative with respect to yaw rate (r)
$C_{l_{\delta_a}}$	Roll moment coefficient derivative with respect to aileron deflection (δ_a)
$C_{l_{\delta_r}}$	Roll moment coefficient derivative with respect to rudder deflection (δ_r)
C_{n_β}	Yaw moment coefficient derivative with respect to sideslip angle (β)
C_{n_p}	Yaw moment coefficient derivative with respect to roll rate (p)
C_{n_r}	Yaw moment coefficient derivative with respect to yaw rate (r)
$C_{n_{\delta_a}}$	Yaw moment coefficient derivative with respect to aileron deflection (δ_a)
$C_{n_{\delta_r}}$	Yaw moment coefficient derivative with respect to rudder deflection (δ_r)
C_{Z_α}	Normal force coefficient derivative with respect to angle of attack (α)
C_{Z_q}	Normal force coefficient derivative with respect to pitch rate (q)
$C_{Z_{\delta_e}}$	Normal force coefficient derivative with respect to elevator deflection (δ_e)
C_{m_α}	Pitch moment coefficient derivative with respect to angle of attack (α)
C_{m_q}	Pitch moment coefficient derivative with respect to pitch rate (q)
$C_{m_{\delta_e}}$	Pitch moment coefficient derivative with respect to elevator deflection (δ_e)

Flight Parameters

In the modeling of missile dynamics, flight parameters play a crucial role in defining the system's state variables. In Figure 2, the following flight parameters are illustrated. Forward Velocity (u) is the missile's velocity component along the body-fixed X-axis. It is assumed to be constant throughout the analysis. Also, Angle of Attack (α) is the angle between the body X-axis and the forward velocity vector. It is used under the small angle assumption.

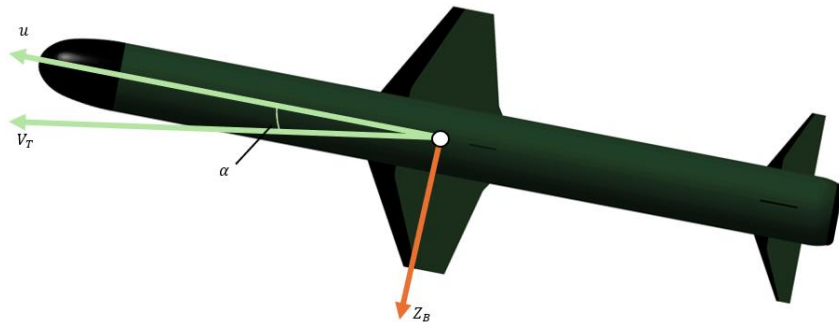


Figure 2. Angle of attack (α) definition

In Figure 3, the Sideslip Angle (β) is shown. It is the angle between the body X-axis and the projection of the velocity vector on the Y-Z plane. It is used under the small angle assumption.

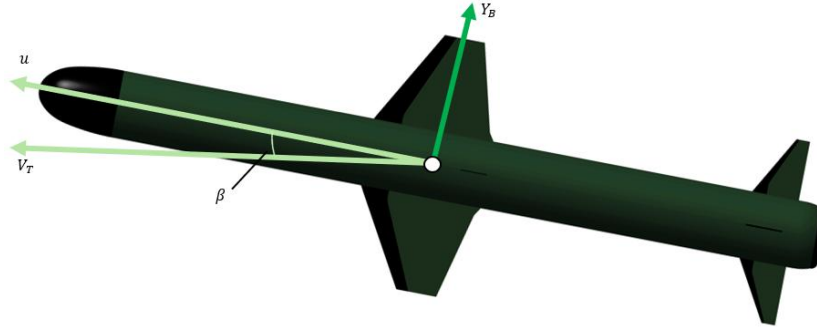


Figure 3. Sideslip angle (β) definition

These parameters are fundamental in the linearization of the missile model and in the formulation of the state-space representation. The use of these parameters and assumptions in missile flight modeling is well established in classical flight dynamics literature (Etkin, 1972).

Translational Kinematic Equations

The translational motion of the missile in the Earth-Fixed Inertial Frame can be represented using the body-fixed velocity components u , v , w and the Euler angles ϕ , θ , ψ . This formulation provides the foundation for describing the missile's motion in three-dimensional space with respect to its center of mass.

$$\dot{X} = u \cos \theta \cos \psi + v(\sin \phi \sin \theta \cos \psi - \cos \phi \sin \psi) + w(\cos \phi \sin \theta \cos \psi + \sin \phi \sin \psi) \quad (15)$$

$$\dot{Y} = u \cos \theta \sin \psi + v(\sin \phi \sin \theta \sin \psi + \cos \phi \cos \psi) + w(\cos \phi \sin \theta \sin \psi - \sin \phi \cos \psi) \quad (16)$$

$$\dot{Z} = -u \sin \theta + v \sin \phi \cos \theta + w \cos \phi \cos \theta \quad (17)$$

These equations describe the instantaneous translational velocity of the missile's center of mass in the Earth-Fixed Inertial Frame and form the basis for modeling the translational dynamics of the missile. Here, u , v and w represent the velocity components along the body-fixed X, Y, and Z axes, respectively. These equations describe the instantaneous translational velocity of the missile's center of mass in the Earth-Fixed Inertial Frame and serve as the basis for modeling the translational dynamics of the missile.

Rotational Kinematic Equations

The orientation changes of the missile are described using Euler angles (ϕ , θ , ψ), and their time derivatives are expressed in terms of the body-fixed angular rates (p , q , r). The rotational kinematic equations for the Euler angles are given as:

$$\dot{\phi} = p + \tan \theta (q \sin \phi + r \cos \phi) \quad (18)$$

$$\dot{\theta} = q \cos \phi - r \sin \phi \quad (19)$$

$$\dot{\psi} = \frac{q \sin \phi + r \cos \phi}{\cos \theta} \quad (20)$$

These equations describe the evolution of the missile's orientation over time based on the angular rates and provide the kinematic model of the rotational motion. This formulation of rotational motion based on Euler angle derivatives is directly aligned with the classical treatment in (Etkin & Reid, 1996).

Linearization

To enable the missile dynamics to be used in control system design, the nonlinear equations of motion are linearized under specific simplifying assumptions. The key assumptions include the small-angle approximation, where angles such as the angle of attack (α), sideslip angle (β), and roll angle (ϕ) are considered small enough to justify the linear relations $\sin \alpha \approx \alpha$, $\cos \alpha \approx 1$, $\sin \beta \approx \beta$, $\sin \psi \approx \psi$, $\sin \phi \approx \phi$, and $\cos \phi \approx 1$. Additionally,

the forward velocity component u is assumed to be constant throughout the flight, leading to the simplification $\dot{u} \approx 0$. Under the mentioned assumptions, the nonlinear equations of motion are linearized around small perturbations from an equilibrium condition. Following the linearization, the system dynamics are decoupled into two independent subsystems: the longitudinal and the lateral-directional planes. The longitudinal plane includes the states w , q , θ , and Z , which represent vertical velocity, pitch rate, pitch angle, and vertical position, respectively. The lateral-directional plane consists of the states v , p , r , ϕ , ψ , and Y , representing lateral velocity, roll rate, yaw rate, roll angle, yaw angle, and lateral position. Separate state-space models are derived for each plane, and the control design is carried out individually based on these linearized subsystems.

State-Space Representation

The linearized missile dynamics are expressed in state-space form separately for the longitudinal and lateral-directional planes. Independent state and input vectors are defined for each plane, and system matrices are constructed accordingly.

Longitudinal Plane State-Space Model

State and input vectors:

$$x_{lon} = [w, q, \theta, Z]^T \quad (21)$$

$$u_{lon} = [\delta_e] \quad (22)$$

State-space equations:

$$\dot{x}_{lon} = A_{lon}x_{lon} + B_{1lon}W_{lon} + B_{2lon}u_{lon} \quad (23)$$

System matrices:

$$A_{lon} = \begin{bmatrix} Z_w & Z_q & -u & 0 \\ M_w & M_q & 0 & 0 \\ 0 & 1 & 0 & 0 \\ 0 & 0 & -u & 0 \end{bmatrix} \quad (24)$$

$$B_{1lon} = [1 \quad 1 \quad 0 \quad 0]^T \quad (25)$$

$$B_{2lon} = [Z_{\delta_e} \quad M_{\delta_e} \quad 0 \quad 0]^T \quad (26)$$

The elements of the system matrices are defined as follows:

$$Z_w = \frac{\rho V_T S_{ref}}{M_{missile}} \cdot C_{Z\alpha} \quad (27)$$

$$Z_q = \frac{\rho S_{ref} l}{2 M_{missile}} \cdot C_{Zq} \quad (28)$$

$$M_w = \frac{\rho V_T S_{ref} l}{I_{yy}} \cdot C_{m\alpha} \quad (29)$$

$$M_q = \frac{\rho S_{ref} l^2}{2 I_{yy}} \cdot C_{mq} \quad (30)$$

$$Z_{\delta_e} = \frac{\rho V_T^2 S_{ref}}{M_{missile}} \cdot C_{Z\delta_e} \quad (31)$$

$$M_{\delta_e} = \frac{\rho V_T^2 S_{ref} l}{I_{yy}} \cdot C_{m\delta_e} \quad (32)$$

Lateral-Directional Plane State-Space Model

State and input vectors:

$$x_{lat} = [v, p, r, \phi, \psi, Y]^T \quad (33)$$

$$u_{lat} = [\delta_a, \delta_r] \quad (34)$$

State-space equations:

$$\dot{x}_{lat} = A_{lat}x_{lat} + B_{1lat}W_{lat} + B_{2lat}u_{lat} \quad (35)$$

System matrices:

$$A_{lat} = \begin{bmatrix} Y_v & Y_p & Y_r & -g \cos(\theta_0) & 0 & 0 \\ L_v & L_p & L_r & 0 & 0 & 0 \\ N_v & N_p & N_r & 0 & 0 & 0 \\ 0 & 1 & 0 & 0 & 0 & 0 \\ 0 & 0 & 1 & 0 & 0 & 0 \\ 1 & 0 & 0 & 0 & 0 & 0 \end{bmatrix} \quad (36)$$

$$B_{1lat} = [1 \ 0 \ 1 \ 0 \ 0 \ 0]^T \quad (37)$$

$$B_{2lat} = \begin{bmatrix} Y_{\delta_a} & L_{\delta_a} & N_{\delta_a} & 0 & 0 & 0 \\ Y_{\delta_r} & L_{\delta_r} & N_{\delta_r} & 0 & 0 & 0 \end{bmatrix}^T \quad (38)$$

The elements of the system matrices are defined as follows:

$$Y_v = \frac{\rho V_T S_{ref}}{M_{missile}} \cdot C_{Y\beta} \quad (39)$$

$$Y_p = \frac{\rho S_{ref} l}{2 M_{missile}} \cdot C_{Yp} \quad (40)$$

$$Y_r = \frac{\rho S_{ref} l}{2 M_{missile}} \cdot C_{Yr} \quad (41)$$

$$L_v = \frac{\rho V_T S_{ref} l}{I_{xx}} \cdot C_{l\beta} \quad (42)$$

$$L_p = \frac{\rho S_{ref}^2 l}{2 I_{xx}} \cdot C_{lp} \quad (43)$$

$$L_r = \frac{\rho S_{ref}^2 l}{2 I_{xx}} \cdot C_{lr} \quad (44)$$

$$N_v = \frac{\rho V_T S_{ref} l}{I_{zz}} \cdot C_{n\beta} \quad (45)$$

$$N_p = \frac{\rho S_{ref}^2 l}{2 I_{zz}} \cdot C_{np} \quad (46)$$

$$N_r = \frac{\rho S_{ref}^2 l}{2 I_{zz}} \cdot C_{nr} \quad (47)$$

$$Y_{\delta_a} = \frac{\rho V_T^2 S_{ref} l}{M_{missile}} \cdot C_{Y\delta_a} \quad (48)$$

$$Y_{\delta_r} = \frac{\rho V_T^2 S_{ref} l}{M_{missile}} \cdot C_{Y\delta_r} \quad (49)$$

$$L_{\delta_a} = \frac{\rho V_T^2 S_{ref} l}{I_{xx}} \cdot C_{l\delta_a} \quad (50)$$

$$L_{\delta_r} = \frac{\rho V_T^2 S_{ref} l}{I_{xx}} \cdot C_{l\delta_r} \quad (51)$$

$$N_{\delta_a} = \frac{\rho V_T^2 S_{ref} l}{I_{zz}} \cdot C_{n\delta_a} \quad (52)$$

$$N_{\delta_r} = \frac{\rho V_T^2 S_{ref} l}{I_{zz}} \cdot C_{n\delta_r} \quad (53)$$

Pure Pursuit Guidance Law

In the Pure Pursuit guidance method, the missile continuously adjusts its flight path to directly aim at the instantaneous position of the target. The missile aligns its velocity vector with the line-of-sight (LOS) vector to the target at every moment. This principle ensures that the missile always attempts to minimize the angular separation between its own heading and the target's location. Although Pure Pursuit is simple to implement and highly intuitive, it may not guarantee interception against highly maneuverable targets, as the missile may tend to follow a curved path that lags behind rapid target movements. Nevertheless, for stationary or low-maneuvering targets, Pure Pursuit provides an effective and computationally efficient guidance strategy, and it is classified under direct (external) guidance methods as illustrated in Figure 4 (Siouris, 2004).

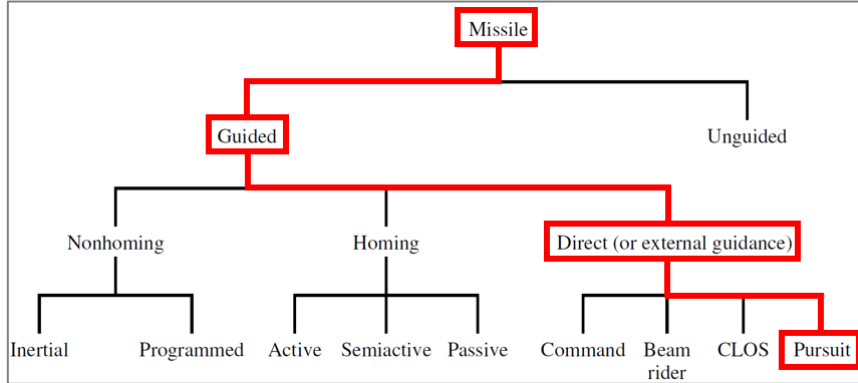


Figure 4. Common missile guidance methods (Adapted from George M. Siouris, *Missile Guidance and Control Systems*, 2004)

Various studies have examined the integration of classical guidance laws such as Pure Pursuit into modern missile control frameworks [10]. In order to steer the missile toward the target position, reference attitude angles are generated using a Pure Pursuit guidance law. The procedure is as follows:

First, the target direction vector is calculated:

$$V_{Target} = \begin{bmatrix} X_{Target} - x \\ Y_{Target} - y \\ Z_{Target} - z \end{bmatrix} \quad (54)$$

Then, the direction vector is normalized:

$$V_{Dir} = \frac{V_{Target}}{\|V_{Target}\|} \quad (55)$$

The reference yaw angle (ψ_{ref}) is computed as:

$$\psi_{ref} = \arctan2(V_{Dir,y}, V_{Dir,x}) \quad (56)$$

The reference pitch angle (θ_{ref}) is computed as:

$$\theta_{ref} = \arctan2(-V_{Dir,z}, \sqrt{V_{Dir,x}^2 + V_{Dir,y}^2}) \quad (57)$$

The reference roll angle (ϕ_{ref}) is set to zero:

$$\phi_{ref} = 0 \quad (58)$$

Since the missile model adopts a Skid-to-Turn (STT) control architecture where roll dynamics are not actively utilized during the guidance phase. This simple approach allows the missile to dynamically adjust its orientation towards the target throughout the flight, as illustrated in Figure 5.

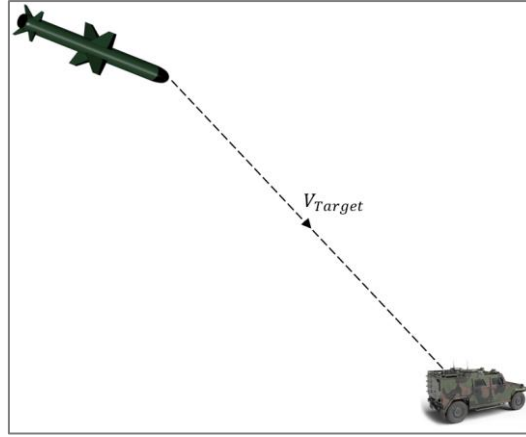


Figure 5. Representation of the target direction vector

Control Design

Control Objectives

The main objectives of the control design for the missile system are summarized in Figure 6. These objectives include ensuring stability in the presence of external disturbances, minimizing their effects through disturbance attenuation, and achieving optimal performance by minimizing the H^∞ norm. Such objectives align closely with the goals of advanced control theory, which aims to maintain performance despite modeling errors and unmeasured perturbations (Mackenroth, 2004).

In this study, the disturbance input is selectively introduced into the angular channels, specifically affecting the pitch (θ) and yaw (ψ) angles, in the form of zero-mean white noise. These perturbations represent realistic environmental effects such as sensor noise or aerodynamic uncertainties. These objectives are addressed through an H^∞ optimization framework formulated using Linear Matrix Inequalities (LMI), which explicitly incorporates stability and disturbance attenuation into the design process.

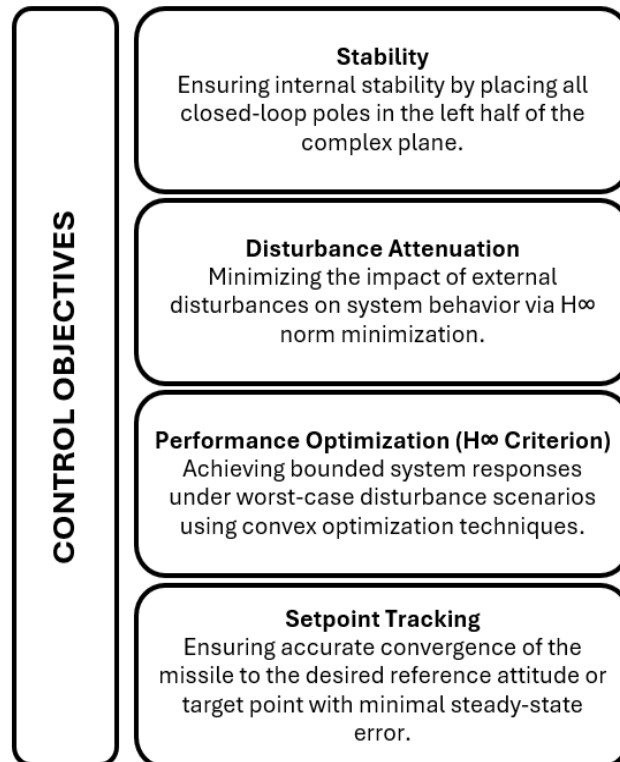


Figure 6. Summary of control objectives considered in the H^∞ -based missile guidance design

State-Feedback H_∞ Controller Design

In order to analyze the closed-loop performance of the missile guidance system under external disturbances, the design equations for a static state-feedback H_∞ controller have been obtained (Boyd et al., 1994). The missile dynamics are represented in the linearized state-space form as:

$$\dot{x}(t) = Ax(t) + B_1w(t) + B_2u(t) + B_{ref}r(t) \quad (59)$$

$$z(t) = C_1x(t) + D_{11}w(t) + D_{12}u(t) \quad (60)$$

In this representation, $x(t) \in R^n$ denotes the state vector of the system, while $w(t) \in R^{m_w}$ represents the exogenous disturbance input acting on the system. The signal $r(t) \in R^{m_r}$ is the reference command, introduced into the system via the input matrix B_{ref} . The term $u(t) \in R^{m_u}$ corresponds to the control input applied to the system. The performance output $z(t) \in R^p$ is defined as the performance variable, which is minimized in the H_∞ sense to ensure stability performance under disturbances. The matrices C_1 , D_{11} , and D_{12} define how the performance output depends on the state, disturbance, and control input, respectively.

To incorporate reference tracking into the H_∞ control framework, the state-space model is augmented with an integral action on the tracking error. This is achieved by extending the system matrices to include the integral of the error between the reference signal $r(t)$ and the corresponding state variable. The extended state vector, input matrices, and output matrices are defined as follows:

$$\begin{bmatrix} \dot{x}(t) \\ e(t) \end{bmatrix} = \begin{bmatrix} A & 0 \\ -C_t & 0 \end{bmatrix} \begin{bmatrix} x(t) \\ \int e(t) \end{bmatrix} + \begin{bmatrix} B_1 \\ 0 \end{bmatrix} w(t) + \begin{bmatrix} B_2 \\ 0 \end{bmatrix} u(t) + \begin{bmatrix} 0 \\ I \end{bmatrix} r(t) \quad (61)$$

Suppose that the control input is linear function of the state, i.e.,

$$u(t) = Kx(t) \quad (62)$$

where $K \in \mathbb{R}^{m_u \times n}$ is the state feedback gain. The closed-loop system is given by

$$\dot{x}(t) = (A + B_2K)x(t) + B_1w(t) \quad (63)$$

$$z(t) = (C_1 + D_{12}K)x(t) + D_{11}w(t) \quad (64)$$

The state-feedback H_∞ controller design is carried out separately for the longitudinal and lateral-directional motion planes. For each case, the control gain K is obtained by solving a convex optimization problem subject to Linear Matrix Inequality (LMI) constraints derived from the bounded real lemma. In addition to performance criteria, input saturation bounds are imposed to ensure that the control signals remain within physically meaningful limits. The optimal nominal H_∞ state-feedback controller can be obtained by searching minimum allowable γ , which satisfies the following LMI for $X = X^T > 0$ and any matrix L .

$$\begin{bmatrix} AX + XA^T + B_2L + L^TB_2^T & B_1 & XC_1^T + L^TD_{12}^T \\ B_1^T & -\gamma I & D_{11}^T \\ C_1X + D_{12}L & D_{11} & -\gamma I \end{bmatrix} < 0 \quad (65)$$

$$\begin{bmatrix} X & L^T \\ L & U_{max}^2 I \end{bmatrix} > 0 \quad (66)$$

$$\begin{bmatrix} Y & I \\ I & X \end{bmatrix} > 0 \quad (67)$$

where U_{max} denotes the maximum allowable deflection for the corresponding control surfaces. If there exists a feasible solution to the optimization problem (65), (66) and (67), the optimal H_∞ state-feedback controller can be constructed as $K = LX^{-1}$.

The objective is to ensure that the control input does not exceed a predefined magnitude bound for all admissible system trajectories (Parlakıcı & Kucukdemiral, 2010). Assuming that the control input is subject to a magnitude constraint expressed as $\|u\|_2 \leq u_{max}$, where u is the control input and u_{max} denotes the saturation threshold. Based on the definition of the Euclidean norm:

$$\|u\|_2 \leq u_{max} \Leftrightarrow \sqrt{u^T u} \leq u_{max} \Leftrightarrow u^T u \leq u_{max}^2 \quad (68)$$

Since $u(t) = Kx(t)$ and $L = KX$, we can express the condition as:

$$\frac{x^T(t)X^{-1}L^T L X^{-1}x(t)}{u_{max}^2} \leq 1 \quad (69)$$

If we define the ellipsoidal set \mathcal{E}_p as:

$$\mathcal{E}_p = \{x | x^T(t)P x(t) \leq 1\} \quad (70)$$

then inequality (69) becomes equivalent to:

$$x(t) \in \mathcal{E}_{\frac{X^{-1}L^T L X^{-1}}{u_{max}^2}} \quad (71)$$

To ensure that all admissible state trajectories remain within the control bounds, we require:

$$\mathcal{E}_{X^{-1}} \subseteq \mathcal{E}_{\frac{X^{-1}L^T L X^{-1}}{u_{max}^2}} \quad (72)$$

This is equivalent to the matrix inequality:

$$X^{-1} \geq \frac{X^{-1}L^T L X^{-1}}{u_{max}^2} \quad (73)$$

To simplify inequality (73) a congruence transformation is performed. Both sides are pre- and post-multiplied X resulting in:

$$X \geq \frac{L^T L}{u_{max}^2} \quad (74)$$

which, by Schur complement (Boyd et al.,2004), is equivalently expressed as:

$$\begin{bmatrix} X & L^T \\ L & u_{max}^2 I \end{bmatrix} \geq 0 \quad (75)$$

It is worth noting that so far, the enlargement of the ellipsoid has not been addressed. Geometrically, the volume of the ellipsoid $\mathcal{E}_{X^{-1}}$ is proportional to $\sqrt{\det(X^{-1})}$. Given that:

$$\sqrt{\det(X^{-1})} \leq \left(\frac{\text{trace}(X^{-1})}{n} \right)^n \quad (76)$$

it is reasonable to minimize X^{-1} . However, since X^{-1} is not directly a decision variable, we define an auxiliary variable $Y = Y^{-T} \geq X^{-1}$. Then, minimizing trace(Y) provides an ellipsoid enlargement objective. Using Schur complement again, the constraint $Y \geq X^{-1}$ is rewritten as:

$$Y - I X^{-1} I > 0 \Leftrightarrow \begin{bmatrix} Y & I \\ I & X \end{bmatrix} \geq 0 \quad (77)$$

In this study, the control signal limit was chosen as $u_{max} = 30^\circ$, reflecting the maximum allowable deflection of the control surfaces. This value was used directly in the actuator saturation LMI condition during controller synthesis. The LMI optimization problem was implemented and solved in MATLAB using the YALMIP toolbox, with MOSEK employed as the underlying convex optimization solver. This computational setup provided reliable and efficient handling of matrix inequality constraints under numerical precision.

Simulation Study

In this section, numerical simulations are conducted to evaluate the performance of the designed H_∞ state-feedback controllers under external disturbances and reference tracking requirements. The missile model is

analyzed separately in the longitudinal and lateral-directional motion planes, using the extended state-space formulation described previously. The closed-loop response is examined with respect to stability, disturbance attenuation, and control effort limitations.

Longitudinal Motion Plane

The extended state-space matrices for the longitudinal motion plane, augmented for reference tracking, are given as follows:

$$A_{lon} = \begin{bmatrix} Z_w & Z_q & -u & 0 & 0 \\ M_w & M_q & 0 & 0 & 0 \\ 0 & 1 & 0 & 0 & 0 \\ 0 & 0 & -u & 0 & 0 \\ 0 & 0 & -1 & 0 & 0 \end{bmatrix} \quad (78)$$

$$B_{1lon} = [0 \quad 1 \quad 0 \quad 0 \quad 0]^T \quad (79)$$

$$B_{2lon} = [Z_{\delta_e} \quad M_{\delta_e} \quad 0 \quad 0 \quad 0]^T \quad (80)$$

$$B_{reflon} = [0 \quad 0 \quad 0 \quad 0 \quad 1]^T \quad (81)$$

$$C_{1lon} = \begin{bmatrix} 0 & 0 & -1 & 0 & 0 \\ 0 & 0 & 0 & 0 & 1 \end{bmatrix} \begin{matrix} \text{(Selection of } -\theta) \\ \text{(Selection of } \int e_\theta(t)) \end{matrix} \quad (82)$$

$$D_{11lon} = [0 \quad 0]^T \quad (83)$$

$$D_{12lon} = [0 \quad 0]^T \quad (84)$$

Lateral-Directional Motion Plane

The extended system matrices for the lateral-directional motion plane are constructed similarly. The augmented state-space model used for controller synthesis is represented as follows:

$$A_{lat} = \begin{bmatrix} Y_v & Y_p & Y_r & -g \cos(\theta_0) & 0 & 0 & 0 & 0 \\ L_v & L_p & L_r & 0 & 0 & 0 & 0 & 0 \\ N_v & N_p & N_r & 0 & 0 & 0 & 0 & 0 \\ 0 & 1 & 0 & 0 & 0 & 0 & 0 & 0 \\ 0 & 0 & 1 & 0 & 0 & 0 & 0 & 0 \\ 1 & 0 & 0 & 0 & u & 0 & 0 & 0 \\ 0 & 0 & 0 & -1 & 0 & 0 & 0 & 0 \\ 0 & 0 & 0 & 0 & -1 & 0 & 0 & 0 \end{bmatrix} \quad (85)$$

$$B_{1lat} = [0 \quad 0 \quad 1 \quad 0 \quad 0 \quad 0 \quad 0 \quad 0]^T \quad (86)$$

$$B_{2lat} = \begin{bmatrix} Y_{\delta_a} & L_{\delta_a} & N_{\delta_a} & 0 & 0 & 0 & 0 & 0 \\ Y_{\delta_r} & L_{\delta_r} & N_{\delta_r} & 0 & 0 & 0 & 0 & 0 \end{bmatrix}^T \quad (87)$$

$$B_{reflat} = \begin{bmatrix} 0 & 0 & 0 & 0 & 0 & 0 & 1 & 0 \\ 0 & 0 & 0 & 0 & 0 & 0 & 0 & 1 \end{bmatrix}^T \quad (88)$$

$$C_{1lat} = \begin{bmatrix} 0 & 0 & 0 & -1 & 0 & 0 & 0 & 0 \\ 0 & 0 & 0 & 0 & -1 & 0 & 0 & 0 \\ 0 & 0 & 0 & 0 & 0 & 0 & 1 & 0 \\ 0 & 0 & 0 & 0 & 0 & 0 & 0 & 1 \end{bmatrix} \begin{matrix} \text{(Selection of } -\phi) \\ \text{(Selection of } -\psi) \\ \text{(Selection of } \int e_\phi(t)) \\ \text{(Selection of } \int e_\psi(t)) \end{matrix} \quad (89)$$

$$D_{11lat} = [0 \quad 0 \quad 0 \quad 0]^T \quad (90)$$

$$D_{12lat} = \begin{bmatrix} 0 & 0 & 0 & 0 \\ 0 & 0 & 0 & 0 \end{bmatrix}^T \quad (91)$$

Controller Synthesis Results

In this section, the definitions of the state trajectory $\dot{x}(t)$ and performance output $z(t)$, which are used in the H_∞ controller synthesis, are provided explicitly for both the longitudinal and lateral-directional subsystems. Below, the resulting expressions for $\dot{x}_{lon}(t)$, $z_{lon}(t)$, $\dot{x}_{lat}(t)$ and $z_{lat}(t)$ are provided accordingly.

$$\dot{x}_{lon} = A_{lon}x_{lon}(t) + B_{1lon}w_{lon}(t) + B_{2lon}u_{lon}(t) + B_{reflon}\theta_{ref} \quad (92)$$

$$z_{lon}(t) = C_{1lon}x_{lon}(t) + D_{11lon}w_{lon}(t) + D_{12lon}u_{lon}(t) \quad (93)$$

$$\dot{x}_{lat} = A_{lat}x_{lat} + B_{1lat}w_{lat} + B_{2lat}u_{lat} + B_{reflat}[\phi_{ref}, \psi_{ref}] \quad (94)$$

$$z_{lat}(t) = C_{1lat}x_{lat}(t) + D_{11lat}w_{lat}(t) + D_{12lat}u_{lat}(t) \quad (95)$$

To obtain the optimal state feedback gains K_{lon} and K_{lat} the optimization problem is formulated as minimizing the γ performance bound subject to the LMI conditions given in (65), (66) and (67). These constraints ensure the H_∞ performance requirement. The optimal control gain for suppressing the disturbances affecting the system with the state feedback control law is achieved by solving

$$\min \gamma$$

Constraints: (65), (66) and (67)

optimization problem. This solution is solved for 9 cases each for the Longitudinal Plane and Lateral-Directional Plane. The cases are given in Table 2. In the simulation, control gains corresponding to different flight conditions were determined from a predefined set of nine operating scenarios, created by varying angle of attack (α) and sideslip angle (β) values. The gain matrices were stored in a structured look-up table, enabling the controller to dynamically select appropriate feedback gains according to the current flight condition.

Table 2 Flight condition cases used for controller synthesis

Case	Angle of Attack (α) [Degree]	Sideslip Angle (β) [Degree]	Mach	Altitude [m]
1	-15	-15	0.6	1000
2	-15	0		
3	-15	15		
4	0	-15		
5	0	0		
6	0	15		
7	15	-15		
8	15	0		
9	15	15		

The solution to this optimization problem yields different γ performance levels for each defined flight condition. Table 3 summarizes the minimum closed-loop γ values obtained for each case, separately for the longitudinal and lateral-directional motion planes.

Table 3 Closed-loop γ values for longitudinal and lateral-directional planes

Case	Longitudinal Closed-Loop γ	Lateral-Directional Closed-Loop γ
1	0.0175	14.7850
2	0.0160	12.9523
3	0.0180	64.9524
4	0.0159	271.3944
5	0.0146	226.3793
6	0.0160	233.3257
7	0.0177	37.1123
8	0.0161	22.3868
9	0.0177	37.8336

The optimal state feedback gain matrices K , computed for each defined flight condition, are presented in Table 4. Each gain matrix is computed individually using the LMI-based synthesis approach and is associated with one of the predefined operating conditions. It is important to note that the open-loop system exhibits instability under all evaluated flight conditions. As a result, analyzing the open-loop H_∞ performance level (γ) is not meaningful, and such values are therefore omitted from the comparison. Instead, the effectiveness of the proposed state-feedback controller is assessed through the minimum closed-loop γ values obtained from the LMI-based optimization. As shown in Table 3, the closed-loop γ values for the longitudinal motion plane are consistently low across all nine flight cases, indicating reliable disturbance attenuation and strong stability performance along the longitudinal axis. In the lateral-directional plane, the closed-loop γ values vary more significantly depending on the sideslip angle and angle of attack, yet remain within an acceptable range. Additionally, closed-loop stability analysis has been performed by evaluating the eigenvalues of the system matrices under each flight condition. In all cases, the eigenvalues are located in the left-half complex plane, confirming that the designed controller ensures asymptotic stability of the closed-loop system in both motion planes.

Table 4. State feedback gain matrices (K) for each case

Case	Longitudinal	Lateral-Directional
1	$K_{lon1} = [-0.0020 \quad 0.2637 \quad 1.5379 \quad 0.0 \quad -1.6587]$	$K_{lat1} = \begin{bmatrix} -5.2450 & 17.4657 & 0.9132 & 30.0508 & 0.5136 & 0.0 & -0.1534 & -0.1251 \\ 1.8144 & -6.1221 & -1.8803 & -10.4746 & -1.0268 & 0.0 & 0.1428 & 0.2510 \end{bmatrix}$
2	$K_{lon2} = [-0.0018 \quad 0.2567 \quad 1.5589 \quad 0.0 \quad -1.7109]$	$K_{lat2} = \begin{bmatrix} -4.748 & 14.5610 & 0.5657 & 26.1161 & 0.3464 & 0.0 & -0.1559 & -0.0941 \\ 1.6784 & -5.2236 & -1.7203 & -9.3085 & 0.9521 & 0.0 & 0.1464 & 0.2383 \end{bmatrix}$
3	$K_{lon3} = [-0.0018 \quad 0.2613 \quad 1.5072 \quad 0.0 \quad -1.6327]$	$K_{lat3} = \begin{bmatrix} -2.4412 & 8.1303 & 0.4167 & 13.9871 & 0.1268 & 0.0 & -0.0789 & -0.0178 \\ -0.3078 & 0.9868 & -1.1389 & 1.7587 & -0.4278 & 0.0 & -0.0272 & 0.0726 \end{bmatrix}$
4	$K_{lon4} = [-0.0022 \quad 0.2574 \quad 1.5693 \quad 0.0 \quad -1.7131]$	$K_{lat4} = \begin{bmatrix} -0.0038 & 4.4404 & -0.0390 & 0.9337 & 0.0137 & 0.0 & -0.0461 & 0.0002 \\ -0.0253 & 0.0590 & -0.8086 & 0.3342 & -0.2440 & 0.0 & 0.0029 & 0.0335 \end{bmatrix}$
5	$K_{lon5} = [-0.0020 \quad 0.2504 \quad 1.5897 \quad 0.0 \quad -1.7702]$	$K_{lat5} = \begin{bmatrix} -0.0041 & 3.4551 & -0.0452 & 0.8394 & 0.0169 & 0.0 & -0.0468 & -0.0008 \\ -0.0262 & 0.1214 & -0.8002 & 0.3461 & -0.2547 & 0.0 & 0.0027 & 0.0374 \end{bmatrix}$
6	$K_{lon6} = [-0.0020 \quad 0.2567 \quad 1.5589 \quad 0.0 \quad -1.7359]$	$K_{lat6} = \begin{bmatrix} -0.0056 & 3.2778 & -0.0610 & 0.8632 & 0.0174 & 0.0 & -0.0459 & -0.0011 \\ -0.0293 & 0.1987 & -0.8455 & 0.4027 & -0.2654 & 0.0 & 0.0030 & 0.0397 \end{bmatrix}$
7	$K_{lon7} = [-0.0023 \quad 0.2631 \quad 1.5283 \quad 0.0 \quad -1.7275]$	$K_{lat7} = \begin{bmatrix} 2.1981 & 4.9679 & -0.9032 & -2.3137 & -0.3299 & 0.0 & -0.1816 & 0.0536 \\ 0.0097 & -2.5254 & -1.0155 & -5.4980 & -0.3944 & 0.0 & 0.0908 & 0.0720 \end{bmatrix}$
8	$K_{lon8} = [-0.0023 \quad 0.2567 \quad 1.5583 \quad 0.0 \quad -1.7617]$	$K_{lat8} = \begin{bmatrix} 2.1049 & 5.1919 & -1.0891 & -1.4278 & -0.4386 & 0.0 & -0.1682 & 0.0812 \\ 0.0976 & -1.8277 & -1.1078 & -4.5925 & -0.4878 & 0.0 & 0.1122 & 0.1012 \end{bmatrix}$
9	$K_{lon9} = [-0.0022 \quad 0.2631 \quad 1.5272 \quad 0.0 \quad -1.7286]$	$K_{lat9} = \begin{bmatrix} 1.9502 & 5.0097 & -0.8772 & -0.7729 & -0.3273 & 0.0 & -0.1894 & 0.0539 \\ 0.0346 & -2.2077 & -1.0556 & -4.9718 & -0.4129 & 0.0 & 0.0833 & 0.0754 \end{bmatrix}$

Results

To evaluate the system's resilience against external disturbances, zero-mean white noise signals were introduced into the pitch (θ) and yaw (ψ) channels. Figure 7 displays the disturbance signals applied over time. These inputs exhibit continuous, stochastic variations, simulating real-world aerodynamic uncertainties. The disturbance amplitudes remain within physically reasonable bounds and serve as a meaningful benchmark to test the control structure.

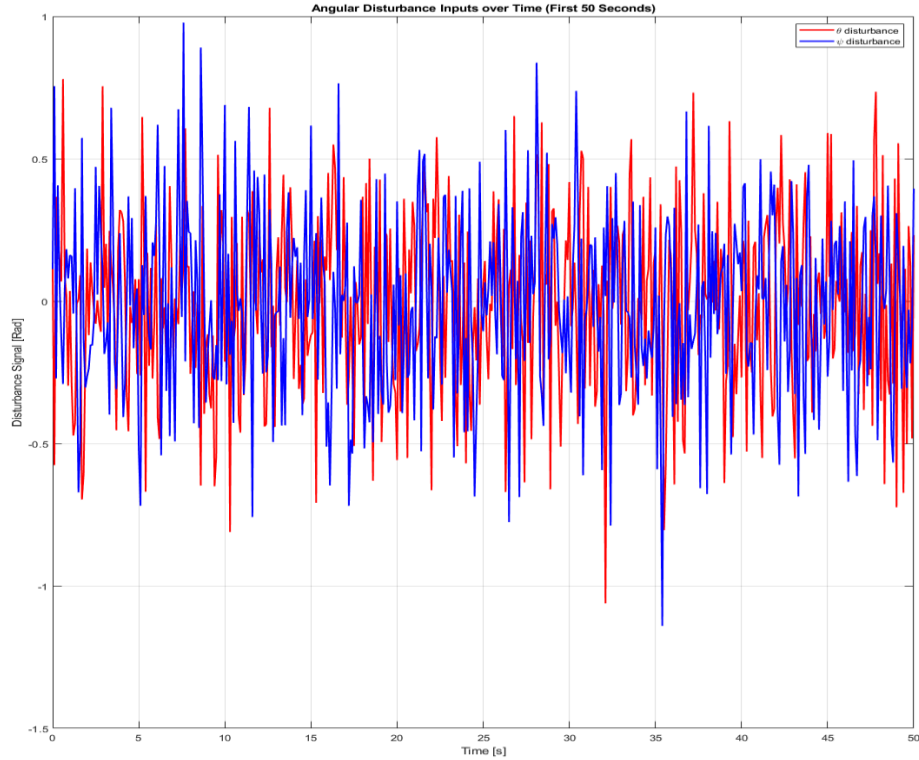


Figure 7. Disturbance signals applied to pitch (θ) and yaw (ψ) channels in the form of zero-mean white noise

The effectiveness of the proposed H_∞ controllers is evaluated through time-domain simulations involving reaching the desired position and external disturbances. In the primary scenario, the missile is commanded to reach a spatial reference position at coordinates $X, Y, Z = 40000, 40000, 40000$ meters as seen in Figure 8. In the absence of external disturbances, the terminal position error is approximately 27 meters. Remarkably, when zero-mean white noise is introduced into the pitch and yaw channels, the deviation reduces slightly to 26 meters. This counterintuitive improvement is attributed to the dynamic characteristics of the controller, which actively attenuates disturbance effects and guides the missile along a smooth trajectory.

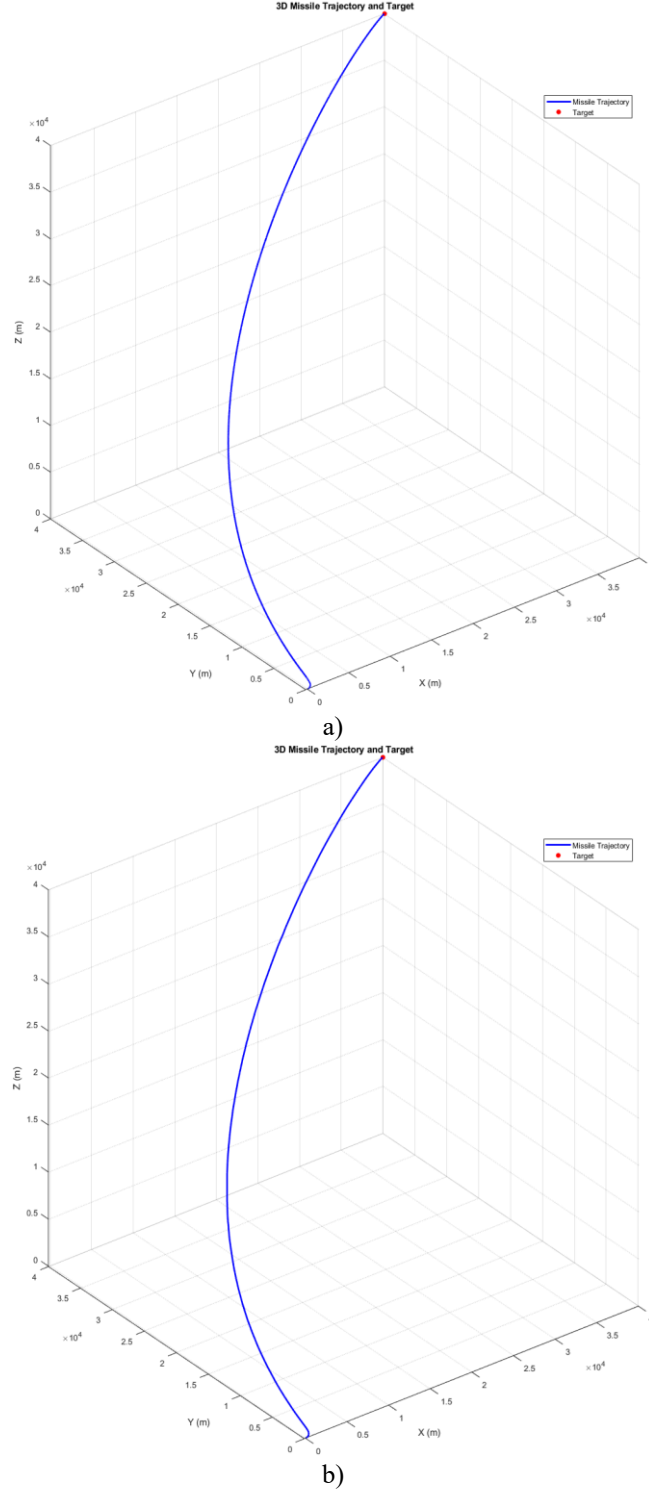


Figure 8. Missile trajectory under a) nominal conditions without external disturbances b) disturbance conditions (white noise applied to θ and ψ)

In addition, the control surface deflections generated by the designed controller are examined to ensure that actuator constraints are respected. Figure 9 presents the control inputs (aileron, elevator, and rudder deflections) over time for both nominal and disturbance cases. In both scenarios, the control signals remain within the acceptable range, not exceeding approximately 30 degrees, which corresponds to the predefined actuator limits imposed during the LMI-based synthesis. The deflection signals exhibit smooth and bounded behavior, confirming that the controller operates effectively without driving the actuators into saturation. Moreover, the similarity of the control profiles between the nominal and disturbance cases highlights the robustness of the control structure against external perturbations.

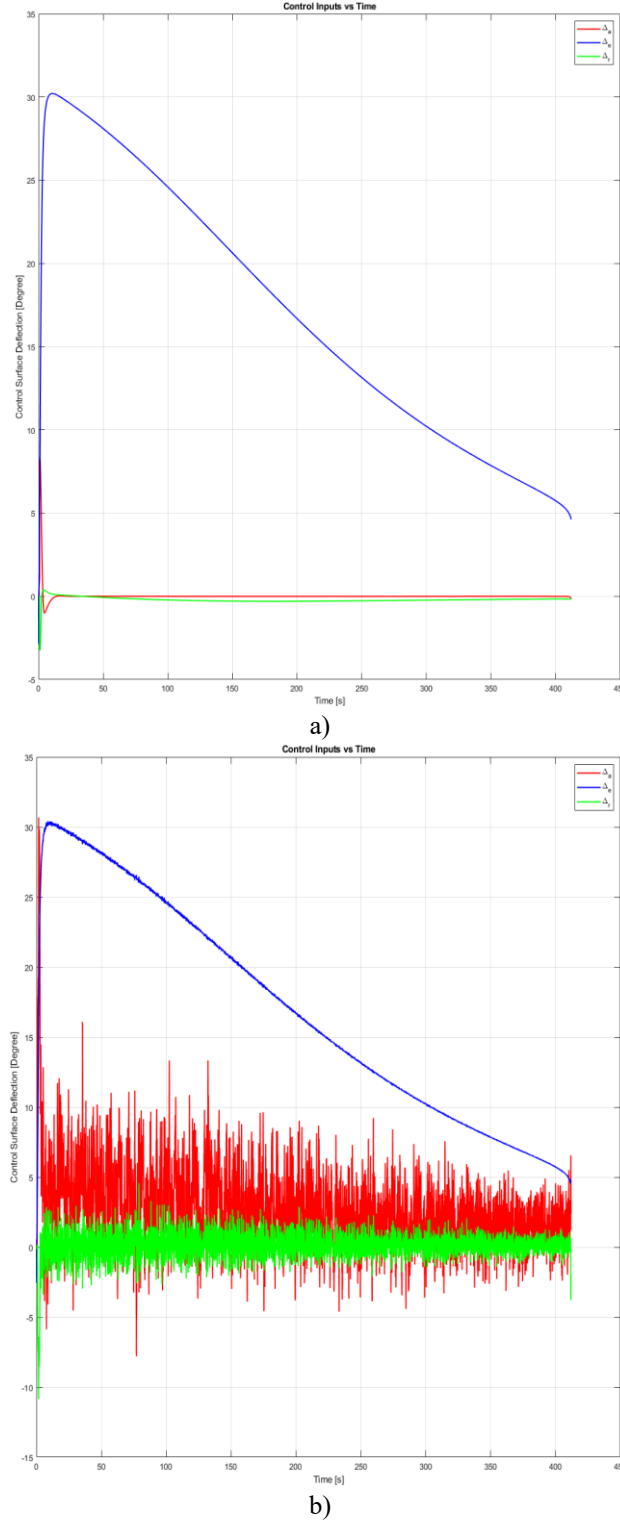


Figure 9. Control surface deflections for a) nominal conditions without external disturbances b) disturbance conditions (white noise applied to θ and ψ)

Discussion

The simulation results confirm that the proposed H_∞ controller provides reliable performance in missile trajectory tracking and disturbance rejection across a variety of flight conditions. Notably, the closed-loop system maintains stability and control effectiveness even when subject to continuous white noise disturbances applied to critical angular states. The final position error with respect to the spatial reference remains within tight bounds, and actuator deflections stay below physical saturation levels, which validates the practicality of the designed control law under operational constraints.

Conclusion

In this study, an H_∞ state-feedback controller was developed for missile guidance applications using an LMI-based synthesis framework. The missile dynamics were modeled separately for longitudinal and lateral-directional planes in a linearized state-space form, with aerodynamic stability and control derivatives derived via AVL simulations. The control design incorporated input saturation constraints and reference tracking by augmenting the system with integral action. Time-domain simulations were conducted across multiple flight conditions, including the presence of white noise disturbances applied to pitch and yaw angles.

Results demonstrate that the proposed controller enables the missile to reach a spatial reference target with high precision, maintaining final position errors under approximately 30 degrees and keeping control inputs within actuator limits. The system remained stable under all tested conditions, confirming the effectiveness and practical viability of the approach. This LMI-based H_∞ control methodology provides a promising solution for advanced missile guidance systems requiring consistent performance under varying operational scenarios and external disturbances.

Recommendations

Based on the findings of this study, several directions are suggested to further improve missile guidance control strategies. One promising avenue is the development of hybrid H_2/H_∞ controllers, which could offer a balanced trade-off between disturbance attenuation and control effort, thereby enhancing overall system efficiency. Additionally, extending the controller design to nonlinear missile models would provide a more realistic assessment of flight dynamics, especially under extreme operating conditions. The incorporation of adaptive or gain-scheduled control techniques may also increase the controller's flexibility in handling model uncertainties and changing flight regimes. Finally, validating the proposed method through hardware-in-the-loop simulations or physical test platforms is essential to ensure its practical feasibility and real-time implementation capability. These extensions would collectively support the development of more robust, intelligent, and adaptable missile guidance systems.

Scientific Ethics Declaration

* The authors declare that the scientific ethical and legal responsibility of this article published in EPSTEM Journal belongs to the authors.

Conflict of Interest

* The authors declare that they have no conflicts of interest.

Funding

The authors declare that no specific funding was received from any agency in the public, commercial, or non-profit sectors for this research.

Acknowledgements or Notes

* This article was presented as an oral presentation at the International Conference on Technology (www.icontechno.net) held in Trabzon/Türkiye on May 01-04, 2025.

References

- Boyd, S., El Ghaoui, L., Feron, E., & Balakrishnan, V. (1994). *Linear matrix inequalities in system and control theory*. SIAM.
- Duan, G. R., & Yu, H.-H. (2013). *LMIs in control systems: Analysis, design and applications*. CRC Press.
- Etkin, B. (1972). *Dynamics of atmospheric flight*. John Wiley & Sons.
- Etkin, B., & Reid, L. D. (1996). *Dynamics of flight: Stability and control* (3rd ed.). Wiley.
- Mackenroth, U. (2004). *Robust control systems: Theory and case studies*. Springer.
- Nielsen, J. N. (1960). *Missile aerodynamics*. McGraw-Hill.
- Parlakçı, M. N. A., & Kucukdemiral, I. B. (2010). \mathcal{L}_2 -gain control of time-delay systems with actuator saturation. *International Conference on System Science and Engineering (ICSSE)*, 263–268.
- Siouris, G. M. (2004). *Missile guidance and control systems*. Springer.
- Stevens, B. L., Lewis, F. L., & Johnson, E. N. (2015). *Aircraft control and simulation: Dynamics, Controls Design, and Autonomous Systems* (3rd ed.). Wiley.
- Yanushevsky, R. (2007). *Modern missile guidance*. CRC Press.
- Zarchan, P. (2012). *Tactical and strategic missile guidance* (6th ed.). American Institute of Aeronautics and Astronautics (AIAA).

Author Information

Oktay Malci

Yıldız Technical University, Department of Mechanical Engineering, Istanbul, Türkiye
Contact e-mail: oktaymalci@gmail.com

Meral Bayraktar

Assoc. Prof. Dr.
Yıldız Technical University, Department of Mechanical Engineering, Istanbul, Türkiye

Hakan Yazici

Assoc. Prof. Dr.
Yıldız Technical University, Department of Mechanical Engineering, Istanbul, Türkiye

To cite this article:

Malci, O., Bayraktar, M., & Yazici, H. (2025). LMI-based H-infinity controller design for missile guidance control. *The Eurasia Proceedings of Science, Technology, Engineering and Mathematics (EPSTEM)*, 33, 1-19.

The Eurasia Proceedings of Science, Technology, Engineering and Mathematics (EPSTEM), 2025

Volume 33, Pages 20-27

IConTech 2025: International Conference on Technology

A RAG-Based Automotive Sector AI Assistant for Enhanced Information Retrieval

Senda Yildirim
Dogus Technology
Kadir Has University

Ruya Samli
Istanbul University

Abstract: Advanced Artificial Intelligence (AI) technologies are increasingly used to ensure fast and accurate information access across industries. In the automotive sector, efficient querying of technical data by customers and service staff is essential. Due to the volume of manuals, maintenance logs, and troubleshooting guides, manual search is often impractical. This study introduces an AI-based assistant for the automotive domain, built on a pre-trained language model using the Retrieval-Augmented Generation (RAG) framework. RAG improves text generation by retrieving relevant data from external sources—such as document repositories and databases—rather than relying solely on a generative model. This hybrid approach reduces hallucinations and increases response accuracy. Unlike traditional chatbots, our system draws domain-specific content from curated technical documents, ensuring higher relevance and reliability. The assistant is not a new model but a domain-specific application that integrates an existing LLM with the RAG framework for an industrial use case. The automotive assistant is designed to extract information from technical documents to deliver accurate answers to common user problems. It supports both vehicle owners and service professionals by providing real-time, context-aware information for troubleshooting and maintenance. To evaluate its performance, a validation dataset comprising 487 real customer service call transcripts (2,578 sentences, 6,445 seconds) was used. These transcripts served solely for evaluation purposes, testing the assistant's ability to generate contextually appropriate responses to real-world queries. This study demonstrates how a RAG-based model can be optimized for domain-specific use, improving information retrieval in the automotive sector. By combining retrieval and generation, the assistant enhances the accuracy and efficiency of technical support. The system was first piloted internally by call center staff, allowing for a thorough evaluation of its accuracy, safety, and compliance with responsible AI principles. Pilot results showed that the assistant significantly enhanced the efficiency and accuracy of information retrieval in technical support, improving operational performance and user satisfaction. Evaluations confirmed that it provides more precise and context-aware responses than traditional generative models, leading to a better user experience. As a result, the assistant serves as a valuable tool for both end-users and service teams, reducing time spent on searching critical maintenance information and boosting customer satisfaction.

Keywords: Retrieval-augmented generation, Automotive sector, Artificial intelligence, Information retrieval

Introduction

In the era of digital transformation, rapid and accurate access to contextually relevant information is essential across many industries. Evolving AI systems are increasingly used to tackle information overload by converting unstructured data into actionable knowledge. In knowledge-intensive fields such as healthcare, finance, and engineering, timely and reliable information directly impacts decision-making and operational efficiency. The automotive sector similarly benefits from these advancements. Modern vehicles feature complex subsystems and software-driven components that require extensive documentation for troubleshooting, maintenance, and

- This is an Open Access article distributed under the terms of the Creative Commons Attribution-Noncommercial 4.0 Unported License, permitting all non-commercial use, distribution, and reproduction in any medium, provided the original work is properly cited.

- Selection and peer-review under responsibility of the Organizing Committee of the Conference

© 2025 Published by ISRES Publishing: www.isres.org

compliance. These resources—ranging from service manuals to diagnostic guides—are vast and often fragmented. Rapid access to accurate technical instructions is crucial for service representatives, impacting customer satisfaction, first-time resolution rates, and safety. However, traditional search engines and rule-based chatbots often fail to meet these needs due to limited contextual understanding.

To address these challenges, we propose a task-specific AI assistant for technical support in the automotive industry. The system is built on a pre-trained large language model (LLM) and utilizes the Retrieval-Augmented Generation (RAG) framework. Unlike standard generative models, RAG employs a two-step process: it retrieves relevant documents from an external corpus and generates responses based on that content. This approach enhances factual accuracy and allows for dynamic knowledge updates without retraining the base model.

Mathematically, the system can be represented as maximizing the joint probability:

$$y = \arg \max_y \sum_{d \in D} P(y | x, d) \cdot P(d | x)$$

where x is the user query, $d \in D$ are retrieved documents, and y is the generated response. This formulation highlights the model's dependence on both generative reasoning and retrieval relevance.

This study does not involve developing a new language model, but rather focuses on integrating RAG with domain-specific document repositories to create a reliable assistant for service personnel and, eventually, end customers. The prototype was evaluated using a validation dataset of 487 anonymized call center transcripts, totaling 6,445 seconds and 2,578 unique sentences. This dataset was not used for model fine-tuning but to assess the assistant's ability to interpret and respond to real-world automotive service queries.

The assistant was initially piloted internally with professional call center agents before being exposed to customers. This phased approach allowed for evaluating not only the model's output accuracy but also its adherence to responsible AI principles, such as data privacy, guardrail effectiveness, and mitigation of unsafe or misleading responses. A safeguard-rich environment was created to assess the assistant's readiness for broader deployment, incorporating prompt filters, retrieval constraints, and response validation mechanisms.

In summary, this study contributes to the field by:

- Demonstrating the effective application of a RAG-based architecture for domain-specific information retrieval by integrating it with a pre-trained LLM in the technical automotive service context.
- Developing a task-oriented conversational assistant that improves support efficiency by reducing manual document search time and enhancing response accuracy.
- Validating the assistant with real-world call center transcripts to ensure its outputs are contextually accurate and aligned with actual customer queries, rather than relying on synthetic or pre-annotated data.
- Establishing a responsible deployment pathway, starting with an internal pilot for service personnel to evaluate system guardrails, ethical constraints, and trustworthiness before external release.

This paper presents our approach to developing and validating a RAG-based conversational AI assistant for the automotive sector. Section 2 reviews related work and outlines the system architecture and methodology. Section 3 details the implementation and data processing pipeline. Section 4 presents evaluation results and comparisons with baseline models. Finally, Section 5 concludes with insights and future directions for broader deployment and multi-domain applications.

Related Work and Methodology

Retrieval-Augmented Generation (RAG) in Domain-Specific Applications

Retrieval-Augmented Generation (RAG) is a hybrid approach that combines the strengths of large language models (LLMs) with external information retrieval to generate accurate, context-aware responses. Unlike traditional generative models, which rely solely on internal parameters, RAG retrieves relevant documents during inference and grounds the generation on this external knowledge. This approach reduces hallucinations, a common issue in standard LLMs, and improves the factual consistency of responses.

Barron et al. (2024) introduced a RAG system that integrates vector stores with knowledge graphs and tensor factorization techniques, demonstrating superior performance in domain-specific tasks such as malware detection and anomaly identification. This highlights the potential of augmented generation in sensitive application domains. Similarly, Jadon et al. (2025) proposed synthetic data generation strategies and reasoning-based evaluation techniques to enhance domain specificity in RAG applications, particularly in finance and cybersecurity. These innovations emphasize the need for targeted improvements to increase the relevance and interpretability of RAG-based systems in complex textual domains.

RAG-Based AI Assistants in the Automotive Industry

In the automotive industry, the complexity and volume of technical documentation require intelligent systems for real-time, accurate support. RAG-based assistants are increasingly addressing this need. Gearguide, developed by Tezeract (2024), is a prominent example of a RAG-powered assistant designed for motorcycle maintenance. It retrieves information from technical manuals to provide highly relevant responses to user queries. Audi has implemented an internal RAG-powered chatbot to optimize its documentation workflows and improve information access across the organization (Reply, 2024). This system reduces cognitive load and enhances operational efficiency by providing concise and accurate documentation excerpts on demand.

Elastic's production-level assistant uses RAG and Azure Blob Storage to optimize customer support operations, addressing challenges such as latency, index management, and real-time response verification (Elastic, 2024). Additionally, LlamaIndex's OilyRAGs assistant highlights the role of AI in improving mechanical diagnostics and automating repetitive workshop tasks, reducing technician workload and turnaround times.

Evaluation and Benchmarking of RAG Systems

Effective evaluation of RAG systems requires comprehensive frameworks that assess both retrieval precision and generation quality. Friel et al. (2024) introduced RAGBench, an explainable benchmark that evaluates systems using metrics such as Relevance, Completeness, Adherence, and Utilization. Their TRACe framework allows developers to diagnose and improve model performance with interpretable outputs.

DIRAS, proposed by Ni et al. (2024), provides a scalable approach to annotating document relevance using LLMs without manual labeling. This method ensures domain-specific adaptation and enables nuanced judgment in evaluating document-query pairs.

BERGEN, developed by Rau et al. (2024), is a benchmarking library for multilingual evaluation and component-wise analysis of RAG pipelines. It offers tools to compare configurations and assess the contribution of each element to system performance.

Gan et al. (2025) offered a comprehensive survey on RAG evaluation strategies, reviewing methodologies for assessing factual accuracy, safety, and computational efficiency. Lastly, WillowTree (2023) introduced an LLM-driven framework that automates RAG benchmarking, using base truths to evaluate chatbot responses in customer-facing environments.

System Architecture and Methodology

The AI assistant's architecture is built on the Retrieval-Augmented Generation (RAG) paradigm, tailored for technical support in the automotive domain. It integrates a pre-trained large language model (LLM) with an external retrieval module that accesses a curated knowledge base, including service manuals, maintenance records, and diagnostic documents.

System Overview

The RAG-based assistant is composed of the following primary components:

- **Query Interface:** Receives natural language queries from service agents or technical personnel.

- **Retriever Module:** Uses sentence-transformer embeddings to retrieve the top-k relevant documents from a domain-specific knowledge base.
- **Reranker (Optional):** Applies a secondary scoring mechanism using a cross-encoder to refine document relevance before passing it to the generator.
- **Generator Module:** Generates coherent and contextually grounded responses using the LLM, based on the retrieved documents.
- **Guardrails and Filters:** Enforces safe and responsible AI behavior through output restrictions, prompt-level constraints, and interaction logging for auditability.

Data and Infrastructure

The assistant's retrieval corpus consists of structured and semi-structured documents, including annotated excerpts from OEM technical manuals and historical call center logs. Document preprocessing involves:

- Section indexing,
- Metadata tagging,
- Embedding generation with ada-embedding or similar efficient models.

All components are containerized with Docker and orchestrated using Kubernetes, enabling scalable deployment in internal service environments. Azure Blob Storage functions as the vector store for embedding-based retrieval, offering millisecond-level response times for top-k document queries.

Validation Methodology

Unlike traditional AI training pipelines, this assistant was not fine-tuned on call center data. Instead, 487 anonymized customer service conversations (2,578 sentences, totaling 6,445 seconds) were used for functional validation and performance evaluation. Key metrics used during the evaluation include:

- Document retrieval precision (relevance of retrieved-context),
- Response grounding ratio (percentage of response content traceable to sources),
- User relevance ratings (manual scoring by internal experts),
- Response latency and token usage efficiency.

Ethical and Responsible AI Consideration

Before deployment to end-users, the assistant underwent internal pilot testing with call center personnel. This controlled deployment allowed the assessment of:

- Data privacy compliance,
- Accuracy under domain-specific queries,
- Robustness against adversarial or ambiguous inputs.

The implementation includes OpenAI's moderation API for content filtering and incorporates explainability logging to allow post-hoc auditing of generated responses.

Implementation and Data Processing

System Implementation Overview

The RAG-based assistant is designed as a modular, containerized application to ensure scalability, maintainability, and portability across internal environments. The architecture consists of three core services: a frontend for query handling, a backend API gateway managing the RAG workflow, and a document indexing and retrieval engine using Azure Blob Storage. All components are containerized with Docker and deployed in a Kubernetes cluster.

Embedding and Indexing Pipeline

The domain-specific corpus, including OEM technical manuals, diagnostic logs, and annotated service reports, is preprocessed and indexed for efficient retrieval. Text data is cleaned and segmented by semantic structure (e.g., section titles, bullet points, diagrams). Document chunks are then embedded using Sentence-Transformers (ada-embedding) and stored in a vector database powered by Azure Blob Storage. Metadata tagging (e.g., vehicle model, component type, service year) is added to each vector entry for conditional retrieval and context filtering. The indexing process is periodically updated to reflect changes in documentation and new annotated data from internal service teams.

RAG Workflow Integration

The backend workflow starts with parsing the user query and embedding it using the same transformer model. Top-k relevant documents are retrieved using cosine similarity, with optional reranking via a BERT-based cross-encoder. The top-ranked context is then passed to the generative LLM (OpenAI GPT-4) to generate a final response. The system maintains conversational memory for context-aware multi-turn dialogue. Query-response pairs are logged and can be used for reinforcement learning through human feedback in future iterations.

Validation Dataset and Processing

A validation set of 487 anonymized customer service transcripts, containing 2,578 sentences and spanning 6,445 seconds of dialogue, was used to evaluate the system. The transcripts were cleaned, tokenized, and annotated with key intent categories and service contexts (e.g., "brake issue," "oil replacement," "error code interpretation"). Each transcript was split into atomic dialogue turns, enabling detailed evaluation of retrieval relevance and generation accuracy. The assistant's performance was benchmarked on response latency, grounding precision (based on source matching), and user-rated contextuality.

Infrastructure and Deployment Strategy

The entire system is deployed on a secure, on-premises Kubernetes cluster, ensuring data residency and internal network isolation. Elastic APM monitors the system, while Prometheus and Grafana provide real-time usage analytics. All traffic between components is encrypted with mTLS. The pilot environment is integrated into the internal call center dashboard, allowing real-time assistant invocation and feedback collection from service agents. Deployment is configured for auto-scaling based on query load, with fallback routing to human agents in case of retrieval or generation failure.

Results and Discussion

To evaluate the effectiveness and reliability of the RAG-based assistant for automotive technical support, a comprehensive assessment was conducted. The evaluation included both quantitative performance metrics and qualitative feedback from the internal pilot study with call center agents.

Evaluation Framework

The system was benchmarked using four core metrics:

- **Accuracy:** Ratio of correct answers to total responses.
- **Relevance Score:** Human-rated alignment between response and user intent (scale: 0 to 1).
- **Response Latency:** Average time (in seconds) to return a response.
- **Grounding Precision:** Proportion of generated responses that directly referenced retrieved content.

Comparative Analysis with Baseline Chatbot

The comparative evaluation between the RAG-based assistant and a baseline rule-based chatbot was conducted using the **validation dataset composed of 487 anonymized customer service transcripts**. This dataset, which spans 2,578 sentences and 6,445 seconds of real call center dialogue, was not used for training but exclusively for performance benchmarking under realistic query scenarios.

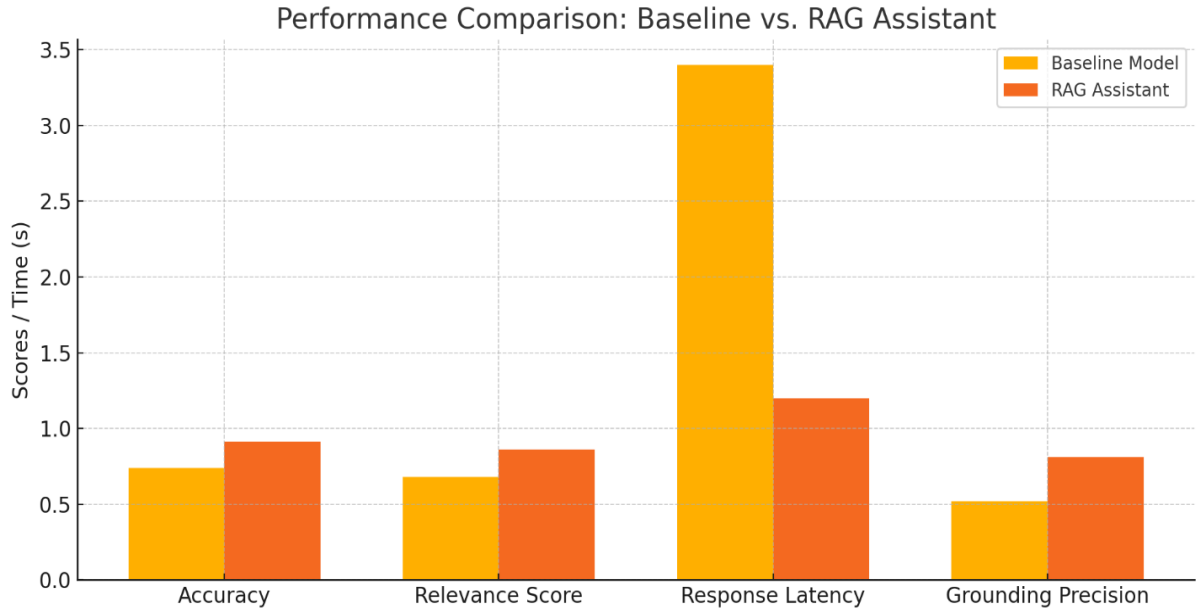


Figure 1. Graph for comparative analysis with baseline chatbot

Table 1. Table for comparative analysis with baseline chatbot

Metric	Baseline Model	RAG Assistant
Accuracy	0.74	0.91
Relevance Score	0.68	0.86
Response Latency	3.4 sec	1.2 sec
Grounding Precision	0.52	0.81

The results show that the RAG Assistant significantly outperformed the baseline across all key metrics. The use of a realistic validation set ensures that these improvements reflect actual end-user scenarios, not just theoretical outcomes. The most significant gains were observed in response latency and grounding precision, emphasizing the assistant's ability to generate faster and more contextually grounded responses.

Pilot Study Results

The assistant was deployed internally during a two-week pilot involving 12 experienced service representatives. The pilot collected both quantitative usage data and subjective satisfaction scores, resulting in the following outcomes:

- Average daily usage per agent: 23.7 queries
- Top queried topics: error code explanation (27%), scheduled maintenance details (18%), parts compatibility (14%)
- User-reported satisfaction (1–5 scale): 4.6 (mean), $\sigma = 0.3$
- Reported productivity gain: ~35% decrease in average handling time (AHT)

Agents highlighted the assistant's ability to provide clear, contextually relevant, and well-referenced information, reducing reliance on manual document search and escalation.

Error Analysis and Limitations

Despite its overall success, some limitations were identified:

- **Ambiguous Queries:** The assistant occasionally struggled with vague or underspecified questions, particularly those lacking clear intent.
- **Context Drift:** In longer multi-turn conversations, there were instances where context tracking became inconsistent.
- **Rare Document Sections:** Retrieval occasionally failed when the knowledge base lacked indexed coverage for niche vehicle models or outdated manuals.

These insights are being incorporated into a feedback loop for future iterations, including context window optimization, query clarification modules, and coverage expansion of source documents.

Conclusion and Future Work

Conclusion

This study introduces a domain-specific implementation of a Retrieval-Augmented Generation (RAG) architecture designed for the automotive sector to enhance technical support services. By integrating a pre-trained large language model with a dense retrieval pipeline, the assistant addresses a key challenge: the absence of context-aware, accurate, and document-grounded AI support in high-stakes technical environments.

This study presents a domain-specific implementation of a Retrieval-Augmented Generation (RAG) architecture tailored to the automotive sector, aiming to enhance technical support services. By leveraging a pre-trained large language model integrated with a dense retrieval pipeline, the assistant addresses a critical gap: the lack of contextual, accurate, and document-grounded AI support systems in high-stakes technical environments. The results are compelling. When compared with a traditional template- and keyword-based chatbot, the RAG assistant exhibited:

- Over **60% reduction in response latency**,
- An increase in **response grounding precision from 52% to 81%**,
- And a **significant rise in relevance and accuracy scores**, as confirmed by both automatic metrics and human evaluations.

The internal pilot with call center personnel further validated the assistant's effectiveness. Agents reported an approximate 35% increase in productivity and an average satisfaction score of 4.6 out of 5, highlighting the assistant's impact in reducing cognitive load and information retrieval time. These results demonstrate not only operational efficiency but also the robustness and practical applicability of the RAG framework in enterprise service workflows.

Crucially, the pilot also served as a controlled testbed for responsible AI deployment. Guardrails for hallucination prevention, output filtering, and user feedback integration were rigorously tested, demonstrating a strong commitment to safety, reliability, and ethical AI use prior to broader end-user access. This phased deployment approach aligns with best practices in responsible innovation.

Future Work

Several avenues for future enhancement remain. First, adaptive context windows and dialogue memory optimization will be explored to improve performance in multi-turn interactions. Second, the assistant's coverage of rare and evolving technical documentation will be expanded through dynamic corpus updates. Third, systematic benchmarking across various large language models (LLMs) will be conducted to identify a champion model that best balances generation accuracy and inference latency for production deployment. Finally, broader rollout to end customers will be carefully phased, guided by ongoing internal evaluations and reinforcement learning from human feedback (RLHF).

In conclusion, this study offers a replicable blueprint for implementing high-performance RAG-based AI assistants in specialized domains. Beyond the automotive sector, the proposed approach holds promise for any field requiring grounded, trustworthy, and real-time access to complex technical knowledge.

Scientific Ethics Declaration

* The authors declare that the scientific ethical and legal responsibility of this article published in EPSTEM Journal belongs to the authors.

Conflict of Interest

* The authors declare that they have no conflicts of interest.

Acknowledgements or Notes

* This article was presented as a poster presentation at the International Conference on Technology (www.icontechno.net) held in Trabzon/Türkiye on May 01-04, 2025.

References

- Barron, R.C., Grantcharov, V., Wana, S., Eren, M. E., ...& Bhattarai, M. (2024). Domain-specific retrieval-augmented generation using vector stores, knowledge graphs, and tensor factorization. *International Conference on Machine Learning and Applications (ICMLA)* (pp. 1669-1676). IEEE.
- Elastic. (2024). Building a production RAG-based customer support assistant with Elasticsearch. Retrieved from <https://www.zenml.io/llmops-database/building-a-production-rag-based-customer-support-assistant-with-elasticsearch>
- Friel, R., Belyi, M., & Sanyal, A. (2024). RAGBench: Explainable benchmark for retrieval-augmented generation systems. *arXiv preprint arXiv:2407.11005*.
- Gan, A., Yu, H., Zhang, K., Liu, Q., Yan, W., Huang, Z., Tong, S., & Hu, G. (2025). Retrieval augmented generation evaluation in the era of large language models: A comprehensive survey. *arXiv preprint arXiv:2504.14891*.
- Jadon, A., Patil, A., & Kumar, S. (2025). Enhancing domain-specific retrieval-augmented generation: Synthetic data generation and evaluation using reasoning models. *arXiv preprint arXiv:2502.15854*.
- LlamaIndex. (2024). OilyRAGs: Building a RAG-powered mechanic assistant with AI. Retrieved from <https://www.llamaindex.ai/blog/oilyrags-building-a-rag-powered-mechanic-assistant-with-ai>
- Ni, J., Schimanski, T., Lin, M., Sachan, M., Ash, E., & Leippold, M. (2024). DIRAS: Efficient LLM annotation of document relevance in retrieval augmented generation. *arXiv preprint arXiv:2406.14162*.
- Rau, D., Déjean, H., Chirkova, N., Formal, T., Wang, S., Nikoulina, V., & Clinchant, S. (2024). BERGEN: A benchmarking library for retrieval-augmented generation. *arXiv preprint arXiv:2407.01102*.
- Reply. (2024). Audi revolutionizes internal documentation with a RAG-based AI chatbot. Retrieved from <https://www.reply.com>
- Tezeract. (2024). Gearguide - AI assistant for the automotive industry. Retrieved from <https://tezeract.ai/ai-case-studies/gearguide-ai-assistant-for-automotive-industry/>
- WillowTree. (2023). Using LLMs to benchmark retrieval-augmented generation (RAG). Retrieved from <https://www.willowtreeapps.com>

Author(s) Information

Senda Yildirim

Dogus Technology, Maslak Mah. Buyukdere Cad.
No:249/6 Saryer, Istanbul/ Türkiye
Department of Industrial Engineering, Faculty of
Engineering and Natural Sciences, Kadir Has University,
Istanbul, Türkiye
Contact e-mail: sendayildirim@outlook.com

Ruya Samli

Department of Computer Engineering, Faculty of
Engineering, Istanbul University-Cerrahpasa, Istanbul,
Türkiye

To cite this article:

Yildirim, S., & Samli, R. (2025). A RAG-based automotive sector AI assistant for enhanced information retrieval. *The Eurasia Proceedings of Science, Technology, Engineering and Mathematics (EPSTEM)*, 33, 20-27.

The Eurasia Proceedings of Science, Technology, Engineering and Mathematics (EPSTEM), 2025

Volume 33, Pages 28-35

IConTech 2025: International Conference on Technology

The Novelties by Using R Programming Language for Simulate Magnetic Hysteresis Loop

Elena Raducan

“Dunarea de Jos” University of Galati

Simona Moldovanu

“Dunarea de Jos” University of Galati

Ciprian Vlad

"Dunarea de Jos" University of Galati

Abstract: Magnetic materials can be classified as hard and soft, depending on the shape of the hysteresis loop. The hysteresis loop describes the magnetic behaviour of the magnetic materials to which an external magnetic field is applied. The shape of the hysteresis loop can be obtained by drawing point by point the B-H dependency by measuring the induced magnetic flux density (B) and the magnetizing force (H), or by visualization with specific laboratory equipment (usually the oscilloscope). Because of the labouring process of these experiments and due to the little research in the computational methods in this direction, nowadays it is impossible to find data sets with a hysteresis loop that can be further used for automatic classification of the magnetic materials and automatic detection of the magnetic materials application field. This paper aims to create and generate the magnetic hysteresis loop in the R programming language with two different approaches. One model was created with a hysteresis package, and one was created by using a synthetic function cloned with an existing mathematical model for magnetic hysteresis.

Keywords: Magnetic materials, Hysteresis loop, R programming language

Introduction

Although the primary property of magnetic materials—the ability to generate a magnetic field and interact with other external fields—was discovered many centuries ago, William Gilbert was the first to analyze and observe modern magnetism in the latter part of the 1600s, and his experiments were published nearly three centuries later (Gilbert & Wright, 1893).

Researchers have discovered it over the years and have advocated for various uses of magnetic materials as well as alternative chemistry to produce materials with magnetic properties. Warburg's creation of the first iron hysteresis loop in 1880 was one of the most significant breakthroughs (Schmool, 2018). The figure below (Figure 1) shows the phases of permanent magnetic material development and improvement based on capabilities per unit volume of material.

Years of study and experimentation have led to observations on the dependence between B (magnetic induction) and H (magnetic field strength). This dependence is known as the hysteresis loop for magnetic materials, and it simply indicates that a remanent induction (B_r) is present in the material following the annulment of the external magnetic field ($H=0$). The applied field must be reversed and then cancelled once more to end the hysteresis loop. The hysteresis loop for ferromagnetic materials is in Figure 2.

- This is an Open Access article distributed under the terms of the Creative Commons Attribution-Noncommercial 4.0 Unported License, permitting all non-commercial use, distribution, and reproduction in any medium, provided the original work is properly cited.

- Selection and peer-review under responsibility of the Organizing Committee of the Conference

© 2025 Published by ISRES Publishing: www.isres.org

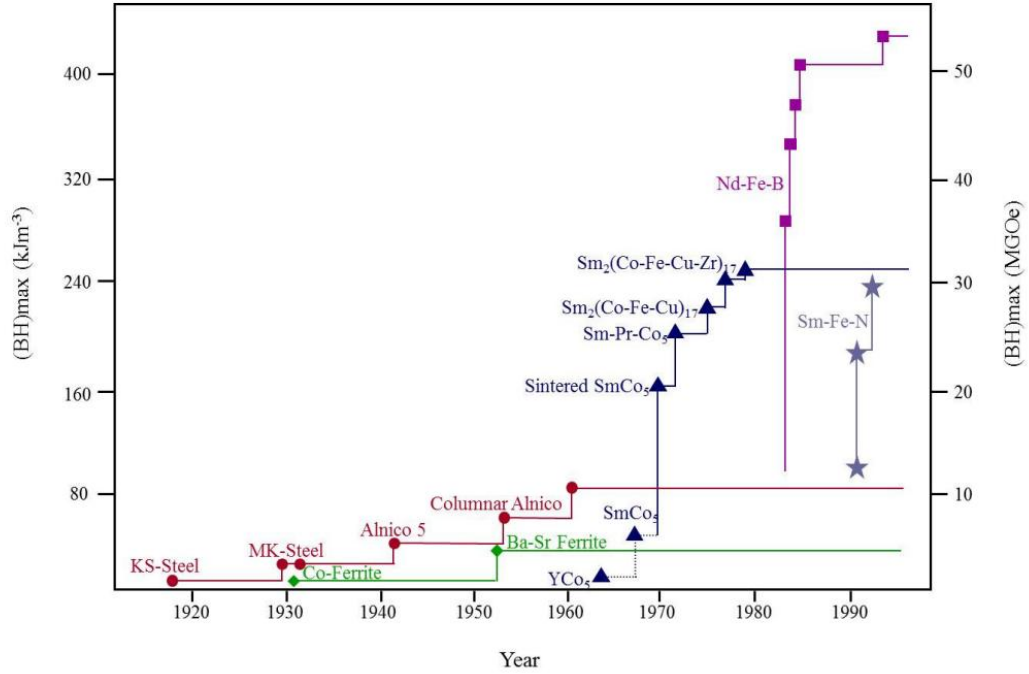


Figure 1. The stages of development and improvement of the permanent magnetic materials between 1920 and 1990 (Coey, 2011)

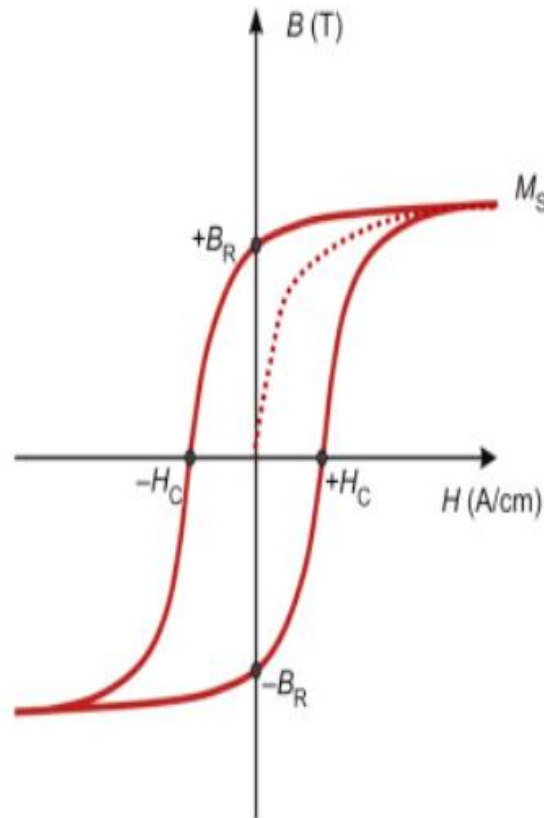
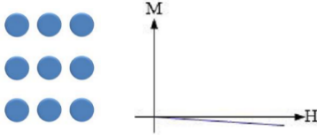
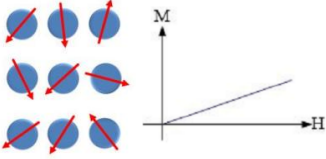
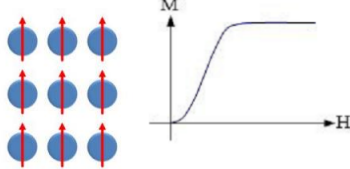
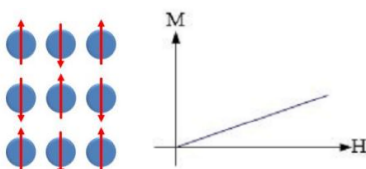
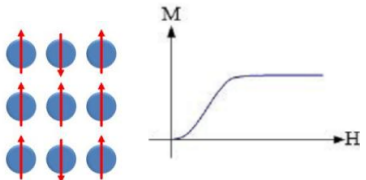


Figure 2. (B, H) dependency for ferromagnetic materials. Histerezis loop (Sieniutycz, 2016)

These three magnetic parameters—saturation magnetisation (M_s), induction remanence (B_r), and coercivity (H_c)—are essential for practically characterising a ferromagnetic material. The magnetic materials were classified into five groups due to their distinct behaviours when exposed to an external magnetic field (different dependencies between M and H). The table below provides a brief description of these groups (Table 1) (Scepka, 2016).

Table 1. Materials classification according to their magnetic susceptibility and atoms magnetic moments

Type	Characteristics for magnetic behavior	Graphics
Diamagnetic materials	Atoms have no magnetic moment. Susceptibility - small and negative	
Paramagnetic materials	Atoms have randomly oriented magnetic moments. Susceptibility- small and positive.	
Ferromagnetic materials	Atoms have parallel aligned magnetic moments. Susceptibility- bigger.	
Antiferromagnetic materials	Atoms have antiparallel aligned magnetic moments. Susceptibility - small and positive.	
Ferrimagnetic materials	Atoms have mixed parallel and antiparallel aligned magnetic moments. Susceptibility -bigger	

The magnetic susceptibility (χ) value and sign indicates the strength of attraction (or not being attracted) of the materials into an external magnetic field. According to their internal magnetism, magnetic materials can be divided in two main categories:

- Hard magnetic materials: magnetism is permanent and are difficult to magnetize and demagnetize into external magnetic field
- Soft magnetic materials: magnetism is temporally and can be easily magnetized and demagnetized into external magnetic field (Prathik, 2024)

The figure below illustrates the (B, H) dependency of the two kinds of magnetic materials (hysteresis loop) as reported by Prathik et al. (2024).

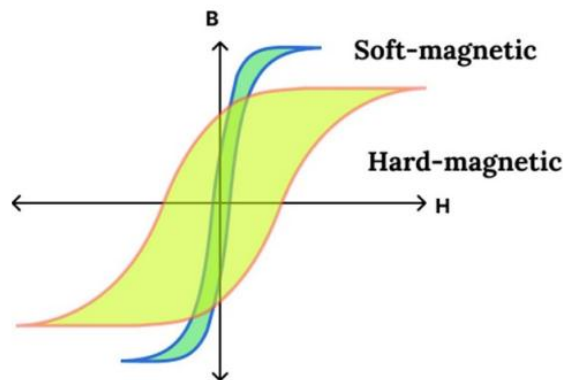


Figure 3. Histerezis loop for hard and soft magnetic materials (Prathik, 2024)

Figure 3 shows that the magnetic hysteresis for hard magnetic materials has a higher coercivity, a smaller saturation of magnetization, and a larger angle of inclination. The inclination angle is smaller for soft magnetic materials, but the saturation and coercivity are larger and smaller, respectively.

Method

The B-H dependency of the magnetic materials that are exposed to an external magnetic field, and several mathematical models have been created over time to simulate behavior. Few models can produce good results when compared to experimental data, but not all of them have been able to accurately simulate the behavior of the complete phenomenon that happens every time a material is exposed to external fields. A brief list of some of the numerous mathematical models is shown here (Morée Gustav, 2023):

- Duhem model
- Coleman-Hodgdon model
- Jiles-Artherton model
- Talukdar-Bailey model
- Flatley-Henretty model, so on.

With the new modern technologies and AI (Artificial Intelligence), the concept included nowadays everywhere, AI algorithms have been implemented to develop new magnetic materials with characteristics requested by advanced applications and equipment. Liccardi et al. (2024) has been developing neural network architecture to model magnetic hysteresis (Liccardi, 2024). According to Liccardi et al. (2024) neural networks are suitable for use to modelling magnetic hysteresis. Liccardi et al. (2024) shown that RNN (Recurrent Neural Network) and CNN (Convolutional Neural Network) models have the capability to predict hysteresis dynamics even in the absence of material information. But, even with this cutting-edge studies, it is impossible to find a data base with hysteresis loops that further can be used for faster classification of magnetics materials. The most used open access datasets as Kaggle, open ML, Sigma AI and Github, are not given datasets with hysteresis loop. In this scope, this paper aim to tackle the programming part that can be used after in generating more hysteresis loops. Two methods are presented for modelling the magnetic hysteresis loop, as follow:

- Using hysteresis package in R programming language
- Creating functions in R programming language that simulate the mathematical model of hysteresis.

Although the R language has been selected for this study, both of these approaches can be effectively implemented in the python programming language as well. A strong tool for statistical programming is the R language. Complex probability issues, linear and logistic regression, ANOVA, time series analysis, multilevel linear and non-linear models, etc., can all be effectively resolved with the R programming language (Long J. D, 2019). Many fields, including economics, physics, engineering, medicine, and more, use the R programming language to solve complex problems. (Field, 2012).

Results and Discussion

1. Hysteresis package in R programming language

Magnetic hysteresis loop occurs because the output variable (magnetization M and inductance B of the material) can have more possible values at the same input value (external magnetic field with the strength H) and depends on the material history (has already being magnetized or not) and on the strength and sign of the applied magnetic field. R programming language has been published in their repository and inserted the new package “Hysteresis” (Maynes, 2021).

The hysteresis package does help to fit, summarize and plot sinusoidal hysteretic processes using two step harmonic least squares. The package fits input and output variables x and y that form a hysteresis loop based on the generalized transcendental equation (Maynes, 2021).

$$x_t = b \cdot x * \cos\left(2\pi \frac{t}{T} + \text{phase.angle}\right) + cx + e_{x,t} \quad (1)$$

$$y_t = b.y * \cos\left(2\pi \frac{t}{T} + \text{phase.angle}\right)^n + \text{retention} * \sin\left(2\pi \frac{t}{T} + \text{phase.angle}\right)^m + cy + e_{y,t} \quad (2)$$

$$t = 0, \dots, n.\text{points} - 1 \text{ times} = \text{'equal'} \quad (3)$$

The functions used and their functionality in the program can be found in the table here below (Table 2).

Table 2. Functions used in hysteresis packhage (S. Maynes, 2021)

Name	Characteristics	Example
mloop	Simulate a hysteresis loop with a variety of possible parameters	<pre>mloop(cx = 0, cy = 0, retention = 0.2, b.x = 0.6, b.y = 0.8, n = 1, m = 1, sd.x = 0, sd.y = 0, phase.angle = 0, n.points = 24, period = 24, extended.classical=FALSE, seed=NULL) mloop2r(cx=0,cy=0,retention.above=0.2,retention.below=0.15,b.x=0.6,b.y=0.8,n=1, m=1,sd.x=0,sd.y=0,phase.angle=0,n.points=24,period=24, extended.classical=FALSE,seed=NULL)</pre>
floop	Fits a hysteresis loop given values of n and m chosen by the user. floop2r fits an asymmetric loop with different values for retention above and below the split line.	<pre>floop(x,y=NULL,n=1,m=1,times="equal",period=NULL, subjects=NULL, subset=NULL,na.action=getOption("na.action"), extended.classical=FALSE,boot=FALSE,method="harmonic2", ...) floop2r(x,y=NULL,n=1,m=1,times="equal",period=NULL, subjects=NULL, subset=NULL,na.action=getOption("na.action"), extended.classical=FALSE,boot=FALSE,method="harmonic2", ...)</pre>
mel	Produces an ellipse based on 1 of 4 possible formulations: 1- Eigenvalues, 2- Hysteresis Coefs, 3- Amplitudes and 4- Algebraic Coefs.	<pre>mel(method=1,seed=NULL,...) mel1(cx=32,cy=39,rote.deg=2,semi.major=7,semi.minor=0.23, phase.angle=0,n.points=24,period=24,sd.x=0,sd.y=0) mel2(cx=32,cy=39,b.x=6.99,b.y=0.244,retention=0.23, phase.angle=0,n.points=24,period=24,sd.x=0,sd.y=0) mel3(cx=32,cy=39,ampx=6.99,ampy=0.335,lag=2.888,phase.angle=0, n.points=24,period=24,sd.x=0,sd.y=0) mel4(x2=0.002293,xy=-.06960,y2=0.9976,x=2.567,y=-75.58,int=1432.7, phase.angle=0,n.points=24,period=24,sd.x=0,sd.y=0)</pre>
fel	Fit a sinusoidal hysteretic (elliptical) process between an input and an output.	<pre>fel(x, y=NULL, method = "harmonic2", period = NULL, subjects = NULL, times="unknown",subset = NULL,na.action= getOption("na.action"), control=nls.control(), boot=FALSE,...)</pre>
summary.fittedloop	Summary methods for classes ellipsefit and fittedloop created by the functions fel and floop. Can bootstrap results to produce parameter estimates with reduced bias and standard errors.	<pre>## S3 method for class 'ellipsefit' summary(object,boot=TRUE, N = 1000, studentize=TRUE, center=FALSE, cbb=NULL, joint=FALSE,seed=NULL,...) ## S3 method for class 'fittedloop' summary(object,boot=TRUE,N=1000, cbb=NULL,joint=FALSE,seed=NULL,...) ## S3 method for class 'loop2r' summary(object,boot=TRUE,N=1000, cbb=NULL,joint=FALSE,seed=NULL,...)</pre>

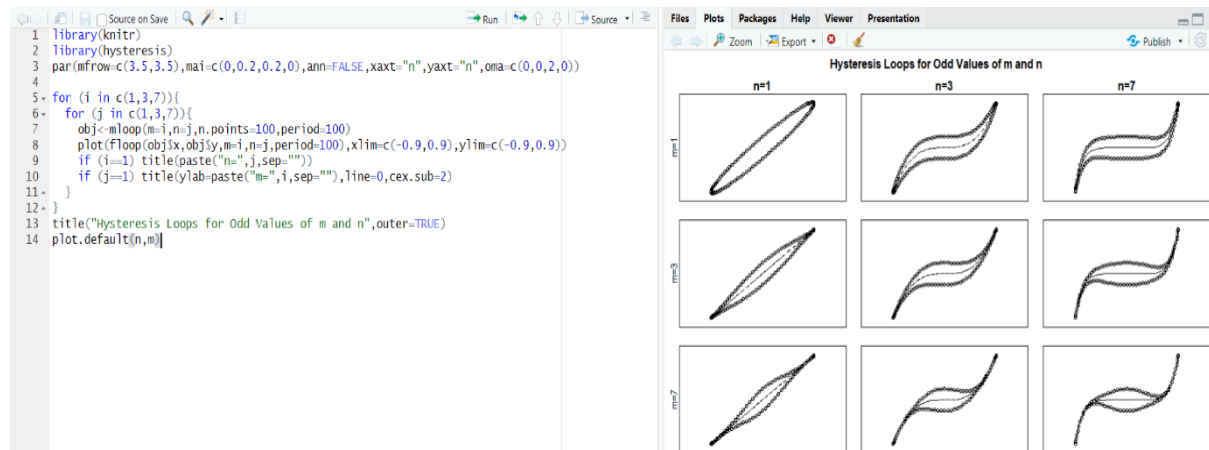


Figure 4. Hysteresis loop for odd values for n and m

The results of plotting the hysteresis loop with the help of “hysteresis” packadge from the R, can be found in the figure here above (Figure 4)

For fitting the hysteresis loop it will be used the next sequence of the code:

```
15 loop <- mloop(n=3, m=5,sd.x=0.05,sd.y=0.1)
```

```
16 fitloop <- floop(loop$x,loop$y,n=3, m=5,period=25,times="equal")
```

```
17 plot(fitloop,main="Fitted Hysteresis Loop")''
```

The results can be seen in the figure here below (Figure 5):

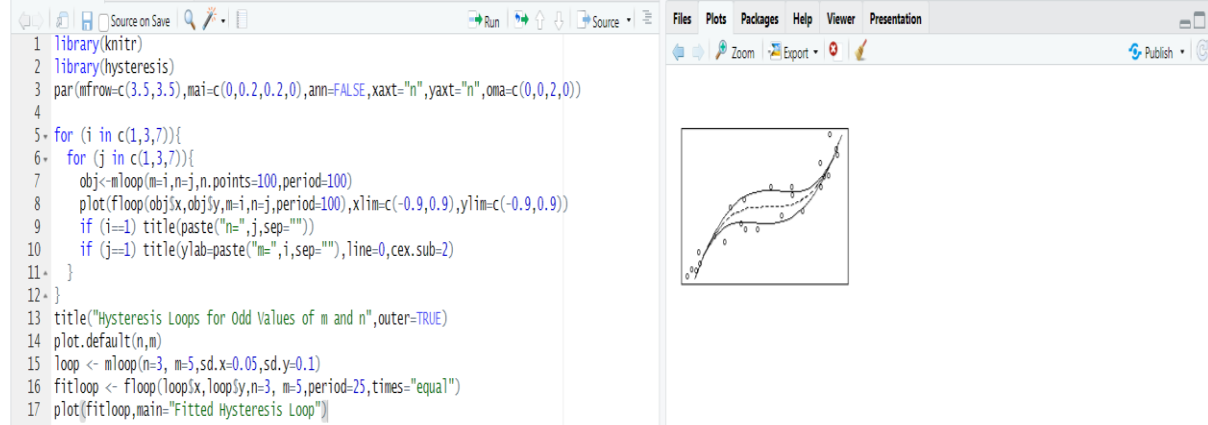
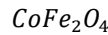


Figure 5. Fitted hysteresis loop

2. Mathematical model of hysteresis implemented in R programming languages

As mentioned previously in Method chapter, many mathematical models were developed to simulate hysteresis loops. For this study it was used as a mathematical model proposed by Pop (2019) in the scientific paper “A model for magnetic hysteresis” (Pop, 2019). In the mathematical models for magnetic hysteresis proposed in this paper, it was successfully prove that equation (4) for the cobalt ferite sample simulate with high accuracy the magnetic hysteresis for this material



(Pop, 2019).

$$M_i = \frac{M_s}{2} \left(\frac{H_e + H_c}{\sqrt{H_e^2 + H_a^2 + 2H_e H_c}} + \frac{H_e - H_c}{\sqrt{H_e^2 + H_a^2 - 2H_e H_c}} \right) \quad (4)$$

$$H_e = H + \alpha'_0 M$$

The data used for this simulation are given in the next table (Table 3)

Table 3. Data used in the R language simulation for magnetic hysteresis for the cobalt ferite materials (Pop, 2019)

Parameter	Meaning	Value
Ms(A/m)	Saturation magnetization	420000
Mr(A/m)	Remanent magnetization	201700
Hc(A/m)	Coercivity	20200
Ha(A/m)	Fictional magnetic field	188700
α'_0	Fitting coefficient	0.478

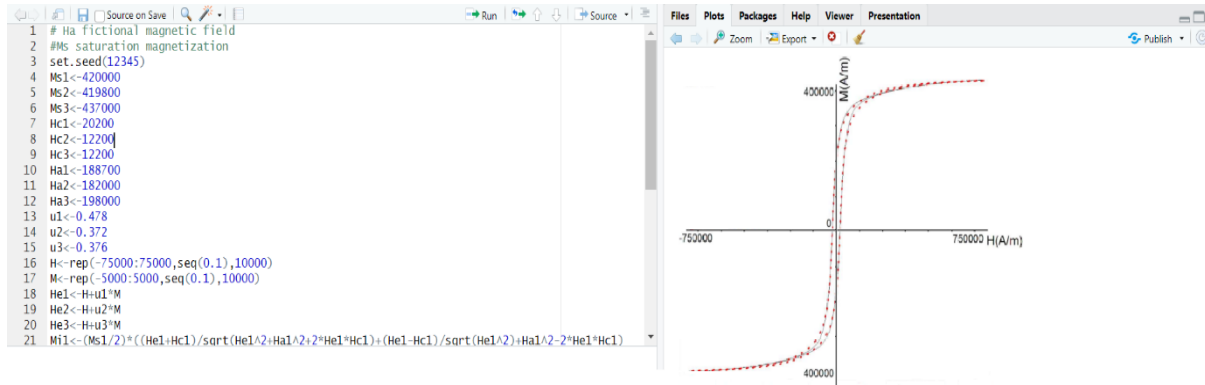


Figure 6. Magnetic hysteresis for cobalt ferite materials by using syntetic function as per eq. (4) and the values from Table 3 in R programming language

Conclusion

Because of the complexity of the physical phenomenon that occurs every time when a magnetic material is supposed to be an external magnetic field, the research to find the best solution to simulate this behavior is still of high interest for the researchers in this domain. Also, the high competences in programming language does not guarantee the disclosure of a general of a model for magnetic hysteresis general valid for all types of materials. With the use of the R programming language, it was accomplished in generation magnetic hysteresis loops from two different approaches. Firs one by using the R package “hysteresis” and the second by using the mathematical model developed with synthetic physical functions for cobalt ferrite materials. Further research aims to develop a generative R programming language for the two types of magnetic materials (hard and soft) for better and faster classification. For this a large amount of laboratory measurement data will be needed.

Scientific Ethics Declaration

The authors declare that the scientific ethical and legal responsibility of this article published in EPSTEM Journal belongs to the authors.

Conflict of Interest

The authors declare that they have no conflicts of interest

Funding

This study received no external funding.

Acknowledgements or Notes

This article was presented as a poster presentation at the International Conference on Technology (www.icontechno.net) held in Trabzon/Türkiye on May 01-04, 2025.

References

- Coey, J. M. D. (2011). Hard magnetic materials: A perspective. *IEEE Transactions on Magnetics* 47(12), 4671-4681.
- Filed, A., Miles, J., & Field, Z. (2012), *Discovering statistics using R*. Sage Publication.
- Gilbert, W., Wright, E., & Mottelay, P. F. (1893). *On the loadstone and magnetic bodies and on the great magnet the earth*. New York, NY: Wiley & Sons.

- Liccardi, S., Ala, G., Francomano, E., ...& Viola, F. (2024), Neural network architectures and magnetic hysteresis: Overview and comparisons. *Mathematics*, 12(21),3363.
- Long, J. D., & Teetor, P. (2019). *R cookbook* (2nd ed.). O'Reilly Publication.
- Mayne, S., Yang F., & Parkhurst, A. (2021). *Package 'hysteresis*. Retrieved from <http://r.meteo.uni.wroc.pl/web/packages/hysteresis/hysteresis.pdf>
- Morée G., & Leijon M. (2023). Review of hysteresis models for magnetic materials. *Energies*, 16(9),3908.
- Pop, N. C. (2019). A model for magnetic hysteresis, *The European Physical Journal Plus*,134(11),567.
- Prathik, N., Ratnadeep, P., & Arockiarajan, A. (2024). Hard magnetism and soft materials—a synergy. *Smart Material Structures*, 33, 043001.
- Schmool, D. S., & Markó, D. (2018). Magnetism in solids: Hysteresis. In *Reference module in materials science and materials engineering*. Elsevier.
- Ščepka, T. (2016), *Noninvasive control of magnetic state in ferromagnetic nanodots by Hall probe magnetometry*. (Doctoral dissertation, Institute of Electrical Engineering).
- Stanisław, S. (2016). *Thermodynamic approaches in engineering systems, contemporary thermodynamics for engineering systems*. Elsevier Inc.

Authors Information

Elena Raducan

"Dunarea de Jos" University of Galati, Faculty of Automatic Control, Computers, Electrical Engineering and Electronics, Electrical Engineering and Energy Conversion Systems Department, Str. Domnească nr. 111, Galați - 800201, Romania
Contact e-mail: elena.raducan@ugal.ro

Simona Moldovanu

"Dunarea de Jos" University of Galati, Faculty of Automatic Control, Computers, Electrical Engineering and Electronics, Computer science Department, Str. Domnească nr. 111, Galați - 800201, Romania

Ciprian Vlad

"Dunarea de Jos" University of Galati, Faculty of Automatic Control, Computers, Electrical Engineering and Electronics, Electrical Engineering and Energy Conversion Systems Department, Str. Domnească nr. 111, Galați - 800201, Romania

To cite this article:

Raducan, E., Moldovanu, S., & Vlad, C. (2025). The novelties by using R programming language for simulate magnetic hysteresis loop. *The Eurasia Proceedings of Science, Technology, Engineering and Mathematics (EPSTEM)*, 33, 28-35.

The Eurasia Proceedings of Science, Technology, Engineering and Mathematics (EPSTEM), 2025

Volume 33, Pages 36-44

IConTech 2025: International Conference on Technology

Enhancing OCTA Image Classification Using Superpixel-Derived Geometric and Texture Features

Stefan Miron

University Dunarea de Jos of Galati

Mihaela Miron

University Dunarea de Jos of Galati

Simona Moldovanu

University Dunarea de Jos of Galati

Marian Barbu

University Dunarea de Jos of Galati

Abstract: Optical Coherence Tomography Angiography (OCTA) is an important imaging technique for diagnosing and monitoring retinal diseases. However, the accurate classification of OCTA images remains challenging due to the complexity of vascular structures and imaging variability. This study introduces a novel approach that enhances OCTA image classification for Diabetic Retinopathy (DR) and Myopia by leveraging superpixel-derived geometric and texture features (Mean Intensity, Area, Perimeter, Compactness, Eccentricity, Contrast and Entropy). The proposed method is evaluated using the FAZID dataset, which contains 304 Superficial Vascular Plexus (SVP) OCTA images classified into Diabetic (107), Myopic (109) and Normal (88) cases. Six machine learning models—Decision Tree, Random Forest, XGBoost, Extra Trees, LightGBM and CatBoost—were tested to assess classification performance. Experimental results indicate that boosting-based classifiers, such as XGBoost, LightGBM and CatBoost, achieved 100% classification performance in terms of accuracy, precision, recall, F1-score and MCC. Among bagging classifiers, Random Forest achieved 95.56% accuracy, 95.67% precision, 95.37% recall, 95.50% F1-score and 93.32% MCC, while Extra Trees obtained 95.84% accuracy, 96.08% precision, 95.58% recall, 95.77% F1-score and 93.76% MCC. Additionally, the Decision Tree classifier achieved 100% accuracy across all metrics. This study highlights the impact of superpixel-based feature representation combined with machine learning techniques, offering a robust solution for automated OCTA image analysis in ophthalmology.

Keywords: Machine learning, Superpixels, Optical coherence tomography angiography

Introduction

Diabetic Retinopathy (DR) and Myopia are two of the most prevalent ocular conditions affecting vision worldwide. DR is a microvascular complication of diabetes that damages the blood vessels in the retina and remains a leading cause of preventable blindness among working-age adults (Cheung et al., 2010; Gandhi et al., 2024). Myopia, on the other hand, is a common refractive error characterized by difficulty seeing distant objects clearly. Its prevalence has increased dramatically in recent decades, particularly in East and Southeast Asia, with global projections suggesting that nearly 50% of the world's population will be myopic by 2050 (Holden et al., 2016).

Optical Coherence Tomography Angiography is an advanced, non-invasive imaging technique in ophthalmology that combines the principles of low-coherence interferometry and motion contrast to produce high-resolution, depth-resolved maps of the retinal and choroidal vasculature (Spaide et al., 2018). This technology allows for detailed visualization of ocular blood flow without the need for dye injection, making it a valuable tool for early detection and monitoring of vascular-related eye diseases. These capabilities make OCTA particularly valuable for detecting and monitoring vascular abnormalities associated with conditions such as diabetic retinopathy, myopic maculopathy and age-related macular degeneration. As technology continues to advance, ongoing improvements in acquisition speed, image quality and the integration of artificial intelligence are set to further enhance the clinical utility and automation of OCTA.

Among the various biomarkers observable through OCTA, the Foveal Avascular Zone (FAZ) is important due to its sensitivity to microvascular changes in retinal disease. The FAZ is a capillary-free region at the center of the macula and its morphology, especially area, perimeter and circularity can reflect the severity of retinal ischemia. In patients with diabetic retinopathy, FAZ enlargement and irregularity have been strongly associated with capillary dropout and visual impairment (Verveka et al., 2015). Similarly, high myopia has been linked to FAZ alterations, often due to retinal thinning and chorioretinal atrophy, which can compromise macular perfusion. OCTA enables precise, layer-specific measurement of the FAZ in both the superficial and deep capillary plexuses, facilitating early diagnosis and longitudinal monitoring of these conditions.

Artificial Intelligence (AI), particularly Machine Learning (ML) and Deep Learning (DL) algorithms, has demonstrated significant potential in enhancing OCTA image classification (Totolici et al., 2024; Wang et al., 2024). The integration of AI in OCTA classification has the potential to identify subtle patterns that may be overlooked by human observers. But despite these advancements, challenges remain. One major concern is the quality and variability of training datasets. OCTA images are sensitive to motion artifacts, segmentation errors and device-specific variations.

In this context, we proposed a ML-based approach for OCTA image classification of DR and Myopia. By fusing superpixel-derived geometric and texture features, we demonstrated that a classification accuracy of 100% can be achieved. The robustness of the proposed approach was validated through the evaluation of six ML algorithms on the FAZID dataset. The paper is organized as follows: The Introduction presents the research context and objectives. The Related Work section reviews relevant literature. The Materials and Methods section details the proposed ML-based framework, including preprocessing steps, the extraction of Superpixel-Derived Geometric and Texture Features and the six machine learning classifiers. The Results and Discussion section presents and analyzes the findings, followed by the Conclusion, which summarizes the key contributions of the study.

Related Work

Machine learning has seen increasing application in ophthalmology, particularly for the analysis of retinal images such as those obtained through OCTA, due to its ability to extract complex patterns and support diagnostic decision-making. Previous research has explored a variety of ML and DL techniques aimed to automate the detection and classification of retinal diseases such as DR, age-related macular degeneration (AMD) and Myopia (Erickson et al., 2017; Meiburger et al., 2021).

For example, Alam et al. (2020) applied transfer learning (TF) using a convolutional neural network (CNN) to classify OCTA images into three categories: healthy, no DR and non-proliferative DR (NPDR). The model achieved an overall accuracy of 87.27%, highlighting the effectiveness of DL, particularly when adapted through TF, in handling complex classification tasks despite limited medical imaging datasets.

Dhodapkar et al. (2022) developed DL-based models to assess the quality of OCTA images, reporting exceptional area under the curve (AUC) values of 0.99 for low-quality and 0.97 for high-quality images. These models significantly outperformed traditional signal strength metrics, demonstrating the potential of ML in improving OCTA image quality control.

Also, the extraction of specific features from OCTA images has proven especially valuable, offering quantitative insights into retinal microvascular health. In this direction, Gao et al. (2023) extracted fractal dimension (FD) and five texture features (contrast, correlation, entropy, energy and homogeneity) from the parafoveal region of OCTA images. Their study demonstrated that these quantitative markers can further facilitate the early detection of DR by capturing the complexity and heterogeneity of the retinal microvasculature.

In addition, Ebrahimi et al. (2023) explored layer fusion strategies in CNN-based classification of OCTA images into control, NoDR and NPDR groups. Among single-layer inputs, the superficial capillary plexus (SCP) produced the best performance, with an accuracy of 87.25%, sensitivity of 78.26% and specificity of 90.10%. However, the intermediate-fusion model achieved the highest overall performance of 92.65% accuracy, 87.01% sensitivity and 94.37% specificity.

Another study, Li et al. (2024) applied ML techniques to classify DR severity by combining clinical data with OCTA features. The study included data from 203 diabetic patients for model development and 169 patients for external validation. Among the models, the RF classifier using both OCTA and clinical data achieved the best performance, with area under the curve (AUC) values of 0.942 for DR, 0.932 for referable DR (RDR) and 0.901 for vision-threatening DR (VTDR) in the internal validation set. In the external validation cohort, the RF model obtained high performance with AUCs of 0.928 (DR), 0.914 (RDR) and 0.884 (VTDR). The most influential predictors included vessel density, retinal thickness, ganglion cell complex thickness as well as body mass index, waist-to-hip ratio and glucose-lowering treatments. These results demonstrate the potential of integrating OCTA features with clinical data for robust and accurate DR screening and staging.

More recently, Thrasher et al. (2025) investigated the use of active learning (AL) techniques to improve retinal disease classification from OCTA images, specifically addressing the limitations posed by insufficient labeled data. Their strategy involved selecting the most informative samples for training a DL model, resulting in more efficient learning and enhanced generalization. The AL approach significantly outperformed traditional methods such as random sampling and class rebalancing, achieving up to a 49% improvement in F1 score. This demonstrates the potential of AL to boost diagnostic accuracy while reducing annotation costs in ophthalmic AI applications.

Finally, Abini et al. (2025) introduced a novel deep learning approach for classifying DR using OCTA images. The model features a custom CNN architecture specifically optimized to capture fine-grained vascular features in OCTA scans, enhancing its ability to detect early microvascular abnormalities associated with DR. The proposed method achieved impressive results, with an accuracy of 97.3%, sensitivity of 96.5%, specificity of 98.1% and an AUC of 0.982, demonstrating both robustness and strong potential for clinical deployment.

These recent innovations, such as texture optimization, layer fusion, clinical feature integration and training efficiency strategies, demonstrate the transformative impact of ML and DL in enhancing the accuracy, performance and clinical relevance of OCTA-based retinal diagnostics.

Materials and Methods

This study is focused on a ML-based framework (Figure 1) for the classification of ischemic alterations such as DR and Myopia within FAZ, using features derived from OCTA images. This represents a pipeline for the classification of OCTA images into three diagnostic categories: Diabetic Retinopathy, Myopia and Normal. First, the OCTA images are loaded and preprocessed by cropping and removing text artifacts which are not relevant and can reduce the model accuracy. Next, the Simple Linear Iterative Clustering (SLIC) superpixel segmentation is applied, followed by the extraction of a comprehensive set of superpixel-based features, including mean intensity, geometric descriptors (area, perimeter, compactness, eccentricity) and statistical texture metrics (contrast and entropy). These features quantitatively characterize the structure and complexity of the FAZ and surrounding vasculature. These are further used to evaluate six MLs: tree-based algorithms (Decision Tree - DT, Random Forest - RF and Extra Trees - ET) and gradient boosting methods (XGBoost, LightGBM and CatBoost). From all the evaluated classifiers, DT and gradient boosting algorithms (XGBoost, LightGBM and CatBoost) achieved perfect classification performance, demonstrating their effectiveness in differentiating between the studied pathologies. The proposed framework shows strong potential for the automated, non-invasive evaluation of retinal vascular health, supporting clinical decision-making in the diagnosis and monitoring of ischemic retinal diseases.

Dataset

In this study, we used the FAZID publicly available dataset (Agarwal et al., 2020). The dataset (Figure 2) contains high-resolution en face OCTA images focused on the superficial vascular plexus (SVP). It has 304 retinal scans, grouped into three clinical categories: 107 diabetic, 109 myopic and 88 normal eyes. Each image captures a 6 mm × 6 mm retinal region, standardized to 420 × 420 pixels. Each image is annotated with a disease label and includes

a manually segmented FAZ region, serving as ground truth for morphological analysis. The annotations were performed by experienced clinicians following standardized protocols.

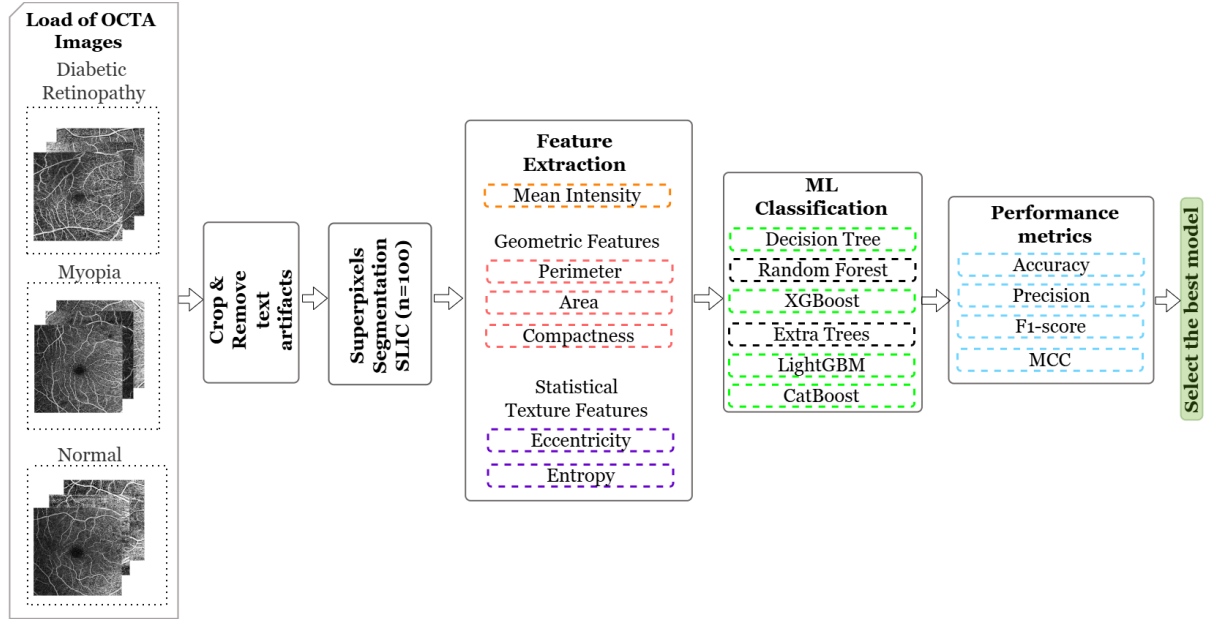


Figure 1. The ML-based framework for superpixel-derived geometric and texture features

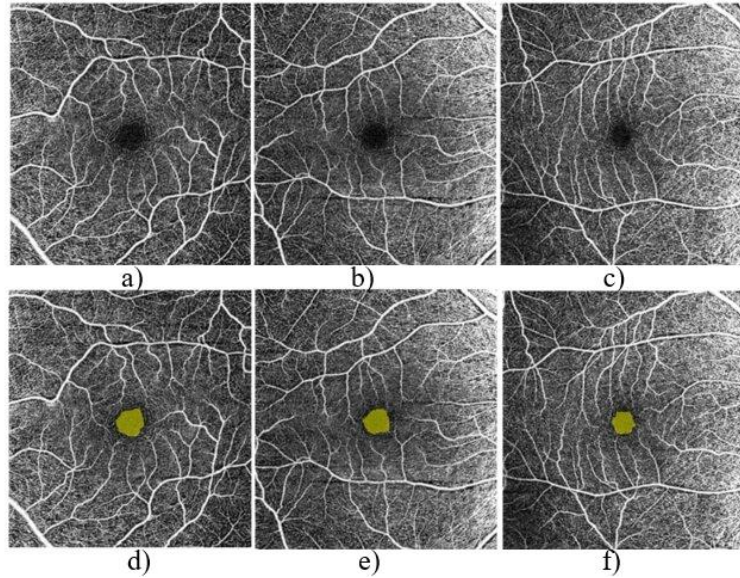


Figure 2. FAZ images: a) Non marked diabetic b) Non marked myopic c) Non marked normal d) Manually marked diabetic e) Manually marked myopic and f) Manually marked normal (Agarwal et al., 2020)

Superpixel-Derived Geometric and Texture Features

To extract regional geometric and texture descriptors from retinal images, superpixel segmentation was performed using the SLIC algorithm (Achanta et al., 2012). The input image was first converted to grayscale to facilitate intensity-based analysis. SLIC segmentation was applied with 100 target superpixels, a compactness value of 20 and a Gaussian smoothing parameter (σ) of 1, generating a spatially coherent and perceptually uniform superpixels.

In Figure 3 is an example of SLIC superpixel segmentation applied to an OCTA image. Red contours indicate the segmented superpixels, highlighting regions of interest (ROIs) used for geometric and texture feature extraction. For each segmented region, a binary mask was generated and analysed using the regionprops function from the Python scikit-image library. The Mean intensity (μ) and the following geometric features were extracted for each

superpixel: Area (A), Perimeter (P), Compactness (C) and Eccentricity (E) (Gonzales et al., 2018). Also, texture features were quantified using the Gray-Level Co-occurrence Matrix (GLCM) (Haralick et al., 1973). For each superpixel, GLCM was computed at 1 pixel and angle of 0° , from which the following features were generated: Contrast (c) and Entropy (e). The extracted features were added to a new CSV format dataset.

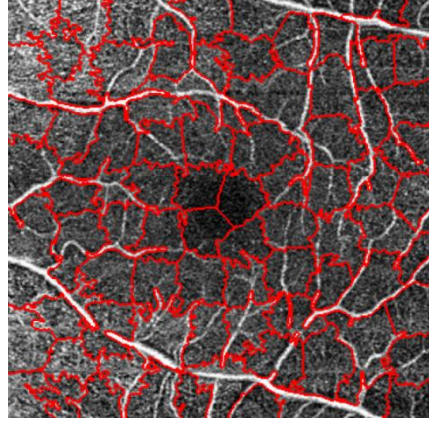


Figure 3. Example of SLIC superpixel segmentation applied to an OCTA image

The mathematical formulas of the features extracted are:

$$\mu = \frac{1}{|R|} \sum_{(x,y) \in R} I(x,y) \quad (1)$$

where $I(x, y)$ is the grayscale intensity at pixel location (x, y) and $|R|$ is the number of pixels in region R .

$$A = |R| \quad (2)$$

where A is the total number of pixels within the superpixel region R .

$$C = \frac{P^2}{4\pi A} \quad (3)$$

where P is the perimeter and A is the area.

$$E = \sqrt{1 - \left(\frac{b}{a}\right)^2} \quad (4)$$

where a is the length of the semi-major axis of the best-fitting ellipse to the region and b is the length of the semi-minor axis of the ellipse.

$$c = \sum_{i=0}^{N-1} \sum_{j=0}^{N-1} (i-j)^2 P(i,j) \quad (5)$$

where $P(i, j)$ is the probability of two neighboring pixels having gray levels i and j , based on the GLCM; N is the number of gray levels in the image and $(i-j)^2$ gives greater weight to larger intensity differences.

$$e = \sum_{i=0}^{N-1} \sum_{j=0}^{N-1} P(i,j) \log_2(P(i,j) + \delta) \quad (6)$$

where $P(i, j)$ is the normalized value of the GLCM at row i and column j , representing the probability of pixel intensity pair (i, j) ; N is the number of gray levels used in the GLCM and δ is a small constant added to avoid computing $\log(0)$.

Machine Learning Models

Several ML have been used for classifying the Superpixel-Derived Geometric and Texture Features into Normal, Diabetic and Myopic. For this purpose, six classifiers were selected: Decision Tree, Random Forest, XGBoost, Extra Trees, LightGBM and CatBoost. These were applied because they are well-suited for handling structured data like superpixel-derived features from OCTA images. DT is easy to interpret; RF and ET improve stability and reduce overfitting through ensembling. XGBoost, LightGBM and CatBoost are advanced gradient boosting algorithms known for their high accuracy, speed and ability to capture complex patterns (Erickson et al., 2017).

The dataset of Superpixel-Derived Geometric and Texture Features was split into training and testing sets using an 80/20 stratified split to preserve class distribution. The ML were trained using default or common hyperparameters, such as 100 estimators for ensemble models and a fixed random seed (42) for reproducibility. XGBoost and CatBoost were configured with `eval_metric='mlogloss'` and `iterations=100`, respectively, while verbosity was suppressed for CatBoost. Model performance was evaluated using multiple metrics: accuracy, precision, recall, F1-score and MCC (Sokolova et al., 2009; Chicco et al., 2020). Additionally, confusion matrices were computed along with true positives (TP), false positives (FP), false negatives (FN) and true negatives (TN), providing further insight into classification behavior.

The ML-based framework was implemented in Google Colab using the default runtime with Python 3.10.12, ensuring a consistent and reproducible environment. It used Pandas and NumPy for data handling, Matplotlib and Seaborn for visualization and Scikit-learn for the machine learning tasks. Gradient boosting was performed using XGBoost, LightGBM and CatBoost. For image segmentation and feature extraction, the framework applies OpenCV for image processing and skimage for advanced operations, including superpixel segmentation, region analysis, texture feature extraction and image reading.

Results and Discussion

In this section are presented the results obtained with the ML-based framework, which evaluated superpixel-derived geometric and texture features for classifying retinal OCTA images into three categories: Normal (class 0), Diabetic (class 1), and Myopic (class 2). In Tables 1 are presented the performance evaluation of the six MLs (Decision Tree, Random Forest, XGBoost, Extra Trees, LightGBM, and CatBoost) with the superpixel-derived texture and geometric features. The results indicate that XGBoost, LightGBM and CatBoost achieved perfect scores (100%) across all metrics, including accuracy, precision, recall, F1 score and MCC. These models also showed zero false positives (FP) and false negatives (FN). In contrast, Random Forest and Extra Trees models, while still performing well, obtained slightly lower metrics. RF achieved an accuracy of 95.56%, with a relatively higher number of FP (227) and FN (227), influencing its recall (95.37%) and MCC (93.32%). ET performed better than RF, with an accuracy of 95.84% and more balanced precision (96.08%), recall (95.58%), F1-score (95.77%), MCC (93.76%) and with FP and FN of 213.

Table 1. The performance evaluation of MLs on superpixel-derived texture and geometric features

MLs	Acc.	Precision	Recall	F1 score	MCC	TN	FP	FN	TP
Decision Tree	1.0000	1.0000	1.0000	1.0000	1.0000	10242	0	0	5121
Random Forest	0.9556	0.9567	0.9537	0.9550	0.9332	10015	227	227	4894
XGBoost	1.0000	1.0000	1.0000	1.0000	1.0000	10242	0	0	5121
Extra Trees	0.9584	0.9608	0.9558	0.9577	0.9376	10029	213	213	4908
LightGBM	1.0000	1.0000	1.0000	1.0000	1.0000	10242	0	0	5121
CatBoost	1.0000	1.0000	1.0000	1.0000	1.0000	10242	0	0	5121

Figure 4 shows the confusion matrices for the six ML. Each matrix visualizes the number of true versus predicted labels for each class, providing insight into each model's classification accuracy and misclassification patterns. In case of RF, are observed some misclassifications, particularly between class 0 (Normal) and class 1 (Diabetic), and between class 0 and class 2 (Myopic). While overall performance is high, this model occasionally confuses diabetic and myopic cases with normal ones. Also, ET model shows a noticeable number of misclassifications in all three classes. Most errors are in class 0 being confused with class 1 and class 2, and vice versa. These results align with the performance metrics (accuracy, F1-score, MCC), which confirm that boosting algorithms are highly effective for classifying ischemic changes in the FAZ using superpixel-derived texture and geometric features.

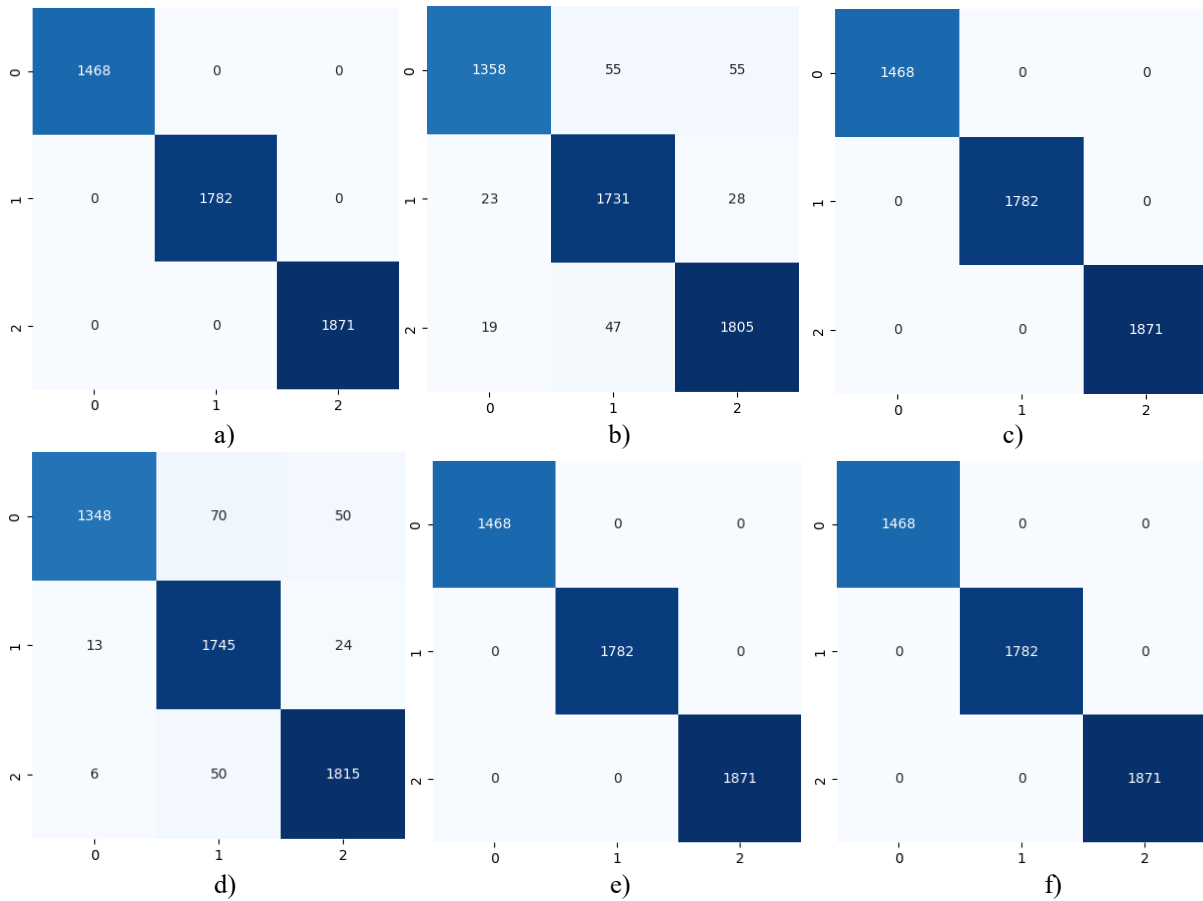


Figure 4. The confusion matrices for the six MLs: (a) DT; (b) RF; (c) XGBoost; (d) ET; (e) LightGBM; and (f) CatBoost.

Conclusion

This study demonstrated the effectiveness of machine learning models in classifying retinal conditions (Normal, Diabetic and Myopic) based on Superpixel-Derived Geometric and Texture Features extracted from OCTA images. A total of six ML classifiers, including DT, RF, ET, XGBoost, LightGBM and CatBoost, were evaluated using stratified training and testing splits. The models were assessed using the performance metrics such as accuracy, precision, recall, F1-score and MCC, providing a comprehensive evaluation of classification performance.

Among the evaluated models, DT, XGBoost, LightGBM and CatBoost achieved high accuracy (100%) and generalization, indicating their suitability for retinal image analysis. The integration of superpixel-based features with robust ML algorithms offers a promising approach for automated retinal disease screening and clinical decision support. Future work may include expanding the dataset, incorporating additional imaging features or biomarkers and exploring deep learning architectures to further enhance diagnostic accuracy and scalability.

Scientific Ethics Declaration

* The authors declare that the scientific ethical and legal responsibility of this article published in EPSTEM Journal belongs to the authors.

Conflict of Interest

* The authors declare that they have no conflicts of interest

Funding

This study received no external funding.

Acknowledgements or Notes

* This article was presented as an oral presentation at the International Conference on Technology (www.icontechno.net) held in Trabzon/Türkiye on May 01-04, 2025.

References

- Abini, A. M., & Priya, S. S. S. (2025). A novel deep learning approach for diabetic retinopathy classification using optical coherence tomography angiography. *Multimedia Tools and Applications*, 1-39.
- Achant, R., Shaji, A., Smith, K., Lucchi, A., Fua, P., & Süsstrunk, S. (2012). SLIC superpixels compared to state-of-the-art superpixel methods. *IEEE Transactions on Pattern Analysis and Machine Intelligence*, 34(11), 2274–2282.
- Agarwal, A., Balaji, J. J., Raman, R., & Lakshminarayanan, V. (2020). The foveal avascular zone image database (FAZID). In *Applications of Digital Image Processing XLIII* (Vol. 11510, p.1151027). SPIE.
- Alam, M., Le, D., Son, T., Lim, J. I., & Yao, X. (2020). AV-Net: Deep learning for fully automated artery-vein classification in optical coherence tomography angiography. *Biomedical Optics Express*, 11(10), 5249–5257.
- Cheung, N., Mitchell, P., & Wong, T. Y. (2010). Diabetic retinopathy. *The Lancet*, 376(9735), 124–136.
- Chicco, D., & Jurman, G. (2020). The advantages of the Matthews correlation coefficient (MCC) over F1 score and accuracy in binary classification evaluation. *BMC Genomics*, 21(1), 6.
- Dhodapkar, R. M., Li, E., Nwanyanwu, K., Rezaei, K. A., & Gill, M. K. (2022). Deep learning for quality assessment of optical coherence tomography angiography images. *Scientific Reports*, 12, 13775.
- Ebrahimi, B., Le, D., Abtahi, M., Dadzie, A. K., Lim, J. I., Chan, R. V. P., & Yao, X. (2023). Optimizing the OCTA layer fusion option for deep learning classification of diabetic retinopathy. *Biomedical Optics Express*, 14(9), 4713–4724.
- Erickson, B. J., Korfiatis, P., Akkus, Z., & Kline, T. L. (2017). Machine learning for medical imaging. *Radiographics*, 37(2), 505–515.
- Gandhi, S., Pattathil, N., & Choudhry, N. (2024). OCTA: Essential or gimmick? *Ophthalmology and Therapy*, 13, 2293–2302.
- Gao, W., Lin, P., Li, B., Shi, Y., Chen, S., Ruan, Y., Zakharov, V. P., & Bratchenko, I. (2023). Quantitative assessment of textural features in the early detection of diabetic retinopathy with optical coherence tomography angiography. *Photodiagnosis and Photodynamic Therapy*, 41, 103214.
- Gonzalez, R. C., & Woods, R. E. (2018). *Digital image processing* (4th ed.). Pearson.
- Haralick, R. M., Shanmugam, K., & Dinstein, I. (1973). Textural features for image classification. *IEEE Transactions on Systems, Man, and Cybernetics*, SMC-3(6), 610–621.
- Holden, B. A., Fricke, T. R., Wilson, D. A., Jong, M., Naidoo, K. S., Sankaridurg, P., Wong, T. Y., Naduvilath, T. J., & Resnikoff, S. (2016). Global prevalence of myopia and high myopia and temporal trends from 2000 through 2050. *Ophthalmology*, 123(5), 1036–1042.
- Li, X., Wen, X., Shang, X., Liu, J., Zhang, L., Cui, Y., Luo, X., Zhang, G., Xie, J., Huang, T., Chen, Z., Lyu, Z., Wu, X., Lan, Y., & Meng, Q. (2024). Identification of diabetic retinopathy classification using machine learning algorithms on clinical data and optical coherence tomography angiography. *Eye*, 38(14), 2813–2821.
- Meiburger, K. M., Salvi, M., Rotunno, G., Drexler, W., & Liu, M. (2021). Automatic segmentation and classification methods using optical coherence tomography angiography (OCTA): A review and handbook. *Applied Sciences*, 11(20), 9734.
- Spaide, R. F., Fujimoto, J. G., Waheed, N. K., Sadda, S. R., & Staurengi, G. (2018). Optical coherence tomography angiography. *Progress in Retinal and Eye Research*, 64, 1–55.
- Sokolova, M., & Lapalme, G. (2009). A systematic analysis of performance measures for classification tasks. *Information Processing & Management*, 45(4), 427–437.
- Thrasher, J., Amireskandari, A., & Gyawali, P. (2025). Enhancing retinal disease classification from OCTA images via active learning techniques. In B. Bhattarai, A. R. Joshi, & R. Garnavi (Eds.), *Data engineering in medical imaging: DEMI 2024* (Lecture Notes in Computer Science, Vol. 15265). Springer.
- Totolici, G., Miron, M., & Culea-Florescu, A.-L. (2024). Automatic segmentation and statistical analysis of the foveal avascular zone. *Technologies*, 12(12), 235.

- Veverka, K. K., AbouChehade, J. E., Iezzi, R., Jr., & Pulido, J. S. (2015). Noninvasive grading of radiation retinopathy: The use of optical coherence tomography angiography. *Retina*, 35(11), 2400–2410.
- Wang, R. Y., Zhu, S. Y., Hu, X. Y., Sun, L., Zhang, S. C., & Yang, W. H. (2024). Artificial intelligence applications in ophthalmic optical coherence tomography: A 12-year bibliometric analysis. *International Journal of Ophthalmology*, 17(12), 2295–2307.

Author(s) Information

Stefan Miron

University Dunarea de Jos Galati, 47 Domneasca Street,
800008, Romania

Mihaela Miron

University Dunarea de Jos Galati, 47 Domneasca Street,
800008, Romania
Contact e-mail: mihaela.miron@ugal.ro

Simona Moldovanu

University Dunarea de Jos Galati, 47 Domneasca Street,
800008, Romania

Marian Barbu

University Dunarea de Jos Galati, 47 Domneasca Street,
800008, Romania

To cite this article:

Miron, S., Miron, M., Moldovanu, S. & Barbu, M. (2025). Enhancing OCTA image classification using superpixel-derived geometric and texture features. *The Eurasia Proceedings of Science, Technology, Engineering and Mathematics (EPSTEM)*, 33, 36-44.

The Eurasia Proceedings of Science, Technology, Engineering and Mathematics (EPSTEM), 2025

Volume 33, Pages 45-61

IConTech 2025: International Conference on Technology

Development and Evaluation of an Advanced Property Management System Using Unified OOAD for Optimizing Real Estate Operations

Riah Elcullada Encaranacion

Caraga State University

Mary Rose Osorio Raz

Caraga State University

Glaicel Anania Araneta

Caraga State University

Abstract: In response to the rapid growth of e-commerce and improvements in supply chain management, there is a pressing need for highly efficient property management system. This study presents the creation and evaluation of an advanced Property Management System (PMS) designed to address property and accommodation challenges and meet the needs of the property owners, managers, and clients specifically in Siargao Island, Philippines, which is considered as one of the world's most popular tourist destinations. The PMS features a robust database for managing property, tenant, and invoice information, and includes essential functionalities such as property search, online payment processing, maintenance request management, lease management, and data analytics. The system development process utilized the Unified Process for Object-Oriented Analysis and Design and carefully detailing the system's technical architecture, security and privacy protocols, as the PMS deals with sensitive information pertaining to properties and payments. The end-users and IT Experts evaluated the system through an online questionnaire using Google Form. The results showed an overall mean rating of 4.52, indicating a high level of satisfaction and compliance with ISO/IEC 25010 Software Quality Standards. Specifically, an average mean results of 4.48 for functional suitability, 4.54 for performance efficiency, 4.49 for compatibility, 4.62 for usability, 4.45 for reliability, and 4.53 for security shows that the developed system met the user requirements. With the developed PMS, the property owners can register and display properties, tenants benefit from an intuitive search interface, and property managers can efficiently handle requests and maintenance. The study offers valuable insights for developers and professionals aiming to create a comprehensive PMS, aligning the system with global trends in smart property management. These innovations will make the PMS highly competitive and better equipped to address the evolving needs of stakeholders in the modern real estate industry.

Keywords: Real estate, Property management system, ISO/IEC 25010, OOAD

Introduction

In a fast-changing world, real estate continues to be a key factor in providing stability, driving economic growth, and fostering innovation, while also contributing to sustainability and improving quality of life. Beyond offering housing, it serves as a critical investment opportunity, a wealth generator, and a driver of urban development. Key industry players—developers, government agencies, and financial institutions—are exploring innovative approaches to ensure continued growth, strengthen market resilience, and secure long-term sustainability in real estate. Adapting to evolving market trends, leveraging technology, and meeting changing consumer demands are essential for success in today's environment (Uriawan et. al., 2023).

- This is an Open Access article distributed under the terms of the Creative Commons Attribution-Noncommercial 4.0 Unported License, permitting all non-commercial use, distribution, and reproduction in any medium, provided the original work is properly cited.

- Selection and peer-review under responsibility of the Organizing Committee of the Conference

© 2025 Published by ISRES Publishing: www.isres.org

These shifts present opportunities for developers, agents, and financial institutions to innovate by adopting versatile and scalable web applications (Shukla, 2024), digital technologies (Avakyan & Pratsko, 2020), blockchain solutions (Patil -Chaitali et al., 2023), and comprehensive tools for real estate management. These innovations will help address the changing demands of a dynamic demographic while fostering growth and diversification within the industry.

The real estate industry in the Philippines is experiencing profound transformation, propelled by the omnipresence of the internet. The shift on how people search for and acquire property is playing a crucial role in the country's economic growth. With a population of 118.2 million and a rising middle class, the demand for industrial, commercial, and residential properties is steadily growing. According to the Accredited Real Estate Salespersons of the Philippines (ACRES), Overseas Filipino Workers (OFWs) are the largest segment of buyers in the market, with sales expected to reach P1 trillion (Sauler, 2024). Foreign investors are also attracted to the Philippine real estate sector due to favorable economic conditions, its strategic location, and strong returns on investment. Additionally, millennials, who now make up 40 percent of the workforce, are influencing the market with their preferences and investment habits (Mendoza, 2024). They place a high value on convenience, sustainability, and technology-driven solutions when purchasing, investing in, or renting properties. Another key driver behind the growth of the real estate sector is the rapid expansion of tourism in the country, particularly in Siargao Island. Known for its stunning beaches and top-tier surfing spots, the island has experienced a significant increase in tourism in recent years (GMA News Integrated, 2024). Siargao's real estate market is booming, driven by rising tourist and expatriate demand, especially for beachfront villas, luxury resorts, and eco-friendly homes. This surge has bolstered the local economy but also highlighted the limitations of the island's accommodation and rental infrastructure. Tourists and residents face challenges such as inefficiencies, limited payment methods, and difficulties finding suitable lodging. Currently, Siargao Island lacks a convenient and automated property management platform, which presents a major obstacle. This research, conducted in Siargao Island, Surigao del Norte, Philippines, leverages the island's unique location and flourishing tourism industry as a backdrop to address property and accommodation challenges. The study seeks to bridge existing gaps by developing system software equipped with tailored algorithms and processes to improve the island's real estate sector.

By introducing a modern and efficient property management system, the research aims to meet the growing demands of a digitally-driven market in Siargao Island, which calls for the advancement of efficient real estate property management systems. This research seeks to align with Sustainable Development Goals (SDGs), or also known as "Global Goals", specifically on Goal 9 that focuses on industry, innovation, and infrastructure. Specifically, the current study sought to answer the following questions: 1) What system architecture and security protocols can be employed for the advanced PMS to optimize real estate operations? 2.) What system features of the advanced web-Based PMS can be developed to optimize real estate operations? 3) What user interfaces can be designed for the advanced web-based Property Management System (PMS)? and 4) What is the level of compliance of the developed PMS in accordance with ISO 20510 software quality standards of functionality suitability, performance efficiency, compatibility, usability, reliability, and security? The web-based PMS has the potential to greatly improve current property management practices and could serve as a model for future advancements in the field. This research does not only develop a more efficient way to manage real estate assets but also sets a standard for the future evolution of property management systems to streamline transactions, enhance the tourist experience, and support the sustainable development of the island's tourism industry. It helps build a resilient infrastructure that can address inclusive and sustainable industrialization to drive employment opportunities.

Literature Review

The Importance of Real Estate Sector

The real estate industry is crucial to economic development, as it helps stabilize the economy by ensuring consistent capital flows for financing (Kaluarachchi, 2021). Many studies have shown the strong connection of real estate to socio-economic development which drives economic growth and social stability. A housing boom can boost household consumption and drive GDP growth (Gao, 2024). Gross domestic product (GDP) measures a country's total economic output and productivity, representing the market value of all finished goods and services produced within a specific period (Sabado, 2023). In addition, Callen (2022) defines GDP as the financial value of goods and services purchased by consumers and produced within a nation during that timeframe.

The Philippines, classified as an emerging economy by the World Bank, has become a key destination for international direct investment, especially after the Asian financial crisis. FDI surged from USD 6.8 billion in 2020 to USD 10.5 billion in 2021, exceeding the Philippine Central Bank's annual target of USD 8 billion (UNCTAD, 2022), attracting significant foreign investment into the economy.

The real estate sector is a major contributor to the Philippine economy, generating approximately PHP1.099 trillion in revenue and providing 101,976 jobs nationwide (PSA, 2019). It also contributes to the 5.7% of Philippines' Gross Domestic Product (GDP), with the related construction industry contributing 7.3% in the same. Likewise, the property sector was responsible for 15.7% of the Philippine Stock Exchange's total market capitalization in 2022 (PSA, 2023). The real estate owners in the Philippines can enhance profitability by focusing on top-line growth, adopting a more aggressive working capital strategy, optimizing the use of productive assets, and leveraging financial opportunities, all of which are expected to positively influence their earnings (Aratea, 2024). For many Filipino families, owning a home is a top aspiration, though it often takes years or decades to achieve. Loans from institutions like Pag-IBIG Fund or private banks help shorten the waiting period. However, the belief persists that commercial real estate investments, such as office buildings and shopping centers, are reserved for the wealthy. This perception is reinforced by the visible success of affluent individuals who earn regular rental income and property value appreciation from such investments (Cadelina, 2023).

The Development of Real Estate Sector in Siargao Island, Philippines

Siargao Island continues to attract tourists and beach enthusiasts, earning a prominent place in an international travel magazine's annual ranking of Asia's best islands. Notably, Siargao was named Condé Nast Traveler's Best Island in Asia in 2021, featured in Time Magazine's "The World's 100 Greatest Places of 2021," and once again recognized in the Condé Nast Traveler Reader's Choice Awards 2023 as one of Asia's top islands (GMA News Integrated, 2024). Post-pandemic, Siargao's tourism industry is making a strong recovery, with visitor numbers rebounding to levels comparable to the pre-pandemic era (Springer, 2024).

Primarily, tourists used to stay in transient houses and homestays due its reasonable prices and strategically located around the island to help them explore the island's world-class tourist spots. With that, property rental businesses are booming due to increased demand from both local and foreign tourists. However, this growth has introduced a set of challenges for the rental businesses. Additionally, securing or managing rentals through a manual system can pose several challenges and problems, which can negatively impact efficiency, accuracy, and customer satisfaction. Moreover, searching for rental accommodation can prove challenging and time consuming, particularly in unfamiliar areas, and there are instances when no available spaces can be found. The automated property management system is very helpful to attract customers and make transactions easier due to the availability of accessible information and the effective and efficient processing of data (Paul, 2019).

The Impact of Real Estate Property Management System

The real estate sector has direct forward linkages with wholesale and retail trade, IT and information services, and telecommunications (Gao, 2024). The use of real estate management system further enhances property management efficiency by centralizing information, streamlining lease and tenant management, providing financial tools, and enabling proactive maintenance tracking.

The Real Estate Management System (REMS) developed by Shukla (2024) provides a holistic solution with a strong database framework for storing and managing data related to properties, tenants, and invoices. Key features include efficient property search options, simplified online payment handling, streamlined maintenance request management, and detailed lease management tools. Additionally, property owners can register and display their properties on the platform, while users benefit from an intuitive interface for property searches based on various criteria.

Deepika et. Al. (2022) also created a web-based Real Estate Management System designed to help users register individual homes or apartments, making it easier to find the ideal rental property. Users can search for rentals in their desired area through the system's search functionality. Key features include the ability for admins to manage property details such as house number, features, rent status, and reviews.

To add tenants, admins can input details like full name, gender, national ID, phone number, email, registration date, house agreement documents, status, and exit date. Additionally, the admin can manage invoices and payments. The application's front end is built with PHP, while the back end uses MySQL.

Property management tasks such as data entry, mathematical computations, and statistical operations are handled using a system developed with a browser/server (B/S) architecture by Mingze (2021). The system is built using Java as the development language within the Spring MVC framework. It utilizes a MySQL database, with database interactions facilitated by the Mybatis framework, and the front-end display powered by the VUE.js framework. Functional modules include owner details, real estate information, engineering equipment, personnel management, and lease management.

Sanket- Donge (2024) created the web-based ABC Real Estate Management using PHP and MySQL to simplify property management for real estate agencies, property managers, and landlords. It features an intuitive interface designed for two main user groups: general users and administrators. General users can search for properties by location and features, use a loan calculator for financial planning, and express interest in listings. Administrators manage user accounts, property listings, and potentially real estate agents, with comprehensive system control. The system prioritizes three core aspects: enhanced user experience, operational efficiency, and robust security. Its user-friendly design ensures easy navigation for both users and administrators. Efficiency is achieved through streamlined property searches and management processes, while role-based access control secures sensitive data by limiting access to authorized users. The system effectively addresses key challenges in property management, creating a secure, efficient, and user-centric platform.

The team of researchers has successfully developed a housing information system featuring fee payments and data management. The system includes functionalities such as displaying resident data, tracking payment history, printing receipts, sending messages to residents, and generating payment reports. By utilizing digital storage with data backup, it eliminates paper-based processes, enhancing efficiency and promoting environmental sustainability. This application is designed to improve service quality in fee payments, providing users with quicker and easier access to payment options. As a result, the system enhances efficiency and service quality in managing resident and fee data (Uriawan, 2023).

Method

The Utilization of Unified Process Model in Object-Oriented Analysis and Design for the Development of the Unified Web-based Property Management System

The Object-Oriented Analysis and Design (OOAD) is a core approach in software engineering for developing reliable and effective software systems (Aratchige et al., 2024). Figure 1.0 presents the Unified Process (UP) in Object-Oriented Analysis and Design (OOAD) used in developing the unified web-based property management system to enhance the real estate business and sustain the needs of real estate stakeholders. The Unified Process (UP) in Object-Oriented Analysis and Design (OOAD) is an iterative and incremental software development methodology that focuses on collaboration, flexibility, and iterative development (Aratchige et al., 2024). It highlights the importance of effective customer communication and simplifies how a system is viewed from the customer's perspective. It emphasizes the critical role of software architecture, guiding architects to prioritize goals such as understandability, adaptability to future changes, and reusability. Its iterative and incremental process flow aligns with the evolutionary approach needed in modern software development (Janis- Osis, 2017).

The model in Figure1 is presented with four major phases having their own series of activities and requirements. The arrows show the flow of control from the first phase to the fifth phase. By substituting the variables of the generic model, the researchers were able to create a unified process model that is suitable to this study. In the *Inception Phase*, the project vision document was created highlighting the project sponsors and project stakeholders who greatly contributed to the success of the project were also identified. It encompasses both customer communication and planning activities. By collaborating with stakeholders, business requirements for the software are identified. The *Elaboration Phase* include project requirements, knowledge requirements and assessment of the stakeholders' needs through an online survey. It focuses on detailed analysis and planning which are undertaken to better understand the problem domain, develop a more concrete project plan, identify and eliminate the high-risk elements of the effort, and to establish a solid architectural foundation for the software to be developed. The software development of the unified web-based PMS system (planning, design, development, testing, and implementation) began with the analysis of the data collected from the online survey in the *Construction* phase. Key activities include developing, testing, and integrating the system components, as

well as continuously verifying that the system meets the requirements. The development phase implements the system, following agile or iterative approaches, with rigorous testing including unit, integration, and system testing. This phase builds a complete, high-quality software product that is ready for deployment. The final stage, *Transition Phase*, highlighted the deployment of a functional and working Unified Web-Based Property Management System. Training and documentation support user adoption, while ongoing maintenance addresses issues and update.

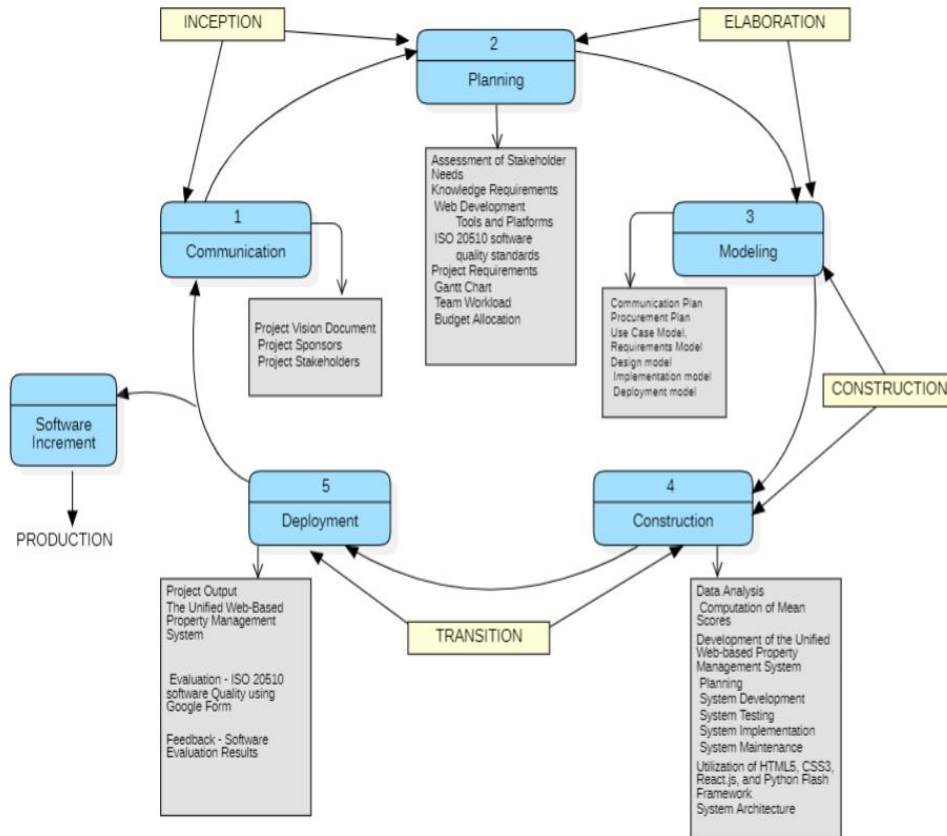


Figure 1. The development of the unified web-based property management system using unified process model in OOAD

Software Evaluation Process

This research utilized both descriptive and developmental methodologies, adhering to a systematic and thorough approach. The developed system underwent essential testing phases, including unit, integration, and system testing, which are critical in software development. Each prototype was evaluated by the developers using predefined test cases. Upon the finalization of the system, the quantitative data were collected through an online questionnaire to assess the system's quality based on the ISO/IEC 25010 System Quality Model Standards (Soares & Franca, 2015). Six criteria from the ISO 25010 software quality standards were used for evaluation, as detailed in Table 1, with each criterion encompassing three specific indicators.

The researchers utilized a verbal interpretation of strongly agree to strongly disagree on a five-point Likert scale to measure respondents' beliefs. The system evaluators are the real estate stakeholders and IT technical experts who were selected through purposive sampling to ensure a diverse representation within the target population. A total of ten (10) real estate participants including tenants, property managers, and property owners utilizing PMS in their performing their tasks were selected for software evaluation. The property manager is responsible for managing all aspects of the properties, including listings, tenants, leases, payments, maintenance, communication, documents, and reports. The tenant is responsible for viewing their lease information, making rent payments, and submitting maintenance requests. While the property owner is responsible for listing properties and managing communication with potential tenants. Meanwhile, five (5) IT experts have validated and evaluated the developed PMS. The feedbacks are essential to further enhance the developed system with regular iterations to meet the changing needs of the real estate stakeholders.

Table 1. The six criteria from ISO 25010 software quality model standards

Functional Suitability	1. <i>Functional completeness</i> - the system covers all the specified tasks and user objectives.
	2. <i>Functional correctness</i> -The system provides the correct results with the needed degree of precision.
	3. <i>Functional appropriateness</i> - The system facilitates the accomplishment of specified tasks and objectives.
Performance Efficiency	1. <i>Time Behavior</i> - The system's response and processing times and throughput rates, when performing its functions, meet requirements.
	2. <i>Resource Utilization</i> - The system's amounts and types of resources used when performing its functions meet requirements.
	3. <i>Capacity</i> - The system's maximum limits of parameters meet requirements.
Compatibility	1. <i>Inter-operability</i> - The system smoothly runs on any device.
	2. <i>Inter-operability</i> - The system is accessible on any device with an internet connection.
Usability	3. <i>Co-existence</i> -The system generates an effective result of data from the prototype.
	1. <i>Appropriateness recognizability</i> - The system allows users to recognize if it is appropriate for their needs.
	2. <i>Learnability</i> - The system allows specified users to achieve specified learning goals effectively, and efficiently and have freedom from risk and satisfaction in a specified context.
Reliability	3. <i>Operability</i> - The system has attributes that make it easy to operate and control.
	1. <i>Maturity</i> - The system meets the need for reliability under regular operation.
	2. <i>Availability</i> - The system is operational and accessible when required for use.
	3. <i>Fault Tolerance</i> - The system can operate as intended despite the presence of hardware or software faults.
Security	1. <i>Confidentiality</i> - The system can be accessed only by the authorized users.
	2. <i>Integrity</i> - The system is secured and protected in terms of data transmission.
	3. <i>Accountability</i> - The system provides its unique account to each end user.

The weighted arithmetic mean was used to calculate the average participant responses, with the interpretation of the weighted mean ranges presented in Table 2.

Table 2. The interpretation of range of the weighted mean

Range of the Weighted Mean	Interpretation
4.51 – 5.00	Strongly Agree (for the questions asked)
3.51 – 4.50	Agree (for the questions asked)
2.51 – 3.50	Moderately Agree (for the questions asked)
1.51 – 2.50	Disagree (for the questions asked)
1.50 and below	Strongly Disagree (for the questions asked)

Results and Discussion

System Architecture and Security Protocols for Optimizing Real Estate Operations

The system architecture of the advanced web-based Property Management System (PMS) is designed to effectively handle various property management functions. The *interaction layer* allows users to interact with a front-end web interface to search for properties, view listings, and manage their accounts. Compliance and regulations are addressed through a module ensuring that the system follows industry standards, legal requirement, and data protection laws such as the Data Privacy Act of 2012 (National Privacy Commission, 2012), and other legal requirements. The *application layer* manages key tasks such as user authentication, property listings, search features, and transactions. The *business logic layer* oversees workflows and notifications, ensuring smooth operation. Data storage is handled by the *data access layer*, while the *integration layer* connects with third-party services like payment gateways and mapping systems. The *infrastructure layer* handles server hosting, load balancing, and scalability, with monitoring and analytics tools tracking system performance and user activity. The technology stack is carefully selected with considerations for scalability, security, and integration capabilities. Frontend development leverage React.js for dynamic user interfaces, complemented by HTML5 and CSS3 for structuring and styling. For backend development, Python Flask Framework provide a robust foundation while MySQL and MongoDB were selected for relational databases

(Shukla, 2024). By leveraging the strengths of Python Flask (Copperwaite, 2015), a lightweight yet robust web application framework used by previous researchers for database management (Suraya, 2022) and document analysis (Revathy, 2024), the developed system includes key functionalities such as property listings, tenant management, rent collection, maintenance tracking, and financial reporting. The API GraphQL facilitates communication between frontend and backend components. To extend functionality, the PMS integrates with third-party services via APIs, such as Gcash, for secure transactions and Google Maps API for geolocation features. Cloud services like AWS or Azure provide scalability and secure cloud data storage. Backup, recovery services, and regulatory compliance are also integral parts of the system.

In the context of property management, where sensitive tenant and property information is involved, the PMS has integrated security and privacy measures, including *authentication*, *authorization*, and *data encryption*. The PMS enhances *authentication security* through multiple mechanisms. It uses *bcrypt algorithm* for password hashing, enforces strong password complexity policies, and requires users to update their passwords every 90 days (password expiration policy). Multi-Factor Authentication (MFA) with the Google Authenticator app generates time-based one-time passwords (TOTP) for added protection. The system also employs OAuth 2.0 for Single-Sign-On (SSO) and secure API authentication, granting external services access based on specific roles. An account lockout policy locks accounts after five failed login attempts, either for 15 minutes or until unlocked via email verification. The *authorization mechanisms* define a user's permissions within the system. The Role-Based Access Control (RBAC) enforces the principle of least privilege, restricting access to data and functionalities based on user roles. Tenants can only access their lease information, submit maintenance requests, and make payments. Property managers can oversee tenants, property listings, financial reports, and maintenance requests. Administrators have complete system control, including user management and access to all data. RBAC helps reduce the risk of unauthorized access and potential damage from security breaches.

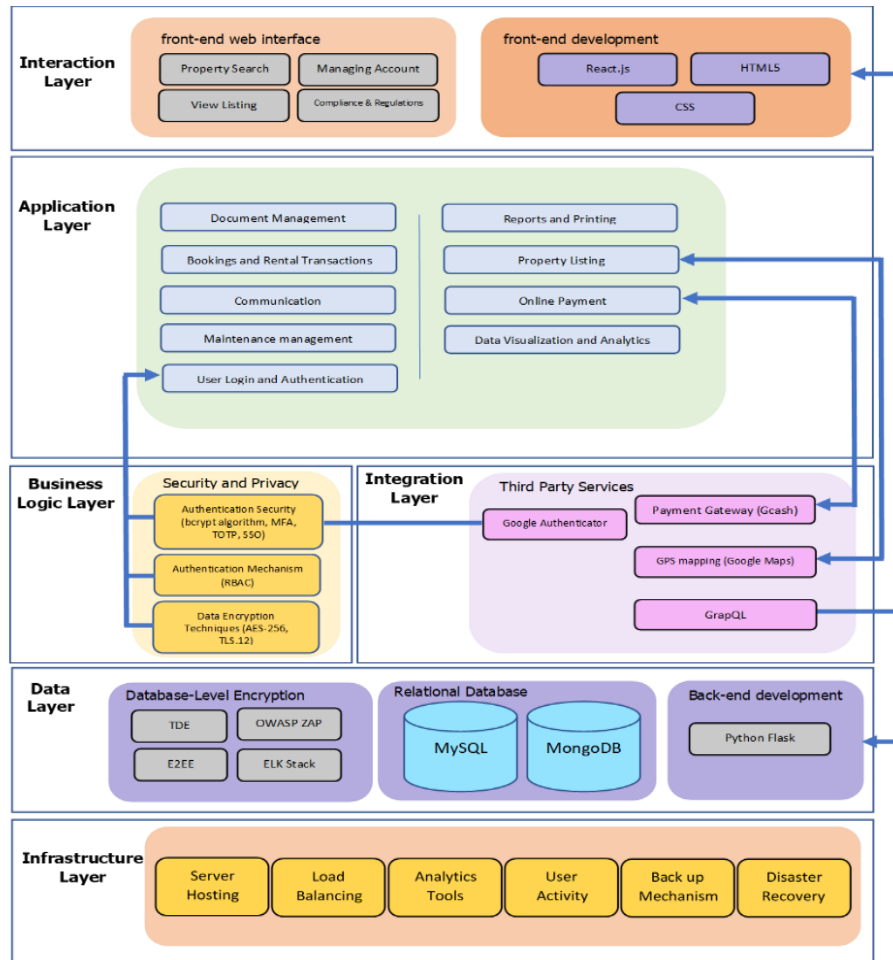


Figure 2. The system architecture and security protocols of the developed advanced PMS

Additionally, audit logs track and securely store user activity, monitoring for suspicious behavior. The *data encryption techniques* in the PMS protect sensitive information by making it unreadable to

unauthorized users. The PMS uses AES-256 encryption for data at rest, including tenant information and payment details, and employs TLS 1.2 for secure communication in transit. Database-level encryption, like Transparent Data Encryption (TDE), automatically encrypts stored data, while end-to-end encryption (E2EE) secures communications between tenants and property managers using protocols like Signal Protocol. The system conducts regular security audits with OWASP ZAP and uses the ELK Stack for real-time monitoring of security events. To safeguard against data loss or system failure, sensitive data is backed up daily at a secure, off-site location, and the disaster recovery procedures are regularly tested to ensure quick data restoration and minimal downtime. Standardizing data formats and ensuring real-time synchronization through webhooks or event-driven architecture facilitates smooth information exchange between the PMS and other systems. Overall, the system aims to provide a secure, scalable, and user-friendly experience for real estate stakeholders, while adapting to market trends and technological advancements.

The System Features of the Developed Unified Web-based Property Management System

The advanced PMS is designed to meet the needs of various stakeholders in the property management ecosystem. The property managers can effortlessly manage property listings, oversee tenant's information, handle maintenance requests, and generate detailed financial reports. The property owners can monitor property performance, financial metrics, and other key indicators with ease. The tenants can have a seamless interface for managing rent payments, maintenance requests, and communication with property managers. The developed system provides the salient features presented in Table 3. These features are from the analyzed user requirements which are suggested in the similar study of Shukla (2024) and Deepika (2022) and Uriawan et al. (2023).

Table 3. Identified features or functions of the developed system

Features / Functions	Description
User Login and Authentication	This function allows users to register and log in to the system.
User Management	This function allows users to register, create accounts, and securely access the system.
Property Listing	This function allows users to list properties for rent complete with details like descriptions, images, amenities, and pricing.
Bookings and Rental Transactions	This function allows handles the booking process and financial transactions related to property reservations. Property managers can create and manage lease agreements, including lease terms, rent payments, and security deposits.
Communication	This function allows property managers to communicate with tenants and vice versa. This could include chatroom mechanism and email messages. There is also the automated notification, keeping users in the loop about property updates, booking confirmations, and reminders
Online Payment	This function allows tenants to make rent payments online.
Document Management	This function allows property managers to store and manage documents related to the properties, such as lease agreements, maintenance records, and inspection reports.
Reports and Printing	This function allows property managers to generate reports on a variety of topics, such as rent payments, maintenance requests, and vacancies.
Data Visualization and Analytics	The system includes graphs and analyzes historical data to assist users in understanding the changes that have occurred more effectively.
Maintenance management	This function allows tenants to submit maintenance requests and property managers to track and manage maintenance requests.

The User Interfaces of the Unified Web-based Property Management System

The advanced web-based system seamlessly organizes real estate assets, streamlining operations and enhancing efficiency. Through intuitive interfaces and robust features, property owners and property managers can effortlessly oversee their portfolios, while tenants enjoy seamless communication and access to essential services.

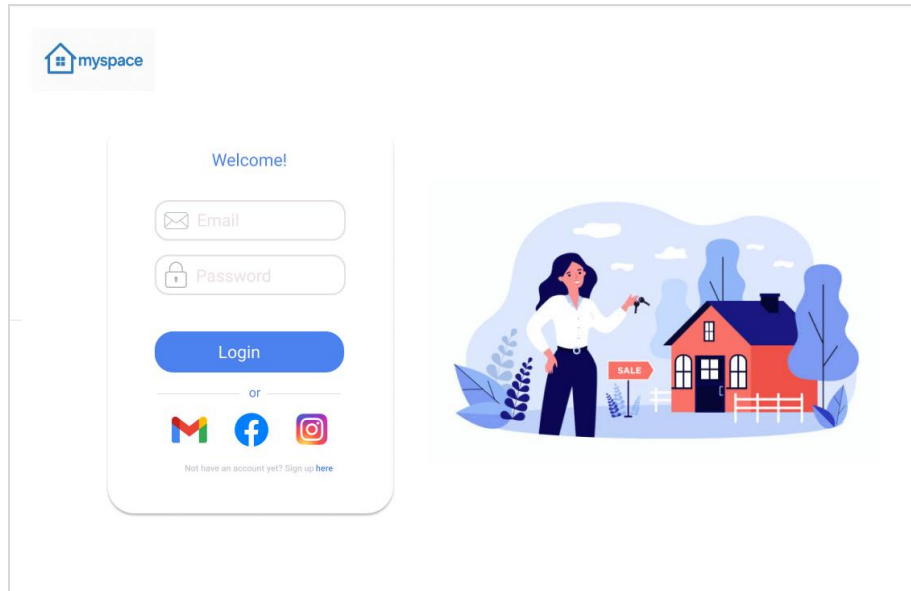


Figure 3. The user's log-in page

The developed system has different parts that make the entire system work seamlessly and smoothly. The user interfaces are designed to be an intuitive and comprehensive that caters to the needs of property managers, owners, and tenants. The login interface (see figure 4) and sign-up interfaces of the advanced web-based PMS is designed to be both secure and user-friendly, ensuring a smooth and efficient entry point for users. The interface features a clean, modern design with clearly labeled fields for username and password.

Figure 4. The user's sign-up page

To gain access to the system, the users are required to follow a straightforward three-step registration process. First, users must thoroughly review and agree to the policy and agreement posted on the website. This step ensures they understand the system's terms and conditions and agree to comply with them. Second, users provide their email and password, as illustrated in Figure 4, or choose to sign up with their Google or Facebook account. This step is vital for creating an account and granting users access to the system. Once registration is complete, a verification email is sent to the user's provided email address. The final step is email verification, which confirms the user's email address, protects personal information, and prevents unauthorized access. After verifying their email, users can log in to the system using their email, password, and user pin. At this point, they can efficiently use the system's features to manage their barangay-related transactions.

Figure 5. The required tenant information page

Upon logging in, users particularly the tenants, are greeted with a sleek, and user-friendly layout. Figure 5 displays the interface for the tenants that allows them to view their records and update their information effortlessly. The tenants must provide accurate and up-to-date information to enable the system to provide efficient and effective services. Tenants are required to upload their valid ID for verification purposes. This step is essential in ensuring the system's security and authenticity, as it verifies the user's identity and confirms that they are authentic users. The tenant can start browsing available properties for renting such as condominiums, rooms, parking lots, etc.

Figure 6. The properties available for rent page

Tenants can pay the property rental fee via online using the Gcash payment method, a very popular online payment system in the Philippines (See Figure 7). While they can also make request for property maintenance online, refer to Figure 8.

myspace
Welcome, Tenant!

- Dashboard
- Tenant Information
- Room Information
- Payment Method**
- Property Information
- Maintenance Request
- Feedback

[Log Out](#)

Payment Method

TOTAL AMOUNT DUE: **4500.00**

Amount Paid: Balance: 45000.00

PAY WITH **GCash**

[SUBMIT](#)

CHOOSE PAYMENT METHOD

Offline Payment

☐ Cash

Online Payment

☒ GCash ☐ GCash

☐ PayMaya ☐ maya

GCash selected

After clicking, you will be redirected to GCash to complete the payment.

[PAY NOW](#)

Figure 7. The payment method page

myspace
Welcome, Tenant!

- Dashboard
- Tenant Information
- Room Information
- Payment Method
- Property Information
- Maintenance Request**
- Feedback

[Log Out](#)

Maintenance Requests

Search

[CREATE MAINTAINANCE REPORT](#)

ID	DATE	NAME	ROOM	DESCRIPTION	STATUS
001	09/01/2024	Isabela Garcia	001		PENDING
002	09/10/2024	Isabela Garcia	002		IN PROGRESS
003	09/15/2024	Diego Cruz	003		IN PROGRESS
004	09/17/2024	Diego Cruz	004		PENDING
005	09/19/2024	Isabela Garcia	005		PENDING
006	09/20/2024	Diego Cruz	006		IN PROGRESS

Showing 6 out of 25 entries

Previous 1 2 3 4 5 Next

Figure 8. The maintenance requests page

After using or renting the property, tenants can provide their feedback to share their experiences and help gauge the quality of the property (see Figure 9).

myspace
Welcome, Tenant!

- Dashboard
- Tenant Information
- Room Information
- Payment Method
- Property Information
- Maintenance Request
- Feedback**

[Log Out](#)

Feedbacks

Search

[ADD FEEDBACK](#)

ID	DATE	NAME	PROPERTY	DESCRIPTION
1	09/20/2024	Carmela Santos	Condominium	I appreciated the clear communication and well-maintained facilities, exceeding my expectations.
2	09/21/2024	Sofia Dela Rosa	House	The property I rented was clean and functional perfectly. I especially appreciated the clear instructions. more
3	09/24/2024	Rafael Mendoza	Condominium	I was very pleased with the overall experience. The customer service was excellent, and the more

Showing 3 out of 25 entries

Previous 1 2 3 9 Next

Figure 9. The tenant feedback page

On the other hand, the administration interface of the developed system is a robust and versatile control center tailored for property managers and owners. It features a comprehensive and sophisticated dashboard that provides an at-a-glance overview of critical system metrics, including property performance, tenant statistics, and financial summaries.

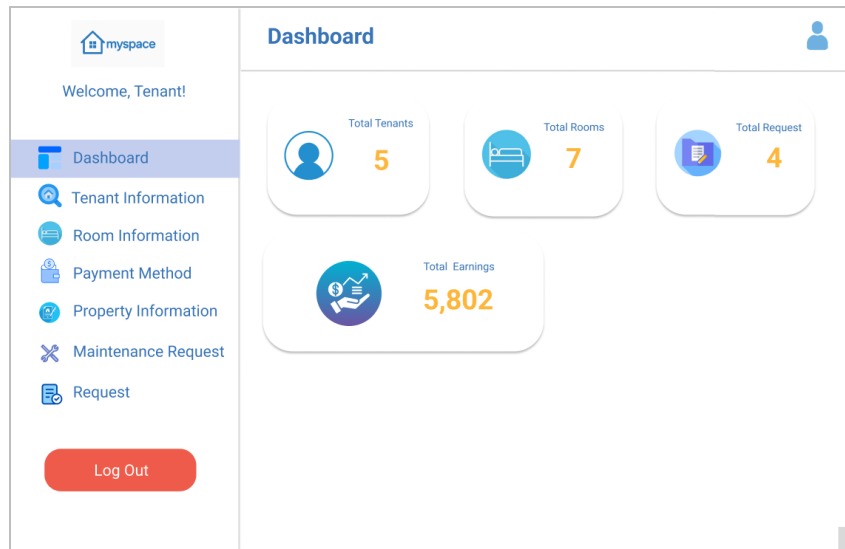


Figure 10. The property manager / owner dashboard page

Figure 10 presents a user-friendly dashboard interface designed for straightforward navigation. Administrators can customize tenant and property information according to their specific requirements, allowing property managers or owners to seamlessly adopt the system. This adaptability ensures an efficient and flexible solution for handling property transactions. Additionally, the dashboard includes tools and features that promote better organization and monitoring of property management activities, enabling more informed decision-making.

The Evaluation of the Developed Advanced Web-based Property Management System in accordance with ISO 20510 Software Quality Standards

The evaluation of the advanced web-based Property Management System (PMS) utilized the ISO 25010 Software Quality Standards, each having three indicators. To assess the system's performance, it was initially deployed in Siargao Islands, Philippines, where it underwent rigorous testing and evaluation. During the evaluation, a varied group of participants provided feedback, including tenants (43%), property managers (30%), and property owners (20%), and IT professionals (7%) with experience in system development. The tenants were the local and international tourists in the island who were active users of the system being evaluated. The following shows the actual result of the system evaluation.

Functional Suitability

Functional suitability implies the presence of the required functionalities and features that address the user's needs under certain conditions. The three indicators represent the completeness, correctness, and appropriateness of every function of the advanced PMS.

Table 4. Results of functional suitability evaluation

Indicators	Mean	Verbal Interpretation	Rank
<i>Functional completeness</i> - the system covers all the specified tasks and user objectives.	4.31	Agree	3
<i>Functional correctness</i> -The system provides the correct results with the needed degree of precision.	4.53	Strongly Agree	2
<i>Functional appropriateness</i> - The system facilitates the accomplishment of specified tasks and objectives.	4.60	Strongly Agree	1
Overall Weighted Mean	4.48	Agree	

The evaluation results in Table 4 indicate that participants strongly agreed that the system offered appropriate and effective functionality. However, they only agreed on the system's completeness, resulting in a slight drop in the weighted mean to 4.24. This finding suggests that, while the system's core features meet users' expectations, there is room for growth through additional functionalities or services. Overall, the outcomes confirm the system's reliability and effectiveness, yet highlight opportunities for further enhancements and refinements to better meet users' needs.

Performance Efficiency

Performance Efficiency represents the system performance relative to the amount of resources used under stated conditions. The response time of the system, the resource utilization, and the limitation of the system were used as the indicators in this area.

Table 5. Results of performance efficiency evaluation

Indicators	Mean	Verbal Interpretation	Rank
<i>Time Behavior</i> - The system's response and processing times and throughput rates, when performing its functions, meet requirements.	4.65	Strongly Agree	12
<i>Resource Utilization</i> - The system's amounts and types of resources used when performing its functions meet requirements.	4.56	Strongly Agree	2
<i>Capacity</i> - The system's maximum limits of parameters meet requirements.	4.40	Agree	3
Overall Weighted Mean	4.54	Strongly Agree	

Performance efficiency obtained the highest weighted mean across all evaluation criteria, indicating that most participants strongly agreed the system satisfies response time and resource utilization requirements. This positive feedback highlights the system's smooth and efficient operation, providing users with a seamless and responsive experience. As a result, the system is better positioned to meet user needs and enhance overall satisfaction. The evaluation underscores performance efficiency as a key strength, suggesting it should be preserved and potentially further refined in future versions.

Compatibility

Compatibility refers to the extent to which a system or component can share information with other products, systems, or components and carry out its functions under the same hardware or software environment. It also underscores the system's ability to adapt to different conditions and environments. Consequently, it is important to assess how the system behaves across various devices and operating systems.

Given that the developed system relies on internet access, it is not surprising that the internet connection is the main factor affecting its performance on different devices. This is reflected in the evaluation results, with the indicator related to running behavior having the lowest mean among the three indicators as shown in Table 6. While this is a limitation of the system, it is not unique to this particular application, and rather a common challenge for any system that relies on internet connectivity. It is important for users to ensure they have a stable internet connection to ensure the system operates optimally. Nonetheless, this finding highlights the importance of considering the impact of external factors, such as internet connectivity, when developing and evaluating digital systems.

Table 6. Results of compatibility evaluation

Indicators	Mean	Verbal Interpretation	Rank
<i>Inter-operability</i> - The system smoothly runs on any device.	4.20	Agree	3
<i>Inter-operability</i> - The system is accessible on any device with an internet connection.	4.35	Agree	2
<i>Co-existence</i> -The system generates an effective result of data from the prototype.	4.92	Strongly Agree	1
Overall Weighted Mean	4.49	Strongly Agree	

Usability

Usability is a critical feature of any software or system, reflecting how well users can accomplish specific objectives with effectiveness, efficiency, and satisfaction under defined conditions. In this evaluation, three indicators—appropriateness recognizability, learnability, and operability—were used to measure how successfully the system meets users' needs.

Table 7. Results of usability evaluation

Indicators	Mean	Verbal Interpretation	Rank
<i>Appropriateness recognizability</i> - The system allows users to recognize if it is appropriate for their needs.	4.75	Strongly Agree	1
<i>Learnability</i> - The system allows specified users to achieve specified learning goals effectively, and efficiently and have freedom from risk and satisfaction in a specified context.	4.63	Strongly Agree	2
<i>Operability</i> - The system has attributes that make it easy to operate and control.	4.47	Agree	3
Overall Weighted Mean	4.62	Strongly Agree	

The developed system is extensive and caters to users across different age groups. If it proves difficult to learn, it may discourage adoption, which could explain the usability findings in Table 7. According to the first two indicators, evaluators strongly agree that the system aligns with their needs and is easy to learn. Meanwhile, its ability to offer a select number of straightforward features enhances user control and serves as an advantage.

Reliability

The Reliability criteria of the developed system was evaluated by looking at how developed system performs specified functions underspecified conditions for a specified period of time. The system's maturity, availability, and fault tolerance which are represented by three indicators were evaluated under reliability.

Table 8. Results of reliability evaluation

Indicators	Mean	Verbal Interpretation	Rank
<i>Maturity</i> - The system meets the need for reliability under regular operation.	4.23	Agree	3
<i>Availability</i> - The system is operational and accessible when required for use.	4.75	Strongly Agree	1
<i>Fault Tolerance</i> - The system can operate as intended despite the presence of hardware or software faults.	3.95	Agree	2
Overall Weighted Mean	4.31	Agree	

Although only two indicators received agreement from the evaluators, the data in Table 8 suggests that the system remains dependable. Notably, availability ranked highest among the indicators, likely due to the system's online accessibility. Since most participants in the area possess mobile phones and enjoy stable internet connections, they can easily access the system. However, the fact that only two indicators were agreed upon indicates potential areas for development. Further evaluation and analysis may help identify specific enhancements needed to strengthen the system's overall functionality and reliability.

Security

Security represents the degree to which the system safeguards information and data. Since the developed system stores sensitive information about the tenants, verifying the security of the information found on the system is essential. In this criterion, data confidentiality and user accountability, regarding the origin of the data, serve as key indicators.

An evaluation of the system's security (Table 9) confirmed that it safeguards resident data without compromising confidentiality. Although two indicators received an "Agree" rating, the overall weighted mean of 4.51 implies that respondents strongly concurred with the system's level of security.

Table 9. Results of security evaluation

Indicators	Mean	Verbal Interpretation	Rank
<i>Confidentiality</i> - The system can be accessed only by the authorized users.	4.80	Strongly Agree	1
<i>Integrity</i> - The system is secured and protected in terms of data transmission.	4.35	Agree	3
<i>Accountability</i> - The system provides its unique account to each end user.	4.45	Agree	2
Overall Weighted Mean	4.53	Strongly Agree	

The developed system was evaluated based on functional suitability, performance efficiency, compatibility, usability, reliability, and security with an overall mean score of 4.52, indicating a high level of agreement among the participants in terms of compliance to the software quality standards (See Table 10). This suggests that respondents found the system both user-friendly and capable of fulfilling its intended functions and requirements. Wulandari and Aristana (2021) emphasized the importance of aligning information systems with ISO 25010 standards to ensure software quality and meet user needs, while Franca and Soares (2015) highlighted ISO 25010 as the most comprehensive quality model for service-oriented architecture.

Table 10. Overall assessment of the participants on the compliance of the developed system to iso 25010 software quality standards

Criteria	Overall Weighted Mean	Descriptive Interpretation
Functional Suitability	4.48	Agree
Performance Efficiency	4.54	Strongly Agree
Compatibility	4.49	Agree
Usability	4.62	Strongly Agree
Reliability	4.45	Agree
Security	4.53	Strongly Agree
Overall Mean	4.52	Strongly Agree

Conclusion

In conclusion, the expected transformation of property management and rental practices highlight the importance of adopting advanced technologies. The advanced Property Management System (PMS) enhances user experience and streamlines transactions by standardizing property information sharing. Stakeholder evaluations indicate strong support for a unified web-based PMS, which offers centralized property data, improved tenant and lease management, advanced financial tools, proactive maintenance tracking, and enhanced communication. This system simplifies core operations, supports better decision-making, and ensures regulatory compliance, aligning with broader trends in digitalization and innovation in real estate. Prospective tenants can easily browse diverse listings through user-friendly portals that address various preferences. The implications of this research extend beyond immediate users, potentially benefiting the wider real estate sector by improving efficiency and effectiveness in property management, leading to positive economic and social outcomes. This study emphasizes the PMS's transformative potential and its critical role in shaping the future of the real estate industry.

Recommendations

Further improvements could transform the PMS into a more robust platform by incorporating blockchain technology, advanced data analytics, AI-driven predictive tools, and IoT for smart building solutions. Blockchain offers significant benefits for secure financial transactions, property record management, smart contracts, and asset tokenization. It can streamline payment processing by transparently recording rental payments and sending notifications to property managers. The PMS can calculate late fees and send reminders, while AI enhances flexibility in payment options and automates rental agreements through smart contracts, reducing manual tasks and speeding up transactions. Blockchain-based identity verification further enhances tenant onboarding security.

Integrating AI and analytics improves the PMS's predictive capabilities, providing insights into maintenance, tenant behavior, and market trends. Predictive analytics can forecast repair needs and tenant turnover, aiding

retention efforts, while AI enhances tenant experiences with personalized services like chatbots. AI also helps optimize rental pricing. IoT integration enables real-time monitoring of utilities and indoor air quality through sensors, as well as smart access management via smartphones. IoT security systems enhance protection, and property managers can control systems from a centralized dashboard. These innovations drive better decision-making and efficiency, adapting to the evolving real estate landscape.

Scientific Ethics Declaration

* The authors declare that the scientific ethical and legal responsibility of this article published in EPSTEM Journal belongs to the authors.

Conflict of Interest

* The authors declare that they have no conflicts of interest

Funding

*This study received no external funding.

Acknowledgements or Notes

* This article was presented as an oral presentation at the International Conference on Technology (www.icontechno.net) held in Trabzon/Türkiye on May 01-04, 2025.

References

- Aratchige, R.M., Ranasinghe, C.,... & Ranasinghe, L. (2024). The object modeling technique in object-oriented analysis and design. *Software Modelling Classwork* , 1 - 4.
- Aratea, J. L. (2024). Determinants of profitability of listed real estate companies in the Philippines. *Philippine Management Review* 2024, 31, 35-48.
- Avakyan, K., & Pratsko, G. (2020). Impact of the coronavirus pandemic in 2020 on the real estate market in Russia: Legal aspects. *E3S Web of Conferences*, 210, 13001.
- Cadelina, A. L. (2023). *Investing in Philippines real estate investment trusts: How REITs can help you own real estate for your portfolioand earn quarterly dividends*. Manila: Arnel Lopez Cadelina.
- Callen, T. (2022). Gross domestic product: An economy's all. *Finance and Development*, 59(2), 14-17.
- Copperwaite, M. A. (2015). *Learning flash framework*. Packt Publishing.
- Deepika S., J. G. (2022). Real estate management system. *Galaxy International Interdisciplinary Research Journal*, 10(6), 108-112.
- Franca, J. M., & Soares, M. S. (2015). Soaqlm: Quality model for soa applications based on iso 25010. *7th International Conference on Enterprise Information Systems (ICEIS)*, 2, 60–70.
- Gao, W. W. (2024). The role of the real estate sector in the economy: Cross-national disparities and their determinants. *Sustainability*, 16(17), 7697.
- GMA News Integrated. (2024, October 18). Boracay, Palawan, Cebu, Siargao among Condé nast traveler's 'best islands' in Asia. Retrieved from <https://www.gmanetwork.com>
- Janis Osis, U. D. (2017). Chapter 2 - software designing with unified modeling language driven approaches. In U. D. Janis -Osis (Ed.), *Computer science reviews and trends, topological UML modeling* (pp. 53 - 82). Elsevier.
- Kaluarachchi, N. D. (2021). Determinants of profitability in the real estate industry: A comparative study between Sri Lanka and Japan. *IOSR Journal of Economics and Finance (IOSR-JEF)*, 11(6), 26-34.
- Ma, M. (2021). Design and realisation of residential property management information system based on browser/server mode. *Applied Mathematics and Nonlinear Sciences*, 6(2),1-10.
- Mendoza, R. (2024, February 24). Estate escapades: 2024's real estate revelations. Retrieved from <https://www.johnclements.com>

- National Privacy Commission. (2012). Republic ACT 10173 data privacy act of 2012. Retrieved from <https://privacy.gov.ph/data-privacy-act/>
- Patil- Chaitali R., Jadhav, A.,...& Gaydhani, A. (2023). Real estate reinvented: Exploring the potential of blockchain technology in property management. *International Journal of Innovative Research in Technology*, 9(11), 733 - 740.
- Paul, A. M. (2019). Spatial progression of estate property management system with customized freeware GIS. *International Journal of Information Technology*, 11, 341–344.
- PSA. (2019). 2019 Annual survey of Philippine business and industry (ASPBI) - real estate activities sector: preliminary results. Retrieved from <https://psa.gov.ph/content/2019-annual-survey-philippine-business-and-industry-aspbi-real-estate-activities-sector>
- PSA. (2023). Annual national accounts linked series (2000-2022). PSA. Retrieved from <https://psa.gov.ph/statistics/national-accounts/data-series>
- Revathy, S. P., Srimathi, R., & Yuvapriya, H. (2024). Document similarity analysis and template matching in health insurance using Python flask. *Journal of Information Technology and Digital World*, 6(2), 179 - 190.
- Sabado, J. N. (2023). The relationship between economic growth and foreign direct investment in the Philippine economy . *Journal of Asian Development*, 9(2), 12 - 31.
- Sankit, D., (2024). ABC real estate management system. *Gurukul International Multidisciplinary Research Journal*, 8(12), 712-722.
- Sauler, N. (2024, March 29). Foundations of real estate in the Philippines in 2024. Lockton. Retrieved from <https://global.lockton.com/ph/en/news-insights/foundations-of-real-estate-in-the-philippines-in-2024>
- Shukla, N. A. (2024). Optimizing efficiency and sustainability in real estate: A comprehensive analysis of advanced real estate property management systems. *International Journal of Innovative Research in Computer Science & Technology (IJIRCST)*, 233- 238.
- Springer, K. (2024, December 19). Siargao, the ‘surf capital of the Philippines,’ is riding a wave of change. CNN Philippines. Retrieved from <https://edition.cnn.com>
- Suraya, S., & Sholeh, M. (2022). Designing and implementing a database for thesis data management by using the Python flask framework. *International Journal of Engineering, Science & Information Technology (IJESTY)*, 2(1), 9 - 14.
- UNCTAD. (2022). International tax reforms and sustainable investment 2022. World Investment Report. Retrieved from <https://unctad.org/>
- Uriawan, W., Enjelianto, I.,... & Lestari, I. S. (2023). Revolutionizing property management: e-Perumahan web-based housing management system. *Preprints*, 1-9.
- Wulandari, D. A. P., & Aristana, M. D. W. (2021). Analysis evaluation management information system audit internal quality. *Annotation*, 5(1), 5-9.

Authors Information

Riah Elcullada Encarnacion

Caraga State University
National Highway, Barangay Ampayon
Butuan City, Philippines
Contact e-mail: reencarnacion@carsu.edu.ph

Mary Rose Osorio Raz

Caraga State University
National Highway, Barangay Ampayon
Butuan City, Philippines

Glaicel Anania Araneta

National Highway, Barangay Ampayon
Butuan City, Philippines

To cite this article:

Encarnacion, R.E., Raz, M.R.O., & Araneta, G.A., (2025). Development and evaluation of an advanced property management system using unified OOAD for optimizing real estate operations. *The Eurasia Proceedings of Science, Technology, Engineering and Mathematics (EPSTEM)*, 33, 45-61.

The Eurasia Proceedings of Science, Technology, Engineering and Mathematics (EPSTEM), 2025

Volume 33, Pages 62-72

IConTech 2025: International Conference on Technology

Implementation of Encryption Using Glushkov Product of Automata

Zhanat Saukhanova

L.N. Gumilyov Eurasian National University

Altynbek Sharipbay

L.N. Gumilyov Eurasian National University

Gulmira Shakhmetova

L.N. Gumilyov Eurasian National University

Alibek Barlybayev

L.N. Gumilyov Eurasian National University

Raykul Sayat

L.N. Gumilyov Eurasian National University

Khasenov Altay

L.N. Gumilyov Eurasian National University

Abstract: This article discusses the software implementation of an encryption algorithm based on the Glushkov product of finite automata. The main focus of this work is on the application of this mathematical model in cryptography, which allows formalizing the process of key generation and construction of block ciphers. The paper provides a theoretical overview of finite automata without output, their properties and features, as well as a formal definition of the Glushkov product. The encryption algorithm is described, its stages are detailed, including the construction of a key automaton and the process of encryption and decryption of data. To confirm the effectiveness of the proposed method, its software implementation in Python was carried out. Experimental results demonstrate the practical applicability of the algorithm, its cryptographic resistance and potential directions for further development. The study shows that the Glushkov product can serve as a basis for the development of new cryptographic schemes with a high degree of protection.

Keywords: Finite automata, Product Glushkov, Permutation automaton, Cryptography, Automata theory

Introduction

Nowadays, automata theory and cryptography are two important areas of theoretical computer science that are actively used in modern information technologies. Automata theory, which studies models of discrete computations and their behavioral characteristics, provides a powerful tool for analyzing and synthesizing data processing algorithms. In turn, cryptography, based on mathematical methods of transforming information, plays a key role in ensuring confidentiality, integrity and authentication of data in digital systems (Idrees et.al., 2020). One of the fundamental concepts of automata theory is the finite state machine model, an abstract computing device that has been successfully applied to describe a variety of processes, including formal languages, pattern recognition, and processing of input data streams. These principles are also reflected in cryptographic algorithms, especially in stream encryption, where the generation of pseudorandom sequences is based on finite state machines.

- This is an Open Access article distributed under the terms of the Creative Commons Attribution-Noncommercial 4.0 Unported License, permitting all non-commercial use, distribution, and reproduction in any medium, provided the original work is properly cited.

- Selection and peer-review under responsibility of the Organizing Committee of the Conference

© 2025 Published by ISRES Publishing: www.isres.org

There are two main classes of finite automata (Shakhmetova et.al.,2024a) – automata with output and automata without output. A finite automaton without output or an automata-recognizer is designed to check whether an input sequence belongs to a certain set. Its main task is to analyze the input data and make a decision on compliance with a given language or rules. In turn, a automata-transducer converts input data into output, thereby implementing an automaton mapping. Both of these types of finite automata are widely used in cryptographic systems.

Automata with outputs, which include Mealy and Moore machines, are widely used in cryptosystems implementing data transformations (Shakhmetova et.al.,2024b). They are used to build both symmetric and asymmetric cryptographic algorithms, providing key generation, stream encryption, and hashing. In particular, Mealy machines are used in cryptosystems based on weak inversion. The founder of the use of finite automata was the scientist Tao Renji, who in 1985 presented a cryptosystem- FAPKC- Finite Automata Public Key Cryptosystem, which has different versions: FAPKC, FAPKC3 and FAPKC4 (Tao&Chen, 1986; Tao et.al.,1997; Tao &Chen, 1999). In 1995 Gysin proposed a One-key cryptosystem based on a non-linear extended Mealy machine (Gysin, 1995). Lakshmi and Gandhi (2012) in their paper considered Mealy/Moore finite automata and recursive functions as applied to cryptographic problems. In (Abubaker&Kui) a system DAFA was proposed that combines elements of DES and finite state machines. Peña and Torres (2016) developed a method for authenticated encryption based on finite state machines with memory (Peña& Torres, 2016). In 2022, a group of scientists Kodada et al. (2022) presented a cryptosystem for cloud computing based on finite-state machines with finite-order memory (Kodada, 2022).

No less interesting for cryptologist scientists were automata without outputs. This group includes cryptographic methods based on deterministic and non-deterministic finite automata that operate without an output. In 2010, P. Domosi's cryptosystem was proposed based on the Rabin-Scott model (Domosi, 2010). In 2015, Horvath and Domosi developed a cryptosystem based on Glushkov's product (permutation automata) (Domosi&Horváth,2015). In 2016, improved cryptographic schemes using nondeterministic finite automata without outputs were presented, including: Modified Domosi cryptosystem (Khaleel et.al.,2016a), a stream cipher based on nondeterministic finite automata (Khaleel et.al., 2016b), a new block cipher based on finite automata systems (Khaleel et.al., 2016c). In (Jawaharlal, 2020), a multi-factor key cryptographic system based on deterministic finite automata was proposed. In 2023, scientists Moatsum Alawida et al. presented a new image encryption scheme for UAV data protection using a combination of DNA encoding and finite automata (Alawida,2023).

This paper studies finite automata without output and the Glushkov product in the context of their application in cryptography. A theoretical overview of key concepts related to finite automata without output, as well as a formal definition and properties of the Glushkov product, is presented. A model of a cryptographic algorithm based on this mathematical construction is described and its formal analysis is carried out. A software implementation of the studied model is carried out, the results of which are confirmed by experimental data demonstrating the efficiency and practical applicability of this cryptographic protocol. Possible directions for further research in the field of application of the Glushkov product in cryptographic systems are also discussed.

Method

Finite Automata without Outputs

An automaton without an output, also known as a finite automata-recognizer, is a mathematical model used to recognize certain sequences of symbols (languages). Unlike automata with outputs, where each state or transition corresponds to a certain output signal, automata without outputs focus exclusively on determining whether the input sequence belongs to a given language. Despite this feature, this type of automata has found its application in data encryption.

According to (Tao, 2008), the finite automata are an algebraic structure $A = \langle X, Q, \delta \rangle$, where: $X = \{x_1, x_2, \dots, x_n\}$ is a non-empty and finite set of the input alphabet; $Q = \{q_1, q_2, \dots, q_m\}$ is a non-empty and finite set of states; $\delta: Q \times X \rightarrow Q$ is the transition function. The elements of the set Q^+ are called states of the finite automata, and the elements of the set X^* are called input symbols, where X^* is the set of all possible words, including the empty set ε , and Q^+ is $Q^+ \setminus \{\varepsilon\}$.

Finite automata without output are divided into deterministic and non-deterministic (Sharipbay, 2015). A *non-deterministic finite automaton (NFA)* is a finite automaton in which the transition function is ambiguous, and

during the operation of the NFA, in one cycle it can make a transition to one or more states different from the initial one. In turn, a *deterministic finite automaton (DFA)* is a special case of an NFA in which for each pair (q, x) there is a unique next state. Further work is based on the use of a deterministic finite automaton without an output, which will be defined in the text as a finite automaton.

The operation of a finite automaton is represented as follows: the relation $(q, ax) \vdash (q', x)$ means that, being in the current state q , reading the input symbol a , the automaton goes to the state q' and then reads the next symbol of the word x . In the row of states q_0, q_1, \dots, q_m ($\{q_0, q_1, \dots, q_m\} \in Q$), the sequence of states q_1, q_2, \dots, q_{m-1} is called *intermediate states*. An extended version of the transition function will be considered:

$$\delta^*: Q \times X^* \rightarrow Q^+,$$

where $\delta^*(q, \varepsilon) = q$, $\delta^*(q, xa) = \delta(q, x) \delta^*(\delta(q, x), a) = q$, $q \in Q, x \in X, a \in X^*$. On other words, under the action of empty word ε , the automaton A does not go anywhere, and for each input word $x_1, x_2, \dots, x_n \in X^+$, where $X^+ = X^* \setminus \varepsilon$, and $x_1, x_2, \dots, x_n \in X$ there exist $q_0, q_1, \dots, q_m \in Q$ with transition functions

$$\delta(q_0, x_1) = q_1, \delta(q_1, x_2) = q_2, \dots, \delta(q_{m-1}, x_n) = q_m$$

such that $\delta(q_0, x_1 x_2 \dots x_n) = q_1 \dots q_m$.

In what follows, the transition function is considered in an expanded form, so we will denote it by δ . For clarity and convenience of presentation of the transition function of a finite automata, it is advisable to use a tabular format (see Table 1).

Table 1. Finite automata transition functions

	q_0	q_1	\dots	q_m
x_1	$\delta(q_0, x_1)$	$\delta(q_1, x_1)$	\dots	$\delta(q_m, x_1)$
x_2	$\delta(q_0, x_2)$	$\delta(q_1, x_2)$	\dots	$\delta(q_m, x_2)$
\dots	\dots	\dots	\dots	\dots
x_n	$\delta(q_0, x_n)$	$\delta(q_1, x_n)$	\dots	$\delta(q_m, x_n)$

In the transition table, the rows correspond to the input symbols of the automaton $x \in X^*$, and the columns correspond to its states $q \in Q$. Each cell of this table contains a state to which the automaton transitions in accordance with the transition function $\delta(q, x)$. If the value of the transition function is not defined for some pair (q, x) , the corresponding cell remains empty.

Product Glushkov of Automata

The Glushkov product of automata is a collection of permutation automata. Each automaton included in this collection changes its state under the influence of a local state transition function and a global input. In this case, the synchronous action of local transitions affects the global transition of the entire collection of automata. Consequently, the result of the Glushkov product of automata is a new finite automaton with a consistent state dynamic (Domosi & Horváth, 2015). Next, we consider the formal definition of the Glushkov product of automata. First, a permutation automaton will be defined.

An automaton $A = \langle X, Q, \delta \rangle$ is called *permutational* if all rows in the transition table are permutations of the set of states. In other words, for each pair $b \in Q, x \in X$, there is only one $a \in Q$ such that $\delta(a, x) = b$. (Dömösi & Horváth, 2015).

Let there be a collection of permutation automata $\mathcal{A}_i = (X_i, Q_i, \delta_i)$, where $i \in \{1, \dots, n\}, n \geq 1$. The feedback function φ_i is defined as a mapping $Q_1 \times \dots \times Q_n \times X \rightarrow X_i$ ($i \in \{1, \dots, n\}$).

The automaton $\mathcal{A} = \mathcal{A}_1 \times \dots \times \mathcal{A}_n(X, (\varphi_1, \dots, \varphi_n))$ is called the Glushkov product of automata \mathcal{A}_i taking into account the feedback function φ_i , which has a set of final states $Q = Q_1 \times \dots \times Q_n$, a finite set of input symbols X , and the transition function δ is defined as follows:

$$\delta((q_1, \dots, q_n), x) = (\delta_1(q_1 \varphi_1(q_1, \dots, q_n, x)), \dots, \delta_n(q_n \varphi_n(q_1, \dots, q_n, x))) \text{ for all } (q_1, \dots, q_n) \in Q \text{ and } x \in X.$$

The feedback function $\varphi_i, i \in \{1, \dots, n\}$ is used in the extended sense: $\varphi_i^*: Q_1 \times \dots \times Q_n \times X^* \rightarrow X_i^*$, where $\varphi_i^*(q_1, \dots, q_n, \varepsilon) = \varepsilon$, and

$\varphi_i^*(q_1, \dots, q_n, ax) = \varphi_i^*(q_1, \dots, q_n, a)\varphi_i(\delta_1(q_1, \varphi_i^*(q_1, \dots, q_n, a)), \dots, \delta_n(q_n, \varphi_n^*(q_1, \dots, q_n, a)), x)$, for all $q_i \in Q, i \in \{1, \dots, n\}, a \in \Sigma^*, x \in X$. Further in the article, $\varphi_i^*, i \in \{1, \dots, n\}$ will be designated as φ_i .

As is known, the automata \mathcal{A}_i used in Glushkov's product must be isomorphic in states to the original automaton. Two finite automata are called *isomorphic in states* if there is a one-to-one correspondence between their sets of states that preserves the structure of transitions and sets of accepted states.

Formally, two automata $\mathcal{A}_1 = (X_1, Q_1, \delta_1)$ and $\mathcal{A}_2 = (X_2, Q_2, \delta_2)$ are considered isomorphic in states if there exist bijections $\sigma_1: Q_1 \rightarrow Q_2, \sigma_2: X_1 \rightarrow X_2$ such that $\sigma_1(\delta_2(q, x)) = \delta_1(\sigma_1(q), \sigma_2(x))$, where $q \in Q_2, x \in X_2$. In the case when $X_2 = X_1$ and $\sigma_2(x) = x$, we can say that \mathcal{A}_2 is an isomorphic automaton \mathcal{A}_1 (Tao, 20).

Encryption Algorithm Glushkov Product of Automata

The paper presents a description of algorithm of the light version of the cryptosystem based on Glushkov Product of automata which was presented in work (Domosi et.al., 2019). This cryptosystem served as a basis for subsequent research in the field of automaton cryptography. The cryptosystem developed by Harvard and Dömösi is of considerable interest to specialists studying the use of alternative mathematical models in cryptography. In this cryptosystem, the key automaton is a sequentially functioning Glushkov product with the following properties:

- The Glushkov product is formed from permutation finite automata that are isomorphic in state.
- The sets of state sets of the automata are identical.
- The automata have identical sets of states and input symbols, which are sets of all strings of fixed length in a given alphabet.

Algorithm:

Let $\mathcal{A}_1 = (X_1, Q_1, \delta_1)$ be a permutation automaton, where $X_1 = Q_1 = \{0, 1, 2, \dots, 255\}$.

At the first stage, the key automaton is constructed in the following way:

Step 1: n and k positive integers are selected. The number n affects the number of automata in the Glushkov product. The number k determines the number of rounds.

Step 2: the initialization vector $r_1 \dots r_n \in X^n$ is generated, which is truly random. It should be taken into account that the alphabet of pseudo-random numbers X is also the alphabet of the open and encrypted text.

Step 3: digraph $D = (V, E)$ with $V = \{1, \dots, n\}, E = \{(n, 1), (1, 2), \dots, (n-1, n)\}$, which defines a D-product: $\mathcal{A}_D = \mathcal{A}_1 \times \dots \times \mathcal{A}_n(X^n, (\varphi_1, \dots, \varphi_n))$ of permutation automata $\mathcal{A}_2, \dots, \mathcal{A}_n$ isomorphic in states to \mathcal{A}_1 , for each $(a_1 \dots, a_n), (x_1 \dots, x_n) \in X^n, i \in \{1, \dots, n\}$ is defined.

Step 4: construct $n-1$ automata isomorphic to \mathcal{A}_1 . For this, generate bijective mappings $\psi_1 \dots \psi_{n-1}$. In order to construct a transition table for isomorphic automata $\mathcal{A}_2, \dots, \mathcal{A}_n$, the formula for states is used:

$$\begin{aligned} \mathcal{A}_2 : \psi_1(\delta_1(q_1, x)) &= \delta_2(\psi_1(q_1), x) \dots \\ \dots \\ \mathcal{A}_n : \psi_{n-1}(\delta_1(q_1, x)) &= \delta_n(\psi_{n-1}(q_1), x) \dots \end{aligned}$$

In this way, transition tables are constructed for all $\mathcal{A}_2, \dots, \mathcal{A}_n$ automata.

The second stage describes the process of encryption of the plaintext using the Glushkov product automaton. The plaintext is read block by block, passing the first block of the plaintext through the key automaton, the first block of the ciphertext is obtained, then the second, third and so on are generated. The blocks of the plaintext are encrypted as follows:

Step 1: the plaintext is split into plaintext blocks $a_1 \dots a_n \in X^n$. The number of symbols in each plaintext block depends on the number of isomorphic automata.

Step 2: a word $w_1, \dots, w_k \in X^n$ of pseudorandom sequences is generated, where $w_1 \dots, w_k \in \Sigma^n$, which are then used in the encryption process as a key at each round. Each vector $w_j = (x_1 \dots x_n), j = 1 \dots k$ has length n .

Step 3: an invertible function φ_i is selected such that

$$\varphi_i: \mathcal{A}_1 \times \dots \times \mathcal{A}_n \times X \rightarrow X_i \text{ for all } i = 1 \dots n$$

$$\mathcal{A}_1 = (X_1, Q_1, \delta_1), \mathcal{A}_2 = (X_2, Q_2, \delta_2), \dots, \mathcal{A}_n = (X_n, Q_n, \delta_n)$$

$$X_1 = X_2 = \dots = X_n = Q_1 = Q_2 = \dots = Q_n = \overline{(0, 255)}$$

$$\varphi_1(a_1 \dots a_n, (x_1, \dots, x_n)) = a_n \oplus x_n$$

$$\varphi_i(a_1 \dots a_n, (x_1, \dots, x_n)) = a_{i-1} \oplus x_{i-1}$$

where \oplus - bitwise addition modulo 2, and $i = 2 \dots n$

4 mar: key automata $\mathfrak{B} = (X^n, X^n, \delta_{\mathfrak{B}})$ is Production Glushkov of automata \mathcal{A}_D , where for any $(a_1 \dots a_n), (x_1 \dots x_n) \in X^n$ has transaction function $\delta_{\mathfrak{B}}((a_1 \dots a_n), (x_1 \dots x_n)) = (b_1 \dots b_n)$. Thus:

$$b_1 = \delta_{\mathcal{A}_1}(a_1, \varphi_1(a_1, \dots, a_n, (x_1, \dots, x_n))), \text{ where } \varphi_1(a_1, \dots, a_n, (x_1, \dots, x_n)) = a_n \oplus x_n$$

$$b_2 = \delta_{\mathcal{A}_2}(a_2, \varphi_2(b_1, a_2, \dots, a_n, (x_1, \dots, x_n))), \text{ where } \varphi_2(b_1, a_2, \dots, a_n, (x_1, \dots, x_n)) = b_1 \oplus x_1$$

...

$$b_n = \delta_{\mathcal{A}_n}(a_n, \varphi_n(b_1, b_2, \dots, a_n, (x_1, \dots, x_n))), \text{ where } \varphi_n(b_1, b_2, \dots, a_n, (x_1, \dots, x_n)) = b_{n-1} \oplus x_{n-1}$$

IIIar 5: $(d_1 \dots, d_n)$ and $(e_1 \dots, e_n)$ vectors are defined.

If $k=1$, these vectors are defined as follows:

$(d_1, \dots, d_n) = (a_1 \dots, a_n)$ – bloc of plaintext.

$$(e_1, \dots, e_n) = \delta_{\mathfrak{B}}((d_1 \dots, d_n), w_1).$$

$$e_1 = \delta_{\mathcal{A}_1}(d_1, \varphi_1(d_1, \dots, d_n, (x_1, \dots, x_n))) = \delta_{\mathcal{A}_1}(d_1, d_n \oplus x_n),$$

$$e_2 = \delta_{\mathcal{A}_2}(d_2, \varphi_2(e_1, d_2, \dots, d_n, (x_1, \dots, x_n))) = \delta_{\mathcal{A}_2}(d_2, e_1 \oplus x_1),$$

...

$$e_n = \delta_{\mathcal{A}_n}(d_n, \varphi_n(e_1, e_2, \dots, d_n, (x_1, \dots, x_n))) = \delta_{\mathcal{A}_n}(d_n, e_{n-1} \oplus x_{n-1}).$$

If $k>1$, encryption is performed in the following way:

$$(e_1 \dots, e_n) = \delta_{\mathfrak{B}}((d_1 \dots, d_n), w_1 \dots w_i)$$

After k rounds, states $(e_1 \dots, e_n)^k$ will be obtained. The ciphertext $c_1 \dots c_n$ is the concatenation of the calculated state blocks (e_1, \dots, e_n) at each round.

The third stage describes the decryption process. The key machine reads the encrypted data in blocks sequentially and, having processed the first block of the ciphertext $c_1, \dots, c_n \in X^n$, calculates the corresponding blocks of the plaintext in the order reverse to their original sequence. This process occurs according to the steps described below:

Step 1: the ciphertext is divided into ciphertext blocks $c_1, \dots, c_n \in X^n$. The number of symbols in each ciphertext block depends on the number of isomorphic automata.

Step 2: a word $w_1, \dots, w_k \in X^n$ of pseudorandom sequences is generated, where $w_1, \dots, w_k \in X^n$, which were used as a key during encryption in each round. Each vector $w_j = (x_1 \dots x_n), j = 1 \dots k$ has length n .

Step 3: an invertible function φ_i is selected similar to that described in step 3 of the encryption stage.

Step 4: during decryption, the inverse automaton $\mathfrak{B}^{-1} = (X^n, X^n, \delta_{\mathfrak{B}^{-1}})$, is used to the key automaton $\mathfrak{B} = (X^n, X^n, \delta_{\mathfrak{B}})$, which was used during encryption. Thus, the vector $(d_1 \dots, d_n)$ is restored as follows:

If $k=1$, the vectors are defined as follows:

$$(e_1, \dots, e_n) = (c_1 \dots, c_n) - \text{ciphertext block}$$

$$(d_1 \dots, d_n) = \delta_{\mathfrak{B}}((e_1 \dots, e_n), w_1).$$

$$d_n = \delta_{\mathcal{A}_n^{-1}}(e_n, \varphi_n(e_1, \dots, e_{n-1}, e_n, (x_1, \dots, x_n))) = \delta_{\mathcal{A}_n^{-1}}(e_n, e_{n-1} \oplus x_{n-1}),$$

$$d_{n-1} = \delta_{\mathcal{A}_{n-1}^{-1}}(e_{n-1}, \varphi_{n-1}(e_1, \dots, e_{n-1}, d_n, (x_1, \dots, x_n))) = \delta_{\mathcal{A}_{n-1}^{-1}}(e_{n-1}, e_{n-2} \oplus x_{n-2}),$$

$$d_1 = \delta_{\mathcal{A}_1^{-1}}(e_1, \varphi_1(e_1, \dots, d_{n-1}, d_n, (x_1, \dots, x_n))) = \delta_{\mathcal{A}_1^{-1}}(e_1, d_n \oplus x_n).$$

If $k > 1$, decryption is done in the following way:

$$(d_1 \dots, d_n) = \delta_{\mathfrak{B}}((e_1 \dots, e_n), w_1 \dots w_i)$$

Thus, we can obtain a block of plaintext after k rounds of inverse transformation.

Results and Discussion

In this section of the article will discuss a demonstration example that will clearly demonstrate the use of the Glushkov product of automata as encryption and decryption of plaintext.

We will further illustrate an example on how to apply product Glushkov of automata on encryption and decryption process. Take $\mathcal{A}_1 = (X_1, Q_1, \delta_1)$ be a permutation automaton, where $X_1 = Q_1 = \{0, 1, 2, 3\}$. The transition table 2:

Table 2. Transition functions of \mathcal{A}_1

	0	1	2	3
0	1	2	3	0
1	0	3	2	1
2	2	1	3	0
3	0	1	3	2

We will choose $n=3$, it is mean that will be constructed two isomorphic automata \mathcal{A}_2 and \mathcal{A}_3 . For that we generate bijective mappings ψ_1 and ψ_2 .

$$\psi_1: \psi_1(0) = 3, \psi_1(1) = 1, \psi_1(2) = 0, \psi_1(3) = 2$$

$$\psi_2: \psi_2(0) = 2, \psi_2(1) = 0, \psi_2(2) = 3, \psi_2(3) = 1$$

According bijective mapping construct transition function for \mathcal{A}_2 and \mathcal{A}_3 (table 3 and table 4).

Table 3. Transition functions of \mathcal{A}_2

	0	1	2	3
0	0	1	3	2
1	3	2	0	1
2	3	1	2	0
3	1	0	2	3

Table 4. Transition functions of \mathcal{A}_3

	0	1	2	3
0	2	1	3	0
1	2	0	1	3
2	0	3	1	2
3	3	0	1	2

Thus, key automata are Glushkov product of automata $\mathcal{A}_D = \mathcal{A}_1 \times \mathcal{A}_2 \times \mathcal{A}_3(X^3, (\varphi_1, \varphi_2, \varphi_3))$

Let, plaintext is 103, for encrypting this text we generate key $w = (x_1, x_2, x_3) = (3, 0, 1)$, $k = 1$.

Define vector $(d_1, d_2, d_3) = (1, 0, 3)$.

Encryption is done as follows:

$$e_1 = \delta_{\mathcal{A}_1}(d_1, \varphi_1(d_1, d_2, d_3, (x_1, x_2, x_3))) = \delta_{\mathcal{A}_1}(d_1, d_3 \oplus x_3) = \delta_{\mathcal{A}_1}(1, 3 \oplus 1) = \delta_{\mathcal{A}_1}(1, 2) = 1$$

$$e_2 = \delta_{\mathcal{A}_2}(d_2, \varphi_2(e_1, d_2, d_3, (x_1, x_2, x_3))) = \delta_{\mathcal{A}_2}(d_2, e_1 \oplus x_1) = \delta_{\mathcal{A}_2}(0, 1 \oplus 3) = \delta_{\mathcal{A}_2}(0, 2) = 3$$

$$e_3 = \delta_{\mathcal{A}_3}(d_3, \varphi_3(e_1, e_2, d_3, (x_1, x_2, x_3))) = \delta_{\mathcal{A}_3}(d_3, e_2 \oplus x_2) = \delta_{\mathcal{A}_3}(3, 3 \oplus 0) = \delta_{\mathcal{A}_3}(3, 3) = 2$$

So, cyphertext $(c_1, c_2, c_3) = (1, 3, 2)$

For decrypting cyphertext we need generate inverse of key automata (table 5, 6, 7).

Table 5. Transition functions of \mathcal{A}_1^{-1}

	0	1	2	3
0	3	0	1	2
1	0	3	2	1
2	3	1	0	2
3	0	1	3	2

Table 6. Transition functions of \mathcal{A}_2^{-1}

	0	1	2	3
0	0	1	2	3
1	2	3	1	0
2	3	1	2	0
3	1	0	2	3

Table 7. Transition functions of \mathcal{A}_3^{-1}

	0	1	2	3
0	3	1	0	2
1	1	2	0	3
2	0	2	3	1
3	1	2	3	0

Key use same us encryption stage $w = (x_1, x_2, x_3) = (3, 0, 1)$

The decryption process is similar to encryption, but in reverse.

$$(e_1, e_2, e_3) = (1, 3, 2)$$

$$d_3 = \delta_{\mathcal{A}_3^{-1}}(e_3, \varphi_3(e_1, e_2, e_3, (x_1, x_2, x_3))) = \delta_{\mathcal{A}_3^{-1}}(e_3, e_2 \oplus x_2) = \delta_{\mathcal{A}_3^{-1}}(2, 3 \oplus 0) = \delta_{\mathcal{A}_3^{-1}}(2, 3) = 3$$

$$d_2 = \delta_{\mathcal{A}_2^{-1}}(e_2, \varphi_2(e_1, e_2, d_3, (x_1, x_2, x_3))) = \delta_{\mathcal{A}_2^{-1}}(e_2, e_1 \oplus x_1) = \delta_{\mathcal{A}_2^{-1}}(3, 1 \oplus 3) = \delta_{\mathcal{A}_2^{-1}}(3, 2) = 0$$

$$d_1 = \delta_{\mathcal{A}_1^{-1}}(e_1, \varphi_1(e_1, d_2, d_3, (x_1, x_2, x_3))) = \delta_{\mathcal{A}_1^{-1}}(e_1, d_3 \oplus x_3) = \delta_{\mathcal{A}_1^{-1}}(1, 3 \oplus 1) = \delta_{\mathcal{A}_1^{-1}}(1, 2) = 1$$

So, we get decrypted text $(d_1, d_2, d_3) = (1, 0, 3)$

The above example is given to illustrate the operation of encrypting and decrypting using Glushkov product of automata work. Obviously, in practice that cryptographic algorithm is much more complicated. For more information on how to build these types of automata, see the work (Domosi et.al., 2019).

The software implementation of the considered cryptosystem was made by the Python programming language. To demonstrate the operation of the algorithm under consideration, a gray image *Airplane.tiff* with size 512x512 pixels was taken (<https://sipi.usc.edu/database>). To encrypt this image, 16 finite automata were taken, and the number of rounds is 8. For images with size 512*512 pixels will be encrypted 16 384 blocks. The key of size 16 is generated randomly, in our case, the same key is used in each round. Results of encrypting and decrypting are shown on figure 1.

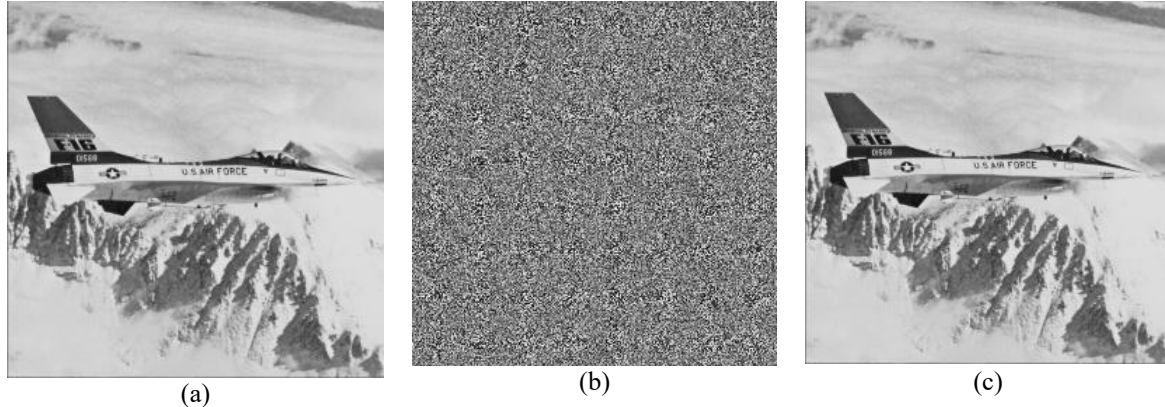


Figure 1. (a) Original image, (b) encrypted image, (c) decrypted image.

NIST Test Results

The statistical tests developed by the National Institute of Standards and Technology (NIST) Information Technology Laboratory are a set of 15 methods designed to assess the degree of randomness of binary sequences. These tests are based on the analysis of various statistical characteristics inherent in random sequences. Successful completion of these tests is interpreted as evidence of high cryptographic strength of the data under study (Pareschi et.al., 2012). Thus, the NIST test set is an effective tool for analyzing the randomness of encrypted information, which in turn indicates the reliability of the cryptographic methods used. Table 8 contains the results of NIST statistical tests on the experimental image.

Table 8. NIST results

Test Name	P-Value	Conclusion
01. Frequency Test:	0.6114533432130285	True
02. Block Frequency Test:	0.9512055879042081	True
03. Run Test:	0.04314964466418219	True
04. Run Test (Longest Run of Ones):	0.37066285180866043	True
05. Binary Matrix Rank Test:	0.7262509735848526	True
06. Discrete Fourier Transform (Spectral) Test:	0.9487819898568091	True
07. Non-overlapping Template Matching Test:	0.8067096223594483	True
08. Overlapping Template Matching Test:	0.5373254259563948	True
09. Universal Statistical Test:	0.9470101746108605	True
10. Linear Complexity Test:	0.8350400376461669	True
11. Serial Test:	0.9804137326823029	True
	0.815036343351716	True
12. Approximate Entropy Test:	0.8733927390000743	True
13. Cumulative Sums (Forward):	0.37820269368211135	True
13. Cumulative Sums (Backward):	0.37820269368211135	True
14. Random Excursion Test:		
STATE	xObs	P-Value
-4	0.3757434402332362	0.9959714520151304
-3	1.997984	0.8494239179678532
-2	4.9027160493827155	0.4278679719139393
		Conclusion
		True
		True
		True

-1	2.0	0.8491450360846096	True
1	8.6	0.12612244119041105	True
2	8.359012345679012	0.13752824367716304	True
3	5.4315200000000001	0.3655134039059185	True
4	4.419958350687214	0.4906636246748899	True
15. Random Excursion Variant Test:			
<i>STATE</i>	<i>COUNTS</i>	<i>P-Value</i>	<i>Conclusion</i>
-9.0	61	0.503594688207976	True
-8.0	71	0.5964828214814786	True
-7.0	80	0.6948866023724733	True
-6.0	74	0.5793585907298551	True
-5.0	70	0.4795001221869535	True
-4.0	89	0.7687675574059754	True
-3.0	93	0.8248125741940059	True
-2.0	94	0.8064959405073401	True
-1.0	99	0.9436280222029834	True
+1.0	109	0.5245182802130763	True
+2.0	125	0.30743416592739536	True
+3.0	128	0.3759205825480747	True
+4.0	111	0.7687675574059754	True
+5.0	111	0.7954250063905932	True
+6.0	110	0.8311704095417624	True
+7.0	107	0.8908084551935809	True
+8.0	128	0.6092056132701683	True
+9.0	150	0.3911725228101395	True

Passing all NIST tests comprehensively demonstrates that the encrypted image meets international standards for cryptographic data strength.

Conclusion

In this research, finite automata without outputs were studied as a basis for constructing encryption algorithms. A cryptographic scheme based on the Glushkov product of automata was implemented in software, allowing for the encryption and decryption of data using a formal automaton-based model. The developed program demonstrates the operation of the encryption process through the sequential composition of isomorphic automata, ensuring high variability and structural complexity of the key automaton.

The considered algorithm has several advantages. It features a clear mathematical structure, flexibility in configuring encryption parameters (such as the number of automata and rounds), and a modular architecture that facilitates software and potentially hardware implementation. The use of isomorphic permutation automata increases resistance to cryptanalytic attacks by introducing combinatorial complexity. Furthermore, the ability to generate pseudorandom transformations on each encryption round contributes to high diffusion and confusion properties, essential for secure encryption. The compositional structure of the Glushkov product contributes to enhancing data protection by increasing the cryptographic strength of the encryption process. The results of NIST statistical tests confirmed the high level of randomness and reliability of the proposed method.

Scientific Ethics Declaration

The authors declare that the scientific ethical and legal responsibility of this article published in EPSTEM Journal belongs to the authors.

Conflict of Interest

The authors declare that they have no conflicts of interest

Funding

This research is funded by the Science Committee of the Ministry of Education and Science of the Republic of Kazakhstan (Grant No. AP19677422).

Acknowledgements or Notes

*This article was presented as an oral presentation at the International Conference on Technology (www.icontechno.net) held in Trabzon/Türkiye on May 01-04, 2025.

References

- Abubaker, S., & Wu, K. (2012). Dafa-a lightweight des augmented finite automaton cryptosystem. *International Conference on Security and Privacy in Communication Systems* (pp. 1-18). Berlin, Heidelberg: Springer.
- Alawida, M., Teh, J. S., & Alshoura, W. H. (2023). A new image encryption algorithm based on DNA state machine for UAV data encryption. *Drones*, 7(1), 38.
- Domosi, P. B., Horvath, G., Medveczki, M. S., & Salga, P. (2019). *U.S. Patent No. 10,419,207*. Washington, DC: U.S. Patent and Trademark Office.
- Domosi, P. (2010). A novel cryptosystem based on finite automata without outputs. In *Automata, formal languages and algebraic systems* (pp. 23-32). https://www.worldscientific.com/doi/abs/10.1142/9789814317610_0002
- Domosi, P., & Horváth, G. (2015). A novel cryptosystem based on Gluškov product of automata. *Acta Cybernetica*, 22(2), 359-371.
- Gysin, M. (1995). A one-key cryptosystem based on a finite nonlinear automaton. *International Conference on Cryptography: Policy and Algorithms* (pp. 165-173). Berlin, Heidelberg: Springer.
- Idrees, B., Zafar, S., Rashid, T., & Gao, W. (2020). Image encryption algorithm using S-box and dynamic Hénon bit level permutation. *Multimedia Tools and Applications*, 79(9), 6135-6162.
- Jawaharlal, S. M., Narayanan, A., Santhar, S., & Sivaramalingam, B. (2019). *U.S. Patent No. 10,320,758*. Washington, DC: U.S. Patent and Trademark Office.
- Khaleel, G., Turaev, S., & Tamrin, M. M. (2016c). A new block cipher based on finite automata systems. *International Journal on Perceptive and Cognitive Computing*, 2(1), 23-26.
- Khaleel, G., Turaev, S., & Zhukabayeva, T. (2016b). A novel stream cipher based on nondeterministic finite automata. In *Information technologies in science, management, social sphere and Medicine* (pp. 439-444). Atlantis Press.
- Khaleel, G., Turaev, S., Tamrin, M. I. M., & Al-Shaikhli, I. F. (2016a). Performance and security improvements of Domosi's cryptosystem. *International Journal of Applied Mathematics & Statistics*, 55(2), 32-45.
- Kodada, B. (2022). FSAaCIT: Finite state automata based one-key cryptosystem and chunk-based indexing technique for secure data de-duplication in cloud computing. *Authorea Preprints*.
- Lakshmi, S. (2012). *On finite state machines and recursive functions—applications to cryptosystems*. (Doctoral dissertation).
- Pareschi, F., Rovatti, R., & Setti, G. (2012). On statistical tests for randomness included in the NIST SP800-22 test suite and based on the binomial distribution. *IEEE Transactions on Information Forensics and Security*, 7(2), 491-505.
- Peña, P. I. S., & Torres, R. E. G. (2016). Authenticated encryption based on finite automata cryptosystems. *13th International Conference on Electrical Engineering, Computing Science and Automatic Control (CCE)* (pp. 1-6). IEEE.
- Shakhmetova, G., Barlybayev, A., Saukhanova, Z., Sharipbay, A., Raykul, S., & Khassenov, A. (2024b). Enhancing visual data security: A novel FSM-based image encryption and decryption methodology. *Applied Sciences*, 14(11), 4341.
- Shakhmetova, G., Saukhanova, Z., Sharipbay, A., Barlybayev, A., Sayat, R., Altay, K., & Saukhanova, M. (2024a). Ontological model of cryptosystems based on the theory of finite automata. In *2024 International Visualization, Informatics and Technology Conference (IVIT)* (pp. 8-13). IEEE.
- Sharipbay, A. (2015). *Theory of language and automata*. Almaty: Evero.
- Tao, R. (2008). *Finite automata and application to cryptography*. Chicago: Springer.
- Tao, R., & Chen, S. (1986). Two varieties of finite automaton public key cryptosystem and digital signatures. *Journal of Computer Science and Technology*, 1(1), 9-18.
- Tao, R., & Chen, S. (1999). The generalization of public key cryptosystem FAPKC4. *Chinese Science Bulletin*, 44, 784-790.

Tao, R., Chen, S., & Chen, X. (1997). FAPKC3: A new finite automaton public key cryptosystem. *Journal of Computer Science and Technology*, 12(4), 289-305.

Author(s) Information

Zhanat Saukhanova

L.N. Gumilyov Eurasian National University
Pushkin street 11, Astana, Kazakhstan

Altynbek Sharipbay

L.N. Gumilyov Eurasian National University
Pushkin street 11, Astana, Kazakhstan

Gulmira Shakhmetova

L.N. Gumilyov Eurasian National University
Pushkin street 11, Astana, Kazakhstan
Contact e-mail: sh_mira2004@mail.ru

Alibek Barlybayev

L.N. Gumilyov Eurasian National University
Pushkin street 11, Astana, Kazakhstan

Raykul Sayat

L.N. Gumilyov Eurasian National University
Pushkin street 11, Astana, Kazakhstan

Khasenov Altay

L.N. Gumilyov Eurasian National University
Pushkin street 11, Astana, Kazakhstan

To cite this article:

Saukhanova, Z., Sharipbay, A., Shakhmetova, G., Barlybayev, A., Sayat, R., & Altay, K. (2025). Implementation of encryption using Glushkov product of automata. *The Eurasia Proceedings of Science, Technology, Engineering and Mathematics (EPSTEM)*, 33, 62-72.

The Eurasia Proceedings of Science, Technology, Engineering and Mathematics (EPSTEM), 2025

Volume 33, Pages 73-79

IconTech 2025: International Conference on Technology

Relay-Aided PDMA with Dynamic Power Control for Cell-Edge User Fairness

Rashed Alsakarnah

Al-Zaytoonah University of Jordan

Mohammad Masoud

Al-Zaytoonah University of Jordan

Shaher Slehat

Al-Zaytoonah University of Jordan

Abstract: Cell-edge users in wireless communication networks often suffer from poor performance due to weak channel conditions. To address this issue, we propose a relay-assisted communication system that employs Pattern Division Multiple Access (PDMA). This approach enhances efficiency and capacity for cell-edge users while maintaining acceptable relay performance. The proposed scheme includes a Base Station (BS), a Relay (R) with better channel conditions, and a cell-edge user. Transmission occurs over two time slots: In the first time slot, the base station (BS) transmits a superimposed signal to both the relay and the cell-edge user. In the second time slot, the relay forwards only the decoded information intended for the cell-edge user. The cell-edge user then applies successive interference cancellation (SIC) to recover the desired signal. To further optimize system performance, we implement an optimal power allocation strategy at the base station that: (1) assigns power to both the signal intended for the relay and the cell-edge user in the superimposed transmission, while (2) allocating higher transmit power to the relay compared to the BS, leveraging the relay's superior channel conditions. This approach enhances the overall system capacity and reliability, particularly benefiting cell-edge users with weak direct links. This approach enhances the overall capacity and reliability of the relay-assisted transmission, thereby improving the quality of service (QoS) for cell-edge users with weak direct links to the BS. As a result, the cell-edge user benefits from both the BS and relay transmissions, enabling the decoding of the superimposed signal by using SIC and ultimately improving spectral efficiency. Furthermore, we introduce a fairness metric to assess the received capacity relative to the actual capacity of each user, providing insights into the equitable distribution of resources. The fairness metric is calculated as the ratio of the received capacity to the actual capacity for each user, allowing for a comparison of how fairly the system allocates resources under different schemes.

Keywords: Relay, Non-orthogonal multiple access, Superposition coding, Decode and forward

Introduction

Superposition Coding (SC) has been recognized as an effective capacity-achieving signaling technique in broadcasting and multicasting scenarios (Silva et al., 2010; Wang, et al., 2013). In this approach, multiple encoded sequences (referred to as layers) are linearly combined into a single composite signal prior to transmission. SC functions as a data multiplexing method for a single user and shares similarities with Non-Orthogonal Multiple Access (NOMA), wherein each layer can be interpreted as representing an individual user (Kim et al., 2015).

At the receiver end, similar to NOMA, low-complexity iterative decoding techniques can be employed. These are enhanced by allocating different power levels to the layers, thereby improving the overall system throughput (Alsakarnah et al., 2017; Chattha et al., 2016). To further enhance the efficiency of superposition-based transmission schemes, Pattern Division Multiple Access (PDMA) has emerged as a promising candidate. PDMA extends the concept of non-orthogonal access by exploiting unique transmission patterns across multiple domains such as power, code, and spatial resources. Unlike conventional SC or NOMA, PDMA allows for more flexible user multiplexing through pattern design, which can effectively reduce inter-user interference and improve spectral efficiency. By integrating PDMA with Superposition Coding, the system can leverage both the layered transmission structure of SC and the pattern diversity of PDMA, leading to improved throughput, user fairness, and overall system performance.

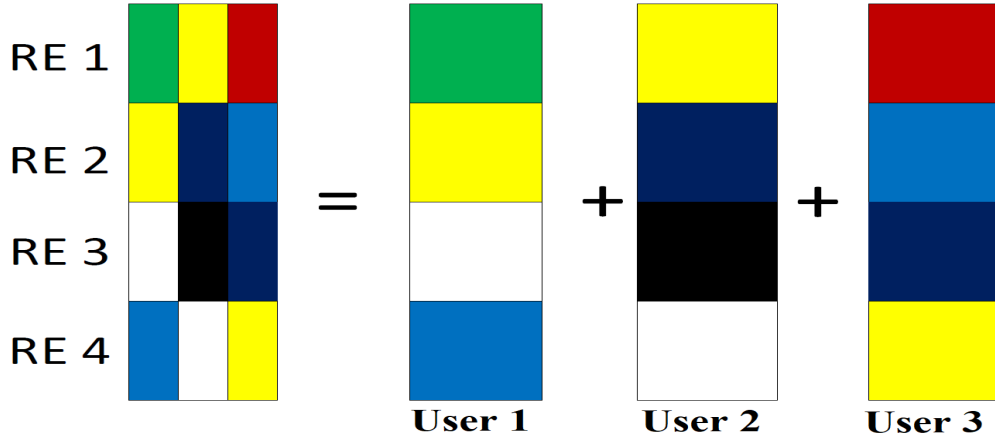


Figure 1. PDMA pattern for three users on 4 Res

Figure 1. shows an example of a PDMA pattern for a network employing a predefined PDMA pattern, in which a single base station (BS) serves three users across two resource elements (REs). Without loss of generality, it is assumed that User 1 utilizes RE1, RE2, and RE3; User 2 accesses RE1, RE2, and RE3; whereas User 3 makes use of all four available REs. To further enhance system efficiency, cooperative communications will be employed, wherein a user located between the base station (BS) and the cell-edge user acts as a relay, forwarding the data intended for the cell-edge user.

Cooperative communication employing relay nodes has demonstrated the potential to enhance both the transmission rate and diversity of wireless networks (Ngo et al., 2009; Narula et al., 1998). However, when all relay nodes function in half-duplex mode, traditional relaying schemes typically require more time compared to direct transmission, as additional time slots are needed for the relays to forward the received signals to their respective destinations.

This paper investigates and compares four downlink transmission schemes in a system comprising a base station (BS), a decode-and-forward (DF) relay, and a far user. These schemes are designed to improve the achievable rate for the far user through a combination of spatial diversity, power-domain multiplexing, and resource element (RE) pattern design. In addition to evaluating the achievable rate, user fairness will also be discussed by introducing a fairness index, which quantifies the users achieved data rates relative to their rates under direct transmission and total data rates transmitted from the base station.

System Model

We consider a downlink transmission scenario in a network comprising a base station (BS), a user acting as a relay (R), and a destination node (D), as illustrated in Figure 2. All transceivers are equipped with single omnidirectional antennas. In this one-way communication setup, the BS transmits following the proposed scheme, while the relay alternates between receiving from the BS and forwarding data to the cell-edge user, following the proposed scheduling scheme. In the first approach (the baseline scheme), the BS communicates directly with the relay and the cell-edge user in two separate time slots. While this method offers a certain degree of spectral efficiency, its overall performance is significantly degraded in the presence of weak channel conditions, and it requires additional transmission time to serve both the relay and the cell-edge user.

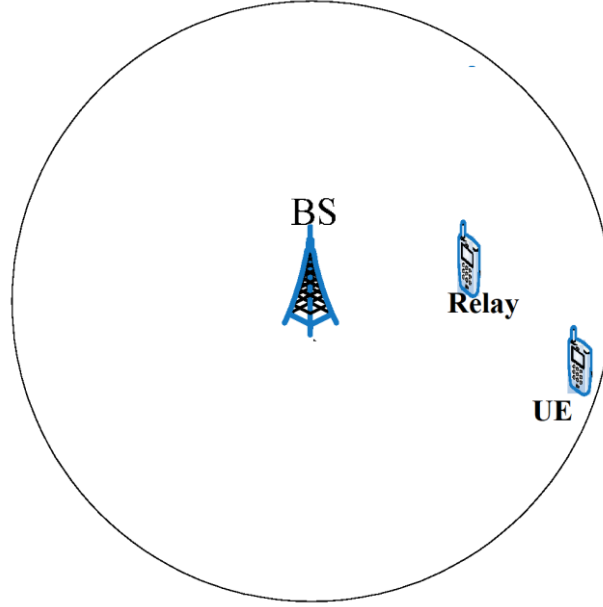


Figure 2. Decode and forward (DF) relay assisted wireless communication

To overcome the limitations of direct transmission in serving cell-edge users with poor channel conditions, cooperative relaying has been widely adopted as an effective strategy. In the decode-and-forward (DF) relaying framework, the communication process is divided into two phases: the base station first transmits data to the relay, which then decodes and re-transmits the signal to the far user. This cooperative strategy enhances link reliability by exploiting spatial diversity, though it introduces a loss in spectral efficiency due to the additional time slots required for relaying. The achievable capacity for the cell-edge user is given by:

$$R_{DF} = \frac{1}{2} \min \{ \log_2 (1 + \text{SNR}_{BR}), \log_2 (1 + \text{SNR}_{RU}) \}$$

Building upon this, non-orthogonal multiple access (NOMA) has been incorporated into relay-assisted systems to improve spectral efficiency by allowing simultaneous transmission to multiple users using power-domain multiplexing. In such configurations, the base station transmits a superimposed signal to both the relay and the far user. In the n th time slot, the BS transmits the signal:

$$s_{BS}(n) = \sqrt{P_T} \cdot (\alpha_1 s_1(n) + \alpha_2 s_2(n))$$

Here, $s_1(n)$ and $s_2(n)$ represent the intended signals for the relay and the cell-edge user, respectively. In this scheme, higher transmission power is allocated to $s_1(n)$, so that $s_2(n)$ to be treated as interference at the relay. However, The relay assists in canceling this interference at the cell-edge user during the second time slot by forwarding it to the cell-edge user. The operation of the proposed Noma relaying scheme is summarized in Table 1.

Table 1. Transmission schedule for relay-assisted NOMA scheme

Time Slot	Transmitter	Recievers	Signal
1	Basestation (BS)	Relay (R), Cell-edge user	$s_{BS}(n) = \sqrt{P_T} \cdot (\alpha_1 s_1(n) + \alpha_2 s_2(n))$
2	Realy (R)	Cell-edge user	$s_2(n)$

The acheivable data rate for the relay after using SIC to cancel $s_2(n)$ in this scheme is given by:

$$\log_2 \left(1 + \frac{|h_1|^2 P_2}{N_0} \right)$$

Where h_1 is the channel coeffiecent between the BS and R, P_2 is the power allocated to the relay. While the acheivable data rate for the cell edge user is given by:

$$\cdot \log_2 \left(1 + \frac{|h_2|^2 P_1}{N_0} \right)$$

It can be noticed that the relay, benefiting from a stronger channel, employs successive interference cancellation (SIC) to decode the far user's message and forwards it in a subsequent time slot. Further enhancement is achieved by enabling both the relay and the far user to apply SIC. In this case, the base station employs superposition coding to transmit a combined signal, while both the relay and cell-edge user decode their respective messages through interference cancellation. The relay then assists the cell-edge user by forwarding its message in the second time slot. This strategy leverages both cooperative and power-domain diversity, improving system performance at the cost of increased receiver complexity. Together, these schemes demonstrate the progressive integration of cooperative and non-orthogonal transmission techniques to support high data rates and reliable communication for users in disadvantaged channel conditions.

To further enhance the efficiency of superposition-based transmission schemes, Pattern Division Multiple Access (PDMA) has emerged as a promising candidate. PDMA extends the concept of non-orthogonal access by exploiting unique transmission patterns across multiple domains such as power, code, and spatial resources. Unlike conventional SC or NOMA, PDMA allows for more flexible user multiplexing through pattern design, which can effectively reduce inter-user interference and improve spectral efficiency. By integrating PDMA with Superposition Coding, the system can leverage both the layered transmission structure of SC and the pattern diversity of PDMA, leading to improved throughput, user fairness, and overall system performance.

Table 2. Transmission schedule for relay-assisted PDMA scheme

Time Slot	Transmitter	Receiver(s)	RE Usage	Signal Flow
1	BS	Relay, Cell-edge user	RE1, RE2	s1(n), s2(n), s3(n)
2	Relay	Cell-edge user	RE1	S2(n)

Table 2 illustrates the operation of the relay-assisted PDMA scheme. In the first time slot, the BS transmits to both the relay and the cell-edge user using two resource elements (REs): s1(n) and s2(n) are superimposed on RE1, while s3(n) is transmitted on RE2 to the cell-edge user. In the second time slot, the relay forwards s2(n) to the cell-edge user. The PDMA pattern matrix for this scheme is expressed as:

$$\mathbf{P} = \begin{bmatrix} 1 & 1 \\ 1 & 0 \end{bmatrix}$$

where the first row corresponds to the cell-edge user access to RE1 and RE2, and the second row indicates the relay's reception on RE1 only. This pattern is designed to ensure that the user benefits from full RE coverage for improved diversity and decoding, while the relay receives selectively to simplify its processing for decode-and-forward operation.

Results and Discussion

In this section, we present a numerical performance evaluation of the proposed PDMA system based on Monte Carlo simulations. The evaluation is carried out by averaging the SNRs and link capacities over 10^5 independent channel realizations for a fixed user position. In the considered scenario, the relay is positioned between the BS and the cell-edge user, such that the channel conditions between the BS and the relay are significantly better than those between the BS and the cell-edge user. We consider the SNR values varying from 0 to 30 dB. It is assumed that the power of the AWGN at both the relay and the cell-edge user is identical, and that the relay transmits with the same power as the BS. Furthermore, we assume that the total transmit power satisfies $P_1 + P_2 = PT$. In both the NOMA and PDMA schemes, the BS's transmit power is allocated such that the relay and the cell-edge user can successfully decode the transmitted signals using successive interference cancellation (SIC). The fairness index is evaluated by comparing the ratio of each user's received capacity to their ideal or target capacity. A fairness index closer to one indicates a more balanced and fair system. A lower fairness index implies that the relay is being favored, whereas a higher fairness index suggests that the BS is allocating more resources in favor of the cell-edge user. In direct transmission, the BS requires two time slots to serve both the relay and the cell-edge user.

The fairness index for this scheme is equal to one, as no specific enhancement is applied to either the relay or the cell-edge user, and both users are allocated one time slot per transmission cycle. In the decode-and-forward relaying scheme, a complete transmission cycle requires three time slots: two time slots for serving the cell-edge user from the relay, and one time slot for the relay to receive data from the BS. In this scheme, due to the improved link to the cell-edge user through the relay, the fairness index exceeded one but we consider it one as it is the maximum value of the fairness index.

The improvement in fairness is attributed to allocating two time slots to the cell-edge user and utilizing a more reliable link compared to direct transmission. For the NOMA and PDMA schemes, additional improvements were made for the cell-edge user by utilizing non-orthogonal transmission technologies. Moreover, the use of a PDMA pattern, which assigns more radio resources to the cell-edge user, further enhances fairness for that user.

Figure 3 shows the SNR values when the BS uses P_t to transmit to only one user. In contrast, in the NOMA and PDMA schemes, the BS superimposes s_1 and s_2 by allocating different power levels to the relay and the cell-edge user based on their respective channel conditions. More power is allocated to the cell-edge user, as it experiences poorer channel conditions, whereas the relay benefits from better channel conditions with both the BS and the cell-edge user.

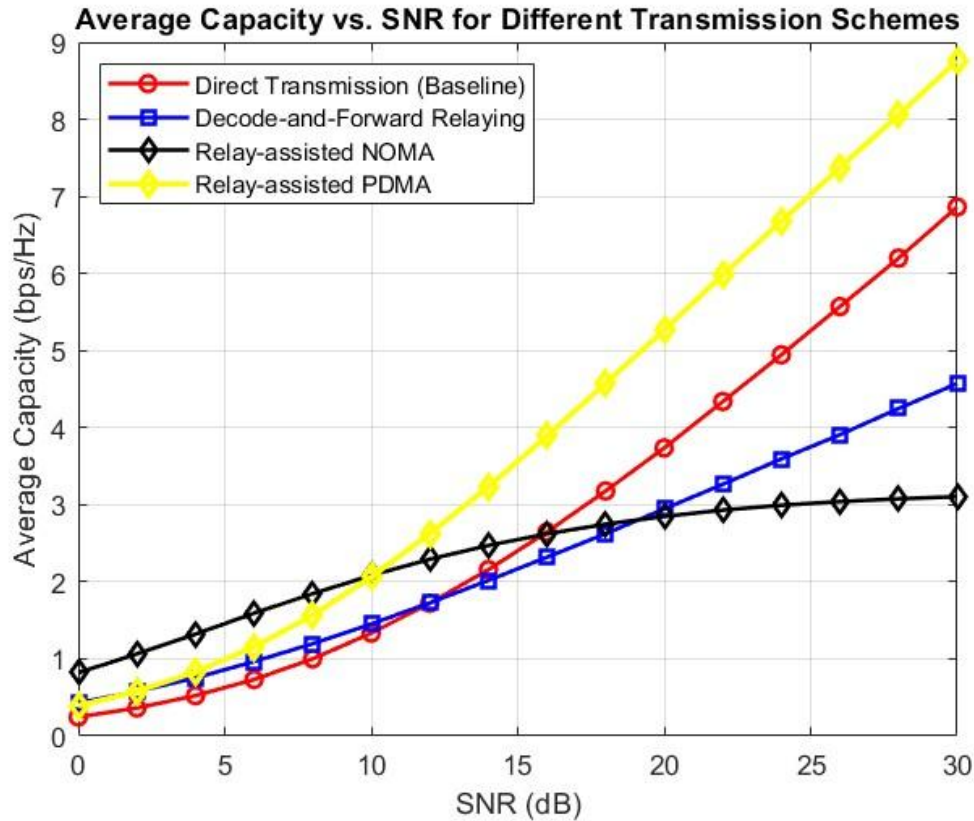


Figure 3. Capacity comparisons of the four different schemes

From Figure 3, the proposed PDMA scheme achieves the highest data rate due to two main factors: (i) the utilization of two radio resources and (ii) the additional gain from the relay. While the relay-assisted NOMA scheme performs well in the low SNR range (0 to 10 dB) and remains acceptable up to around 15 dB, its performance degrades significantly beyond that point. This degradation is primarily due to the interference caused by the superposition of signals in NOMA, specifically, the interference from the data intended for the relay negatively impacts the decoding performance at the cell-edge user.

Conclusion

In this work, we investigate relay-based transmission in a wireless system employing NOMA and PDMA coding schemes. The proposed schemes consist of two key components: (i) signal layering at the source

combined with multiplexed coding at the relay, and (ii) power allocation to facilitate SIC (Successive Interference Cancellation) decoding. While source-layering enables the recovery of only the base layer at the destination via the direct path, multiplexed coding through over-the-air signal superposition allows full utilization of system resources for decoding the intended information at the cell-edge user. Using network average capacity as the performance metric, the proposed PDMA scheme demonstrates excellent performance, comparable to single-relay superposition coding schemes, and effectively mitigates interference caused by relaying. The main advantage of the proposed scheme lies in its ability to enhance bandwidth efficiency by leveraging relay assistance, non-orthogonal multiple access, and PDMA patterning.

Scientific Ethics Declaration

* The authors declare that the scientific ethical and legal responsibility of this article published in EPSTEM Journal belongs to the authors.

Conflict of Interest

* The authors declare that they have no conflicts of interest

Funding

*This study received no external funding.

Acknowledgements or Notes

* This article was presented as an oral presentation at the International Conference on Technology (www.icontechno.net) held in Trabzon/Türkiye on May 01-04, 2025.

* Authors would like to acknowledge Al-Zaytoonah University of Jordan for financially supporting this study.

References

- Alsakarnah, R., & Ilow, J. (2017). Superposition coding in alternate DF relaying systems with inter-relay interference cancellation. *13th International Conference on Wireless and Mobile Computing, Networking and Communications (WiMob)* (pp. 104-109). IEEE.
- Chattha, J., & Uppal, M. (2016). Layered multiplexed-coded relaying in wireless multicast using QAM transmissions. *IEEE Communications Letters*, 20(4), 760-763.
- Chen, S., Ren, B., Gao, Q., Kang, S., Sun, S., & Niu, K. (2016). Pattern division multiple access—A novel nonorthogonal multiple access for fifth-generation radio networks. *IEEE Transactions on Vehicular Technology*, 66(4), 3185-3196.
- Kim, J. B., & Lee, I. H. (2015). Capacity analysis of cooperative relaying systems using non-orthogonal multiple access. *IEEE Communications Letters*, 19(11), 1949-1952.
- Kim, J. B., & Lee, I. H. (2015). Capacity analysis of cooperative relaying systems using non-orthogonal multiple access. *IEEE Communications Letters*, 19(11), 1949-1952.
- Liu, K. J. R., A. K. Sadek, A. K., Su, W., & Kwasinski, A. (2009). *Cooperative communications and networking*. New York, NY: Cambridge University Press.
- Narula, A., Lopez, M. J., Trott, M. D., & Wornell, G. W. (1998). Efficient use of side information in multiple-antenna data transmission over fading channels. *IEEE Journal on Selected Areas in Communications*, 16(8), 1423-1436.
- Ngo, D. T., Tellambura, C., & Nguyen, H. H. (2009, January). Efficient resource allocation for OFDMA multicast systems with fairness consideration. *IEEE Radio and Wireless Symposium* (pp. 392-395). IEEE.
- Silva, M., Correia, A., Dinis, R., Souto, N., & Silva, J. C. (2010). *Transmission techniques for emergent multicast and broadcast systems*. CRC Taylor & Francis Group.

Sundaresan, K., & Rangarajan, S. (2014). Cooperation versus multiplexing: Multicast scheduling algorithms for OFDMA relay networks. *IEEE/ACM Transactions on Networking*, 22(3), 756–769.

Author(s) Information

Rashed Alsakarnah

Al-Zaytoonah University of Jordan

Amman, Jordan

Contact e-mail: r.alsakarnah@zu.edu.jo

Mohammad Masoud

Al-Zaytoonah University of Jordan

Amman Jordan

Shaher Slehat

Al-Zaytoonah University of Jordan

Amman, Jordan

To cite this article:

Alsakarnah, R., Masoud, M., & Slehat, S., (2025). Relay-aided PDMA with dynamic power control for cell-edge user fairness. *The Eurasia Proceedings of Science, Technology, Engineering and Mathematics (EPSTEM)*, 33, 73-79.

The Eurasia Proceedings of Science, Technology, Engineering and Mathematics (EPSTEM), 2025

Volume 33, Pages 80-95

IconTech 2025: International Conference on Technology

Emerging Trends in Volatility Forecasting Using Machine Learning: A Bibliometric Analysis

Beste Alpaslan

OSTIM Technical University

Abstract: Volatility forecasting remains a cornerstone of financial economics, offering critical insights into risk management, asset valuation, and investment strategy development. With the increasing complexity of financial markets, machine learning (ML) and deep learning (DL) techniques have significantly influenced the way volatility in financial time series is modeled and analyzed. This study presents a bibliometric analysis of academic publications from 2000 to 2025 that explore the use of ML and DL techniques within the context of volatility forecasting. The analysis is based on data extracted from the Web of Science database, a leading source of reliable and comprehensive scholarly literature in this field. The study analyzes the methodological development of models, such as Long Short-Term Memory (LSTM) networks, Support Vector Machines (SVM), and other ML-based models, which stand out for their capacity to model the complex and nonlinear dynamics of financial time series. In recent years, hybrid modeling strategies, based on the integration of traditional statistical methods with artificial intelligence algorithms, have emerged as prominent approaches in volatility forecasting. The study also highlights emerging trends, such as the use of transformer architectures and meta-learning strategies in high-frequency trading markets and cryptocurrency markets, where volatility is especially pronounced. Comparative analyses across different asset types and timeframes offer a comprehensive framework for understanding how these models perform under various financial conditions. The analysis conducted in this study critically examines the evolving paradigms of volatility forecasting, tracking methodological innovations and scientific developments. In doing so, it underscores the potential of ML and DL techniques to enhance forecasting accuracy, with an expectation that advancements in this field will guide future research directions. The insights derived from the findings not only contribute to the existing academic literature but also facilitate a more effective visualization of the structural dynamics of the literature, analyzed through the VOSviewer software.

Keywords: Volatility forecasting, Machine learning, LTSM, SVM, Financial time series

Introduction

Due to their inherent structure, financial markets are prone to high levels of volatility, which becomes particularly evident during periods of economic crises and market shocks. Volatility during such periods has the potential to significantly influence investor behavior and market dynamics (Schwert, 1989). As volatility forecasting plays an active role in financial decision-making processes, it relies on a robust framework composed of multiple components. The primary purposes of such forecasting include risk management, derivative pricing, investment strategy development, and portfolio optimization (Andersen et al., 2006; Poon & Granger, 2003). With the increasingly dynamic structure of financial markets, traditional econometric models—such as ARCH and GARCH—have become insufficient in capturing the nonlinear and complex patterns inherent in financial time series (Bollerslev, 1986; Engle, 1982).

In recent years, rapid advancements in technology have led to a transformative shift in forecasting financial time series through the integration of ML and DL techniques. These data-driven approaches play an effective role in

- This is an Open Access article distributed under the terms of the Creative Commons Attribution-Noncommercial 4.0 Unported License, permitting all non-commercial use, distribution, and reproduction in any medium, provided the original work is properly cited.

- Selection and peer-review under responsibility of the Organizing Committee of the Conference

© 2025 Published by ISRES Publishing: www.isres.org

identifying the intricate features of market volatility. In particular, algorithms such as LSTM and SVM have gained prominence due to their high performance in pattern recognition and time series learning (Fischer & Krauss, 2018; Zhang et al., 2017). As the application of these algorithms expands within the finance domain, a methodological transition from traditional statistical models to AI-supported frameworks has been increasingly observed.

This study provides a bibliometric analysis of academic publications (2000–2025) that apply ML and DL techniques to volatility forecasting models. The dataset used in this research was retrieved from the Web of Science database, one of the most comprehensive sources in the field. The analysis indicates a growing emphasis on the application of advanced AI techniques—such as meta-learning strategies—especially during periods of heightened volatility in high-frequency trading and cryptocurrency markets. Additionally, hybrid approaches combining ML methods with conventional econometric models have been investigated, highlighting their respective advantages (Kim et al., 2024). By visualizing the structural dynamics of the literature through the VOSviewer software, this research enhances comprehension of the academic landscape. Accordingly, by critically evaluating methodological trends, the study reveals that ML and DL approaches offer superior performance in volatility forecasting and shed light on the evolution of innovation in the field.

Literature

The concept of ML was first introduced in 1959 by computer scientist Arthur Samuel. According to Samuel's definition, ML is a scientific field that enables computers to perform specific tasks by systematically learning and improving their performance over time. This approach allows systems to learn from their own experiences and make decisions accordingly without being explicitly programmed, thus differing from the traditional understanding of software development (Samuel, 1959). ML is methodologically grounded within subfields of mathematics, particularly probability theory, statistics, and optimization. In this context, models developed using ML are capable of learning specific patterns from historical data and making future predictions based on these patterns. In contrast, classical software development processes require the programmer to identify data-based patterns through observation and code them manually. However, since these methods rely heavily on the individual judgment of the programmer, they tend to be unsystematic and often fail to accurately reflect real-world conditions (Grigorev, 2020). ML is now widely used in many fields where uncertainty is high and conventional methods prove inadequate. In this regard, notable application areas include the classification of diseases with overlapping symptoms, forecasting stock market movements under volatile conditions, filtering spam emails, and predicting future travel preferences based on customer experience (Keles et al., 2020).

The frequent fluctuations observed in financial markets and the growing economic uncertainty on a global scale have significantly increased the demand for accurate, timely, and reliable market forecasts by both financial institutions and individual or institutional investors. In the literature, it is observed that traditional methods used in volatility forecasting remain limited in handling complex and dynamic datasets. Specifically, the inability of linear models to adequately represent stock market data has led to the insufficiency of conventional analytical methods, which in turn has made the application of artificial intelligence, ML and DL techniques to such data increasingly widespread and effective (Egeli et al., 2003). In one study, based on economic and financial factors affecting the BIST-50 index, ML algorithms and artificial neural networks were employed, and stock performance was classified accordingly (Filiz et al., 2017). Sahin (2023) analyzed market volatility using both GARCH-type models and artificial neural networks (ANN), and determined that hybrid models produced more accurate results than classical ones. Aksehir and Kılıc (2019), in their study on stock index prediction, achieved successful results in forecasting bank stock prices using methods such as regression, random forest, and decision trees.

Akusta (2023) applied a machine learning-based method to monitor Bitcoin price movements and perform price forecasting. The findings indicated that this approach contributed to more rational investment decisions and risk reduction while enabling more effective monitoring of price movements in cryptocurrency markets. Moreover, this study provided an important framework regarding the potential impact of ML methods in financial markets, particularly in Bitcoin price forecasting. Sonmez and Arslan (2024), taking into account the complex and volatile structure of stock indices, used LSTM networks instead of traditional methods and achieved effective results in index forecasting by successfully modeling long-term relationships in time series. Ozcan (2023) asserted that ML methods were the most effective approach for predicting future movements in stock indices and securities markets using past data. His study compared nine different ML algorithms applied to the BIST100 index and evaluated their performance in predicting increases and decreases in the index. The findings revealed that linear methods yielded more accurate results compared to others. In their study on forecasting the

BIST100 index, Akbulut and Adem (2023) concluded that the LSTM model was an effective and successful method. Urgenc (2023) aimed to predict change points in Bitcoin prices using ML methods and comparatively evaluated their forecasting performance. Oncu (2022) assessed the applicability of ML methods in predicting the price trends of carbon futures based on carbon emissions. Based on the findings, given the increasing economic and environmental importance of carbon markets, data-driven models were applied to improve the accuracy of price forecasting. The results suggested that ML algorithms could model the complex structural characteristics of carbon contracts and contribute to risk management and strategic decision-making processes for market participants. In Ceyhan's (2023) study, it was determined that ML and DL methods were predominantly used in predicting future prices of financial assets, identifying financial risks, and optimizing portfolios. The analysis revealed that, in most cases, the performance of multiple algorithms was compared to determine the most efficient one.

In a study conducted by Colak (2025), a deep learning-based model was used to analyze stock price forecasts for Nike (NKE). The findings indicated that LSTM and GRU models produced reliable results in long-term analyses of financial time series. In another study, the predictability of the BIST100 index was measured using the LSTM model—one of the DL methods with high learning capacity—and the results showed that LSTM outperformed classical models, particularly in capturing nonlinear structures (Abizada, 2024). In their study, Gur and Esidir (2023) conducted a comparative analysis using DL, ML and ensemble learning methods to forecast the future values of scrap steel imports in Turkey. Their findings showed that LSTM achieved the highest success in learning long-term dependencies. Budak (2023), aiming to forecast the prices of financial instruments during global market crises, utilized ML algorithms—one of the emerging data science technologies—for price forecasting. A review of the related literature reveals that researchers such as Sarkar and Ali (2022), Wijayanti and Taufik (2022), Bhuriya et al. (2017), Lin et al. (2013), and Nuchitprasitchai et al. (2023) have utilized ML algorithms for forecasting a wide range of financial instruments. Their findings indicated that even in the presence of complex data structures, AI-based linear models demonstrated high forecasting performance. Eylasov and Cicek (2024), in their study on cryptocurrency price forecasting, compared ARIMA-GARCH and LSTM methods and evaluated the most effective forecasting approaches. In another study, SVM have been widely adopted for financial volatility modeling due to their robustness in handling nonlinear patterns (Gavrishchaka & Banerjee, 2006). Chen et al. (2010) demonstrated that SVM, as an advanced alternative to traditional artificial neural networks (ANN), have gained increasing attention in financial forecasting applications. In their study, SVM was applied within a volatility forecasting framework and evaluated using both simulated data and real-world datasets, including daily GBP exchange rates and the NYSE stock index. In their 2009 study, Tang et al. addressed the limitation of standard SVM kernels in capturing volatility clustering by developing a multidimensional wavelet kernel function. Their findings confirmed the effectiveness of the wavelet support vector machine (WSVM) in forecasting stock market volatility using both simulated and real-world data.

Method

The aim of this study is to conduct a comprehensive bibliometric analysis of the academic literature on volatility forecasting using ML and DL techniques, based on publications from the years 2000 to 2025. The research utilizes bibliographic data retrieved from the Web of Science database and aims to identify major publication trends, leading authors and institutions, frequently co-occurring keywords, and methodological developments within the field. The bibliometric analysis method employed in this study refers to the quantitative evaluation of scholarly publications related to a specific academic domain by analyzing various bibliographic indicators—such as authorship, countries of publication, keywords, institutional affiliations, citation counts, publication years, and source journals—using mathematical and statistical techniques (Pritchard, 1969).

Findings and Discussion

Publications related to volatility were examined by searching relevant keywords in the Web of Science database for the period between 2000 and 2025. The search was conducted using the Keywords Plus feature, with the Boolean combination of terms as follows: “Volatility Forecasting” OR “Volatility Modeling” AND “Machine Learning” OR “Deep Learning” OR “LSTM” OR “SVM” AND “Financial Time Series”.

This approach was adopted to capture a broad yet focused set of studies at the intersection of volatility analysis and emerging computational techniques. Accordingly, a total of 2,278 publications were identified during the specified years. The annual distribution of these publications is presented in Table 1.

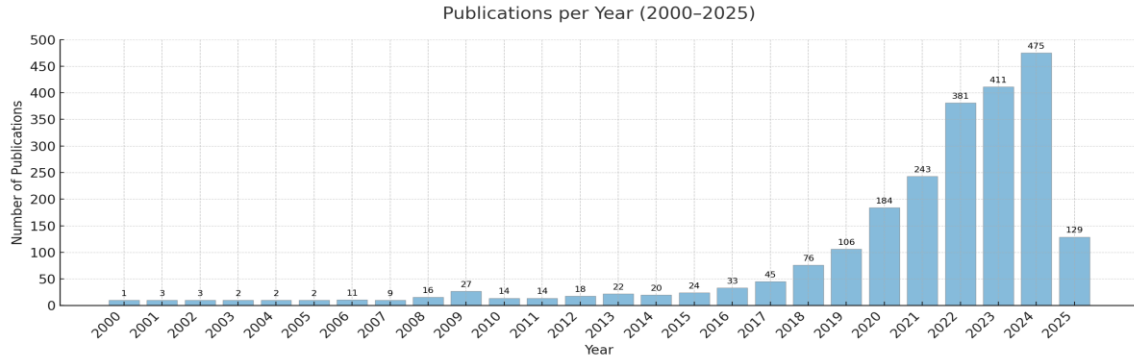


Figure 1. Publications per year (2000-2025)

As shown in Figure 1, the number of publications started to increase from 2006 onward, with the highest number recorded in 2024. Since only a certain period of 2025 was included in the analysis, it is anticipated that related studies in the field will continue to increase in the coming years based on the trend observed in previous years. In recent years, ML and DL techniques have emerged as prominent topics in financial forecasting. Among these techniques, models such as LSTM networks and SVM have attracted attention due to their ability to model nonlinear and complex patterns in financial time series data. As a result, these methods are increasingly applied to volatility forecasting, reflecting their growing importance as trending topics in academic literature and practical financial applications.

Table 1. Publications per year (2000-2025)

Years	Count	Years	Count	Years	Count
2000	1	2010	14	2020	184
2001	3	2011	14	2021	243
2002	3	2012	18	2022	381
2003	2	2013	22	2023	411
2004	2	2014	20	2024	475
2005	2	2015	24	2025	129
2006	11	2016	33		
2007	9	2017	45		
2008	16	2018	76		
2009	27	2019	106		

Based on the data obtained from the analyzed publications, the authors with the highest number of publications and their respective counts are presented in Figure 2. According to the results, Zhang, Yaojie stands out as the most prolific author with 25 publications, indicating the author's active involvement in the research field. Other prominent researchers include Ma, Feng (22 publications), Ting, Daniel S. W. (16 publications), Wang, Yiyi (15 publications), Karniadakis, George Em (14 publications), Liang, Chao (13 publications), and Gupta, Rangan (11 publications). Additionally, Wong, Tien Yin (8 publications), Feng, Xin-Long (7 publications), and Wei, Yu (7 publications) have also made notable contributions to the literature.

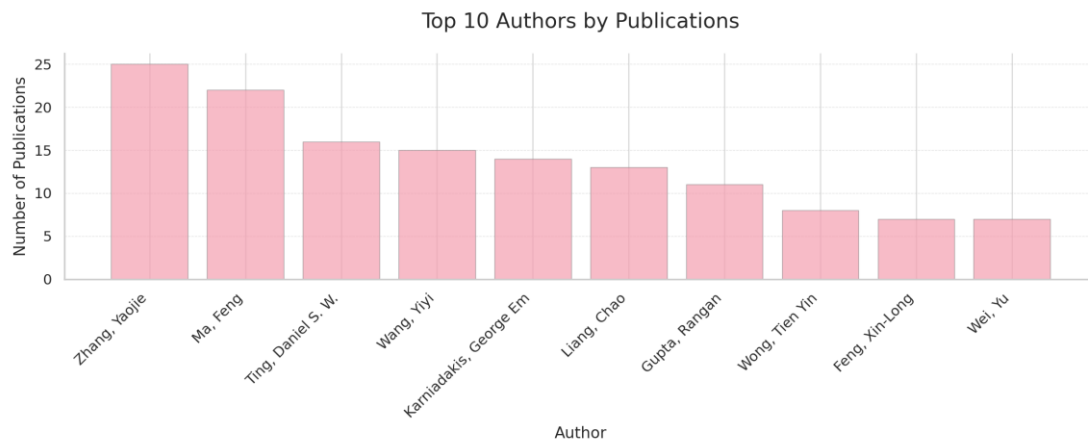


Figure 2. Top 10 authors by publications

The distribution of the total 2,278 publications examined from the Web of Science database by document type is presented in Figure 3. According to this distribution, original research articles constitute the dominant publication type, accounting for 78.3% of the total. These are followed by review articles (13.8%) and conference papers (4.6%). Additionally, early access publications make up 1.5%, book chapters 0.8%, and editorial materials 0.7%. The dataset also includes a small proportion of retracted publications (0.1%) and books (0.1%). This distribution indicates that the relevant research field is largely shaped by original research articles, while review studies occupy a secondary position.

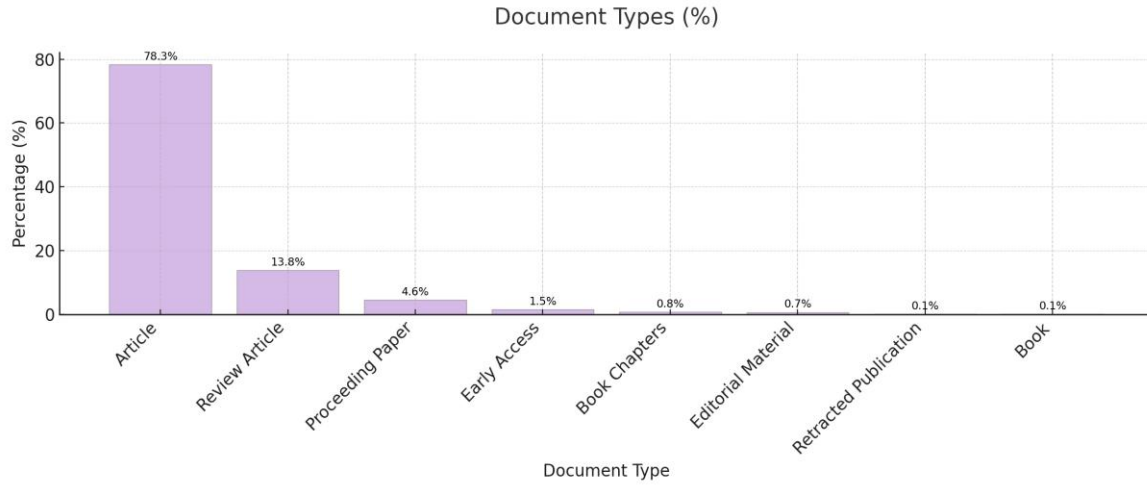


Figure 3. Types of data analyzed

As a result of the analysis conducted in this study, the distribution of the relevant literature by subject categories is presented in Figure 4. Accordingly, the majority of the studies were conducted in the field of Electrical and Electronic Engineering. This is followed by categories such as Economics, Computer Science—Information Systems, and Artificial Intelligence. In addition, a considerable number of publications were observed in areas like Business and Finance, Telecommunications, Computer Science—Interdisciplinary Applications, and Computer Science—Theory and Methods. Based on the figure, it was found that studies combining ML and financial applications are relatively prominent. The results of the distribution suggest that the research has evolved toward an interdisciplinary direction focused on technology, economics, and computer science. In particular, the concentration of studies in the fields of artificial intelligence and information systems indicates that research trends are increasingly shaped around themes of digitalization and automation.

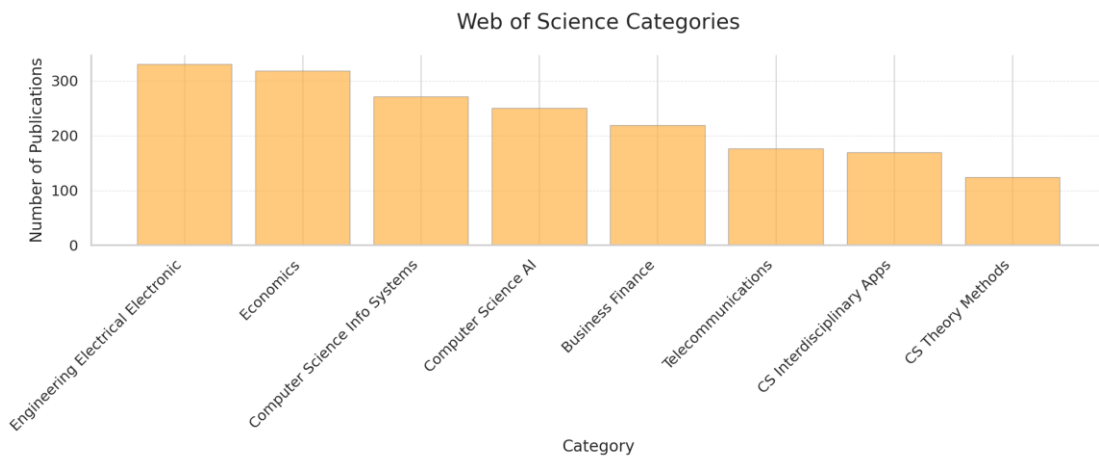


Figure 4. Categories of analyzed publications

Considering the research outputs, the country-wise distribution of the analyzed publications is presented in Figure 5. The analysis reveals that China ranks first with 864 publications, followed by the United States with 478 publications, and India in third place with 188 publications. The significantly higher number of publications from China and the U.S. indicates a strong academic interest in this research field within these countries. Other major contributors include the United Kingdom (144 publications), Australia (113 publications), and Germany

(104 publications), suggesting a broad geographical distribution of research activity. Additionally, South Korea (102 publications) and Canada (87 publications) have also demonstrated notable contributions, reflecting substantial interest in the field. This distribution highlights that countries from Asia, North America, and Europe have played a prominent role in the scientific output, suggesting that the research area has garnered global attention and is the focus of active academic work across diverse regions.

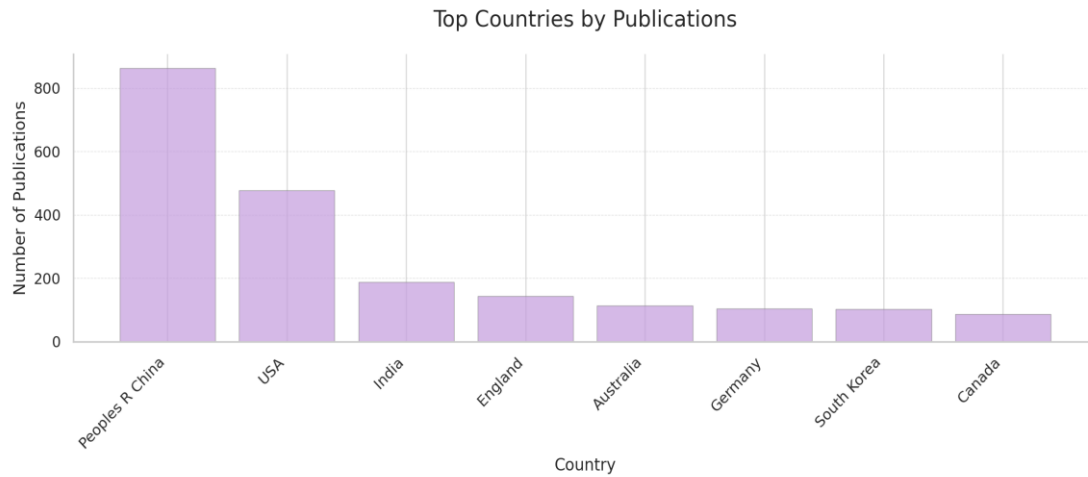


Figure 5. Distribution of analyzed publications by country

Based on the data presented in Figure 6, the top 10 institutions contributing most significantly to the research field are ranked by the number of publications. Leading the list is the Chinese Academy of Sciences (CAS) with 61 publications, followed by Southwest Jiaotong University with 56. Institutions such as the University of California System (45 publications) and Nanjing University of Science and Technology (41 publications) are at the forefront of both theoretical and applied research. These are followed by prominent Asian universities including Shanghai Jiao Tong University (35), National University of Singapore (34), University of Chinese Academy of Sciences CAS (34), and Zhejiang University (34). Tsinghua University (32) and, notably, Harvard University (29) — recognized for its global influence and prestige — also stand out in this ranking.

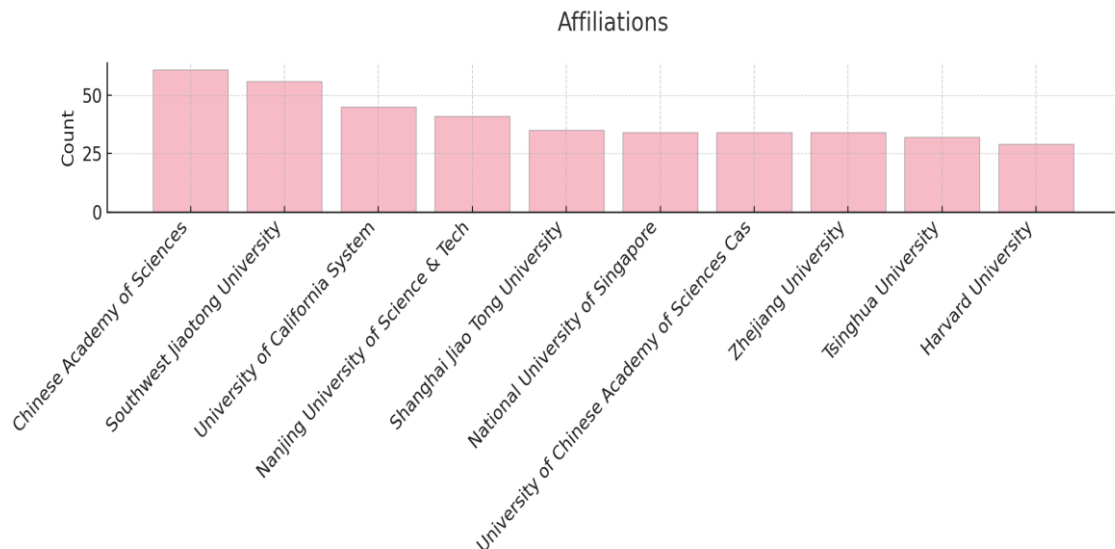


Figure 6. Leading 10 institutions contributing to the literature

According to the findings presented in Figure 7, computer science (675) and engineering (586) emerge as the disciplines contributing the most to the literature. Business and economics (460) highlight the impact of ML in financial applications, followed by mathematics (189) and physics (176). The inclusion of fields such as telecommunications (176), mechanical engineering (95), and medical imaging (71) indicates that the study has a multidisciplinary structure and spans a broad range of areas.

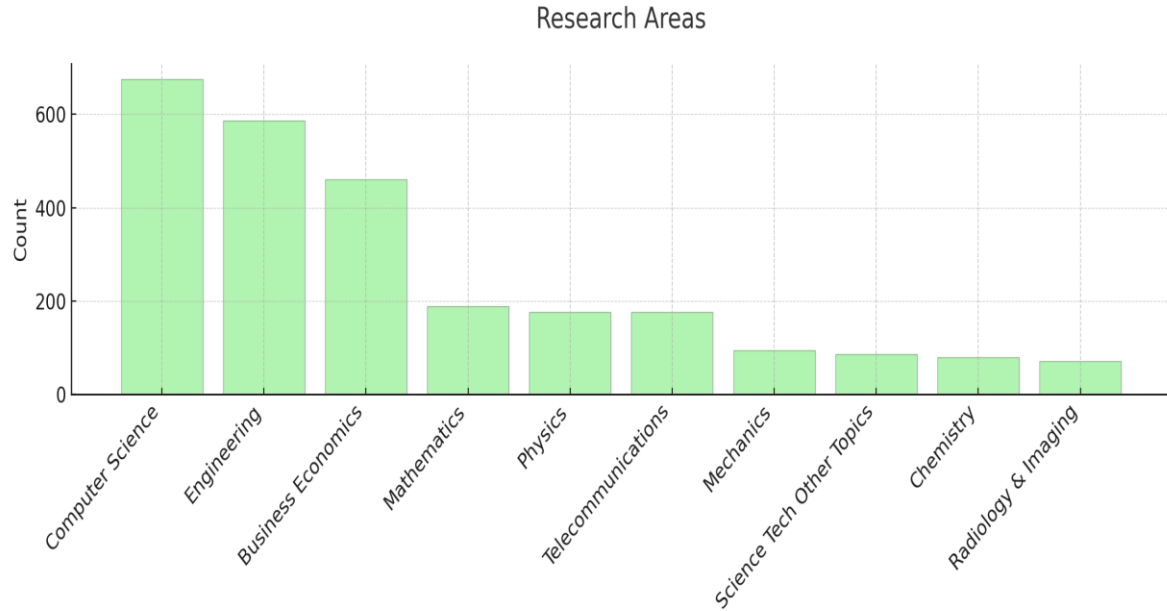


Figure 7. Distribution of research areas in the relevant literature

Based on the observations from the literature review, the mid-level (meso) distribution of citation topics shows that the literature predominantly focuses on areas such as economics (579), artificial intelligence and ML (255), and modeling and simulation (255), as shown in Figure 8. Additionally, the inclusion of topics like image processing, telecommunications, engineering, and health-related subjects indicates that the research has a multidisciplinary nature.

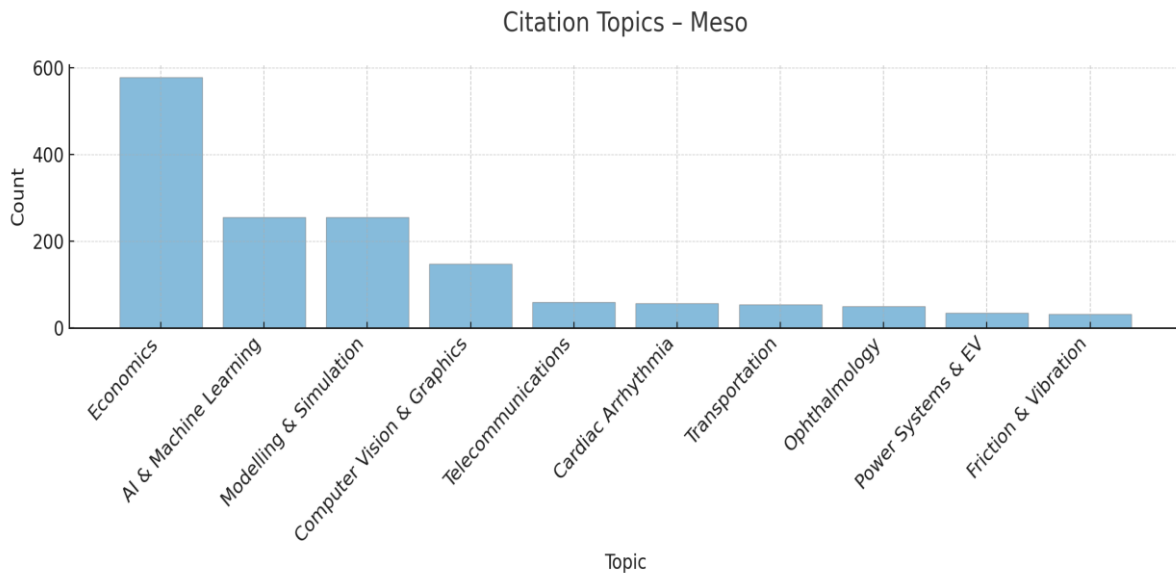


Figure 8. Citation topics at the meso level

In the second part of the methodology, bibliometric maps—such as keyword co-occurrence, author collaboration, and country-based publication networks—were created using VOSviewer software as part of the bibliometric analysis method. In this context, visualizations based on the frequency of keywords and cluster analysis were conducted. In addition to these network analyses, raw publication data (e.g., number of publications by year, document types, institutional distribution, etc.) presented in the first part of the methodology were processed and visualized using the Python programming language (version 3.10). In this section, a comprehensive analysis is planned by evaluating content maps based on VOSviewer in conjunction with Python-based statistical distribution graphs. Based on the data presented in Table 2, the most frequently used keywords in the literature are identified according to the results of the relevant research.

Table 2. The most frequently used keywords in the literature

Keyword	Occurrences	Total link strength
Deep Learning	437	1254
Machine Learning	226	785
Artificial Intelligence	202	634
Feature Extraction	64	453
Training	35	274
Data Models	26	261
Intrusion Detection	53	230
Neural Networks	51	196
Anomaly Detection	32	176
Internet of Things	34	172
Convolutional Neural Networks	30	169
Network Security	26	167
Classification	42	159
Computational Modeling	17	155
Intrusion Detection	31	140
Convolutional Neural Network	56	135
Security	17	125
Predictive Models	13	120
Accuracy	11	112
Feature Selection	25	105

In this study, the keyword analysis conducted using VOSviewer software presents the development and connection intensity of keywords over time in Figure 9. This visualization illustrates how the connection intensity and frequency of each keyword have changed over time, showing the evolution of the most frequently used keywords. On the other hand, the intensity of keywords is further detailed in Figure 10. In this visualization, the connection intensity and frequency of keywords are highlighted through color tones, with keywords that exhibit stronger relationships and higher levels of focus being emphasized more intensely and distinctly. The goal of this visualization is to identify thematic clusters within the research field and determine the most interactive topics in the literature.

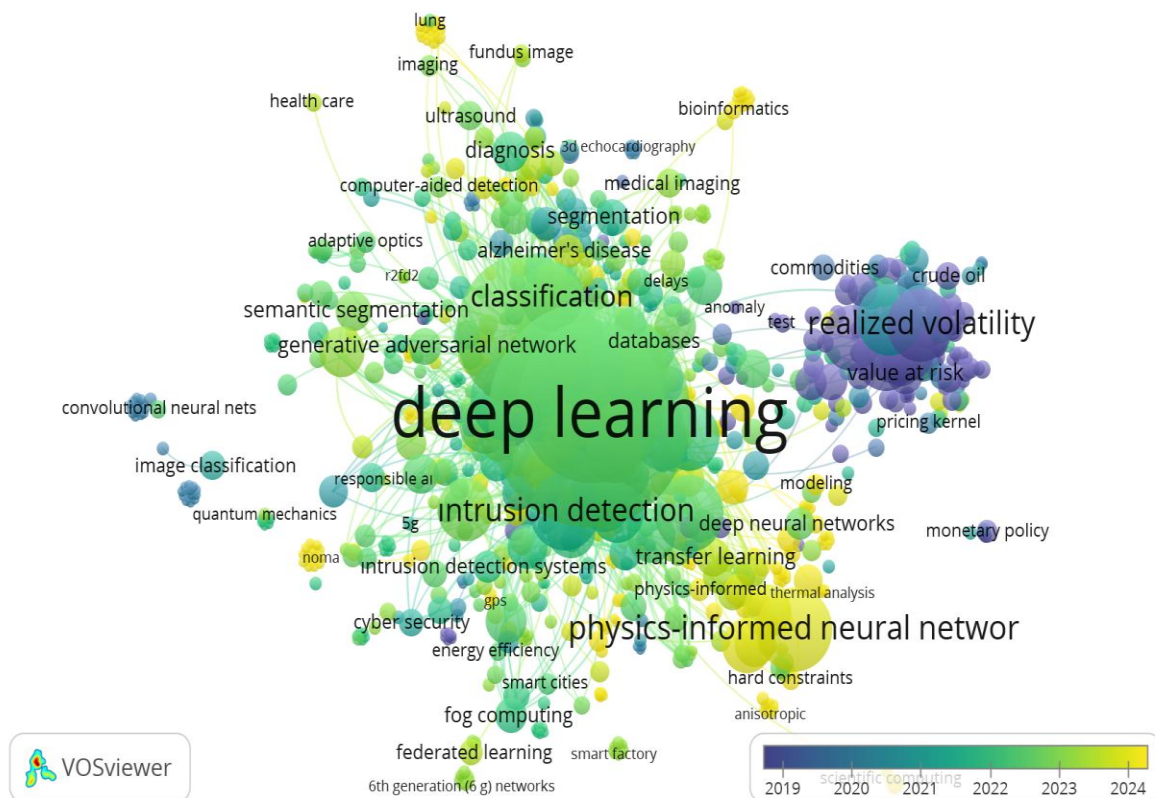


Figure 9. Keyword co-occurrence visualization (VOSviewer output)

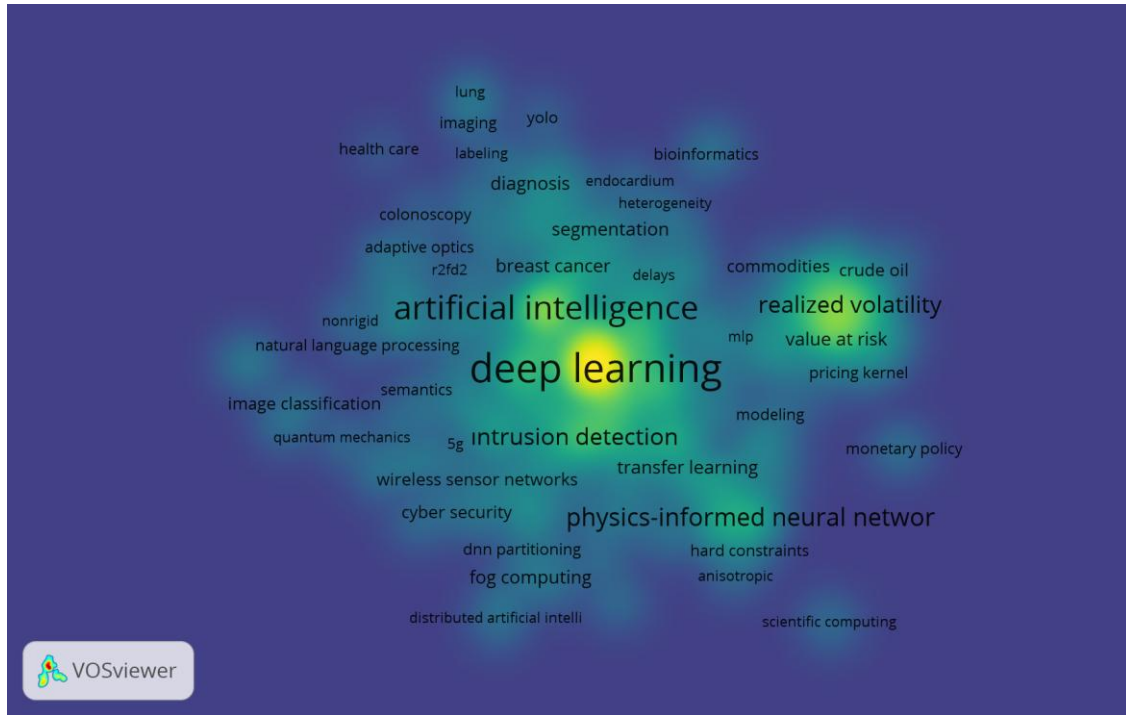


Figure 10. VOSviewer density visualization of most frequent keywords

Based on the data presented in Table 3, the co-authorship network between authors, derived from the author collaboration analysis conducted using the VOSviewer database, is provided. As a result of this analysis, the number of publications authored by each researcher, the citation count received, and the total link strength values with other relevant authors were calculated.

Table 3. Co-authorship and impact indicators of leading authors

Author	Documents	Citations	Total link strength
Zhang, Yaojie	25	1092	49
Li, Huating	3	93	47
Wong, Tien Yin	6	78	42
Park, Yongkeun	2	71	38
Sheng, Bin	4	138	37
Tan, Gavin Siew Wei	3	22	36
Guan, Zhouyu	2	92	34
Jia, Weiping	2	92	34
Bee, Yong Mong	2	24	31
Li, Fei	3	21	31
Lim, Lee-ling	2	24	31
Sabanayagam, Charumathi	2	24	31
Chikama, Tai-ichiro	2	1	30
Kato, Naoko	2	1	30
Kitaguchi, Yoshiyuki	2	1	30
Lim, Gilbert	4	186	30
Maehara, Hiroki	2	1	30
Miyazaki, Dai	2	1	30
Nejima, Ryohei	2	1	30
Oda, Masahiro	2	1	30

In Figure 11, the network structure obtained visually represents both the individual scientific productivity and the interaction strength of authors within the network. Through this network structure, pioneering authors in the literature are assessed alongside bibliometric indicators such as the number of publications, citation counts, and total link strength. The density visualization in Figure 12 highlights the identification of the most influential authors and the dense collaboration clusters in the literature. In this context, the brightness levels on the map are defined according to the authors' publication counts, citations received, and total link strength, thereby clearly illustrating the academic focal points with the highest interaction in the literature.

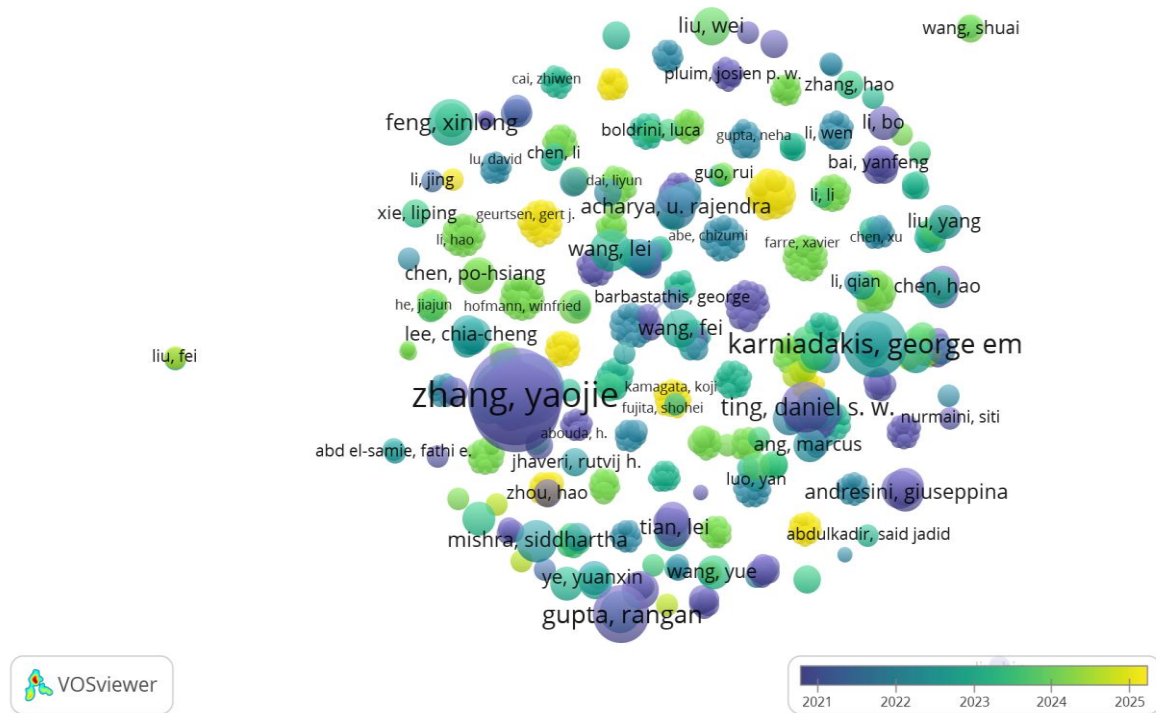


Figure 11. Overlay visualization of author collaboration network (VOSviewer output)



Figure 12. Density visualization of author collaboration network (VOSviewer output)

Based on the bibliometric analysis, the institutions that have made the most significant contributions to the field, according to the number of publications, citation levels, and total link strength, are presented in Table 4. The evaluation shows that the Chinese Academy of Sciences and the University of Chinese Academy of Sciences stand out, while institutions such as MIT, Brown University, and Monash University, despite having fewer publications, create a substantial impact through high citation levels.

Table 4. Organizational-level bibliometric indicators

Organization	Documents	Citations	Total link strength
Chinese Acad Sci	49	1509	109
Univ Chinese Acad Sci	34	1229	101
Hong Kong Polytech Univ	27	643	91
Singapore Natl Eye Ctr	14	343	85
Natl Univ Singapore	21	760	83
Nanjing Univ Sci & Technol	41	1778	73
Shanghai Jiao Tong Univ	33	821	71
Southwest Jiaotong Univ	54	2058	70
Sun Yat Sen Univ	18	343	69
Chinese Univ Hong Kong	15	210	67
Mit	22	1051	65
Tsinghua Univ	30	534	64
Duke Nus Med Sch	9	368	61
Asia Univ	7	238	56
Wuhan Univ	19	712	50
Monash Univ	17	329	47
Zhejiang Univ	34	301	47
Univ Miami	6	247	45
Brown Univ	23	2847	43
Deakin Univ	11	398	43

According to Figure 13, which illustrates the institutional collaboration network, institutions are color-coded based on the number of publications, citations received, and total link strength, with the periods of most intense collaboration highlighted through distinct tones. Based on the data presented in Table 4, Brown University emerges as the institution with the highest number of citations. The corresponding density map, displayed in Figure 14, emphasizes the points of academic interaction between institutions through color intensity, where brighter regions indicate institutions characterized by both high productivity and strong collaborative linkages. According to this visualization, the highest concentration is observed for Brown University, followed closely by Southwest Jiaotong University.

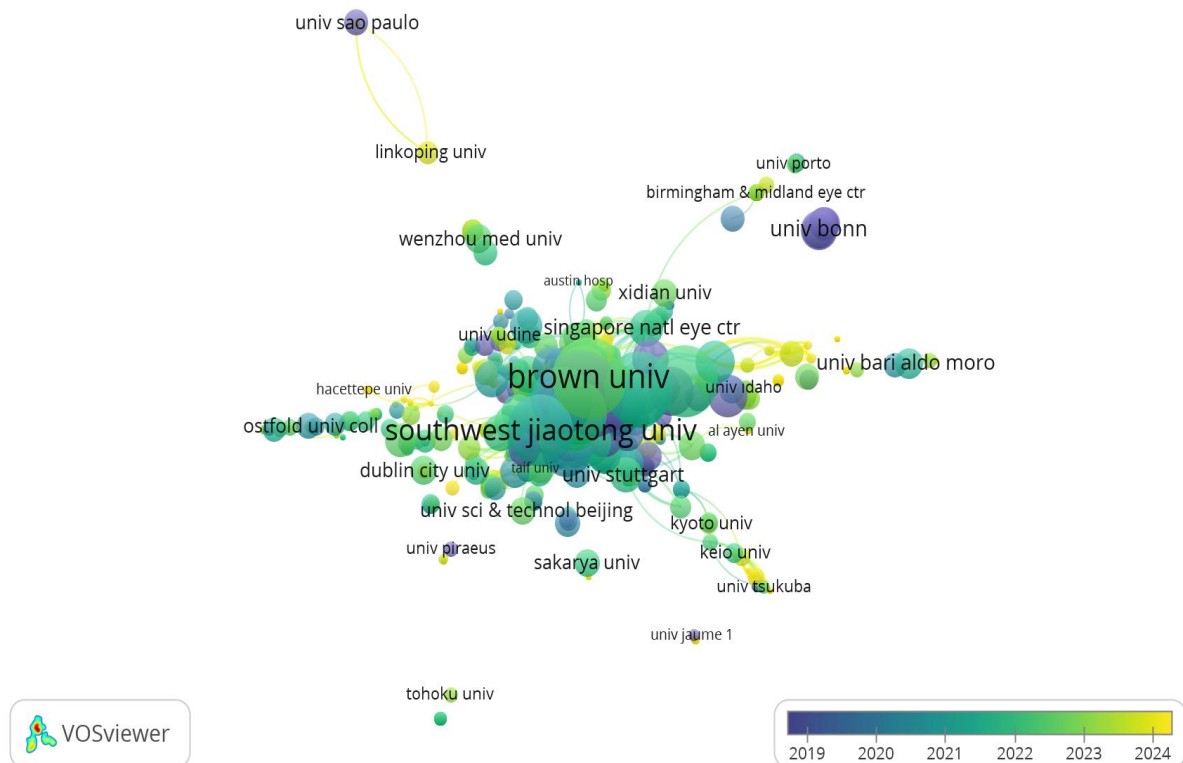


Figure 13. Overlay visualization of institutional collaboration network

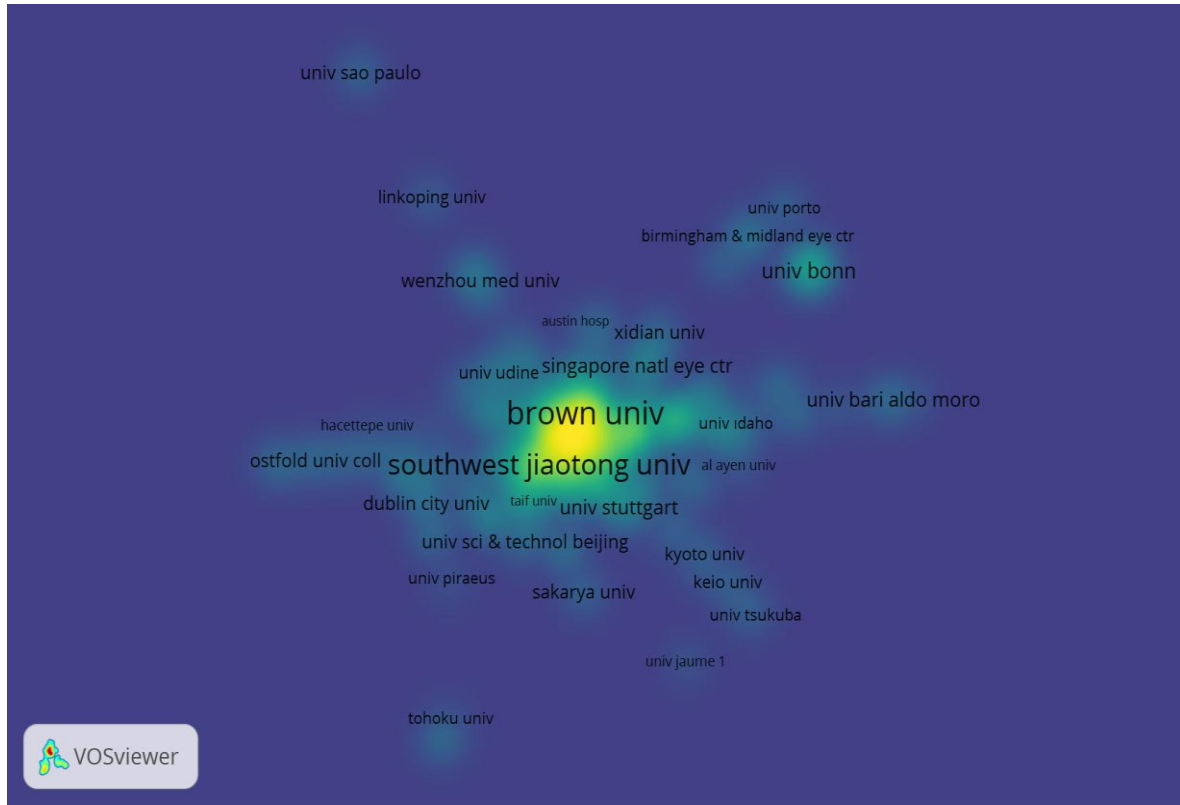


Figure 14. Density visualization of institutional co-authorship

Table 5. Top contributing countries by documents, citations, and total link strength

Country	Documents	Citations	Total link strength
Usa	473	24541	393
Peoples R China	853	18099	353
Australia	111	3628	193
England	143	6509	193
Canada	85	4124	145
Italy	81	1814	132
Germany	104	2724	121
France	66	2473	111
India	186	2389	111
Singapore	52	1909	100
Spain	66	1028	99
Saudi Arabia	53	941	96
South Korea	100	1682	81
Netherlands	37	1464	70
Pakistan	33	562	67
Taiwan	62	962	66
Switzerland	36	1278	65
Malaysia	36	549	60
Iran	32	883	52
Sweden	24	378	51

The bibliometric analysis conducted on the reviewed literature presents key findings at the country level in Table 5, highlighting scientific productivity, citation impact, and collaboration strength. Within this framework, China and the United States stand out with high publication volumes and citation metrics, while the United Kingdom, Australia, Canada, and several European countries also emerge as prominent actors within the collaboration network. Based on the findings, the temporal distribution of international scientific collaborations is illustrated through color mapping in Figure 15. Furthermore, Figure 16 displays a density map emphasizing the countries with the highest levels of interaction and collaboration clusters, where brighter areas represent nations with strong link strength and significant academic influence within the field.

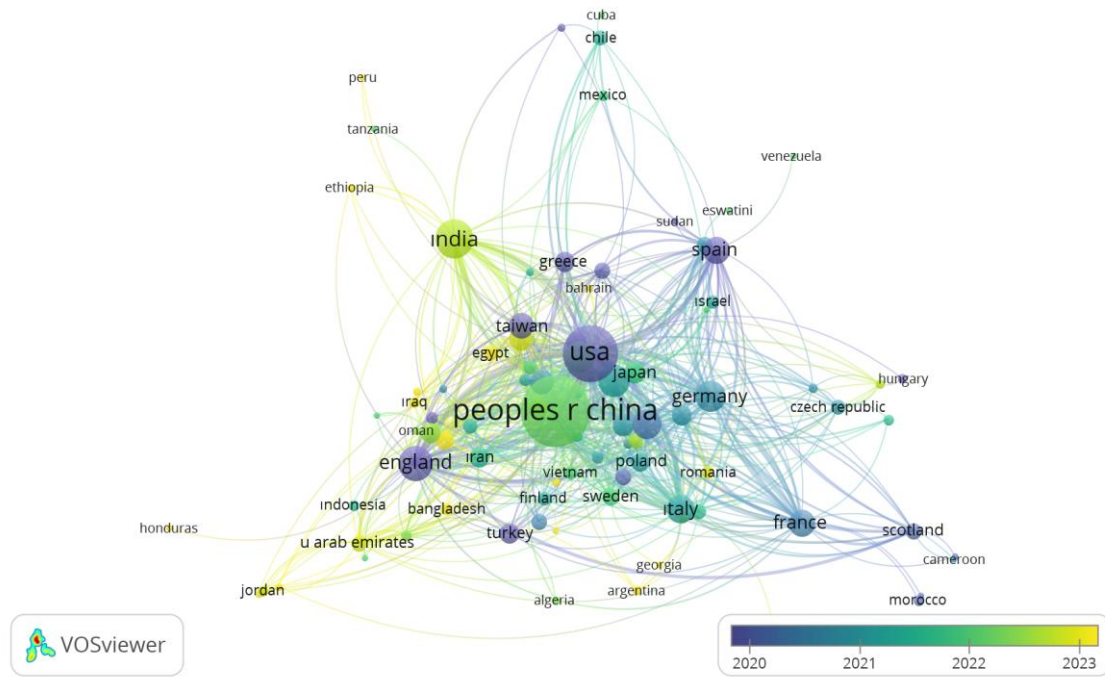


Figure 15. Overlay visualization of country collaboration network (VOSviewer output)

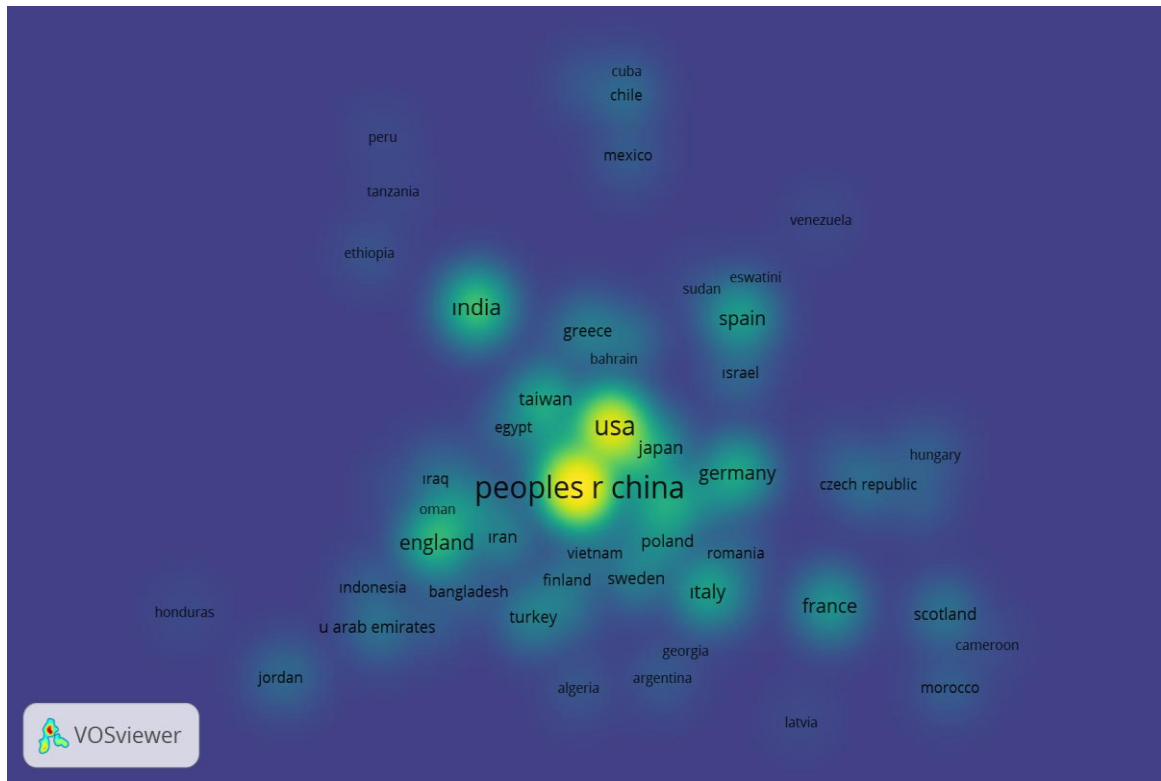


Figure 16. Density visualization of international research collaboration (VOSviewer output)

Conclusion

This bibliometric study provides a comprehensive examination of how ML and DL techniques have evolved in the context of volatility forecasting between 2000 and 2025, highlighting key emerging trends. The findings indicate that hybrid models integrating traditional econometric methods with AI algorithms—particularly

LSTM, SVM, and related approaches—have gained prominence. Network visualizations generated through VOSviewer reveal that the majority of research outputs are concentrated in China and the United States, with notable collaboration networks also present across parts of Asia, North America, and Europe. In parallel with the increasing use of deep learning-based models in financial time series analysis in recent years, the keyword “deep learning” has appeared with growing frequency in the literature.

Furthermore, thematic and keyword co-occurrence analyses suggest a growing interest not only in well-established areas such as financial econometrics and time series modeling, but also in emerging topics like meta-learning and transformer-based models. The network maps visually capture the structural evolution of the literature and clearly reflect which themes have gained prominence over time.

By mapping the scientific landscape of ML applications in volatility forecasting, this study sheds light on the interdisciplinary nature and shifting methodological foundations of the field. The results emphasize the increasing success of ML models in addressing the nonlinear structures, uncertainty, and structural breaks inherent in financial time series, thereby offering both conceptual insight and future research directions.

Recommendations

Future research could enhance modeling accuracy and applicability by focusing on advanced AI techniques that remain underexplored in the volatility forecasting literature, such as transformer architectures, meta-learning, and other cutting-edge approaches.

Scientific Ethics Declaration

* The author declares that the scientific ethical and legal responsibility of this article published in EPSTEM journal belongs to the author.

Conflict of Interest

* The author declares that there is no conflict of interest

Funding

*This study received no external funding.

Acknowledgements or Notes

* This article was presented as an oral presentation at the International Conference on Technology (www.icontechno.net) held in Trabzon/Türkiye on May 01-04, 2025.

References

- Abizada, R. (2024). *Finansal serilerin ongorusunda derin ogrenme ve klasik yontemlerin karsilastirilmesi: BIST100 ornegi* (Master's thesis, Marmara University).
- Akbulut, S., & Adem, K. (2023). Derin ogrenme ve makine ogrenmesi yontemleri kullanilarak gelismekte olan ulkelerin finansal enstrumanlarının etkilesimi ile Bist 100 tahmini. *Nigde Omer Halisdemir Universitesi Muhendislik Bilimleri Dergisi*, 12(1), 52-63.
- Aksehir, Z. D., & Kılıc, E. (2019). Makine ogrenmesi teknikleri ile banka hisse senetlerinin fiyat tahmini. (2), 30-39.
- Akusta, A. (2023). *Bitcoin fiyat hareketliliğinin makine öğrenmesi ile tahmin edilmesi* (Doctoral dissertation, Necmettin Erbakan University).

- Andersen, T. G., Bollerslev, T., Christoffersen, P. F., & Diebold, F. X. (2006). Volatility and correlation forecasting. In *Handbook of economic forecasting* (Vol. 1, pp.777-878). Elsevier.
- Bhuriya, D., Kaushal, G., Sharma, A., & Singh, U. (2017). Stock market predication using a linear regression. *International Conference of Electronics, Communication and Aerospace Technology (ICECA)*, 2, 510-513.
- Bollerslev, T. (1986). Generalized autoregressive conditional heteroskedasticity. *Journal of Econometrics*, 31(3), 307-327.
- Budak, M. Y. (2023). *Kuresel finansal kriz donemlerinde para ve sermaye piyasası araçları fiyatlarının makine öğrenmesi ile tahmin edilmesi*. (Master's thesis, Balıkesir University, Turkey).
- Ceyhan, I. F. (2023). Finans alanında makine ve derin öğrenmenin kullanılması: Lisansustu tezlerde sistematik literatur taraması. *Insan ve Toplum Bilimleri Arastirmaları Dergisi*, 12(3), 2187-2209.
- Chen, S., Härdle, W. K., & Jeong, K. (2010). Forecasting volatility with support vector machine-based GARCH model. *Journal of Forecasting*, 29(4), 406-433.
- Colak, Z. (2025). Derin öğrenme modelleri ile hisse senedi fiyat tahmini: Lstm, Gru, Rnn, Mlp modellerinin karşılaştırmalı analizi. *Yonetim Bilimleri Dergisi*, 23(56), 1250-1286.
- Egeli, B., Ozturan, M., & Badur, B. (2003). Stock market prediction using artificial neural networks. *Decision Support Systems*, 22, 171-185.
- Engle, R. F. (1982). Autoregressive conditional heteroscedasticity with estimates of the variance of United Kingdom inflation. *Econometrica: Journal of the Econometric Society*, 50, 987-1007.
- Eylasov, N., & Cicek, M. (2024). Kripto para fiyatlarının tahmini: ARIMA-GARCH ve LSTM yöntemlerinin karşılaştırılması. *Finans Ekonomi ve Sosyal Arastirmalar Dergisi*, 9(1), 48-62.
- Filiz, E., Karaboga, H. A., & Akogul, S. (2017). BIST-50 endeksi değişim değerlerinin sınıflandırılmasında makine öğrenmesi yöntemleri ve yapay sinir ağları kullanımı. *Cukurova Universitesi Sosyal Bilimler Enstitusu Dergisi*, 26(1), 231-241.
- Fischer, T., & Krauss, C. (2018). Deep learning with long short-term memory networks for financial market predictions. *European Journal of Operational Research*, 270(2), 654-669.
- Keles, M. B., & Keles, A. (2020). Makine öğrenmesi yöntemleri ile ucus fiyatlarının tahmini. *Euroasia Journal of Mathematics, Engineering, Natural & Medical Sciences*, 7(11), 72-78.
- Gavrishchaka, V. V., & Banerjee, S. (2006). Support vector machine as an efficient framework for stock market volatility forecasting. *Computational Management Science*, 3(2), 147-160.
- Grigorev, A. (2020). *Machine learning bookcamp MEAP V06*. Manning Publications. Retrieved from <https://www.manning.com/books/machinelearning-bookcamp>
- Gur, Y. E., & Esidir, K. A. (2024). Türkiye hurda demir çelik ithalatının gelecek değerlerinin derin öğrenme, makine öğrenmesi ve topluluk öğrenme yöntemleri ile öngörülmesi. *Alanya Akademik Bakış*, 8(3), 885-908.
- Kim, H. S., & Choi, S. Y. (2024). investigating the impact of agricultural, financial, economic, and political factors on oil forward prices and volatility: A SHAP analysis. *Energies*, 17(5), 1001.
- Lin, S. Y., Chen, C. H., & Lo, C. C. (2013). Currency exchange rates prediction based on linear regression analysis using cloud computing. *International Journal of Grid and Distributed Computing*, 6(2), 1-10.
- Oncu, E. (2022). *Bölüm IX makine öğrenmesi ile karbon gelecek sözleşmeleris fiyatlarının tahmini* (p.169). İşletme ve İktisadi Bilimler.
- Ozcan, K. A. (2023). Borsa endeksi yönünün makine öğrenmesi yöntemleri ile tahmini: BIST 100 örneği. *Gumushane Universitesi Sosyal Bilimler Dergisi*, 14(3), 1001-1018.
- Nuchitprasitchai, S., Chantarakasemchit, O., & Nilsiam, Y. (2023). Sliding-window technique for enhancing prediction of Forex rates. *International Conference on Computing and Information Technology*, 209-219.
- Poon, S. H., & Granger, C. W. J. (2003). Forecasting volatility in financial markets: A review. *Journal of Economic Literature*, 41(2), 478-539.
- Pritchard, A. (1969). Statistical Bibliography or bibliometrics?. *Journal of Documentation*, 25(4), 348-349.
- Samuel, A. L. (1959). Some studies in machine learning using the game of checkers. *IBM Journal of Research and Development*, 3(3), 210-229.
- Sarkar, M. S. A., & Ali, U. M. E. (2022). Eur/usd exchange rate prediction using machine learning. *International Journal of Mathematical Sciences and Computing*, 8(1), 44-48.
- Schwert, G. W. (1989). Why does stock market volatility change over time?. *The Journal of Finance*, 44(5), 1115-1153.
- Sonmez, L., & Arslan, M. C. (2024). LSTM modeli ile volatilite temelli borsa tahmini. *Uluslararası Muhasebe ve Finans Arastirmaları Dergisi*, 6(2), 48-61.
- Sahin, C. (2023). Garch ve yapay sinir ağları modelleri yardımıyla volatilite tahmini: Turk borsası örneği. *Kastamonu Universitesi İktisadi ve İdari Bilimler Fakultesi Dergisi*, 25(2), 572-595.

- Tang, L. B., Tang, L. X., & Sheng, H. Y. (2009). Forecasting volatility based on wavelet support vector machine. *Expert Systems with Applications*, 36(2), 2901-2909.
- Urgenc, S. (2023). *Makine öğrenmesi yöntemleri ile Bitcoin trend donuslerinin tahmin edilmesi* (Master's thesis, Mimar Sinan Fine Arts University).
- Wijayanti, T. and Taufik, M. R. (2022). Analyzing the exchange rate usd/idr under the impact of Covid-19 by using linear regression in Indonesia. *AIP Conference Proceedings*, 2575(1), 1-44.
- Zhang, L., Aggarwal, C., & Qi, G. J. (2017). Stock price prediction via discovering multi-frequency trading patterns. *23rd ACM SIGKDD International Conference on Knowledge Discovery and Data Mining* (pp. 2141-2149).

Author Information

Beste Alpaslan

OSTIM Technical University

Ankara, Türkiye

Contact e-mail: beste.alpaslan@ostimteknik.edu.tr

To cite this article:

Alpaslan, B. (2025). Emerging trends in volatility forecasting using machine learning: A bibliometric analysis. *The Eurasia Proceedings of Science, Technology, Engineering and Mathematics (EPSTEM)*, 33, 80-95.

The Eurasia Proceedings of Science, Technology, Engineering & Mathematics (EPSTEM), 2025

Volume 33, Pages 96-104

IConTech 2025: International Conference on Technology

Enhancing Low-Resolution Facial Recognition in Classroom Environments Using YOLOv8

Gheri Febri Ananda

University of Gadjah Mada

Hanung Adi Nugroho

University of Gadjah Mada

Igi Ardiyanto

University of Gadjah Mada

Abstract: Accurate facial recognition is essential in modern classroom environments, enabling automated attendance tracking and real-time monitoring of student participation. However, classroom settings present unique challenges, including low-resolution images caused by distance, varied lighting conditions, and occlusions, which significantly reduce identification accuracy. While previous approaches often employed super-resolution methods to address these issues, they required high computational resources and offered suboptimal accuracy. This study proposes using YOLOv8 to enhance face detection and recognition specifically tailored for classroom conditions. Experiments were conducted with four YOLOv8 variants—YOLOv8-S, YOLOv8-M, YOLOv8-L, and YOLOv8-X—in real classroom settings involving 40 students within a 6 m x 5 m space. The results demonstrate that YOLOv8-X delivered the best performance, achieving 92% precision, 88% recall, and an mAP50 of 95%, proving highly effective for detecting students in challenging classroom scenarios. YOLOv8-L closely followed with 94% precision and 84% recall. In contrast, YOLOv8-M and YOLOv8-S showed limited effectiveness, with YOLOv8-S achieving only 82% precision and 70% recall. These findings highlight the suitability of YOLOv8-L and YOLOv8-X for addressing the complex challenges of classroom environments, providing robust solutions for improving facial recognition accuracy and efficiently automating classroom management systems.

Keywords: Low resolution, Face recognition, YOLOv8

Introduction

Facial recognition in the classroom holds significant potential in supporting the concept of a smart classroom, particularly for automatic attendance tracking, monitoring student engagement, and personalizing learning interventions (Akash et al., 2023; Pabba & Kumar, 2022; Yin Albert et al., 2022). This technology enables teachers to track student attendance more efficiently, monitor student activities in real-time, and provide personalized learning interventions tailored to individual need. However, the classroom environment presents several challenges for facial recognition, such as variations in lighting, the distance between students and the camera, low image resolution, and occlusions, which can affect the accuracy of facial recognition (Gu et al., 2022; Shi & Tang, 2022). Therefore, addressing these challenges is essential for the system to be reliably implemented in educational settings.

One of the main problems in classroom settings is the low resolution of images caused by the distance between students and the camera, as well as the large number of individuals being monitored simultaneously. Numerous studies were conducted to address low-resolution challenges, focusing on techniques such as Super-Resolution

- This is an Open Access article distributed under the terms of the Creative Commons Attribution-Noncommercial 4.0 Unported License, permitting all non-commercial use, distribution, and reproduction in any medium, provided the original work is properly cited.

- Selection and peer-review under responsibility of the Organizing Committee of the Conference

© 2025 Published by ISRES Publishing: www.isres.org

Convolutional Neural Networks (SRCNN) (Dong et al., 2016), Deep Convolutional Neural Networks (DCNN) (Hornig et al., 2022), Super-Resolution Generative Adversarial Networks (SRGAN) (Zhao et al., 2023), and Enhanced Super-Resolution Generative Adversarial Networks (ESRGAN) (Song et al., 2021). While these methods have shown promising results in improving image quality, These methods were primarily tested on general datasets and typically focus on recognizing individual faces rather than multiple faces within a classroom context. Additionally, these super-resolution methods require high computational power, which often poses a limitation when applied to devices with limited resources in educational settings. Most of these studies have yet to be tested under classroom conditions, where multitasking and simultaneous face recognition are crucial.



Figure 1. Illustration of challenges in the classroom environment

Various approaches have been developed to address the problem of face detection to support good performance in face recognition, particularly using enhanced multitask cascaded convolutional neural networks (MTCNN) and optimization of YOLOV3 with Bayesian (Gu et al., 2022; Shi & Tang, 2022). On the other hand, deep learning technology has also applied in facial recognition to improve the accuracy and efficiency of automatic identification processes (Khan et al., 2019; Nguyen et al., 2021). However, previous research still encountered issues with suboptimal accuracy. Additionally, several studies using YOLOv8 have successfully focused on small object detection in small images within remote sensing (Yue et al., 2024), manufacturing (Tao et al., 2023), and autonomous vehicles (Wang et al., 2024).

Therefore, this study aims to adopt YOLOv8 with the capability to recognize small objects and scale variations in classroom conditions. Furthermore, it seeks to provide a more effective and efficient solution to support smart classroom management. The study also aims to enhance system accuracy on a larger scale, making it applicable in classrooms with more students and diverse environmental conditions

Method

Dataset Collection

The dataset used in this study was collected from a real classroom environment, capturing various student orientations, lighting conditions, and distances from the camera. This dataset was specifically gathered to ensure that the designed system could be effectively adopted in real-world classroom settings. It consists of 181 images taken over multiple days, with 159 images used for training, 15 for validation, and 7 for testing. The images feature 40 students in different seating arrangements for each image. The dataset was captured using the classroom's existing camera, providing a realistic representation of typical classroom conditions. Figure 2 presents an example of the dataset used.



Figure 2. Example of image dataset used

To evaluate the system's performance on low-resolution facial recognition, face detection was carried out using the MTCNN method, followed by cropping the detected faces to analyze the resolution of individual faces across different seating positions. This approach aimed to demonstrate how face resolution fluctuates based on a student's proximity to the camera. Specifically, students seated in the front row exhibited face resolutions of approximately 40 x 52 pixels, those in the middle row had around 22 x 27 pixels, and those in the back row displayed face resolutions of about 16 x 21 pixels. Figure 3 provides examples of the cropped faces, illustrating the varying image resolutions captured from the dataset.

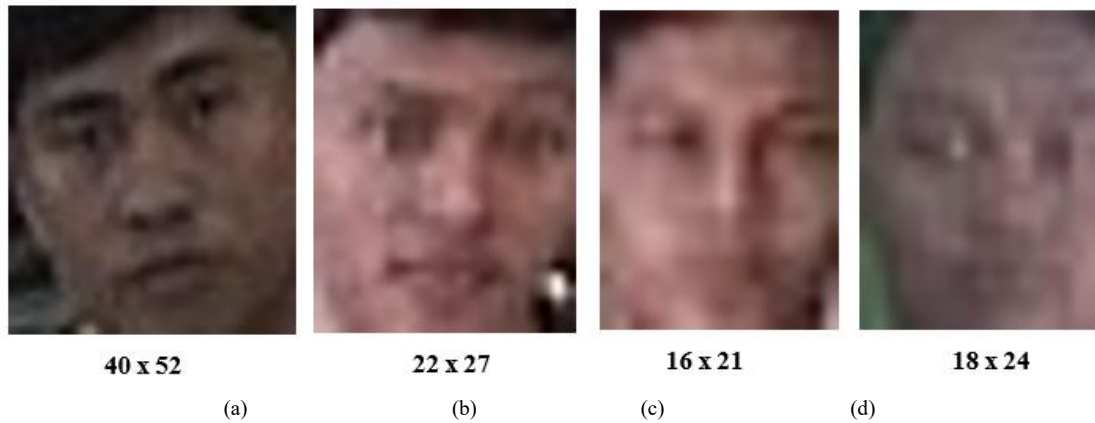


Figure 3. Face image resolution in the dataset (a) front row students, (b) middle row students, and (c), (d) back row students.

This data collection method highlights the challenges of recognizing all students in a classroom setting, particularly due to scale variation and low-resolution faces caused by distance from the camera. These differences present significant obstacles for facial recognition systems, emphasizing the need for models that can handle these variations to ensure robustness and effectiveness in real-world scenarios.

Architecture of Yolov8

The architecture of YOLOv8 builds upon the innovations introduced in its predecessors, integrating several advanced components designed to enhance performance in object detection tasks. It employs a custom backbone that features the C2f (Cross Stage Partial 2-Fusion) structure, which optimizes feature extraction by improving information flow between layers while reducing computational complexity (Tao et al., 2023). The neck incorporates SPPF (Spatial Pyramid Pooling Fast), allowing the model to effectively capture features at multiple scales, which is crucial for accurately detecting objects of varying sizes (Gunawan et al., 2023). The head of YOLOv8 introduces separate classification and detection heads, transitioning from an anchor-free to an anchor-based approach to improve localization and classification precision.

YOLOv8 also transitions from an anchor-free detection system to an anchor-based approach, which increases the precision of object localization and classification (Terven et al., 2023). The model further enhances performance by using Focal Loss for classification instead of Binary Cross-Entropy (BCE), and Distribution Focal Loss (DFL) for regression, improving bounding box predictions. Furthermore, the integration of Complete IoU (CIoU) loss refines the accuracy of bounding box dimensions, leading to higher detection precision (Yan et

al., 2023). These architectural improvements collectively result in significant gains in both accuracy and efficiency, making YOLOv8 particularly effective for real-time object detection applications. The architecture of YOLOv8 is illustrated in Figure 4.

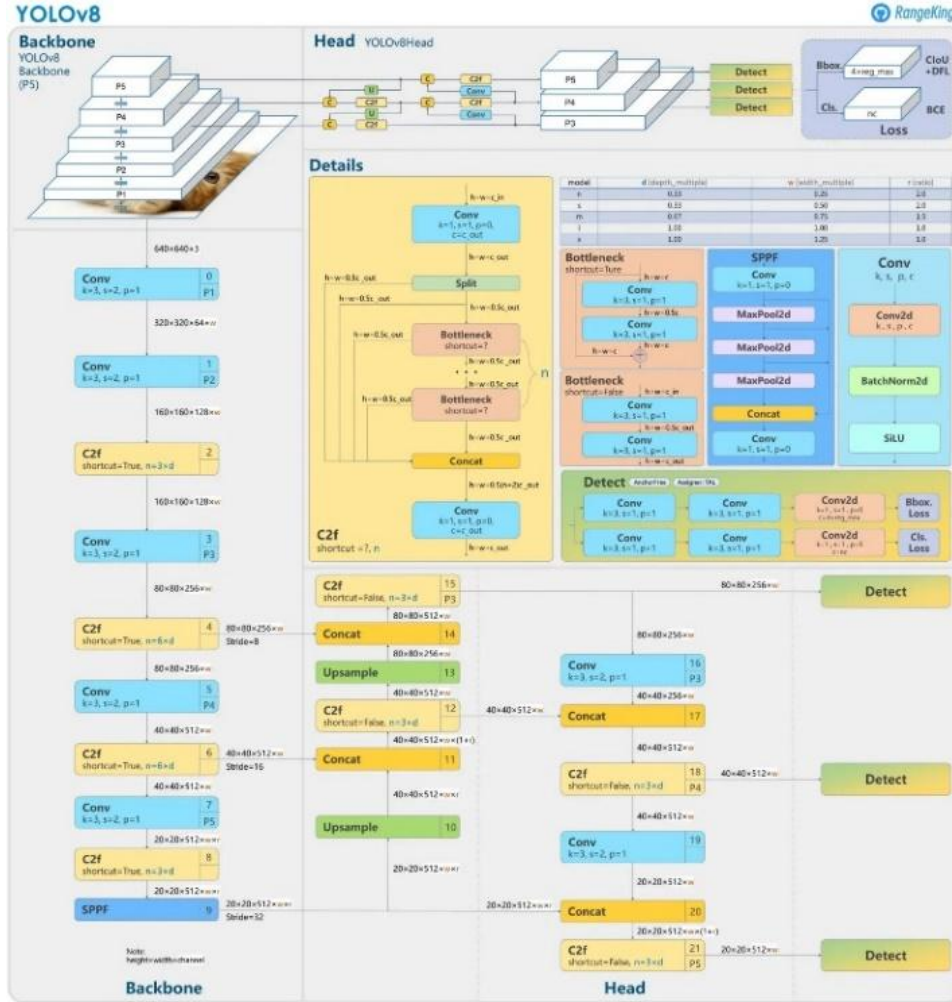


Figure 4. The architecture of YOLOv8 (Gunawan et al., 2023)

Model Selection and Training

In this study, several versions of YOLOv8 (YOLOv8-S, YOLOv8-M, YOLOv8-L, and YOLOv8-X) were trained and tested to determine the most effective model for face recognition in low-resolution classroom environments. The purpose of testing these different variants was to determine which version of YOLOv8 performed best in the specific case of low-resolution classroom environments. Each version was evaluated based on its ability to balance speed and accuracy, ensuring the optimal model for face detection in this setting was identified. Each variant presents different levels of complexity, characterized by the number of layers, parameters, and computational requirements (GFLOPs), as detailed in Table 1

Table 1. YOLOv8 model variant details

Model Variant	Layers	Parameters	GFLOPs
YOLOv8-S	225	11.151.080	28.7
YOLOv8-M	295	25.879.480	79.2
YOLOv8-L	365	43.660.680	165.6
YOLOv8-X	365	68.191.128	258.3

To handle the computational demands of training, all models were trained for 100 epochs with a batch size of 16, using an image resolution of 640 x 640 pixels and an initial learning rate of 0.01. This training was conducted on Google Colab with an NVIDIA A100 GPU, providing the high processing power needed to

efficiently manage the models' computational requirements. The training configuration was standardized across all tests, as shown in Table 2.

Table 2. Hyperparameter setting

Hyperparameter	Value
Image Size	640 x 640
Epochs	100
Batch Size	16
Learning Rate	0.01
Processor Used	NVIDIA A100 (Google Colab)

These standardized hyperparameter settings were chosen to ensure consistent and fair comparison across the YOLOv8 variants.

Model Evaluation

After training, the performance of the YOLOv8 model is measured using several metrics, including precision, recall, and mean Average Precision (mAP). Precision is defined as the ratio of the number of true positive predictions (TP) to the total number of positive predictions made by the model, while Recall measures the ratio of the number of true positive predictions to the total number of actual positive objects present in the image, as expressed in Equations 1 and 2 below:

$$\text{Precision} = \frac{TP}{TP + FP} \quad (1)$$

$$\text{Recall} = \frac{TP}{TP + FN} \quad (2)$$

Next, Average Precision (AP) is calculated as the area under the Precision-Recall curve, with the formula stated in Equation 3:

$$AP = \int_0^1 P(R) dR \quad (3)$$

This metric provides an overview of the model's performance at various threshold values. For further evaluation, mAP@0.5 is utilized to measure the accuracy of the model's detections at an Intersection over Union (IoU) threshold of 0.5. Additionally, mAP@0.5:0.95 calculates the average AP value across a range of IoU thresholds from 0.5 to 0.95, providing a comprehensive assessment of the model's performance. These metrics are expressed in Equations 4 and 5 :

$$mAP_{0.5} = \frac{1}{N} \sum_{i=1}^N AP_i, \text{IoU} = 0.5 \quad (4)$$

$$mAP_{0.5 : 0.95} = \frac{1}{N} \sum_{i=1}^N AP_i, \text{IoU} = 0.5 : 0.05 : 0.95 \quad (5)$$

These metrics collectively give a detailed evaluation of the model's ability to detect and localize objects accurately across varying levels of detection difficulty.

Results and Discussion

Training Process Results

To evaluate the effectiveness of the YOLOv8 models, we conducted a series of experiments to compare their performance across key metrics: precision, recall, mAP50, mAP50-95, and various loss values. The training was carried out on four model variants—YOLOv8-S, YOLOv8-M, YOLOv8-L, and YOLOv8-X—using the same dataset and hyperparameters to ensure consistency and fairness in the comparison. This comparative analysis aims to highlight the capability of each model in detecting and classifying objects, guiding the selection of the most appropriate variant for classroom scenarios. The training process results are illustrated in Figure 5 below.

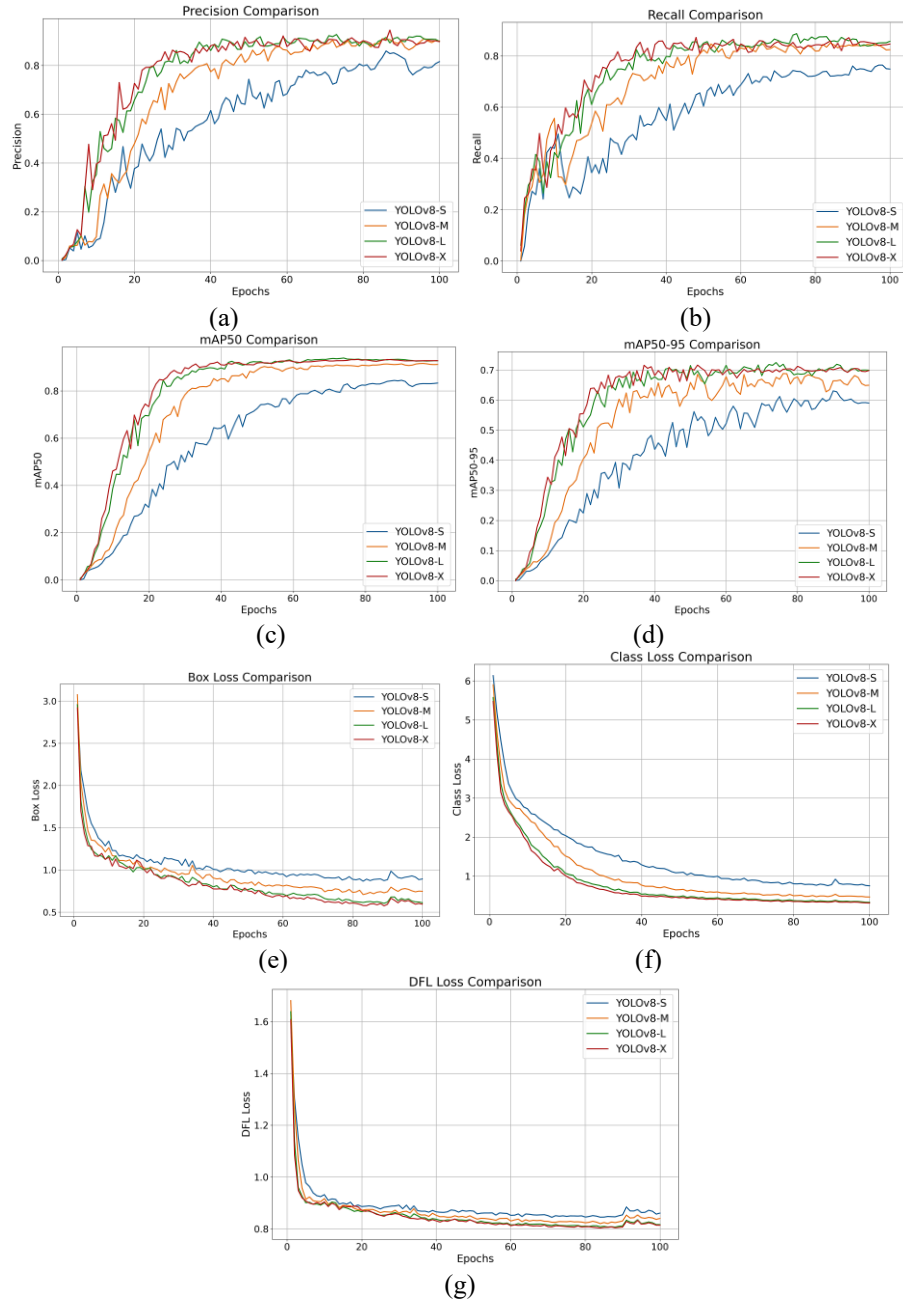


Figure 5. Evaluation metrics graph of four types of YOLOv8 during the training process (a) Precision, (b) Recall, (c) mAP50, (d) mAP50-9, (e) Box Loss, (f) Class Loss, (g) DFL Loss

During the training process, YOLOv8-L demonstrated the best stability in the recall metric, consistently achieving values in the 0.84-0.85 range over the last five epochs, indicating reliable and accurate object detection capabilities. YOLOv8-X also exhibited strong performance with high precision in the 0.89-0.91 range, although there were minor fluctuations in the recall metric compared to YOLOv8-L. On the other hand, YOLOv8-M had good precision around 0.91, but lower recall stability, with inconsistent values, reflecting poorer performance in detecting all objects in the images. Meanwhile, YOLOv8-S displayed the weakest performance, with precision around 0.82 and recall around 0.75, significantly lagging behind the other three models.

Training Process Results

To test the generalization capability of the model, an evaluation was conducted using test data that the model had never encountered during the training process. This testing aims to assess how well the model can recognize objects in previously unseen data and provides a more accurate representation of the model's performance in

real-world scenarios. The results of the evaluation are presented in the table 3, which lists key metrics such as precision, recall, mAP50, and mAP50-95 for each variant of the YOLOv8 model after training.

Table 3. Evaluation metric on four types of YOLOv8

Yolov8 Types	Precision	Recall	mAP 50	mAP 50-95
Yolov8s	0.82	0.7	0.82	0.63
Yolov8m	0.91	0.83	0.91	0.71
Yolov8l	0.94	0.84	0.93	0.72
Yolov8x	0.92	0.88	0.95	0.74

Table 3 shows that YOLOv8-X outperforms with a precision of 0.92 and a recall of 0.88, accompanied by mAP50 of 0.95 and mAP50-95 of 0.74. This indicates that YOLOv8-X has excellent detection accuracy and can handle various object variations in the test data. YOLOv8-L also demonstrates strong performance with a precision of 0.94 and a recall of 0.84, as well as mAP50 of 0.93 and mAP50-95 of 0.72, reflecting the model's stability in detecting complex objects. In contrast, YOLOv8-M lags slightly behind with a precision of 0.91 and a recall of 0.83, along with an mAP50 of 0.91 and mAP50-95 of 0.71. This suggests that although YOLOv8-M has reasonably good accuracy, it may be less optimal in handling more complicated object variations compared to YOLOv8-L and YOLOv8-X. YOLOv8-S exhibits the lowest performance among the four models, with a precision of 0.82, recall of 0.70, mAP50 of 0.82, and mAP50-95 of 0.63, indicating that this model is less effective in detecting diverse objects in the test data.

Overall, the results from this testing reinforce the findings from the training phase, where YOLOv8-L and YOLOv8-X again demonstrate superior performance in object detection with high accuracy. These two models are more suitable for implementation in environments that require a high and diverse level of detection, such as the classroom scenarios being tested. Next, we present an overview of the tests performed with each model, aimed at deepening our understanding of their performance success in addressing the challenges of face recognition in demanding classroom environments. These examples are illustrated in Figure 6.



Figure 6. View on testing each type of YOLOv8 (a) YOLOv8-S, (b) YOLOv8-M, (c) YOLOv8-L, (d) YOLOv8-X

Figure 6 shows the effectiveness of the YOLOv8 model in recognizing faces under various challenging classroom conditions. These results highlight YOLOv8-L's robustness and adaptability, making it a valuable tool for applications in educational settings where reliable face recognition is essential. The high accuracy and

efficiency observed in these tests reinforce the model's potential for enhancing classroom management and student engagement through effective facial recognition technology.

Conclusion

Our experiments with various YOLOv8 models demonstrate that YOLOv8-L and YOLOv8-X are highly effective for face recognition in complex classroom environments. Both models exhibit high precision and recall, showcasing their ability to accurately identify and classify faces even in challenging real-world scenarios. YOLOv8-L stands out for its stability and reliability, while YOLOv8-X delivers superior precision, making it ideal for applications requiring extremely accurate results. In contrast, the limitations observed in YOLOv8-M and YOLOv8-S suggest that these models may not perform optimally in scenarios with significant variations in facial appearances. These findings emphasize the importance of selecting the most appropriate model based on the specific requirements of the operational context. Moreover, the success of YOLOv8 in addressing challenges with small or low-resolution faces in classrooms eliminates the need for super-resolution methods before face recognition. Consequently, adopting YOLOv8 not only improves accuracy but also reduces the computational load typically associated with super-resolution techniques.

Recommendations

Future research can focus on further improving YOLOv8's performance by training it with a larger and more diverse dataset that reflects a wider range of classroom scenarios. Integrating YOLOv8 with other image enhancement techniques could also enhance the model's accuracy and robustness, especially in challenging environments. Additionally, developing real-time face recognition systems for classroom settings will be critical for practical applications. These systems could include intuitive interfaces for teachers and administrators, enabling them to monitor and analyze student engagement more effectively. The implementation of this technology may hold the potential to create modern classrooms that are more interactive and innovative. By integrating face recognition systems with AI-based technologies, teachers may identify student engagement patterns in real-time, personalize teaching methods, and enhance the efficiency of the learning process.

Scientific Ethics Declaration

The authors declare that the scientific ethical and legal responsibility of this article published in EPSTEM Journal belongs to the authors.

Conflict of Interest

* The authors declare that they have no conflicts of interest

Funding

* The writing and publication of this article were supported and funded by Lembaga Pengelola Dana Pendidikan (LPDP) Indonesia.

Acknowledgements or Notes

* This article was presented as an oral presentation at the International Conference on Technology (www.icontechno.net) held in Trabzon/Turkey on May 01-04, 2025.

References

- Akash, S., Dinesh, V., Muthamil Selvan, S., Alfred Daniel, J., & Srikanth, R. (2023). Monitoring and analysis of students' live behaviour using machine learning. *2023 7th International Conference on Intelligent Computing and Control Systems (ICICCS)*, 98–103.
- Dong, C., Loy, C. C., He, K., & Tang, X. (2016). Image super-resolution using deep convolutional networks. *IEEE Transactions on Pattern Analysis and Machine Intelligence*, 38(2), 295–307.
- Gu, M., Liu, X., & Feng, J. (2022). Classroom face detection algorithm based on improved MTCNN. *Signal, Image and Video Processing*, 16(5), 1355–1362.
- Gunawan, F., Hwang, C.-L., & Cheng, Z.-E. (2023). ROI-YOLOv8-based far-distance face-recognition. *2023 International Conference on Advanced Robotics and Intelligent Systems (ARIS)*, 1–6.
- Horng, S.-J., Supardi, J., Zhou, W., Lin, C.-T., & Jiang, B. (2022). Recognizing very small face images using convolution neural Networks. *IEEE Transactions on Intelligent Transportation Systems*, 23(3), 2103–2115.
- Khan, M. Z., Harous, S., Hassan, S. U., Ghani Khan, M. U., Iqbal, R., & Mumtaz, S. (2019). Deep unified model for face recognition based on convolution neural network and edge computing. *IEEE Access*, 7, 72622–72633.
- Nguyen, D. D., Nguyen, X. H., Than, T. T., & Nguyen, M. S. (2021). Automated attendance system in the classroom using artificial intelligence and internet of things technology. *2021 8th NAFOSTED Conference on Information and Computer Science (NICS)*, 531–536.
- Pabba, C., & Kumar, P. (2022). An intelligent system for monitoring students' engagement in large classroom teaching through facial expression recognition. *Expert Systems*, 39(1), e12839.
- Shi, D., & Tang, H. (2022). A new multiface target detection algorithm for students in class based on bayesian optimized YOLOv3 Model. *Journal of Electrical and Computer Engineering*, 2022(1), 1–12.
- Song, C., He, Z., Yu, Y., & Zhang, Z. (2021). Low resolution face recognition system based on ESRGAN. *3rd International Conference on Applied Machine Learning (ICAML)*, 76–79.
- Tao, Q., Chen, Y., & Chen, H. (2023). A detection approach for wafer detect in industrial manufacturing based on YOLOv8. *2023 CAA Symposium on Fault Detection, Supervision and Safety for Technical Processes (SAFEPROCESS)*, 1–6.
- Terven, J., Córdova-Esparza, D.-M., & Romero-González, J.-A. (2023). A comprehensive review of YOLO architectures in computer vision: From YOLOv1 to YOLOv8 and YOLO-NAS. *Machine Learning and Knowledge Extraction*, 5(4), 1680–1716.
- Wang, H., Liu, C., Cai, Y., Chen, L., & Li, Y. (2024). YOLOv8-QSD: An improved small object detection algorithm for autonomous vehicles based on YOLOv8. *IEEE Transactions on Instrumentation and Measurement*, 73, 1–16.
- Yan, M., Fan, Y., Jiang, Y., & Fang, Z. (2023). A fast detection algorithm for surface defects of bare PCB based on YOLOv8. *2023 3rd International Conference on Electronic Information Engineering and Computer Communication (EIECC)*, 559–564.
- Yin Albert, C. C., Sun, Y., Li, G., Peng, J., Ran, F., Wang, Z., & Zhou, J. (2022). Identifying and monitoring students' classroom learning behavior based on multisource information. *Mobile Information Systems*, 2022(1), 9903342.
- Yue, M., Zhang, L., Zhang, Y., & Zhang, H. (2024). An improved YOLOv8 detector for multi-scale target detection in remote sensing images. *IEEE Access*, 12, 114123–114136.
- Zhao, Y., Yao, C., Li, X., & Shen, L. (2023). Face recognition using the improved SRGAN. *2023 8th International Conference on Image, Vision and Computing (ICIVC)*, 120–123.

Author Information

Gheri Febri Ananda

University of Gadjah Mada

Yogyakarta, Indonesia

Contact e-mail: gherifebriananda1998@mail.ugm.ac.id

Hanung Adi Nugroho

University of Gadjah Mada

Yogyakarta, Indonesia

Igi Ardiyanto

University of Gadjah Mada

Yogyakarta, Indonesia

To cite this article:

Ananda, G.F. Nugroho, H. A & Ardiyanto, I. (2025). Enhancing low-resolution facial recognition in classroom environments using YOLOv8. *The Eurasia Proceedings of Science, Technology, Engineering and Mathematics (EPSTEM)*, 33, 96-104.

The Eurasia Proceedings of Science, Technology, Engineering and Mathematics (EPSTEM), 2025

Volume 33, Pages 105-113

IConTech 2025: International Conference on Technology

The Application of Big Data Algorithm in the Personalized Management of Students by College Counselors

Jing Gui

Chiang Mai University

Jirawit Yanchinda

Chiang Mai University

Abstract: The specific application of the student's personal knowledge is one of the contents of university Counselors management of students; however, the traditional ant colony algorithm has certain limitations for solving accounting information problems, and its effect is relatively unsatisfactory. Therefore, this paper proposes a specific application in the students personal Counselors management of students the student's personal knowledge of colleges and universities based on big data algorithm and analyzes the specific application in the students personal Counselors management of students the student's personal knowledge of colleges and universities. Firstly, Plan the relevant data in the business index to form an index system, which is convenient for later calculation. Big data is applied in various fields and is also suitable for implementation in personal Counselors management of students, and the results were comprehensively analyzed. The simulation results based on MATLAB show that under certain evaluation standards, the specific application scheme of the students personal knowledge based on the big data algorithm shows obvious advantages in terms of the accuracy of the specific application in the service and the processing time of the influencing factors of the specific application in the students personal knowledge, and can achieve more ideal results than the traditional ant colony algorithm.

Keywords: Data set theory, Big data algorithms, Specific applications

Introduction

The specific application in the students' personal knowledge plays an important role in the students' personal counselors management of students at universities, which can realize the precise positioning and real-time control of the specific application in the students' personal knowledge (Akhtar, et al., 2024). However, the accuracy of specific application solutions in traditional the student's personal knowledge has the problem of poor accuracy, which adversely affects the effect of specific applications in the students' personal knowledge (Alshemaimri, et al., 2025). Studies in recent years considered that the big data method has a remarkable effect on personal Counselors management of students (Chen et al., 2024). It can effectively optimize specific application solutions in the students' personal knowledge and provide reliable support (Chou, et al., 2025). The optimization model is specifically applied in the students' personal knowledge of big data algorithms, and its effectiveness is verified and evaluated in detail (Delnevo et al., 2024). By making full use of the decentralization, non-tampering and smart contract characteristics of big data algorithms, the model realizes the credibility improvement and automatic execution of specific application solutions in the students' personal knowledge (Elfeky et al., 2024). Through a large number of experiments and data analysis, the results show that comprised with the traditional scheme, the optimization model based on big data algorithm has significant advantages in the accuracy of specific application in the students' personal knowledge (Gao, Zhang & Wei, 2024). The accuracy of specific applications in the students' personal knowledge and the ability to suppress interference factors and can effectively improve the quality and efficiency of specific application in the students' personal knowledge (Gao et al., 2024).

Related Concepts

Mathematical Description of Big Data Algorithms

The big data method comprehensively applies business management data, realizes the integration and analysis of knowledge, and completes the promotion of personal knowledge, which finds that the unqualified value parameter of the specific application in the Students personal knowledge is y_i , and integrates the function of the specific application scheme in the Students personal knowledge, and finally judges the feasibility of the specific application in the Students personal knowledge, and the calculation is z_i shown in Equation (1).

$$\lim_{x \rightarrow \infty} (y_i \cdot t_{ij}) = \lim_{x \rightarrow \infty} y_{ij} \geq \max(t_{ij} \div 2) \quad (1)$$

Among them, the judgment of outliers is $tol(y_i \cdot t_{ij})$ shown in Equation (2).

$$\max(t_{ij}) = \partial(t_{ij}^2 + 2 \cdot t_{ij}) \succ \frac{1}{2} (\sum t_{ij} + 4) M \quad (2)$$

Big data algorithms combine the advantages of computer technology and use specific applications in the students' personal knowledge for quantification, which can improve the accuracy of specific applications in the students' personal knowledge (Han & Ren, 2024).

Suppose I The specific application requirements in the Students personal knowledge is t_i , the specific application scheme in the Students personal knowledge is set_i , the satisfaction of the specific application scheme in the Students personal knowledge is y_i , and the judgment function of the specific application scheme in the Students personal knowledge is $F(t_i \approx 0)$ as shown in Equation (3).

$$F(d_i) = \prod \sum t_i \bigcap \xi \cdot \sqrt{2} \rightarrow \prod y_i \cdot 7 \quad (3)$$

Selection of Specific Application Solutions in the Students' Personal Knowledge

Hypothesis II The specific application function in the students' personal knowledge is $g(t_i)$ and the weight coefficient is w_i Kulasegaram, et al.(2024).then, the specific application in the students personal knowledge requires the specific application in the unqualified the students' personal knowledge, as shown in equation (4).

$$g(t_i) = \ddot{x} \cdot z_i \prod F(d_i) \frac{dy}{dx} - w_i \sqrt{a^2 + b^2} \quad (4)$$

Combining various assumptions, a comprehensive function for specific applications in the students' personal knowledge Li(2025).It can be obtained, and the result is shown in equation (5).

$$\lim_{x \rightarrow \infty} g(t_i) + F(d_i) \leq \bigcap \max(t_{ij}) \quad (5)$$

In order to improve the effectiveness of the reliability of specific applications in the students' personal knowledge, it is necessary to standardize all data, and the result is shown in equation (6).

The overall analysis of personal knowledge should be considered from the aspects of knowledge quantity and knowledge accumulation (Li, 2025). It is necessary to measure personal knowledge, and the specific results are shown in formula (6).

$$g(t_i) + F(d_i) \leftrightarrow \text{mean}(\sum t_{ij} + 4) \phi \quad (6)$$

Analysis of Specific Application Scenarios in the Students' Personal Knowledge

With the help of big data computing, students' personal knowledge is comprehensively analyzed, mapping the specific application requirements in the students' personal knowledge to the specific application library in the students' personal knowledge (Wu et al., 2024). The data in the above equation (6) are analyzed, a relatively standard calculation formula is obtained, and the system parameters are added to the formula, and the results are shown in equation (7).

$$No(t_i) = \frac{g(t_i) + F(d_i)}{\text{mean}(\sum t_{ij} + 4)} \sqrt{2} \Lambda \quad (7)$$

Among them, it is $\frac{g(t_i) + F(d_i)}{\text{mean}(\sum t_{ij} + 4)} \leq 1$ stated that the scheme needs to be proposed, otherwise the scheme integration is required, and the result is $Zh(t_i)$ shown in equation (8).

$$Zh(t_i) = \bigcap [\sum g(t_i) + F(d_i)] \quad (8)$$

Conduct comprehensive analysis of specific applications in the student's personal knowledge and set the thresholds and indicator weights of specific application solutions in the service to ensure the accuracy of big data algorithms. The specific application in the service is the specific application solution in the test service system, and accurate analysis is required. If the specific application in the service is $unno(t_i)$ in a non-normal distribution, the specific application scheme in the service will be affected, reducing the accuracy of the specific application in the overall service, and the calculation result is $accur(t_i)$ shown in equation (9).

$$accur(t_i) = \frac{\min[\sum g(t_i) + F(d_i)]}{\sum g(t_i) + F(d_i)} \times 100\% \quad (9)$$

According to the students' personal knowledge and knowledge preparation, it is found that the distribution between knowledge and needs is reasonable, especially business data. The specific application in the student's personal knowledge is not directional, indicating that the specific application scheme in the student's personal knowledge has strong randomness, so it is regarded as high analysis and research. If the specific random function applied in the student's personal knowledge is $randon(t_i)$, then the calculation of Equation (9) can be expressed as Equation (10).

$$accur(t_i) = \frac{\min[\sum g(t_i) + F(d_i)]}{\sum g(t_i) + F(d_i)} + randon(t_i) \quad (10)$$

Conduct a comprehensive analysis of students' personal knowledge, the key qualities and repetitive programs in students' personal knowledge, supplement some insufficient data, adjust the corresponding personal relationships, and make any correlation between different programs.

Optimization Strategies for Specific Applications in the Students' Personal Knowledge

The strategy based on randomness optimization is adopted for the specific application of big data algorithms in the students' personal knowledge, and the optimization of specific application solutions in the student's personal knowledge is realized by adjusting internet information parameters. The optimization process involves classifying specific applications in the students' personal knowledge into different levels and randomly selecting different solutions for implementation. However, it extracts the knowledge and content of students, analyzes the relevance of the implementation of each program and the impact of the program, continuously excavates the value of each program, and uses the method of the highest value to put forward feasible policies and countermeasures for the corresponding program, and completes the accurate judgment and evaluation of the program.

Practical Examples of Specific Applications in Students' Personal Knowledge

A. Introduction to Specific Applications in the Individualized Management Mode of Students

To facilitate the specific application in the individualized management mode of students, the specific application in complex cases is the research object, there are 12 paths, the test time is 12h, and the specific application scheme of the specific application in the Individualized management mode of students is shown in Table I.

Table 1. Specific application requirements in the individualized management mode of students

Scope of application	Grade	Accuracy	Specific applications in the Individualized management mode of students
Knowledge base building	I	87.81	89.64
	II	93.24	90.67
Knowledge gathering	I	87.58	91.23
	II	90.44	88.47
Knowledge collation	I	90.08	90.36
	II	92.32	88.33

The specific application process in the individualized management mode of students in Table 1 is shown in Figure 1.

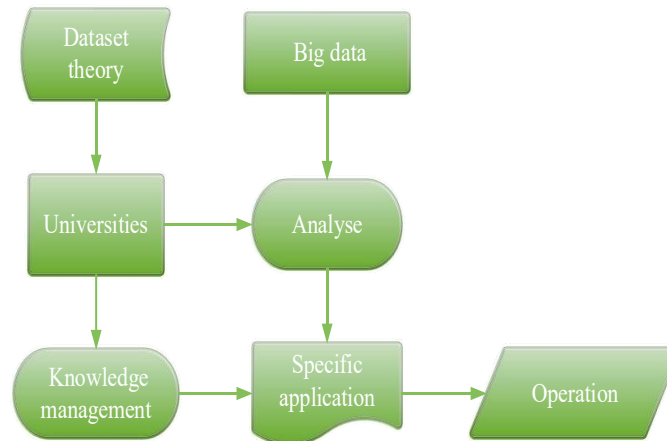


Figure 1. The analytical process of a specific application in the individualized management mode of students

Comprised with the ant colony algorithm, the big data algorithm is closer to the specific application requirements of the actual the Individualized management mode of students in the specific application scheme of the Individualized management mode of students. From the perspective of rationality and accuracy of specific applications in the Individualized management mode of students, big data algorithms have more advantages than ant colony algorithms. The changes in Figure II show that the solution accuracy of the big data algorithm is higher and more reliable. Therefore, big data algorithms perform better in terms of speed, accuracy and stability of specific application scenarios in the Individualized management mode of students.

B. Specific Applications in the Individualized Management Mode of Students

Students should consider different results, must consider the problems of individual students and the problems of the school, and choose different plans according to the actual situation of students. To improve the test results of the program, the program should be sampled and analyzed, which is to complete the analysis of key values, and the results are shown in Table 2

Table 2. The overall situation of the specific application scenario in the individualized management mode of students

Category	Random data	Reliability	Analysis rate
Knowledge base building	88.71	92.37	90.97
Knowledge gathering	87.84	90.10	90.00
Knowledge collation	89.01	89.97	91.20
Mean	89.33	92.27	89.45
X6	91.88	87.32	89.29
	P=1.249		

C. Specific Applications and Stability in the Individualized Management Mode of Students

To verify the accuracy of the big data algorithm, the specific application scheme in the Individualized management mode of students is comprised with the ant colony algorithm, and the specific application scheme in the service is shown in Figure 2.

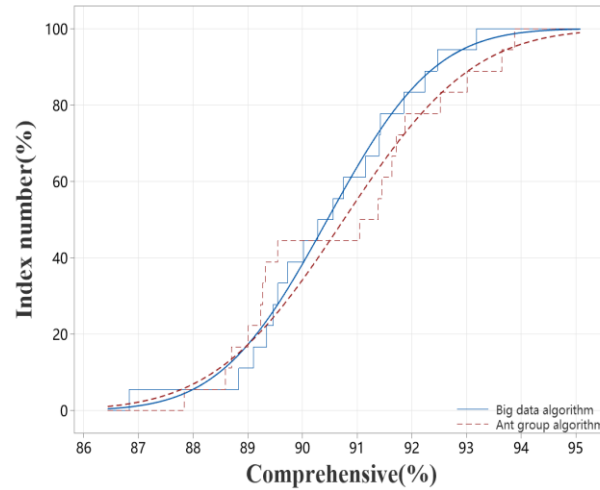


Figure 2. Specific applications of different algorithms in the individualized management mode of students

In Figure 2, the nootropic analysis of different methods is carried out to reduce the error rate between methods, and the corresponding analysis results can be obtained from Table 3.

Table 3. Comparison of the accuracy of specific applications in different methods of the individualized management mode of students

Algorithm	Survey data	Specific applications in the Individualized management mode of students	Magnitude of change	Error
Big data algorithms	90.56	89.24	91.31	89.40
Ant colony algorithm	89.55	91.38	93.63	87.64
P	88.84	89.27	91.57	88.04

According to the data analysis in Table III, there is a problem of insufficient accuracy of ant colony algorithm in specific applications in the Individualized management mode of students, resulting in large changes in results and high error rate. In contrast, the specific application of big data algorithms in the Individualized management mode of students shows higher general results and higher accuracy in specific application in services, which is better than ant colony algorithms. In addition, the accuracy rate of the specific application of big data algorithms in the

Individualized management mode of students exceeds 90% and has a more stable accuracy performance, and there is no obvious major change.

To further verify the effectiveness of the proposed method, other methods are used to comprehensively analyze the big data algorithm, and the specific results can be referred to Figure III. This professional analysis data further verify the superiority of big data algorithms in specific applications in the Individualized management mode of students.

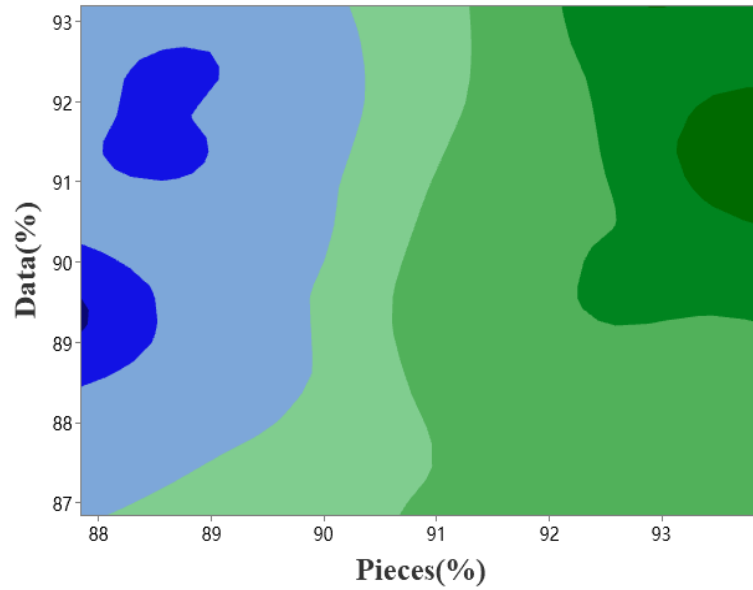


Figure 3. Specific applications of big data algorithms in the individualized management mode of students

From the data distribution in Figure 3, you can see that the yellow data represents a high degree of influence, and the green data represents a low degree of impact.

D. Reasonableness of Specific Applications in the Individualized Management Mode of Students

To verify the accuracy of the big data algorithm, the specific application scheme in the Individualized management mode of students is comprised with the ant colony algorithm, and the specific application scheme in the service is shown in Figure 4.

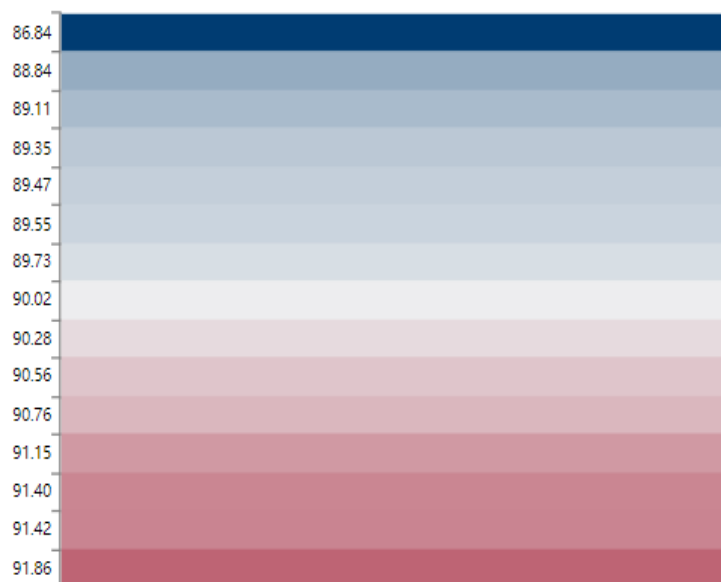


Figure 4. Specific applications of different algorithms in the individualized management mode of students

In the analysis of Figure 4, it can be known that different colors replace the application degree of college students' personal knowledge, and the accuracy of the algorithm for the data analysis results of college students is more reasonable, and it can also be preliminarily judged that the algorithm can be used as one of the application methods. The introduction of big data algorithms provides a decentralized data storage and management platform for specific applications in the Individualized management mode of students to ensure the security and reliability of results. Through big data algorithms, each is given a unique identification code, and the relevant data and scheme is recorded on the big data algorithm in a chain structure. The characteristics of this big data algorithm provide data immutability and traceability, effectively preventing data tampering and fraud.

E. The Effectiveness of Specific Applications in the Individualized Management Mode of Students

Effective implementation of the program is analyzed through effectiveness, and the individual only has a high analytical value in the possibility analysis, so I should make a comprehensive judgment on the credibility of the student, and the specific results are shown in the figure below.

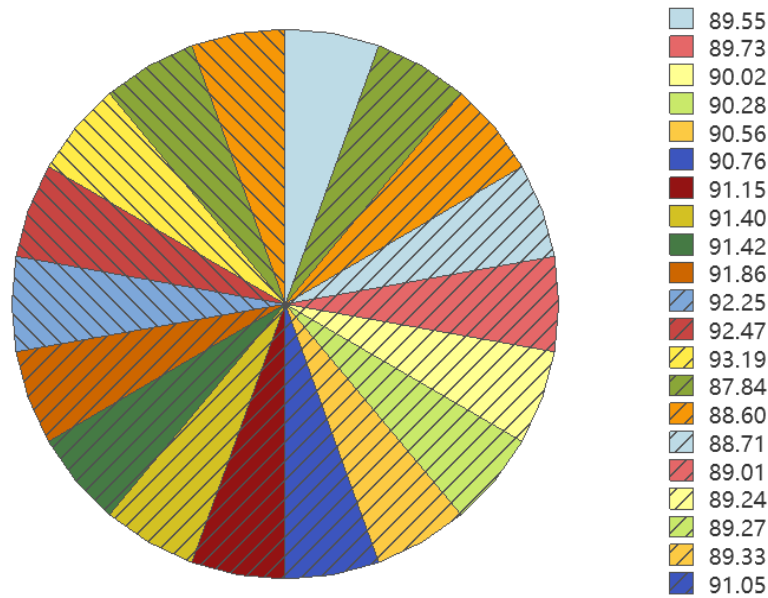


Figure 5. Specific applications of different algorithms in the individualized management mode of students

In the analysis in Figure 5, big data has a high accuracy for the management of personal knowledge, but there are certain differences between the data results, and the specific results are shown in Table 4 for physiological reasons for different differences

Table 4. Comparison of the effectiveness of specific applications in different methods of the individualized management mode of students

Different management methods	Survey data	Specific applications in the Individualized management mode of students	Magnitude of change	Increase rate of students' knowledge
Big data algorithms	89.73	92.53	94.24	92.46
Ant colony algorithm	90.02	91.64	92.44	87.13
Degree of concentration of knowledge	86.84	91.05	90.31	88.61

For the analysis of any data in the table, it will be found that there are certain changes in the deviation of the data, and the repetition of the changes is high, which indicates that the data is standardized and comprehensive, and verifies the overall validity of the results. The general results of big data algorithms are higher in specific applications in the Individualized management mode of students, which is better than ant colony algorithms. At the same time, the specific application of big data algorithms in the Individualized management mode of students is greater than 90%, and the accuracy has not changed significantly. To further verify the superiority of big data algorithms. To further verify the effectiveness of the proposed method in this paper, the general analysis of big data algorithms is carried out by different methods, Figure 6 shown.

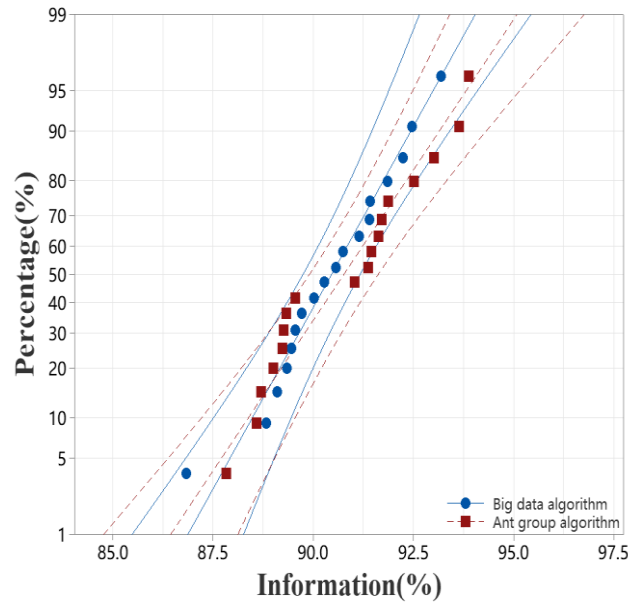


Figure 6. Specific applications of big data algorithm in the individualized management mode of students

In the analysis of personal Counselors management of students, ant colony algorithm can improve the indicators in management, and the original algorithm is equal and difficult, so it is relatively difficult to adjust the coefficients and norms, so it is necessary to conduct a comprehensive analysis of personal management data, and the overall analysis is relatively good.

Conclusion

Many people think that the counselor's management of students' big data function is obvious, this paper proposes a comprehensive optimization method based on big data algorithms and computer technology. First, by using the decentralized nature of big data algorithms and data immutability, the security and reliability of data is ensured. At the same time, the data is analyzed and processed by applying computer technology to extract potential features. Secondly, this paper deeply analyzes the key indicators of accuracy and reliability of specific applications in the Individualized management mode of students and constructs a complete Internet information collection system to provide accurate application results in the Individualized management mode of students. However, it should be noted that in the process of applying big data algorithms, the selection of specific application indicators in the Individualized management mode of students needs to be reasonably considered to give full play to the advantages of big data algorithms.

Scientific Ethics Declaration

* The authors declare that the scientific ethical and legal responsibility of this article published in EPSTEM Journal belongs to the authors.

Conflict of Interest

* The authors declare that they have no conflicts of interest

Funding

*This study received no external funding.

Acknowledgements or Notes

* This article was presented as an oral presentation at the International Conference on Technology (www.icontechno.net) held in Trabzon/Türkiye on May 01-04, 2025.

References

- Akhtar, P., Moazzam, M., Ashraf, A., & Khan, M. N. (2024). The interdisciplinary curriculum alignment to enhance graduates' employability and universities' sustainability. *International Journal of Management Education*, 22(3), 101037.
- Alshemaimri, B., Badshah, A., Daud, A., Bukhari, A., Alsini, R., & Alghushairy, O. (2025). Regional computing approach for educational big data. *Scientific Reports*, 15(1), 7619.
- Chen, X. X., Zhang, D., Wang, B., & Ahmad, K. (2024). Application-based big data development framework for health sciences libraries. *Health Information and Libraries Journal*, 41(3), 324-329.
- Chou, S. F., Horng, J. S., Liu, C. H., Yu, T. Y., Gan, B., Chang, W. J., & Lin, J. Y. (2025). The concepts of sustainability value and the application of big data in enhancing the ability of sustainability marketing. *Marketing Intelligence & Planning*, 43(3), 519-540.
- Delnevo, G., Ghini, V., Fiumana, E., & Mirri, S. (2024). A support tool for emergency management in smart campuses: reference architecture and enhanced web user interfaces. *Sensors*, 24(18), 5887.
- Elfeky, A. I. M., Najmi, A. H., & Elbyaly, M. Y. H. (2024). Effects of big data analytics in learning management systems for improving learners' academic success. *Profesional De La Informacion*, 33(1), e33016.
- Gao, D. N., Zhang, Y., & Wei, G. X. (2024). Athlete-focused student physique test and evaluation system utilizing body test big data: Enhancing performance and health monitoring. *Revista Internacional De Medicina Y Ciencias De La Actividad Fisica Y Del Deporte*, 24(97), 492-511.
- Gao, Y. L., Dong, Q., & Chen, Z. P. (2024). Leveraging the synergy of IPv6, generative ai, and web engineering to create a big data-driven education platform. *Journal of Web Engineering*, 23(2), 197-226.
- Han, F., & Ren, J. Y. (2024). Analyzing big data professionals: Cultivating holistic skills through university education and market demands. *IEEE Access*, 12, 23568-23577.
- Kulasegaram, K., Grierson, L., Barber, C., Chahine, S., Chou, F. C., Cleland, J., ...& Touchie, C. (2024). Data sharing and big data in health professions education: Ottawa consensus statement and recommendations for scholarship. *Medical Teacher*, 46(4), 471-485.
- Li, H. J. (2025). Multicultural data assistance mining analysis for ideological and political education in smart education platforms using artificial intelligence. *Wireless Networks*, 31(1), 567-581.
- Li, X. L. (2025). The curriculum planning and implementation for mindfulness education and diversified humanism based on big data. *Scientific Reports*, 15(1), 10588.
- Wu, X. Q., Chen, C., & Quan, L. L. (2024). Visual analysis and interactive interface design of students' abnormal behavior introducing clustering algorithm. *Technology and Health Care*, 32(6), 4947-4963.

Author Information

Jing Gui

Chiang Mai University
College of Arts, Media and Technology,
Thailand
Contact e-mail: jalways@163.com

Jirawit Yanchinda

Chiang Mai University
College of Arts, Media and Technology,
Thailand

To cite this article:

Gui, J., & Yanchinda, J. (2025). The application of big data algorithm in the personalized management of students by college counsellors. *The Eurasia Proceedings of Science, Technology, Engineering and Mathematics (EPSTEM)*, 33, 105-113.

The Eurasia Proceedings of Science, Technology, Engineering and Mathematics (EPSTEM), 2025

Volume 33, Pages 114-119

IConTech 2025: International Conference on Technology

The Impact of Artificial Intelligence and Robotics on the Nursing Labor Market: Transformations, Opportunities, and Challenges

Rumyana Stoyanova

Medical University of Plovdiv

Abstract: This report critically analyzes the effects of Artificial Intelligence (AI) and robotics on the nursing labor market, focusing on shifts in job roles, skills, and workforce dynamics. Utilizing a systematic review, the study examines AI's transformative potential in nursing practice, particularly through automating routine tasks, augmenting clinical decision-making, and streamlining patient care processes. AI technologies such as predictive analytics, natural language processing, and robotics offer substantial opportunities to enhance efficiency, reduce administrative burdens, and improve patient outcomes. However, the rapid adoption of AI also presents challenges, including potential job displacement, the widening of skill gaps, and ethical concerns related to data privacy and patient safety. The findings highlight the need for continuous professional development with a strong focus on digital literacy and skill enhancement to prepare nurses for changing roles in a technology-driven healthcare environment. The report also stresses the importance of regulatory oversight to address ethical implications and ensure equitable access to AI tools across different healthcare settings. Ultimately, the study calls for a strategic approach to AI integration, advocating for technology that supports and enhances, rather than replaces the nursing workforce. By fostering collaboration between AI developers, healthcare providers, and policymakers, the nursing profession can adapt to the digital era while maintaining its critical role in patient-centered care.

Keywords: Artificial intelligence, Robotics, Nursing labor market

Introduction

The shortage of nurses in Bulgaria has remained an unresolved issue for the past 30 years (IME, 2024), significantly affecting the efficiency and quality of healthcare services. The healthcare system is under increasing strain due to an aging population, a growing burden of chronic diseases, and an overall rise in demand for medical care. At the same time, the number of active nursing professionals continues to decline, as many leave the profession due to low wages, challenging working conditions and limited career development opportunities. This persistent workforce crisis leads to staff shortages, increased workloads, and burnout among the remaining nurses, further exacerbating the problem.

Demographic trends indicate that Bulgaria will continue to face serious challenges in maintaining a sufficient nursing workforce. Another major concern is the aging nursing workforce, with a large number of experienced nurses nearing retirement while too few new professionals are entering the field to fill the gap. Furthermore, the emigration of healthcare workers to countries with better pay and working conditions worsens the crisis, creating an urgent need for systemic reforms and innovative solutions (Mihaylova & Alakidi, 2023; Shopov & Stoeva, 2022). In this context, artificial intelligence (AI) and robotics have been proposed as potential solutions to alleviate nursing shortage. According to research, these technologies can assist in various nursing-related tasks, such as diagnostics, patient monitoring, medication administration, and administrative processes (Bin et al., 2022; Raymond et al., 2022; Tiase & Cato, 2021). However, the integration of AI and robotics into healthcare raises critical questions about their impact on nursing roles, required skills, and workforce dynamics.

- This is an Open Access article distributed under the terms of the Creative Commons Attribution-Noncommercial 4.0 Unported License, permitting all non-commercial use, distribution, and reproduction in any medium, provided the original work is properly cited.

- Selection and peer-review under responsibility of the Organizing Committee of the Conference

© 2025 Published by ISRES Publishing: www.isres.org

This study critically analyzes the effects of AI and robotics on the nursing labor market, focusing on how these technologies reshape job roles, influence skill requirements, and alter workforce structures.

Materials and Methods

A systematic search was conducted for scientific articles investigating and assessing the possibilities and limitations of AI or robotics to replace the activities performed by nurses, which would lead to overcoming the chronic shortage of labor in this category of personnel.

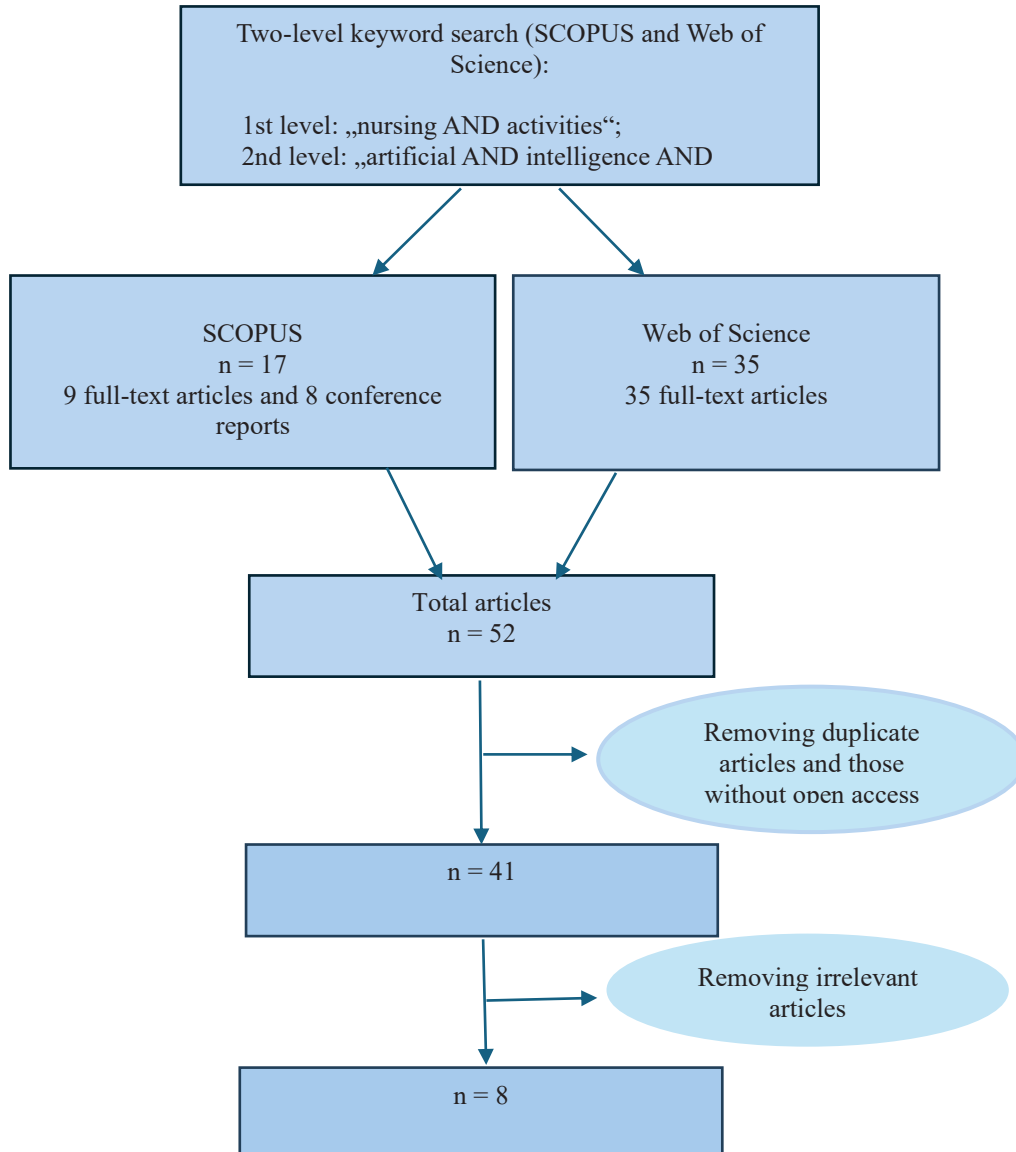


Figure 1. Stages in the selection of scientific publications.

The search was carried out using keywords in the international databases SCOPUS and Web of Science in early September 2024. In the first database, using the keywords "nursing AND activities" and subsequently "artificial AND intelligence AND robotics," 9 full-text articles and 8 conference reports were found, while in the second, 35 full-text articles were identified. When comparing the results from the two databases, it was found that some of the articles overlapped, and a significant share did not refer to activities performed by nurses but rather by rehabilitators or other medical specialists (mostly in neurosurgery and neurology). After removing the duplicate articles, 41 publications remained, of which only 25 were open access and were subjected to content analysis. As a result of content screening, only 8 articles remained that met the research objectives (see Figure 1). They were subjected to critical analysis.

Results and Discussion

Studies show a consensus on the potential of AI and robotics to automate routine and administrative tasks, but not to completely replace nurses. For instance, a significant number of activities have been identified that can be taken over by technologies - such as monitoring, registration, medication dosing and patient transport. However, this automation does not reduce the demand for nurses; instead, it transforms their roles, necessitating new skills to collaborate effectively with technology. On the other hand, the conclusions of the studies clearly indicate that although AI and robotics can ease the burden on nurses, they cannot replace them in providing care that requires human attention, emotional support and complex medical decisions. These findings are synthesized in Table 1, which summarizes key insights from the reviewed studies.

Table 1. Summary of key findings

Study	Activities performed by nurses that can be done by new technologies	Study Conclusion
Bin et al. (2022)	<ol style="list-style-type: none"> 1. Automation of patient registration, reducing administrative burden on nurses. 2. Assisted monitoring and initial screening, leading to faster referral to physician care. 	<ol style="list-style-type: none"> 1. Reduced nurses' workload, allowing focus on complex medical tasks. 2. Increased need for new technological skills. 3. Automation will not replace human care.
Pailaha (2023)	<ol style="list-style-type: none"> 1. AI-driven automation of documentation. 2. Improved patient monitoring and diagnosis. 3. AI handling routine tasks. 	<ol style="list-style-type: none"> 1. Freed time for advanced care. 2. Need for reskilling and technological competencies.
Tiase and Cato (2021)	<ol style="list-style-type: none"> 1. Monitoring vital signs and reporting anomalies. 2. Automated medication dosing. 3. Automated documentation. 	<ol style="list-style-type: none"> 1. Reduced demand for nurses in routine tasks. 2. Expanded nursing roles in technology management and advanced care.
Raymond et al. (2022)	<ol style="list-style-type: none"> 1. Clinical decision-making and diagnostic support. 2. Risk assessment. 3. Patient triage and referral to specialized care. 4. Automated patient monitoring. 	<ol style="list-style-type: none"> 1. AI will enhance efficiency as a tool. 2. Necessity of nurse retraining.
Blechar and Zalewska (2019)	<ol style="list-style-type: none"> 1. Robots performing routine tasks (e.g., delivering food/medications). 2. Robots conduct invasive/non-invasive procedures. 3. Robotic therapy for stress reduction. 	<ol style="list-style-type: none"> 1. Nurses gain time to focus on humanistic care. 2. Increased efficiency and reduced staff stress.
Zachariae et al. (2024)	<ol style="list-style-type: none"> 1. Automated patient transport. 2. Transport of medical supplies. 3. Robotic monitoring for emergencies. 	<ol style="list-style-type: none"> 1. Relief from physically demanding tasks. 2. Need for new skills and training in robotic systems.
Mlakar et al. (2022)	<ol style="list-style-type: none"> 1. Physical assistance and mobility support for patients. 2. Automated vital sign measurement. 3. Social support via humanoid robots. 	<ol style="list-style-type: none"> 1. Reduced nurse workload. 2. Need for additional training in robotic systems. 3. Concerns about dehumanization of care.
Georgadarellis et al. (2024)	<ol style="list-style-type: none"> 1. Robotic systems for diagnostics and surgeries. 2. Patient-assistance robots. 	<ol style="list-style-type: none"> 1. Reduced workload through automation. 2. Nurses must acquire new technological skills.

The analyzed studies underscore the increasingly significant role of artificial intelligence (AI) and robotics in healthcare, particularly within nursing. The primary impact of these technologies lies not in replacing nurses but

in transforming their responsibilities and enhancing the efficiency of healthcare delivery. One key finding is that AI and robotic systems can automate numerous routine tasks, including patient registration, medical documentation, vital sign monitoring, triage, patient allocation, medical supply transportation, and medication dispensing. By alleviating administrative and physical burdens, these innovations enable nurses to dedicate more time to complex, patient-centered care.

Conversely, research unanimously emphasizes that automation, while improving efficiency, cannot supplant the irreplaceable human element in nursing. Emotional support, clinical decision-making, managing complex medical conditions, and personalized care remain inherently dependent on human expertise. Rather than reducing the demand for nurses, technological advancements necessitate the acquisition of new skills, such as collaborating with AI systems. This shift highlights the urgent need for updated nursing education programs and continuous professional development.

It is important to note that despite the advantages of AI and robotics, their implementation poses several challenges. Among these are ethical concerns related to the dehumanization of healthcare, the risk of dependency on technology, and potential algorithmic errors. Additionally, there are concerns about possible resistance from medical personnel and shifts in the labor market that may require the retraining of a significant number of professionals.

Another crucial challenge is the issue of accountability - who will bear responsibility for errors caused by artificial intelligence? The lack of clear regulatory frameworks could complicate the integration of these technologies into clinical practice. Furthermore, while AI offers substantial benefits in terms of efficiency, risks remain related to algorithmic biases and the lack of personalized care for patients.

In the future, hybrid work models may become necessary, in which nurses and AI work in synergy. This will require a reevaluation of existing medical protocols and the establishment of new standards for working with intelligent systems. It is also possible that the demand for specialists who oversee AI operations and ensure patient safety will increase.

In conclusion, artificial intelligence and robotics represent powerful tools for improving nursing care, but they cannot fully replace nurses. Instead, they lead to a redefinition of their role and require a balance between technological innovations and the preservation of the human aspect in healthcare. To achieve successful integration, strategic planning, effective staff training, and the establishment of clear regulatory frameworks for these technologies are essential.

Conclusion

The integration of AI and robotics into the nursing labor market presents transformative potential for addressing Bulgaria's persistent nursing shortage. By automating routine tasks such as patient registration, medication administration, and documentation, these technologies can alleviate administrative burdens and physical strain on nurses, enabling them to prioritize complex care, patient interaction, and critical decision-making. However, the findings underscore that AI and robotics are not replacements for human nurses but tools to augment their roles. The human elements of empathy, ethical judgment, and personalized care remain irreplaceable.

To harness these technologies effectively, Bulgaria must prioritize workforce adaptation through targeted upskilling programs, integrating digital literacy and AI management into nursing education. Ethical challenges - such as algorithmic bias, accountability for errors, and data privacy: require robust regulatory frameworks and collaboration between policymakers, healthcare institutions, and AI developers. Additionally, addressing concerns about dehumanization and ensuring equitable access to AI tools across healthcare settings will be critical.

Strategic implementation should focus on hybrid models where nurses and AI systems collaborate synergistically. This approach not only enhances healthcare efficiency but also preserves the core values of patient-centered care. For Bulgaria, leveraging AI and robotics could mitigate workforce strain, improve retention by reducing burnout, and attract new professionals through modernized roles. Ultimately, the successful integration of these technologies depends on balancing innovation with ethical governance and continuous investment in the nursing workforce.

Recommendations

To optimize the integration of AI and robotics in nursing, healthcare institutions should prioritize workforce reskilling through targeted training programs that equip nurses with technological competencies, such as managing AI-driven systems and robotic tools. Concurrently, workflows should be redesigned to delegate routine tasks (e.g., patient registration, medication delivery) to automation, freeing nurses to focus on complex care and human-centric interactions. Ethical guidelines must be established to prevent dehumanization, ensuring technologies complement - rather than replace - human judgment, particularly in emotionally sensitive scenarios. Policymakers should advocate for funding to support infrastructure upgrades and update nursing curricula to include digital literacy and AI ethics. Finally, interdisciplinary collaboration between clinicians, engineers, and ethicists is critical to designing systems that align with clinical needs while monitoring outcomes like reduced burnout and improved diagnostic accuracy. By balancing automation with workforce development and ethical oversight, healthcare systems can enhance care quality, reduce administrative burdens, and ensure sustainable adaptation to technological advancements.

Scientific Ethics Declaration

* The author declares that the scientific ethical and legal responsibility of this article published in EPSTEM Journal belongs to the author.

Conflict of Interest

* The author declares that there is no conflict of interest

Funding

*This study received no external funding.

Acknowledgements or Notes

* This article was presented as an oral presentation at the International Conference on Technology (www.icontechno.net) held in Trabzon/Türkiye on May 01-04, 2025.

References

- Bin, K. J., Melo, A. A. R., da Rocha, J. G. M. F., de Almeida, R. P., Cobello Junior, V., Maia, F. L., & Ono, S. K. (2022). The impact of artificial intelligence on waiting time for medical care in an urgent care service for COVID-19: A single-center prospective study. *JMIR Formative Research*, 6(2), e29012.
- Blechar, L., & Zalewska, P. (2019). The role of robots in the improving work of nurses. *Pielęgniarstwo XXI wieku/Nursing in the 21st Century*, 18(3), 174–182.
- Georgadarellis, G. L., Cobb, T., Vital, C. J., & Sup, I. V. F. C. (2024). Nursing perceptions of robotic technology in healthcare: A pretest–posttest survey analysis using an educational video. *IISE Transactions on Occupational Ergonomics and Human Factors*, 12(1–2), 68–83.
- IME. (2024, December 19). *Deset resheniya na problema s meditsinskite sestri: Analiz na IPI* 19.12.2024. Retrieved from <https://ime.bg/wp-content/uploads/2024/12/deset-resheniya-na-problema-s-meditsinskite-sestri-analiz-na-ipi-19.12.2024.pdf>
- Mihaylova, V., & Alakidi, A. (2023). Professional challenges for healthcare professionals. *Bulgarian Journal of Public Health*, 15(2), 27–34.
- Mlakar, I., Kampic, T., Flis, V., Kobilica, N., Molan, M., Smrke, U., & Bergauer, A. (2022). Study protocol: A survey exploring patients' and healthcare professionals' expectations, attitudes and ethical acceptability regarding the integration of socially assistive humanoid robots in nursing. *BMJ Open*, 12(4), e054310.
- Pailaha, A. D. (2023). The impact and issues of artificial intelligence in nursing science and healthcare settings. *SAGE Open Nursing*, 9, 23779608231196847.

- Raymond, L., Castonguay, A., Doyon, O., & Paré, G. (2022). Nurse practitioners' involvement and experience with AI-based health technologies: A systematic review. *Applied Nursing Research*, 66, 151604.
- Shopov, D., & Stoeva, T. (2022). Age structure of working nurses in Bulgaria. *Information for Nursing Staff*, 54(1), 9–14.
- Tiase, V. L., & Cato, K. D. (2021). From artificial intelligence to augmented intelligence: Practical guidance for nurses. *OJIN: The Online Journal of Issues in Nursing*, 26(3), 4.
- Zachariae, A., Plahl, F., Tang, Y., Mamaev, I., Hein, B., & Wurll, C. (2024). Human-robot interactions in autonomous hospital transports. *Robotics and Autonomous Systems*, 179, 104755.

Author Information

Rumyana Stoyanova

Medical University of Plovdiv

15a Vassil Aprilov blvd., Plovdiv, Bulgaria

Contact e-mail: rumi_stoqnova@abv.bg

To cite this article:

Stoyanova, R. (2025). The impact of artificial intelligence and robotics on the nursing labor market: Transformations, opportunities, and challenges. *The Eurasia Proceedings of Science, Technology, Engineering and Mathematics (EPSTEM)*, 33, 114-119.

The Eurasia Proceedings of Science, Technology, Engineering and Mathematics (EPSTEM), 2025

Volume 33, Pages 120-129

IConTech 2025: International Conference on Technology

Fuzzy SVM Inverter-Based Field-Oriented Control of a DFIG used in a Wind Turbine

Azzedine Khati

Hassiba Benbouali University of Chlef

Taieb Bessaad

Hassiba Benbouali University of Chlef

Hamza Sahraoui

Hassiba Benbouali University of Chlef

Abstract: This research paper presents an advanced control strategy for Doubly Fed Induction Generators (DFIGs) used in wind turbines (WT), focusing on the implementation of a Field-Oriented Control (FOC) method combined with a fuzzy space vector modulation (FSVM) inverter approach. The proposed FSVM inverter-based direct vector control aims to optimize the performance of the DFIG by reducing stator current harmonics and active and reactive power ripples under varying wind conditions. The control strategy utilizes the FSVM algorithm to enhance the voltage and current control of the system, ensuring improved dynamic performance and stability. The paper outlines the mathematical modeling of the DFIG system, the design of the FSVM-based control algorithm, and simulation results demonstrating the effectiveness of the approach in achieving higher efficiency and better system response compared to traditional control techniques.

Keywords: Doubly fed induction generators (DFIGs), Fuzzy logic, Space vector modulation (SVM)

Introduction

Although the doubly-fed induction generator (DFIG) has the disadvantage of requiring collector brushes, which reduce its robustness and necessitate frequent maintenance, its adoption in renewable energy systems continues to grow. This is due to its operational principle, which enables power adjustment on the rotor, facilitating the control of the power delivered to the grid through the connection between the rotor and the grid [Khati (2024)-Decai (2020)]. This widespread interest is reflected in the extensive body of research and publications that focus on the application of DFIG in Wind Turbine Systems (WTS) (Maksud, 2024; Yaichi, 2023).

On the other hand, various control techniques have been employed for torque and power management of the DFIG, such as Sliding Mode (SM) (Kouadria, 2024), Neural Network (NN) (Sharadbhai, 2021), Field Oriented Control (FOC) (Zoubir, 2018) and Backstepping (Anwar, 2016; Adekanle, 2017) among others. However, these methods often result in high Total Harmonic Distortion (THD) in the stator currents and significant power ripples (Benbouhenni, 2018), particularly when combined with Pulse Width Modulation (PWM) inverters, which are commonly used in electrical machine control. Unfortunately, these inverters also introduce additional harmonics in flux, power, and torque.

To solve this problem, Gouaamar (2025) proposed a new method for controlling the converter, known as Space Vector Modulation (SVM). The advantage of SVM is its ability to minimize THD, with its underlying principle discussed in Reghioui (2019). However, this method also has some limitations, such as variable switching frequency and high ripples caused by hysteresis regulators.

To enhance the control of active and reactive powers in DFIG, this study suggests substituting the hysteresis blocks in SVM with fuzzy logic controllers for improved performance. This approach is referred to as Fuzzy SVM (see Fig. 5). In addition, fuzzy logic technology is not based on a complex mathematical model (Khati, 2020). Moreover, the Fuzzy SVM minimizes harmonic distortion in the stator currents.

This article is structured as follows: first, we introduce the DFIG using the d-q reference model. Next, we provide a detailed explanation of the DVC of DFIG with inverter SVM. We then describe the fuzzy logic system to be applied to the inverter SVM. Finally, we simulate the overall control strategy of the system.

DFIG Model

The DFIG is represented in the Park (d-q) model by the following equations [2]:

$$\begin{cases} V_{sd} = R_s \cdot I_{sd} + \frac{d\psi_{sd}}{dt} - \omega_s \cdot \psi_{sq} \\ V_{sq} = R_s \cdot I_{sq} + \frac{d\psi_{sq}}{dt} + \omega_s \cdot \psi_{sd} \\ \omega_r = \omega_s - p \cdot \Omega \\ V_{rd} = R_r \cdot I_{rd} + \frac{d\psi_{rd}}{dt} - \omega_r \cdot \psi_{rq} \\ V_{rq} = R_r \cdot I_{rq} + \frac{d\psi_{rq}}{dt} + \omega_r \cdot \psi_{rd} \end{cases} \quad (1)$$

$$\begin{cases} \psi_{sd} = L_s \cdot I_{sd} + M \cdot I_{rd} \\ \psi_{sq} = L_s \cdot I_{sq} + M \cdot I_{rq} \\ \psi_{rd} = L_r \cdot I_{rd} + M \cdot I_{sd} \\ \psi_{rq} = L_r \cdot I_{rq} + M \cdot I_{sq} \end{cases} \quad (2)$$

Where, R_s, R_r, L_s, L_r and M : Parameters of the generator.

ψ_{sdq} and ψ_{rdq} : Stator and rotor flux.

ω_s and ω_r : Stator and rotor pulsation.

Ω : Mechanical speed.

p : Number of pair of poles

The mechanical equation of the system is expressed as:

$$T_e = T_r + J \frac{d\Omega}{dt} + f\Omega \quad (3)$$

Where: T_e : Electromagnetic torque

T_r : Load torque

J : Inertia

f : Viscous friction coefficient

And the electromagnetic torque can be expressed as:

$$T_e = p \cdot M (I_{rd} \cdot I_{sq} - I_{rq} \cdot I_{sd}) \quad (4)$$

Similarly, the active power and reactive power of the stator are given by the following expressions:

$$\begin{cases} P_s = \frac{3}{2} (V_{sd} \cdot I_{sd} + V_{sq} \cdot I_{sq}) \\ Q_s = \frac{3}{2} (V_{sq} \cdot I_{sd} - V_{sd} \cdot I_{sq}) \end{cases} \quad (5)$$

Where: P_s : Stator's active power, Q_s : Stator's reactive power

Field-Oriented Control

The principle of this control is to align the stator flux vector with the “d” axis, thereby eliminating it along the “q” axis [4] (Fig. 1), also called Direct Vector Control (DVC).

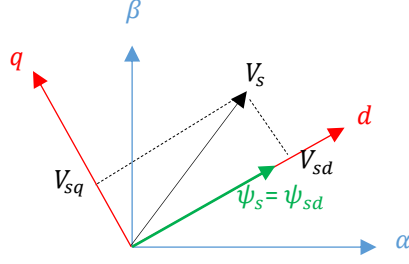


Figure 1. Stator flux oriented along the “d” axis

$$\psi_s = \psi_{sd} \text{ and } \psi_{sq} = 0$$

With negligible R_s from (1), we can write:

$$\begin{cases} V_{sd} = 0 \\ V_{sq} = \omega_s \cdot \psi_{sd} \end{cases} \quad (6)$$

$$\begin{cases} I_{sd} = -\frac{M}{L_s} I_{rd} + \frac{\psi_s}{L_s} \\ I_{sq} = -\frac{M}{L_s} I_{rq} \end{cases} \quad (7)$$

And (5) becomes:

$$\begin{cases} P_s = -\frac{3}{2} \frac{\omega_s \psi_s M}{L_s} I_{rq} \\ Q_s = -\frac{3}{2} \left(\frac{\omega_s \psi_s M}{L_s} I_{rd} - \frac{\omega_s \psi_s^2}{L_s} \right) \end{cases} \quad (8)$$

Also (4) becomes:

$$T_e = -\frac{3}{2} p \cdot \frac{M}{L_s} \cdot I_{rq} \cdot \psi_s \quad (9)$$

Figure 2 depicts the concept of the DVC technique using an SVM inverter to control the DFIG. In contrast,

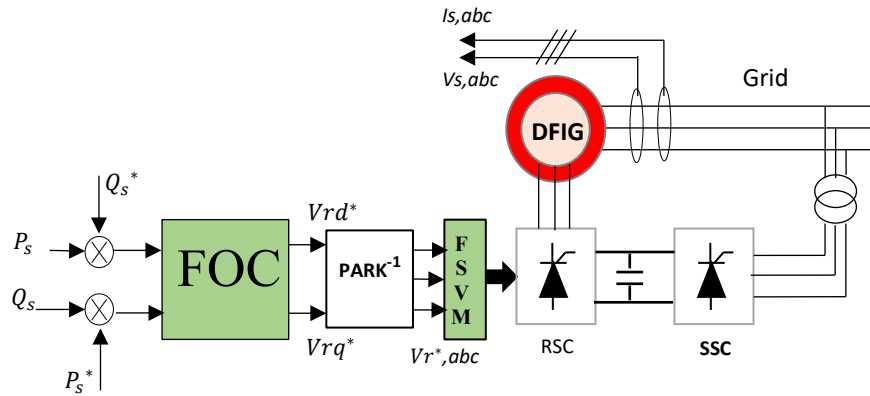


Figure 2. DVC of DFIG scheme

Fuzzy SVM

The inverter can be controlled using various methods. Many studies have utilized the Pulse Width Modulation (PWM) technique, while others have applied alternative methods such as Discrete Pulse Width Modulation (DPWM), as shown in Gaballah (2013). Additionally, Su (2025) proposed the Space Vector Modulation (SVM) technique, which is also commonly used to modulate inverters. This method relies on calculating the angles and parameters of sectors. However, Benbouhenni (2018) introduced a new SVM inverter that eliminates the need for

sector and angle calculations. Instead, it computes the maximum and minimum of balanced voltages (Fig. 3). This version of SVM offers several advantages, including the absence of sector identification, no need for angle information, and no reliance on lookup tables to calculate switching times. Furthermore, it delivers high performance in real-time control systems (Qiu,2025).

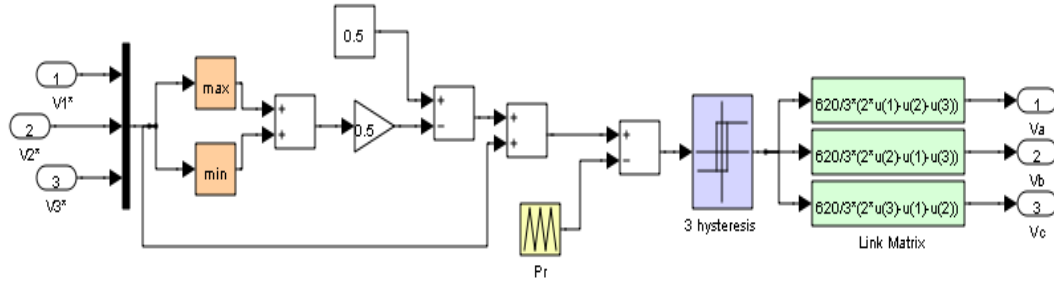


Figure 3. SVM inverter command

In this section, we propose replacing the hysteresis blocks in SVM with fuzzy logic controllers to improve the control performance. This approach is referred to as Fuzzy SVM (Fig. 4). On the other hand, fuzzy logic technology does not require a complex mathematical model (Khatai, 2020). Additionally, the Fuzzy SVM minimizes harmonic distortion in stator currents.

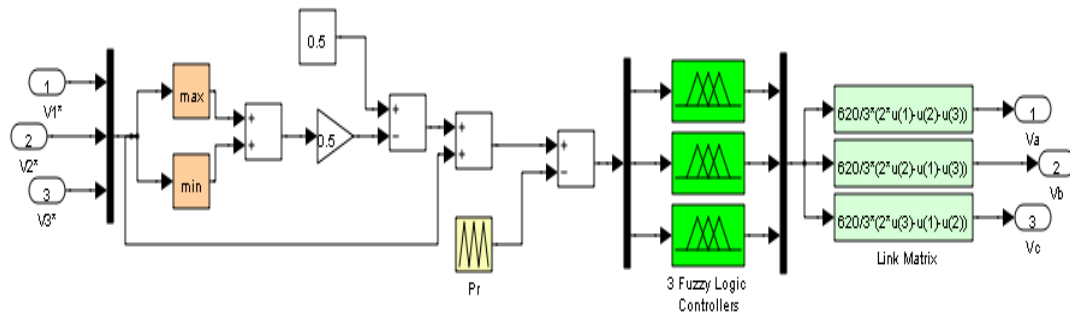


Figure 4. Fuzzy SVM inverter

Figure 5 illustrates the main structure of the Fuzzy logic controller. The proposed Fuzzy Logic controller is based on hysteresis controllers. The most commonly used fuzzy controller is the e - Δe controller, which is a two-input fuzzy controller that generates a command output. Here, e represents the error, and Δe denotes the variation in error.

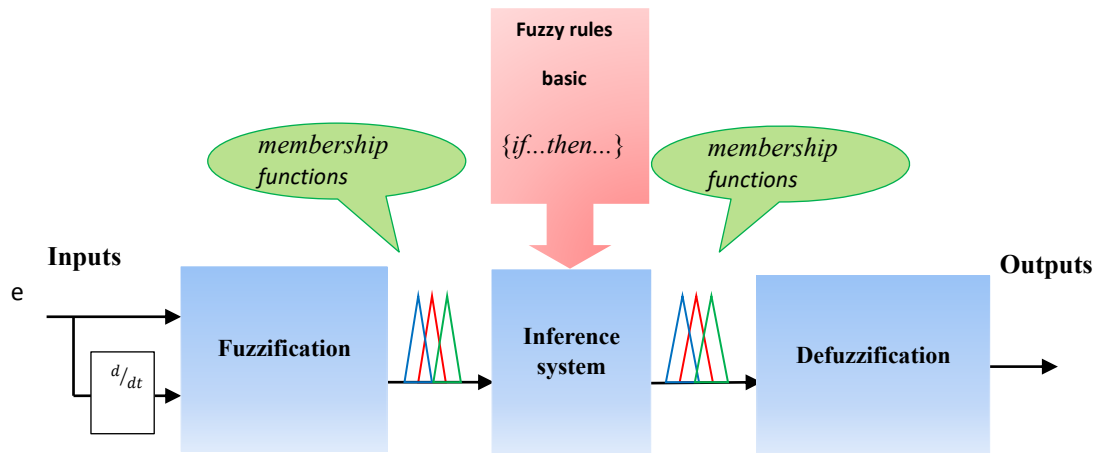


Figure 5. Internal structure of fuzzy rules

To generate a fuzzy command, several components must be chosen, including the linguistic information model, the inference process, the aggregation process, and the defuzzification process. For the linguistic variables e

(error) and Δe (error variation), the following linguistic values are defined: Negative Big (**NB**), Negative Middle (**NM**), Negative Small (**NS**), Positive Small (**PS**), Positive Big (**PB**), Positive Middle (**PM**), and Equal Zero (**EZ**). The definition of the membership function for both the input and output is provided in Figure 6.

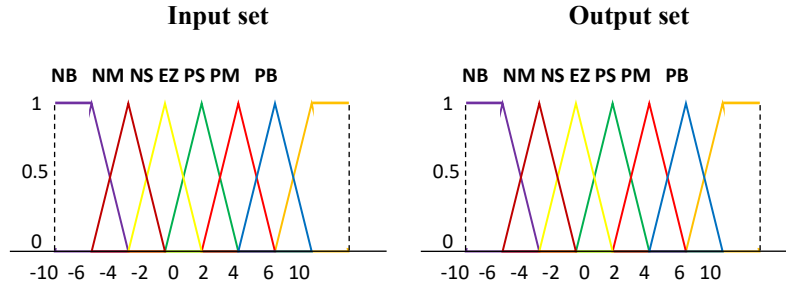


Figure 6. Membership function for the input and output

The fuzzy rules governing this system are formulated as follows:

{IF e is NB and Δe is NB THEN s is NB
 (IF e is NB and Δe is NM THEN s is NB
 {IF e is PB and Δe is PM THEN s is PBT

The seven fuzzy sets, defined by their membership functions for both e and Δe , allow the construction of 49 distinct rules. These rules are presented in Table 1 (Sunori, 2025).

Table 1. Inference matrix							
$e \backslash \Delta e$	NB	NM	NS	EZ	PS	PM	PB
NB	NB	NB	NB	NB	NM	NS	EZ
NM	NB	NB	NB	NM	NS	EZ	PS
NS	NB	NB	NM	NS	EZ	PS	PM
EZ	NB	NM	NS	EZ	PS	PM	PB
PS	NM	NS	EZ	PS	PM	PB	PB
PM	NS	EZ	PS	PM	PB	PB	PB
PB	EZ	PS	PM	PB	PB	PB	PB

Figure 7 illustrates the parameters of the fuzzy controller. To view this figure, simply type ">> fuzzy" in the MATLAB workspace window.

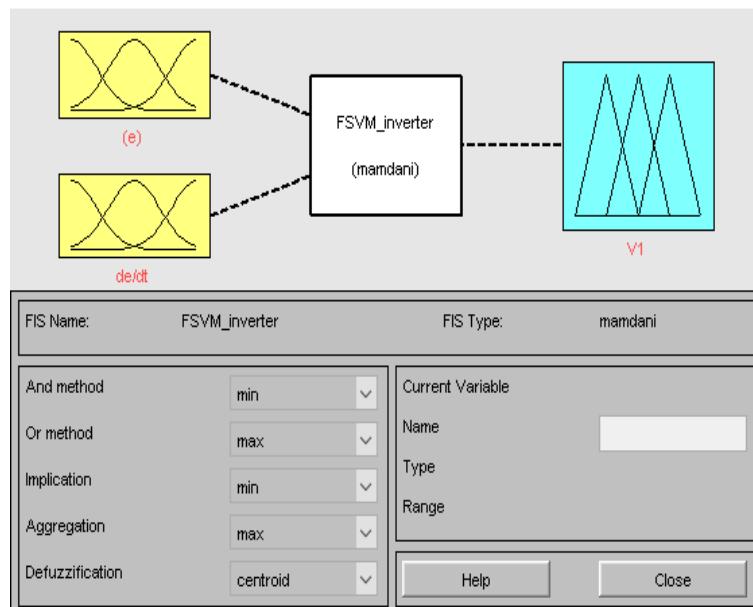


Figure 7. Fuzzy controller parameters

Simulation Results

To simulate the diagram shown in Fig. 2, we used MATLAB/Simulink software. The parameters of the DFIG are provided in the following table. To improve the system's response time and achieve optimal energy performance, it is necessary to maintain the reactive power at zero, ensuring a unity power factor. However, to test the reference tracking, we increased the reactive power reference after one second.

Table 2. DFIG parameters

$P_n=1.5$ (MW)
$V_s=398$ (V)
$f_s=50$ (Hz)
$P=2$
$R_r=0.021$ (Ω)
$R_s=0.012$ (Ω)
$L_r=0.0136$ (H)
$L_s=0.0137$ (H)
$M=0.0135$ (H)
$f=0.0024$ (Nm/s)
$J=1000$ (Kg.m ²)

Reference Tracking Test

The simulation results for reference tracking of stator currents, torque, active and reactive power are presented in Figs. 8-10. As shown in Fig. 8, both the active power and reactive power successfully track their references with a highly acceptable response time of approximately 0.03s. It is clearly observed that the active power ripples, reactive power ripples, and torque ripples are all zero. This is undoubtedly attributed to the inverter's Fuzzy SVM. Finally, Figs. 9-10 demonstrate that the stator currents and torque track their respective references without any overshoot.

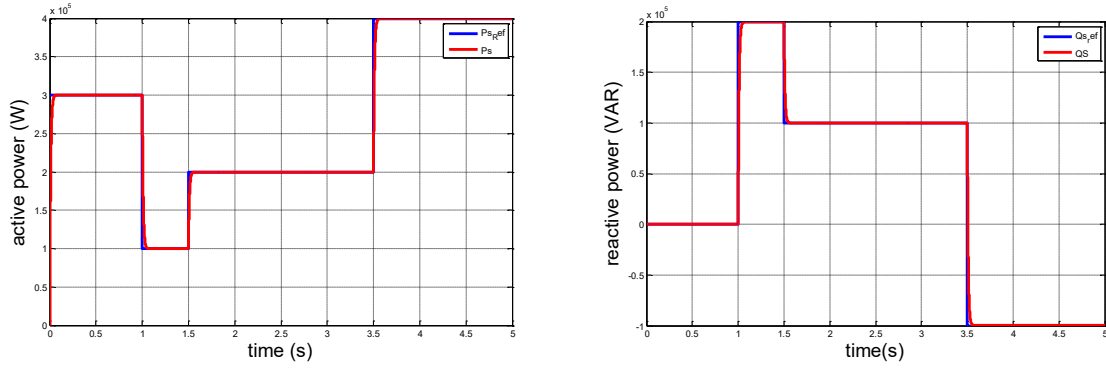


Figure 8. Active and reactive power (Reference tracking test)

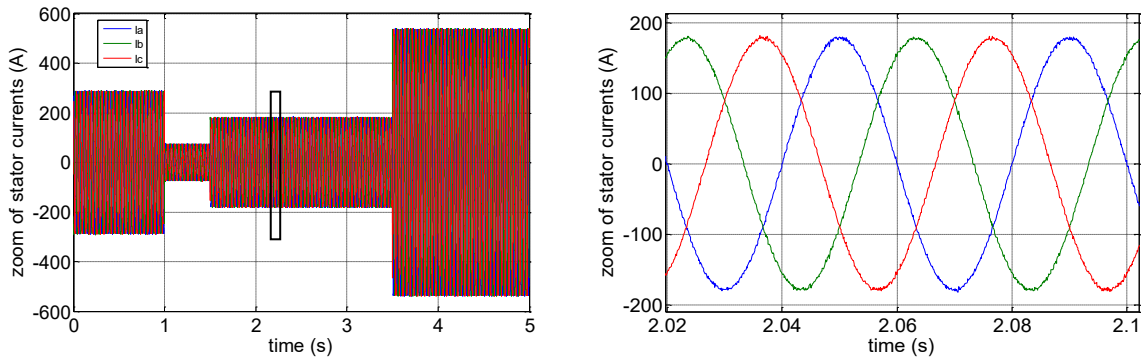


Figure 9. Stator currents (Reference tracking test)

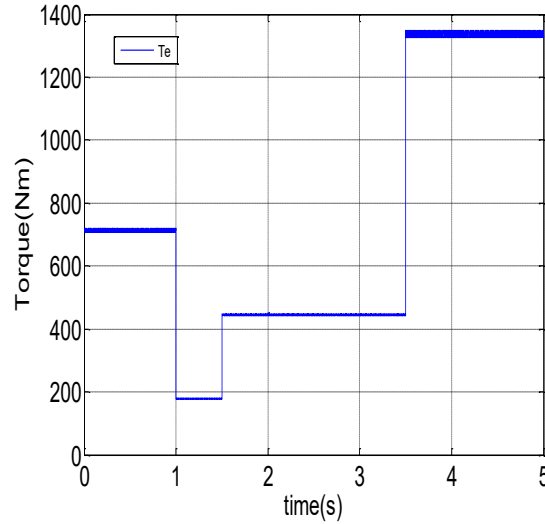


Figure 10. Torque (Reference tracking test)

Robustness Test

The robustness test involves modifying the electrical and magnetic parameters of the machine to evaluate the accuracy and reliability of the proposed control method. In this test, the rotor and stator resistances are increased, while the rotor, stator inductance and mutual inductances are reduced to 75% of their nominal values at the 0.5 second. The results demonstrate that the selected method is insensitive to variations in machine parameters. As shown in Figs. 11-13, the active power, reactive power, torque, and stator currents remain unaffected by these variations, despite some ripples that become noticeable after 0.5 seconds of simulation.

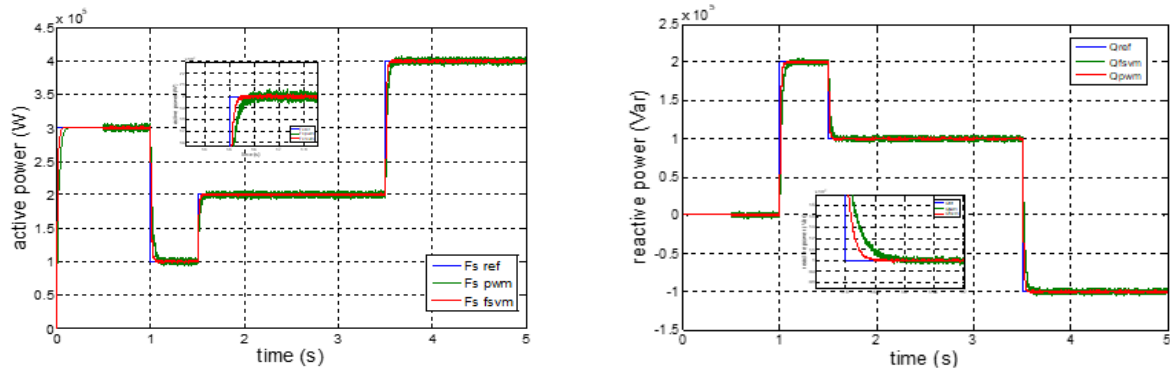
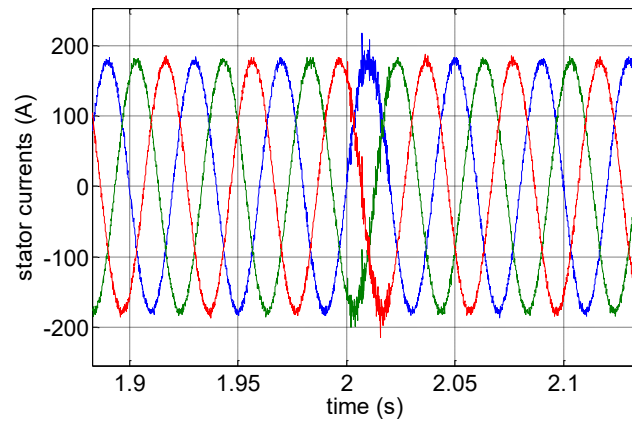


Figure 11. Active and reactive power for variations of machine parameters at 2s



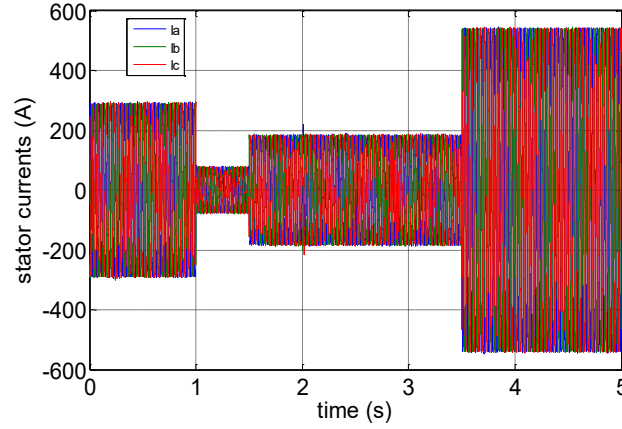


Figure 12. Stator currents for variations of machine parameters at 2s

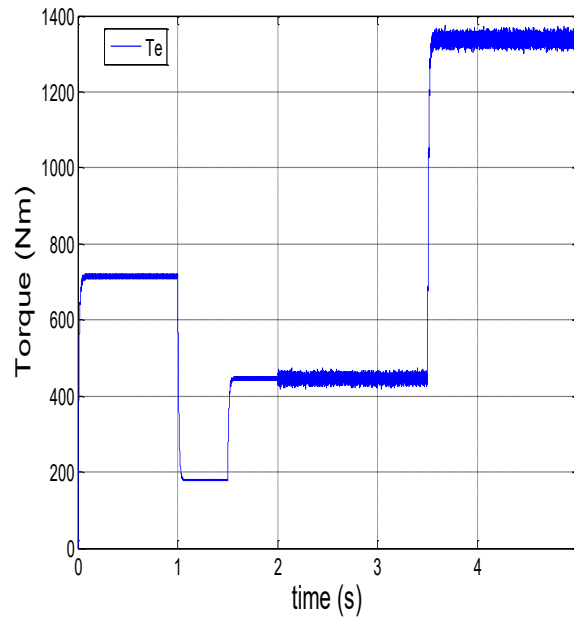


Figure 13. Torque for variations of machine parameters at 2s

Conclusion

This research utilizes artificial intelligence to control the active and reactive power of a DFIG using the Space Vector Modulation (SVM) technique. The proposed method is straightforward to implement and takes into account the estimation of key variables such as electromagnetic torque, stator active and reactive power, and stator currents. Furthermore, the integration of a Fuzzy SVM converter significantly reduces stator current ripples. The combination of the direct Vector Control (DVC) strategy with the Fuzzy SVM-based converter enhances the overall performance of the machine drive system.

Scientific Ethics Declaration

* The authors declare that the scientific ethical and legal responsibility of this article published in EPSTEM Journal belongs to the authors.

Conflict of Interest

* The authors declare that they have no conflicts of interest

Funding

*This study received no external funding.

Acknowledgements or Notes

* This article was presented as a/an oral/poster presentation at the International Conference on Technology (www.icontechno.net) held in Trabzon/Türkiye on May 01-04, 2025.

* The authors would like to thank the organizing and scientific committees of the 5th International Conference on Technology (IConTech).

References

- Adekanle, O., Guisser, M., Abdelmounim, E., & Aboulfatah, M. (2017, November). Adaptive backstepping control of grid-connected doubly-fed induction generator during grid voltage dip. *International Conference on Electrical and Information Technologies (ICEIT)* (pp. 1-6). IEEE.
- Anwar, G., Ahmed, G., Ali, C., & Ghada, M. (2016). Integral backstepping control for stability enhancement of doubly fed induction generator. *2nd International Conference on Electrical Engineering and Automatic Control (ICEEAC)*, 1-6.
- Decai, L., Meiyuan, C., Wei, Y. & Jihong, W (2020). Study of doubly fed induction generator wind turbines for primary frequency control. *IEEE 4th Conference on Energy Internet and Energy System Integration (EI2)*. (pp. 2690-2695).
- Gaballah, M., & El-Bardini, M. (2013). Low-cost digital signal generation for driving space vector PWM inverter. *Ain Shams Engineering Journal*, 4, 763–774.
- Gouaamar, R., El Fadl, A., Bri, S., & Mekrini, Z. (2025). Higher performance enhancement of direct torque control by using Space Vector Modulation for doubly fed induction machine. In *E3S Web of Conferences*, 601,16.
- Khati, A. (2024). Multivariable prediction control for direct vector control of a DFIG-based wind turbine using a fuzzy space vector modulation converter. *Iranian Journal of Electrical & Electronic Engineering*, 20(3), 25-37.
- Khati, A., Kansab, A., Taleb, R., & Khoudmi, H. (2020). Current predictive controller for high frequency resonant inverter in induction heating, *International Journal of Electrical and Computer Engineering*, 10(1), 255-264.
- Kouadria, M. A., Kouadria, S., & Chaib, H. (2024). Sliding mode control for doubly fed induction generators system-based a wind turbine. *Studies in Engineering and Exact Sciences*, 5(2), e7199.
- Makhsud, B., Furkat, T., Nuralibek R. & Alim H. (2024). The possibility of using hybrid winding in doubly fed induction generator. *III International Scientific and Technical Conference "Actual Issues of Power Supply Systems (ICAIPSS2023)*.
- Qiu, X., & He, X. (2025). Fuzzy Logic based scheduling optimization and risk control in power systems. *International Conference on Intelligent Systems and Computational Networks (ICISCN)*.
- Reghioui, H., Belhamdi, S., Abdelkarim, A., & Lallouani, H. (2019). Enhancement of space vector modulation based-direct torque control using fuzzy PI controller for doubly star induction motor. *Advances in Modelling and Analysis C*, 74(2-4), 63-70.
- Sharadhai, P. T., & Gupta, S. (2021). Artificial neural network based control of doubly fed induction generator for active filtering capabilities. *4th International Conference on Recent Developments in Control, Automation & Power Engineering (RDCAPE)*, 107-112.
- Su, H., Ovr, S. E., Xu, Z., & Alfayad, S. (2024). Exploring the potential of fuzzy sets in cyborg enhancement: a comprehensive review. *IEEE Transactions on Fuzzy Systems*, 33(3), 810-827.
- Sunori, S. K., Joshi, P., Mittal, A., & Juneja, P. (2025). Fuzzy logic based dynamic spectrum allocation in wireless communication. *International Conference on Electronics and Renewable Systems (ICEARS)* (pp. 831-838). IEEE.
- Yaichi, I (2023). Control of doubly fed induction generator using artificial neural network controller. *Revue Roumaine Des Sciences Techniques — Série Électrotechnique Et Énergétique*, 68(1), 46-51.

Zoubir, Z., Linda, B., & Abdelkader, L. (2018). Field oriented control of doubly fed induction generator integrated in wind energy conversion system using artificial neural networks. *International Conference on Electrical Sciences and Technologies in Maghreb (CISTEM)*, 1-7.

Author(s) Information

Azzedine Khati

Hassiba Benbouali University
El-hassania, Chlef, Algeria
Contact e-mail : a.khati@univ-chlef.dz

Taieb Bessaad

Hassiba Benbouali University
El-hassania, Chlef, Algeria

Hamza Sahraoui

Hassiba Benbouali University
El-hassania, Chlef, Algeria

To cite this article:

Khati, A., Bessaad, T., & Sahraoui, H. (2025). Fuzzy SVM inverter-based field-oriented control of a DFIG used in a wind turbine. *The Eurasia Proceedings of Science, Technology, Engineering and Mathematics (EPSTEM)*, 33, 120-129.

The Eurasia Proceedings of Science, Technology, Engineering and Mathematics (EPSTEM), 2025

Volume 33, Pages 130-139

IConTech 2025: International Conference on Technology

Influence of Different Behavior in Tension and Compression on Longitudinal Fracture of Inhomogeneous Beams Under Impact

Victor Rizov

University of Architecture, Civil Engineering and Geodesy

Abstract: The current paper has for its purpose to develop a theoretical investigation of the effect of different mechanical behavior in tension and compression on the longitudinal fracture in continuously inhomogeneous beam structures subjected to impact loading. The basic motive for carrying-out this investigation is the fact that in many situations in engineering practice various beam structures are under impact loading which may be induced, for instance, by falling objects which strike the structure. This kind of loading threatens the structural integrity and reliable functioning of engineering constructions. Therefore, it is important to study in detail different aspects of the behavior of structures under impact. This paper is focused on the influence of different mechanical behavior in tension and compression on the longitudinal fracture. The beams under consideration are non-linear elastic and exhibit continuous inhomogeneity along their thickness. The integral J is applied for studying the longitudinal fracture under impact loading. The strain energy release rate is obtained to verify the solution of the integral J . Results illustrating the effect of different behavior in tension and compression are derived and presented in graphical form.

Keywords: Impact loading, Longitudinal fracture, Inhomogeneous beam structure

Introduction

The quick development of continuously inhomogeneous (functionally graded) structural materials has a significant influence on the state of various branches of modern engineering (Kaul, 2014; Toudehdeghghan et al., 2017; Gandra et al., 2011). The strong interest which the representatives of the international engineering community around the globe show towards the continuously inhomogeneous materials is conditioned mainly by their excellent properties (Mahamood & Akinlabi, 2017). Among them, one of the most important advantages of these new engineering materials in comparison with the traditional homogeneous materials like metals or heterogeneous (fiber reinforced) composites is the continuous variation of their properties along one or more directions in a given structural member (Radhika et al., 2020; Rizov, 2018). Besides, the variation of the material properties can be tailored during manufacturing in order to achieve some predefined goals (Gururaja Udupa et al., 2014; Fanani et al., 2021). However, the increasing application of these highly efficient materials requires elaboration and practical use of different methods for analyzing the behavior and performance of structural members and components subjected to various external influences. In the context of safety, studying fracture behavior of continuously inhomogeneous structural members under different loading conditions is of primary importance (Dowling, 2007; Rizov, 2019, 2024).

The current paper focuses on analyzing the effects of different mechanical behavior in tension and compression on longitudinal fracture in continuously inhomogeneous load-bearing beam structures under impact loading. The beams under consideration have non-linear elastic behavior. The material exhibits continuous inhomogeneity along the beam thickness. The beam hosts a longitudinal crack. The impact loading is induced by a falling object that strikes the beam. The longitudinal fracture behavior of the beam under impact is analyzed by applying the integral J .

The strain energy release rate (SERR) under impact loading is derived for verification of the integral J solution. A parametric study is carried out by applying the solution. The results of the parametric study are reported in the form of graphs. The study provides a useful knowledge for the influence of different mechanical behavior in tension and compression on longitudinal fracture of continuously inhomogeneous non-linear elastic engineering structures subjected to impact loading.

Theoretical Investigation

The load-bearing beam structure depicted in Figure 1 is subjected to impact loading by a small object of weight, P , which falls from height, h_p , and strikes the upper surface of the beam in point, B_4 .

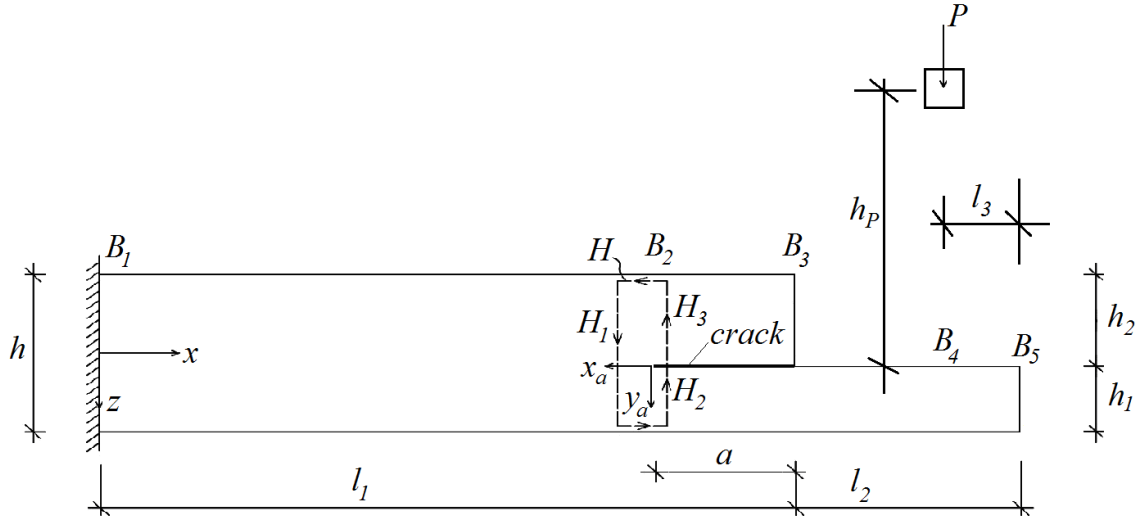


Figure 1. Inhomogeneous beam structure under impact loading

The beam is clamped in its left-hand end. The right-hand end of the beam is free. The thickness of the beam in portion, B_1B_3 , is h . In section, B_3 , the beam thickness changes abruptly. In portion, B_3B_5 , the thickness is h_1 . The beam hosts a longitudinal crack of length, a , in portion, B_2B_3 .

The material of the beam has non-linear elastic behavior that obeys the Ramberg-Osgood law (Dowling, 2007). In compression, the behavior is described by the stress-strain relation presented in Eq. (1).

$$\varepsilon_c = \frac{\sigma_c}{E_c} + \left(\frac{\sigma_c}{D_c} \right)^{\frac{1}{n_c}}, \quad (1)$$

where ε_c is the strain, σ_c is the stress, E_c , D_c and n_c are material parameters. The stress-strain relation in tension is presented in Eq. (2).

$$\varepsilon_t = \frac{\sigma_t}{E_t} + \left(\frac{\sigma_t}{D_t} \right)^{\frac{1}{n_t}}. \quad (2)$$

Here, ε_t is the strain, σ_t is the stress, E_t , D_t and n_t are material parameters in tension.

The material of the beam is continuously inhomogeneous along the thickness. The change of material parameters across the beam thickness is given below.

$$E_c = E_{cup} + \frac{E_{clw} - E_{cup}}{h^\alpha} \left(\frac{h}{2} + z \right)^\alpha, \quad (3)$$

$$D_c = D_{cup} + \frac{D_{clw} - D_{cup}}{h^\beta} \left(\frac{h}{2} + z \right)^\beta, \quad (4)$$

$$n_c = n_{cup} + \frac{n_{clw} - n_{cup}}{h^\eta} \left(\frac{h}{2} + z \right)^\eta, \quad (5)$$

$$E_t = E_{tup} + \frac{E_{tlw} - E_{tup}}{h^\lambda} \left(\frac{h}{2} + z \right)^\lambda, \quad (6)$$

$$D_t = D_{tup} + \frac{D_{tlw} - D_{tup}}{h^\rho} \left(\frac{h}{2} + z \right)^\rho, \quad (7)$$

$$n_t = n_{tup} + \frac{n_{tlw} - n_{tup}}{h^\omega} \left(\frac{h}{2} + z \right)^\omega \quad (8)$$

where

$$-\frac{h}{2} \leq z \leq \frac{h}{2} \quad (9)$$

Here E_{cup} , D_{cup} and n_{cup} are the values of E_c , D_c and n_c on the upper surface of the beam, E_{clw} , D_{clw} and n_{clw} are the values of E_c , D_c and n_c on the lower surface of the beam. Analogically, E_{tup} , D_{tup} and n_{tup} are the values of E_t , D_t and n_t on the upper surface of the beam, while E_{tlw} , D_{tlw} and n_{tlw} are the values of properties in tension on the lower surface of the beam. The parameters, α , β , η , λ , ρ and ω , govern the change of E_c , D_c , n_c , E_t , D_t and n_t , respectively.

The longitudinal fracture under impact is analyzed theoretically by using the integral J (Broek, 1986). The integration is performed long the contour H that is shown in Figure 1. Since the contour H has three portions, H_1 , H_2 and H_3 , the solution of J is obtained as

$$J = J_{H1} + J_{H2} + J_{H3}. \quad (10)$$

The solution of J in portion, H_1 , is given in Eq. (11).

$$J_{H1} = J_{H1c} + J_{H1t}, \quad (11)$$

where J_{H1c} and J_{H1t} are the solutions in the compression and tension zones, respectively. J_{H1c} and J_{H1t} are presented below, i.e.

$$J_{H1c} = \int \left[u_{0c} \cos \alpha_c - \left(p_{xac} \frac{\partial u}{\partial x_a} + p_{yac} \frac{\partial v}{\partial x_a} \right) \right] ds, \quad (12)$$

$$J_{H1t} = \int \left[u_{0t} \cos \alpha_t - \left(p_{xat} \frac{\partial u}{\partial x_a} + p_{yat} \frac{\partial v}{\partial x_a} \right) \right] ds \quad (13)$$

The components of J_{H1c} are found as

$$u_{0c} = \int \sigma_c d\varepsilon, \quad (14)$$

$$\cos \alpha_c = 1, \quad (15)$$

$$p_{xac} = -\sigma_c, \quad (16)$$

$$\frac{\partial u}{\partial x_a} = \varepsilon, \quad (17)$$

$$p_{yac} = 0, \quad (18)$$

$$ds = dz_1, \quad (19)$$

where σ_c is the stress in the compression zone, ε is the strain, α_c is the inclination of the integration contour, u is the axial displacement, v is the transversal displacement, z_1 is the vertical centric axis of the beam cross-section.

The quantities involved in Eq. (13) are determined as written below

$$u_{0t} = \int \sigma_t d\varepsilon, \quad (20)$$

$$\cos \alpha_t = 1, \quad (21)$$

$$p_{xat} = \sigma_t, \quad (22)$$

$$\frac{\partial u}{\partial x_a} = \varepsilon, \quad (23)$$

$$p_{yat} = 0, \quad (24)$$

$$ds = dz_1, \quad (25)$$

where σ_t is the stress in the tension zone.

The stresses are found by using the dynamic coefficient, k_{dyn} , i.e.

$$\sigma_c = k_{dyn} \sigma_{cst}, \quad (26)$$

$$\sigma_t = k_{dyn} \sigma_{tst}, \quad (27)$$

where σ_{cst} and σ_{tst} are the stresses in compression and tension induced by the static force of magnitude, P , applied in point, B_4 , on the upper surface of the beam. The dynamic coefficient is determined by applying the approach reported in (Obodovski & Hanin, 1981). This approach leads to Eq. (28) for k_{dyn} .

$$k_{dyn} = 1 + \sqrt{1 + 2 \frac{h_p}{\delta_{st}} \frac{P}{P + G_{bm}}} , \quad (28)$$

where δ_{st} is the static displacement of point, B_4 . G_{bm} is the deadweight of the beam structure.

The static displacement is found by using the integrals of Maxwell-Mohr, i.e.

$$\delta_{st} = \sum \int \kappa_i M_i dx , \quad (29)$$

where κ_i is the curvature, M_i is the bending moment induced by a unit vertical force applied in point, B_4 .

In order to derive the curvatures, we first analyze the distribution of the strains along the thickness of the beam in portion, B_1B_2 , by applying Eq. (30).

$$\varepsilon = \kappa_i (z_1 - z_{1n}) , \quad (30)$$

Where

$$-\frac{h}{2} \leq z_1 \leq \frac{h}{2} . \quad (31)$$

Here, z_{1n} is the neutral axis coordinate.

Then, the curvature and the neutral axis coordinate are determined by using Eqs. (32) and (33).

$$N = \iint_{(A_c)} \sigma_c dA + \iint_{(A_t)} \sigma_t dA , \quad (32)$$

$$M = \iint_{(A_c)} \sigma_c z_1 dA + \iint_{(A_t)} \sigma_t z_1 dA , \quad (33)$$

where N is axial force, M is the bending moment, A_c and A_t are the areas of compression and tension zones of the beam cross-section, respectively. N and M are found as

$$N = 0 , \quad (34)$$

$$M = P(l_1 + l_2 - l_3 - x) , \quad (35)$$

where the distances, l_1 , l_2 and l_3 , are defined in Figure 1. The MatLab is used for solving Eqs. (32) and (33).

The solution of the J integral in portion, H_2 , of the integration contour is derived by performing replacements in Eqs. (11) – (25).

The upper crack arm is free of stresses. Therefore, we have

$$J_{H3} = 0 \quad (36)$$

Finally, the J integral solution is found by using Eq. (10). The integration is performed by the MatLab.

The SERR, G , is derived to verify the J integral solution. For this purpose, the expression reported in (Rizov, 2018) is applied, i.e.

$$G = \frac{1}{b} \left(\iint_{(A_{H2c})} u_{0H2c}^* dA + \iint_{(A_{H2t})} u_{0H2t}^* dA - \iint_{(A_{H1c})} u_{0c}^* dA - \iint_{(A_{H1t})} u_{0t}^* dA \right), \quad (37)$$

where A_{H2c} and A_{H2t} are the compression and tension zones in the cross-section of the lower crack arm behind the crack tip, A_{H1c} and A_{H1t} are the compression and tension zones in the cross-section of the beam ahead of the crack tip, u_{0H2c}^* and u_{0H2t}^* are the complementary strain energy densities in compression and tension in the lower crack arm behind the crack tip, u_{0H1c}^* and u_{0H1t}^* are the complementary strain energy densities in compression and tension in the beam ahead of the crack tip. The complementary strain energy densities in compression and tension in the beam ahead of the crack tip are obtained by Eqs. (38) and (39), respectively.

$$u_{0H1c}^* = \sigma_c \varepsilon - u_{0c}, \quad (38)$$

$$u_{0H1t}^* = \sigma_t \varepsilon - u_{0t}, \quad (39)$$

where u_{0c} and u_{0t} are determined by Eq. (14) and Eq. (20), respectively. The complementary strain energy densities in compression and tension in the lower crack arm behind the crack tip are found by performing replacements in Eqs. (38) and (39). The SERR found by using Eq. (37) matches the solution of the integral J derived by Eq. (10) which is a verification of the solution.

Parametric Study

The parametric study reported in this section of the paper aims to evaluate how the longitudinal fracture of the inhomogeneous beam under impact loading is affected by the different mechanical behavior in tension and compression.

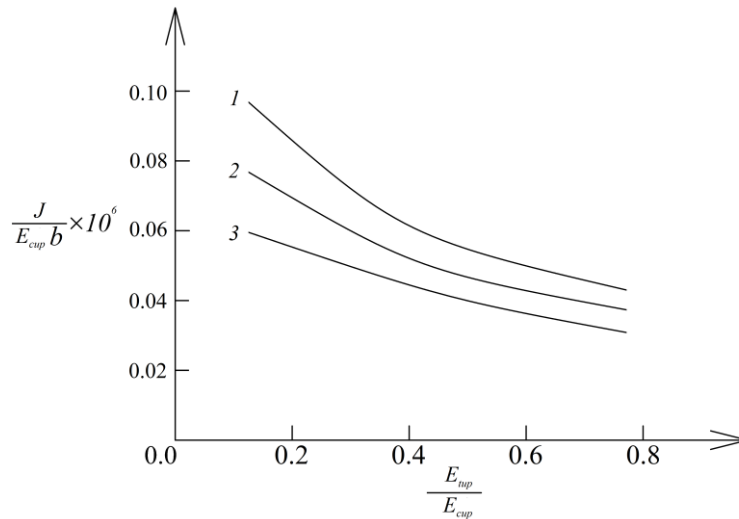


Figure 2. The integral J plotted versus E_{tup} / E_{cup} ratio

The effects of material inhomogeneity and the impact loading parameters are evaluated too. It is assumed that $b=0.015$ m, $h=0.020$ m, $l_1=0.300$ m, $l_2=0.300$ m, $l_3=0.050$ m, $a=0.150$ m, $\alpha=0.4$, $\beta=0.4$, $\eta=0.4$, $\lambda=0.6$, $\rho=0.6$ and $\omega=0.6$. The parametric study yields the results shown in graphical form in Figures 2, 3, 4, 5 and 6.

Figure 2 illustrates how the integral J in normalized form changes when E_{tup}/E_{cup} ratio varies at $l_3/l_1=1/6$ (curve 1), $l_3/l_1=2/6$ (curve 2) and $l_3/l_1=3/6$ (curve 3). The ratio, l_3/l_1 , determines the location of the impact loading application point on the beam surface.

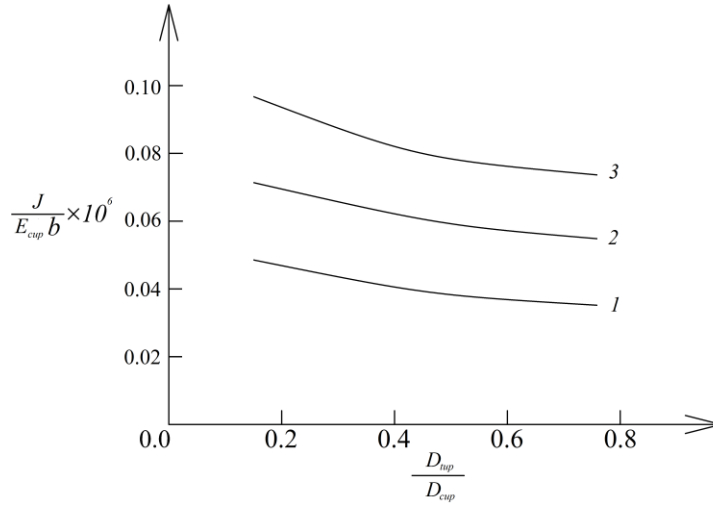


Figure 3. The integral J plotted versus D_{tup}/D_{cup} ratio

It can be seen in Figure 2 that the value of the integral J reduces as a result of increase of l_3/l_1 ratio (this is due to decrease of the bending moment in the beam). Increase of E_{tup}/E_{cup} ratio leads also to reduction of the integral J (Figure 2).

One can observe the effect of D_{tup}/D_{cup} ratio on the value of the integral J at $h_p/l_2=0.3$ (curve 1), $h_p/l_2=0.6$ (curve 2) and $h_p/l_2=0.9$ (curve 3) in Figure 3.

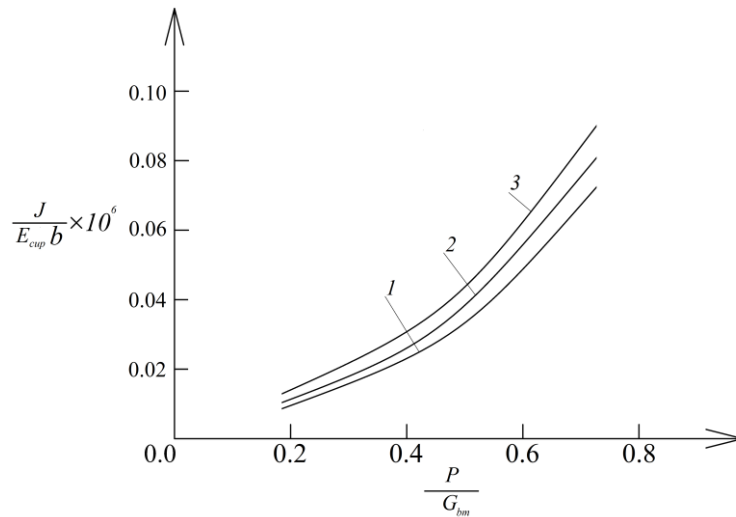


Figure 4. The integral J plotted versus P/G_{bm} ratio

The graphs indicate that the integral J decreases when D_{tup} / D_{cup} ratio grows. However, grow of h_p / l_2 ratio induces a significant rise of the value of the integral J (Figure 3). This observation is attributed to increase of the impact energy. The graphs reported in Figure 4 illustrate how the integral J is affected by the change of P / G_{bm} ratio at $n_{tup} / n_{cup} = 0.2$ (curve 1), $n_{tup} / n_{cup} = 0.5$ (curve 2) and $n_{tup} / n_{cup} = 0.8$ (curve 3).

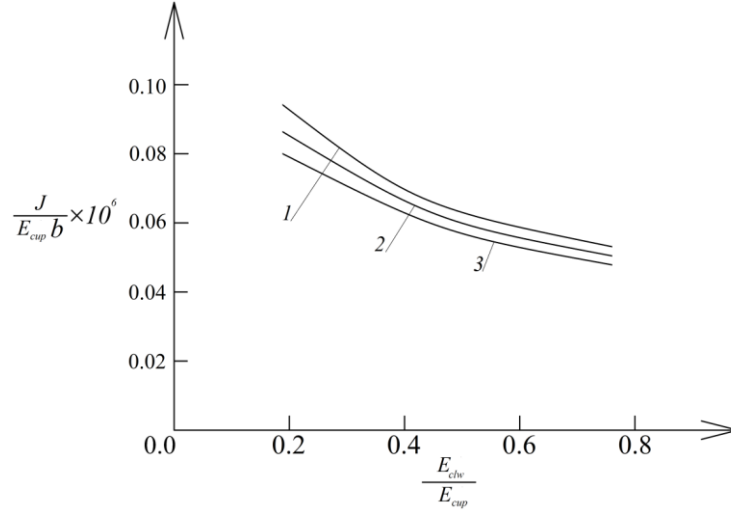


Figure 5. The integral J plotted versus E_{clw} / E_{cup} ratio

It can be seen in Figure 4 that the integral J increases its value when n_{tup} / n_{cup} ratio grows. Increase of the integral J value is observed also at increase of P / G_{bm} ratio (this behavior is due to rise of the impact energy).

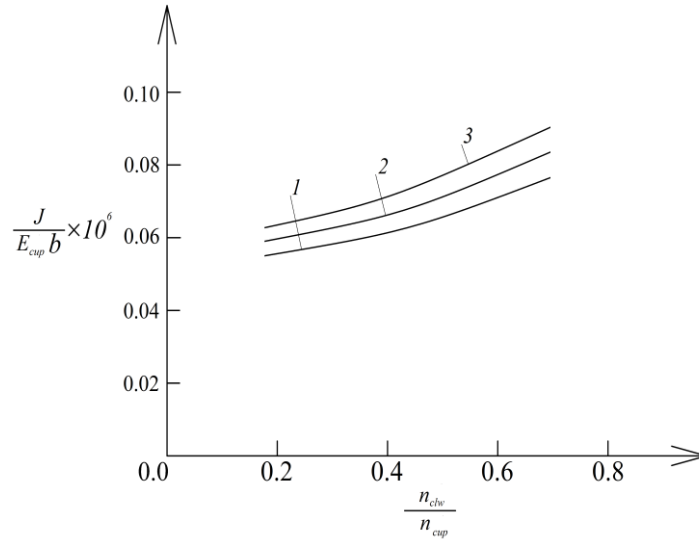


Figure 6. The integral J plotted versus n_{clw} / n_{cup} ratio

One can get an idea for the variation of the value of the integral J due to continuous material inhomogeneity from the graphs shown in Figures 5 and 6. The inhomogeneity is characterized by the E_{clw} / E_{cup} , D_{clw} / D_{cup} , n_{clw} / n_{cup} and n_{tlw} / n_{tup} ratios. The graphs in Figure 5 illustrate the effect of E_{clw} / E_{cup} ratio at $D_{clw} / D_{cup} = 0.2$ (curve 1), $D_{clw} / D_{cup} = 0.5$ (curve 2) and $D_{clw} / D_{cup} = 0.8$ (curve 3). Figure 6 shows the effect of n_{clw} / n_{cup} ratio at $n_{tlw} / n_{tup} = 0.3$ (curve 1), $n_{tlw} / n_{tup} = 0.5$ (curve 2) and $n_{tlw} / n_{tup} = 0.8$ (curve 3). The graphs in Figure 5 indicate a reduction of the value of the integral J when the

E_{clw} / E_{cup} and D_{clw} / D_{cup} ratios grow. Increase of n_{clw} / n_{cup} and n_{tlw} / n_{tup} ratios generate growth of the J integral value as can be seen in Figure 6.

Conclusion

The effect of different mechanical behavior in tension and compression on the longitudinal fracture of continuously inhomogeneous beam structures subjected to impact loading is investigated theoretically. Solution of the integral J is obtained. The SERR under impact loading is derived for verification of the solution. A parametric study is performed by using the solution. The study indicates that the longitudinal fracture is affected significantly by the different behavior in tension and compression. For example, it is observed that the value of the integral J reduces when E_{tup} / E_{cup} and D_{tup} / D_{cup} ratios grow. The growth of n_{tup} / n_{cup} ratio generates rise of the J integral. It is found that the integral J value decreases when l_3 / l_1 ratio grows. An increase of the value of the integral J is detected when h_p / l_2 ratio rises. The study of the effect of material inhomogeneity reveals reduction of the integral J when E_{clw} / E_{cup} and D_{clw} / D_{cup} ratios grow. The rise of n_{clw} / n_{cup} and n_{tlw} / n_{tup} ratios, however, leads to growth of the integral J value.

Recommendations

The theoretical investigation developed in this paper can be used in structural design of continuously inhomogeneous beams with different mechanical behavior in tension and compression under impact loading.

Scientific Ethics Declaration

* The author declares that the scientific ethical and legal responsibility of this article published in EPSTEM Journal belongs to the author.

Conflict of Interest

* The author declares that he has no conflicts of interest.

Funding

*This study received no external funding.

Acknowledgements or Notes

* This article was presented as an oral presentation at the International Conference on Technology (www.icontechno.net) held in Trabzon/Türkiye on May 01-04, 2025.

References

- Broek, D. (1986). *Elementary engineering fracture mechanics*. Springer.
- Dowling, N. (2007). *Mechanical behavior of materials*. Pearson.
- Fanani, E.W.A., Surojo, E., Prabowo, A. R., & Akbar, H. I. (2021). Recent progress in hybrid aluminum composite: manufacturing and application. *Metals*, 11(12), 1919-1929.
- Gandra, J., Miranda, R., Vilaça, P., Velinho, A., & Teixeira, J.P. (2011). Functionally graded materials produced by friction stir processing. *Journal of Materials Processing Technology*, 211(11), 1659-1668.

- Kaul, A. B. (2014). Two-dimensional layered materials: Structure, properties, and prospects for device applications. *Journals of Materials Research*, 29, 348-361.
- Mahamood, R. C., & Akinlabi, E. T. (2017). *Functionally graded materials*. Springer.
- Obodovski, B. A., & Hanin, S. E. (1981). *Strength of materials*. Vista.
- Radhika, N., Sasikumar, J., Sylesh, J. L., & Kishore, R. (2020). Dry reciprocating wear and frictional behaviour of B4C reinforced functionally graded and homogenous aluminium matrix composites. *Journal of Materials Research and Technology*, 9, 1578-1592.
- Rizov, V. I. (2018). Non-linear delamination in two-dimensional functionally graded multilayered beam. *International Journal of Structural Integrity*, 9, 646-663.
- Rizov, V. I. (2024). Analysis of delaminated multilayered rod under centric impact. *AIP Conference Proceedings*, 3078, 060007.
- Rizov, V.I. (2019). Influence of material inhomogeneity and non-linear mechanical behaviour of the material on delamination in multilayered beams. *Frattura ed Integrità Strutturale*, 13(47), 468-481.
- Toudehdeghghan, J., Lim, W., Fool, K. E., Ma'arof, & M. I. N., Mathews J. (2017). A brief review of functionally graded materials. *MATEC Web of Conferences*, 131, 03010.
- Udupa, G., Rao, S. S., & Gangadharan, K. V. (2014). Functionally graded composite materials: an overview. *Procedia Materials Science*, 5, 1291-1299.

Author Information

Victor Rizov

Department of Technical Mechanics
University of Architecture, Civil Engineering and Geodesy
1 Chr. Smirnensky blvd. 1046 – Sofia, Bulgaria
Contact e-mail: v_rizov_she@uacg.bg

To cite this article:

Rizov, V. (2025). Influence of different behavior in tension and compression on longitudinal fracture of inhomogeneous beams under impact. *The Eurasia Proceedings of Science, Technology, Engineering and Mathematics (EPSTEM)*, 33, 130-139.

The Eurasia Proceedings of Science, Technology, Engineering and Mathematics (EPSTEM), 2025

Volume 33, Pages 140-147

IConTech 2025: International Conference on Technology

The Advantages of Employing Transfer Learning in the Classification of Breast Cancer Histopathological Images

Simona Moldovanu

Dunarea de Jos University of Galati

Elena Raducan

Dunarea de Jos University of Galati

Mihaela Miron

Dunarea de Jos University of Galati

Carmen Sirbu

Dunarea de Jos University of Galati

Abstract: Digital pathology represents a significant advancement in contemporary medicine, offering enhanced diagnostic capabilities and improved patient outcomes. Pathological examinations, which need particular steps in the diagnostic process, are standard in medical protocols and the law. Today, a new challenge is to use cutting-edge algorithms, like Convolutional Neural Networks (CNN), to classify histological images into different groups. So, the Invasive Ductal Carcinoma (IDC) dataset was used to use some well-known CNNs, such as VGG16, DenseNet169, and EfficientNetV2B3 pre-trained networks, as well as two new custom-built CNNs with four (CNN1) and five (CNN2) layers. The results show that for a 70% training to 30% testing ratio, CNN1 (0.895), CNN2 (0.882), VGG16 (0.983), DenseNet169 (0.971), and EfficientNetV2B3 (0.979) all got the best results on the test set. The results obtained with pre-trained CNNs are superior to proposed custom-built CNNs. This outcome denotes the main advantage of leveraging pre-trained CNNs in classifying breast cancer histopathological images.

Keywords: Convolutional neural networks, VGG16, DenseNet169, EfficientNetV2B3

Introduction

According to Siegel et al. (2017) and the cancer statistics report in the United States in 2022 (Siegel et al., 2022), breast cancer (BC) is one of the leading causes of cancer-related deaths among women of all ages. Conventional techniques for categorizing breast cancer molecular subtypes predominantly depend on histopathology analysis, which can be laborious, subjective, and occasionally incorrect in interpretation. The accuracy of this method in diagnosing pathologies and characterizing tissues is well known. Furthermore, such technologies, although promising, are costly and may not be easily accessible in multiple nations and healthcare systems (Rashmi et al., 2021)

Deep learning (DL) has recently become a revolutionary tool in various domains, particularly in medical image processing. Deep learning, a subset of machine learning, employs multilayered neural networks to discern complex patterns in unprocessed data without the necessity for manual feature extraction, representing a significant advancement over conventional techniques (Szilágyi & Kovács, 2024; Ragab et al., 2022). Convolutional Neural Networks are enabled to differentiate the malignant versus non-malignant (benign) tissue,

which exhibits alterations in the normal pattern of breast parenchyma that are not directly associated with the progression to malignancy.

Many researchers have been motivated to use deep learning techniques for histopathology image classification as a result of the recent significant advancements and outstanding results in the fields of computer vision (CV) and image processing (IP). Convolutional neural networks (CNNs) are the dominant type of deep learning architecture, excelling in both the classification of images and feature extraction (Litjens et al., 2017). Pre-trained CNN models are neural networks that have undergone training on extensive datasets, usually for general image recognition purposes, and are accessible for external utilization.

This study examines three distinct pre-trained CNNs: VGG16, DenseNet169, and EfficientNetV2B3, for feature extraction from breast cancer histopathology images. The histopathological images of breast cancer are sourced from the publicly accessible Invasive Ductal Carcinoma (IDC) dataset. This work utilized transfer learning to construct four pre-trained models using the IDC dataset instead of employing a model with arbitrary weights from inception. The results obtained are comparable to those described in the following studies.

Simonyan et al. (2023) focused on the accurate classification of breast cancer using deep learning models for medical image processing, employing four pre-trained models: DenseNet201, ResNet50, ResNet101, and MobileNet-v2. Kumar and Murali (2024) discussed the importance of early breast cancer detection and the use of EfficientNetB6, ResNet34, VGG-19, MobileNetV2, and ResNet50 for the classification of medical histopathological images.

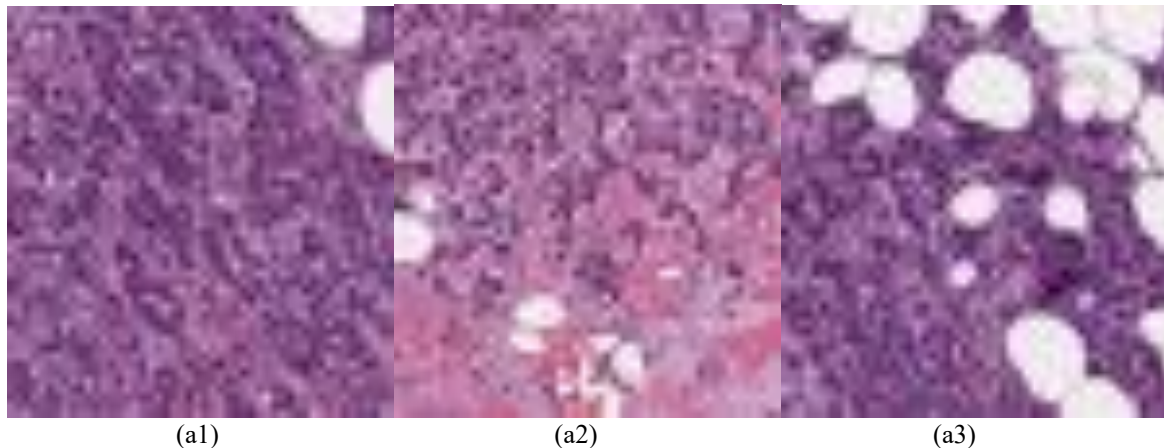
An approach for classifying the same BC histopathology images using pre-trained CNNs by Abdulaal et al. (2024) was proposed. This study included Inception V3 Net, VGG19, Alex Net, ResNet-18, Google Net, Shefflenet, Mobile Net, ResNet 101, Inception ResNetV2 Net, and Squeeze Net. Sumitha and Isaac (2024) proposed one pre-trained CNN model (ResNet152v2) for the automated classification of benign and malignant BC using histopathological images. Only one pre-trained CNN was proposed by Mani et al. (2023) The suggested model (VGG-16) classifies breast histopathology images as benign or cancerous, yielding superior results.

Recently, an interesting result was presented by Korkmaz and Kaplan (2025). This study includes three pre-trained models: VGG16, MobileNet, DenseNet201, and a custom-built CNN. The higher accuracy rate was obtained using the custom-built CNN model (Korkmaz & Kaplan, 2025).

Materials and Methods

Image Dataset

A 40x scan of 162 whole-mount slide images of BC specimens made up the original dataset. A total of 277,524 patches measuring 50 x 50 were retrieved, comprising 198,738 non-IDC and 78,786 IDC samples. The images have a PNG extension and are labeled with “0” for non-IDC and “1” for IDC samples. The dataset is stored at the web address, and the data of the last access is 19 February 2025 (<https://www.kaggle.com>) (Janowczyk& Madabhushi, 2016). In this study, the dataset was split into 70% for training and 30% for testing. The same samples are shown in Figure 1.



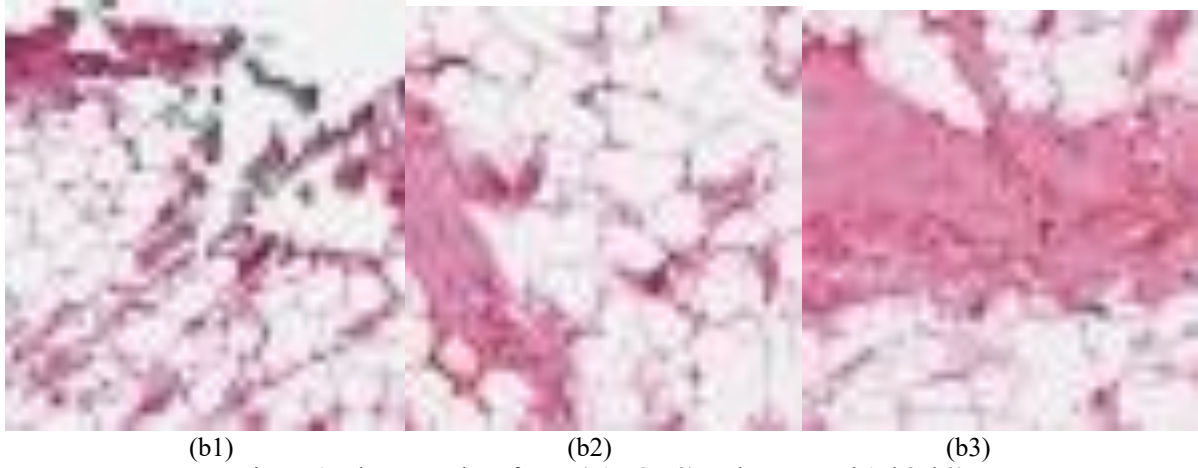


Figure 1. The examples of IDC (a1, a2, a3) and non-IDC b1, b2, b3)

Hardware and Software

All experiments were run on a PC with the architecture Apple Mac Studio (2022), Apple M1 Max, 32GB, 1TB SSD, and 32-core GPU. The programming environment was Python (3.12.9), with the following main libraries: (i) TensorFlow (2.18.0), (ii) Keras (3.6.0), and (iii) Visualekera (0.1.4.3).

Pre-trained CNN

Transfer learning approaches are utilized to retrain CNNs already trained in a given domain, enabling their application to various datasets. The primary advantage is the conservation of resources, as the model is partially reutilized, with scenarios varying from retraining the network entirely to retraining only selected components, generally associated with categorization (Tsaler et al., 2021).

VGG-16 is a CNN of 16 layers. A trained version of the network trained on over a million images is available for loading from the ImageNet database. The pre-trained network is capable of classifying images into 1000 object classes (Abdulaal et al., 2024; Kumar & Murali, 2024; Mani et al., 2023). Convolutional neural networks yield effective outcomes in image processing, particularly in object detection and classification applications. This effort aims to train a convolutional neural network for classifying photos from the CIFAR-10 database using Keras.

The DenseNet-169 CNN is pre-trained on ImageNet and CIFAR-10 using the Keras tool. Her architecture consists of convolutional layers succeeded by subsampling layers (average This CNN facilitates the identification of features and edges inside the image (Mani et al., 2023). The EfficientNetV2B3 belongs of EfficientNet CNN family intoruced by Tan and Le (2021). EfficientNet's fundamental concept is a novel scaling approach that consistently adjusts all dimensions of depth, width, and resolution using a compound coefficient.

Custom-built CNN

Besides pre-trained CNNs, this paper presents a customized, optimal, and efficient model to illustrate the application of a CNN-based technique for IDC classification in histopathological images. The proposed architectures utilized a 4-convolutional-layer (CNN1) model, Figure 2.(a), and a 5-convolutional-layer (CNN2) model, Figure 2.(b), respectively. Their implementation keeps on the following steps:

- i Access publicly available Invasive Ductal Carcinoma (IDC) dataset;
- ii Load images onto Python environment.
- iii Configure hyperparameters and pre-processing options for image data augmentation.
- iv The previous images are the inputs of the custom-built CNN model.
- v Dropout layer is added to prevent the overfitting process.
- vi The convolutional layers give the depth of CNN.
- vii MaxPooling layers are proposed to reduce the spatial dimensions of the input volume data.

viii Output size is depicted by the FC layer, and the SoftMax function is applied to obtain a binary classification.

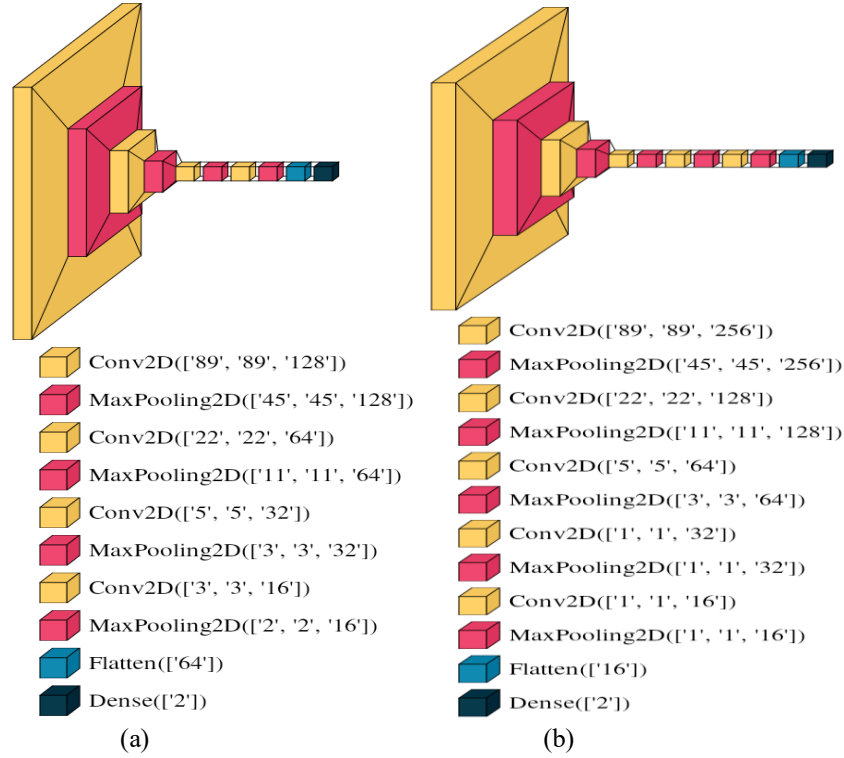


Figure 2. Custom-built CNNs: (a) four layers (CNN1); (b) five layers (CNN2).

The hyperparameters used for all CNNs were the size of images 180x180, the batch size of 16, the canal number of 3 and 20 epochs.

Performance Evaluation

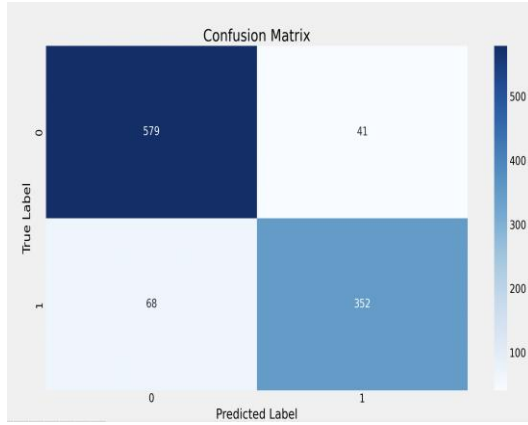
The objective of this study was to assess efficacy custom-built and pre-trained CNNs. The confusion matrix having the form $\begin{bmatrix} TP & FP \\ FN & TN \end{bmatrix}$ (TN-true positive, FP-false positive, FN-false negative and TN true negative) is used in this sense. The relevant metric what reflect the prediction of model is accuracy, it has the equation $Accuracy = (TP + TN)/(TP + TN + FP + FN)$ (Tăbăcaru et al., 2024).

Results and Discussions

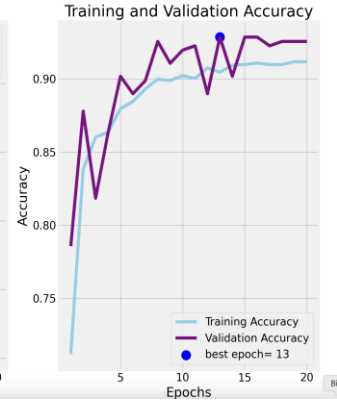
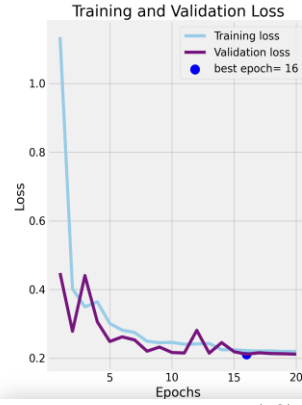
In this section, we assessed the efficacy of suggested deep learning models by analyzing the predicted accuracy. Initially, we emphasized the performance indicated by pre-trained CNNs and then for custom-built CNNs, followed by a discussion on the competitiveness of our suggested models to recently published studies, particularly with the classification of BC histopathology images.

The VGG16, DenseNet169, and EfficientNetV2B3 (Moldovanu et al., 2024; Tabacaru et al., 2023) models yielded excellent outcomes when analyzing the histopathological images for the classification of IDC. The confusion matrix obtained for the test stage for each CNN is shown in Figure 3, first column. The accuracy and loss function for training validation stages for each epoch are shown in Figure 3; also, the best epoch, when the accuracy is maximum, is marked in the second column.

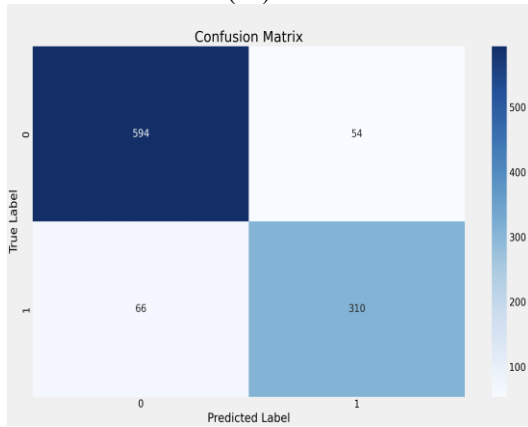
As shown in the first column, several histopathological BC images were incorrectly classified. The DNN1 and DNN2 had a low performance; these misclassified more samples in comparison with pre-trained. Table 1 shows all the information provided by the runs performed. In addition to the accuracy and loss metrics computed for the test stage, the complementary details of the same metrics are provided for the training and testing stages.



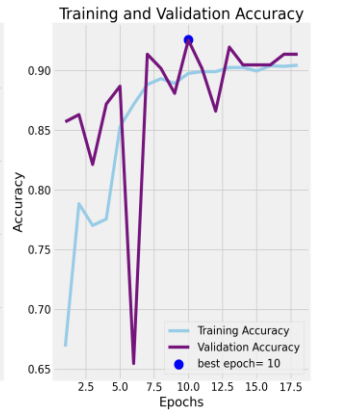
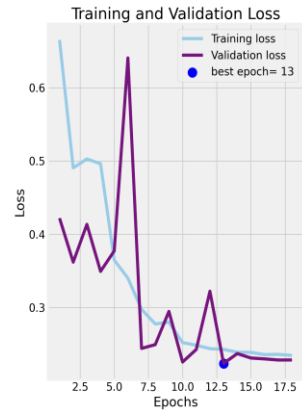
(a1)



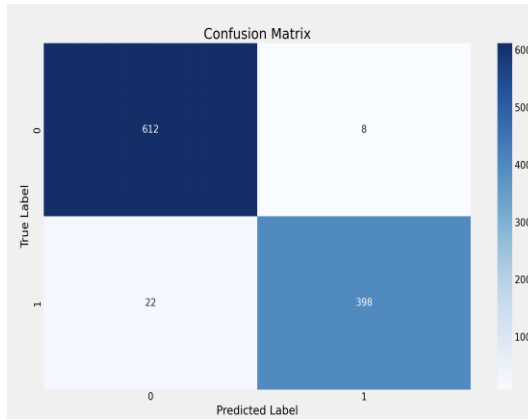
(a2)



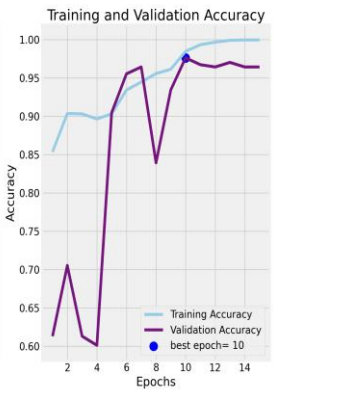
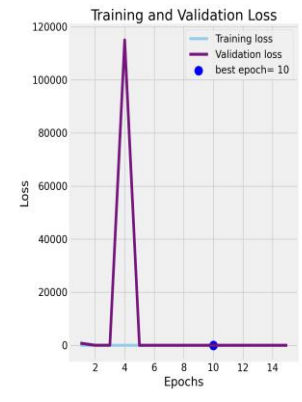
(b1)



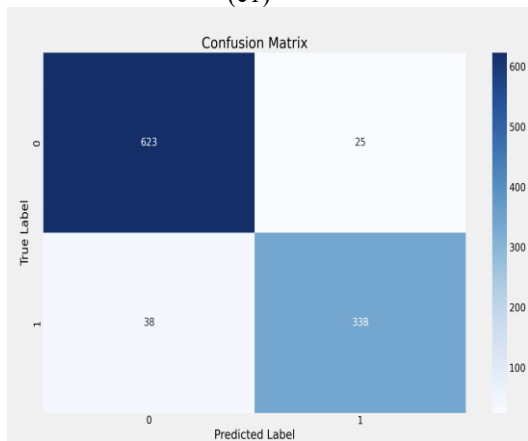
(b2)



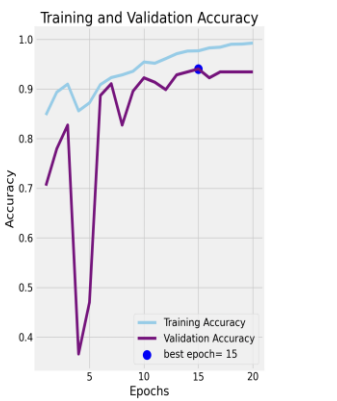
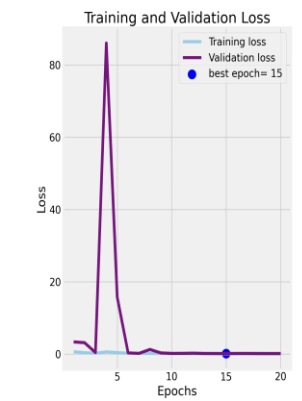
(c1)



(c2)



(d1)



(d2)

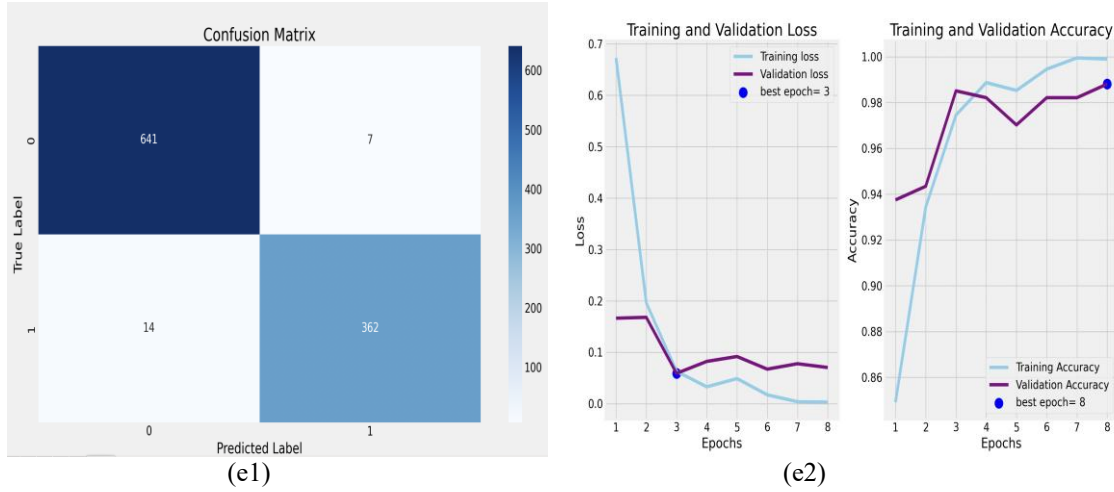


Figure 3. (a) DNN1; (b) DNN2; (c) DenseNet169; (d) VGG16; (e) EfficientNetV2B3

Table 1. The metrics computed for each CNN and run stage

CNN	Metrics	Training	Validation	Testing
VGG16	Loss	0.120	0.169	0.166
	Accuracy	0.957	0.940	0.938
DenseNet169	Loss	0.055	0.063	0.071
	Accuracy	0.980	0.976	0.971
EfficientNetV2B3	Loss	0.012	0.059	0.068
	Accuracy	0.995	0.985	0.979
CNN1	Loss	0.22	0.211	0.236
	Accuracy	0.908	0.928	0.895
CNN2	Loss	0.238	0.223	0.269
	Accuracy	0.904	0.919	0.882

Table 2 Comparing with state-of-the-art-methods

References/year	Pre-trained CNNs	The best accuracy
(Simonyan et al., 2023)	DenseNet201, ResNet50, ResNet101 MobileNet-v2	DenseNet201(91.37%)
(Kumar and Murali, 2024)	EfficientNetB6, ResNet34, VGG-19, MobileNetV2, ResNet50	MobileNetV2 (99%) ResNet50 (99%)
(Abdulaal et al., 2024)	Inception V3 Net, VGG19, AlexNet, ResNet-18, Google net, Shefflenet, Mobile net, Resnet 101, Inception ResnetV2 Net, Squeeze net	Inception-V3Net (99.1%)
(Sumitha and Isaac, 2024)	ResNet152v2	ResNet152v2 (96.47%)
(Mani et al., 2023)	VGG-16	VGG-16 (96.9%)
(Korkmaz and Kaplan, 2025)	VGG16, MobileNet, DenseNet201 A custom-built CNN	Custom-built CNN (93.80%)
The proposed method	EfficientNetV2B3	97.9%

The efficacy of our suggested method can be evaluated against several cutting-edge studies utilized for the classification of BC histopathology images. Many of these innovative deep learning methodologies are based on pre-trained CNNs (Ashraf et al., 2024; Abdullhussain et al., 2022; Kucharski et al., 2020); the exception is the paper (Davri et al., 2022), which, besides pre-trained CNNs, uses a custom-built. Table 2 shows the recent state-of-the-art method, as well as the proposed method. The best value obtained by a CNN among those proposed in terms of accuracy is mentioned in the last column.

In summary, the findings indicated that our proposed deep learning model is capable of extracting features from histopathological images of BC and using the Softmax function to classify them. The comparison method revealed that the outcomes of our suggested pre-trained CNNs are competitive with several state-of-the-art research studies utilizing comparably larger datasets.

Conclusion

This research utilizes two custom-built CNN models for extracting features and classification tasks on BC histopathological images. The publicly available dataset was archived by several institutions. The BC histopathological images dataset consists of two categories, namely, non-IDC and IDC samples. The custom-built CNN1 with four layers observed in this research achieved in the test stage an accuracy of 89.5%. Also, this research investigated the classification of BC histopathological images using pre-trained CNN models. The performance of three pre-trained models, including VGG16, DenseNet169, and EfficientNetV2B3, was evaluated using the same dataset. The EfficientNetV2B3 outperformed the best accuracies of 97.9 in the testing stage. Future directions of this research entail the augmentation of our dataset and the incorporation of images for multi-class classification challenges. Additionally, the integration of other pre-trained models is necessary in subsequent work. At some point, it would be intriguing to apply analogous CNNs to histopathology images of various cancers, including lung and colon cancer.

Scientific Ethics Declaration

The authors declare that the scientific ethical and legal responsibility of this article published in EPSTEM Journal belongs to the authors.

Conflict of Interest

The authors declare that they have no conflicts of interest

Funding

This study received no external funding.

Acknowledgements or Notes

* This article was presented as an oral presentation at the International Conference on Technology (www.icontechno.net) held in Trabzon/Türkiye on May 01-04, 2025.

References

- Abdulaal, A.H., Valizadeh, M., Amirani, M.C., & Shah, A.S. (2024). A self-learning deep neural network for classification of breast histopathological images, *Biomed. Signal Process. Control*, 87, 105418.
- Janowczyk, A., Madabhushi, A. (2016) Deep learning for digital pathology image analysis: a comprehensive tutorial with selected use cases. *Journal of Pathology Informations*, 7, 29.
- Ashraf, A., Nawi, N.M., Shahzad, T., Aamir, M., Khan, M.A., & Ouahada, K. (2024). Dimension reduction using dual-featured auto-encoder for the histological classification of human lungs tissues. *IEEE Access*, 12, 104165–104176.

- Abdulhussain, F.A., Adnan, M., Radhi, HAl-Mualm, M., Hasen -Alubaidy, M., Salih, M., & Saadoon S.J. (2022). Automatic diagnosis of breast cancer in histopathologic images based on convolutional autoencoders and reinforced feature selection. *Majlesi Journal of Electrical Engineering*, 16(4), 89-95.
- Davri, A., Birbas, E., Kanavos, T., Ntritsos, G., Giannakeas, N., Tzallas, A.T., & Batistatou, A. (2022). Deep learning on histopathological images for colorectal cancer diagnosis: A systematic review. *Diagnostics*, 12, 837.
- Korkmaz, M., & Kaplan, K. (2025). Effectiveness analysis of deep learning methods for breast cancer diagnosis based on histopathology images, *Applical Sciences*, 15(3), 1005.
- Kucharski, D., Kleczek, P., Jaworek-Korjakowska, J., Dyduch, G., & Gorgon, M. (2020). Semi-supervised nests of melanocytes segmentation method using convolutional autoencoders. *Sensors*, 20, 1546.
- Kumar, V., & Murali G., (2024). Optimized deep learning approaches for lung and colon cancer classification using histopathological images. *Proceedings from 3rd International Conference on Automation, Computing and Renewable Systems (ICACRS)*, 1665-1669.
- Litjens, G., Kooi, T., Bejnordi, B. E., Setio, A. A. A., Ciompi, F., Ghafoorian, M., ... & Sánchez, C. I. (2017). A survey on deep learning in medical image analysis. *Medical Image Analysis*, 42, 60-88.
- Mani, C., Kamalakannan, R. K., Pandu Rangaiah, J., & Anand Y. (2023). Bio-inspired method for breast histopathology image classification using transfer learning. *Journal of Artificial Intelligence and Technology*, 4(2), 89-101
- Moldovanu, S., Tăbăcaru, G., & Barbu, M. (2024). Convolutional neural network-machine learning model: hybrid model for meningioma tumour and healthy brain classification. *Journal of Imaging*, 10(9), 235.
- Ragab, M., Albukhari, A., Alyami, J., & Mansour R.F. (2022). Ensemble deep-learning-enabled clinical decision support system for breast cancer diagnosis and classification on ultrasound images. *Biology*, 11(3), 439.
- Rashmi, R., Prasad, K., & Udupa, C. B. K. (2022). Breast histopathological image analysis using image processing techniques for diagnostic purposes: A methodological review. *Journal of Medical Systems*, 46(1), 7.
- Siegel, R.L., Kimberly M. D., Hannah, F. E., & Ahmedin, J. (2022). Cancer statistics. *CA: Cancer Journal for Clinicians*, 72 (1), 7-33.
- Siegel, R.L., Miller K.D., Jemal A. (2017). Cancer statistic. *CA: Cancer Journal for Clinicians*, 67(1), 7-30.
- Simonyan, E.O., Badejo, J.A., & Weijin, J.S. (2023). Histopathological breast cancer classification using CNN, *Materials Today: Proceedings*, 105, 268-275.
- Sumitha, R. S., Isaac, R. (2024). Transfer learning-based CNN model for the classification of breast cancer from histopathological images. *International Journal of Advanced Computer Science & Applications*, 15(4), 270.
- Szilágyi, L., & Kovács, L. (2024). Artificial intelligence technology in medical image analysis. *Applied Sciences*, 14(5), 2180.
- Tăbăcaru, G., Moldovanu, S., Răducan, E., & Barbu, M. (2023). A robust machine learning model for diabetic retinopathy classification. *Journal of Imaging*, 10(1), 8.
- Tan, M., & Le, Q. (2019, May). Efficientnet: Rethinking model scaling for convolutional neural networks. In *International conference on machine learning* (pp. 6105-6114). PMLR.
- Tsalera, E., Papadakis, A., & Samarakou, M. (2021). Comparison of pre-trained CNNs for audio classification using transfer learning. *Journal of Sensor and Actuator Networks*, 10(4), 72

Author(s) Information

Simona Moldovanu

Dunarea de Jos University of Galati,
47 Domneasca Str., 800008 Galati, Romania
e-mail: simona.moldovanu@ugal.ro

Elena Raducan

Dunarea de Jos University of Galati,
47 Domneasca Str., 800008 Galati, Romania

Mihaela Miron

Dunarea de Jos University of Galati,
47 Domneasca Str., 800008 Galati, Romania

Carmen Sirbu

Dunarea de Jos University of Galati,
47 Domneasca Str., 800008 Galati, Romania

To cite this article:

Moldovanu, S., Raducan, E., Miron, M., & Sirbu, C. (2025). The advantages of employing transfer learning in the classification of breast cancer histopathological images. *The Eurasia Proceedings of Science, Technology, Engineering and Mathematics (EPSTEM)*, 33, 140-147.

The Eurasia Proceedings of Science, Technology, Engineering and Mathematics (EPSTEM), 2025

Volume 33, Pages 148-154

IConTech 2025: International Conference on Technology

Classification of Industrial Wastewater Generated by Food and Beverage Industry

Slav Valchev

University of Food Technology

Nenko Nenov

InnoSolv Ltd.

Abstract: A classification of wastewater generated by food and beverage industry based on their various indicators: temperature, level of impurities, type of impurities, acidity, cyclicity of generation was made. Samples of industrial wastewater, taken immediately upon their receipt, were studied. Physical parameters - density, dynamic viscosity, content of non-volatile impurities, electrical conductivity, acidity and optical transmission of different types of wastewaters from canning, dairy, meat processing, brewing and aromatic industries in temperature range between 25 and 80 °C were obtained. The possibilities for recycling industrial wastewater using mechanical vapour recompression method are commented on. It has been found that a large part of industrial wastewater generated from food and beverage industry is suitable for recycling by mechanical vapour recompression method at low energy costs due to its high temperature and low content of dry organic matter. The resulting recycled water has the physical characteristics of pure distilled water.

Keywords: Wastewater treatment, Mechanical vapour recompression, Food and beverage industry

Introduction

Overview

Food industry enterprises use large amounts of fresh water in their production processes. These businesses have high energy costs associated with transporting and treating fresh water. At the same time, these same enterprises are generators of large amounts of wastewater, and they have to pay high costs for treatment and disposal. The separation of large quantities of wastewater in a given production means high costs for purification and landfilling. If wastewater has a high outlet temperature, it means that enterprise loses energy in form of heat, and this leads to increased production costs. The transition from an open to a closed water cycle of water use in production process is the main goal of energy managers in enterprises: in addition to reducing energy costs in the production process, the goals of a circular economy are also achieved (Stoyanova, 2011; Tabakov, 2004; Valchev & Nenov, 2014). The main methods for water treatment are as follows:

- mechanical methods: precipitation, separation of solid suspended particles with centrifuges and hydrocyclones, filtering (retain finely dispersed pollutants substances);
- physicochemical methods: coagulation and flocculation, flotation, sorption, ionic exchange, extraction, evaporation, crystallization, electrolysis, membrane processes (electrodialysis, reverse osmosis, ultrafiltration) (Gertsen & Sonderby, 2009; Smith, 2005; Shrivastava et al., 2022; Semerdzhieva et al., 2024; Rilling, 2012; Ramalho, 1977).

Wastewater treatment using mechanical vapour recompression (MVR) heat pump system is method, which is applied to extraction of volatile organic pollutants from some wastewater - ammonia, phenols, anilines, amines

- This is an Open Access article distributed under the terms of the Creative Commons Attribution-Noncommercial 4.0 Unported License, permitting all non-commercial use, distribution, and reproduction in any medium, provided the original work is properly cited.

- Selection and peer-review under responsibility of the Organizing Committee of the Conference

© 2025 Published by ISRES Publishing: www.isres.org

and others. The method consists in heating and boiling wastewater and as a result separation from impurities according to their different volatility (Russel, 2006; Ng, 2006). The wastewater generated by enterprises in food and beverage industry is characterized by different temperature, dynamic viscosity, level and type of impurities, electrical conductivity, acidity, optical transmission and cyclicity of generation. The values of parameters are discussed above determine possibility of wastewater treatment using method of mechanical vapour recompression.

Studying Indicators of Wastewater

Temperature of Wastewater

This parameter is important for energy characteristics of MVR heat pump system. In addition, temperatures of wastewater and used fresh water determine efficiency of recycling process according to proposed method. Certain technological operations in enterprises (e.g. rinsing, hydrotransport, washing with fresh water, etc.) using fresh water at ambient temperature and generated wastewater is at the same temperature levels. In others (e.g. cooling) consumed cold fresh water is heated to temperatures higher than ambient temperature, and in others (e.g. washing with hot water) used hot fresh water is also discarded as hot wastewater (Waldron, 2007). According to temperature wastewater can be classified into the following groups:

Group A1 – cold wastewater with ambient temperature (in range of 10-30°C).

Group A2 – warm wastewater with temperatures higher than ambient temperature (in range of 30-50°C).

Group A3 – hot wastewater with temperature up to 100 °C. The upper limit of this interval is determined by the fact that wastewater disposal is carried out in the environment at atmospheric pressure (in range 50-95°C).

Level of Impurities in Wastewater

The wastewater generated by enterprises in food and beverage industry are characterized by varying degrees of pollution. It could be expressed through different indicators- biologically required oxygen (BOD), chemically required oxygen (COD), content of dissolved or total dissolved and undissolved non-volatile impurities. For the purpose of the present study, most appropriate indicator of evaluation is total content of non-volatile impurities. The low content of non-volatile substances, as a rule, leads to a higher degree of regeneration of wastewater (Ghimpușan et al., 2017; Syed, 2006; Valchev et al., 2016). According to level of impurities wastewater can be classified into the following groups:

Group B1 – low-polluted wastewater with a content of non-volatile impurities up to 200 mg/dm³;

Group B2 – moderately polluted wastewater with a content of non-volatile impurities from 200 to 600 mg/dm³;

Group B3 – highly polluted wastewater with a content of non-volatile impurities over 600 mg/dm³;

Type of Impurities in Wastewater

It is established that industrial wastewater, contains impurities of various origins (inorganic, vegetable, animal, chemical), chemical and physical composition and structural-mechanical properties. The type of impurities contained in a given wastewater determine properties related to boiling process in MVR heat pump system- density, dynamic and kinematic viscosity, surface tension, coefficient of thermal conductivity, specific heat capacity, physico-chemical temperature depression, etc. This properties determine intensity of heat exchange, the dynamics of scale formation on heat exchanger surfaces and the intensity of microorganism development in water (Muller & Marechal, 2008). According to type of impurities wastewater can be classified into the following groups:

Group C1 – volatile impurities. This includes water soluble and insoluble liquids (organic acids, etc.) with boiling temperatures lower than boiling temperature of distilled water at the same pressure and dissolved gases (air, ammonia, amines, decomposition products, etc.). When wastewater is boiled, impurities will be released together with evaporated water.

Group C2 – non-volatile impurities of inorganic natural origin. Water soluble and insoluble mineral particles such as soil, grains of sand, dust, salt, etc. are included here. They are characterized by great stability during storage and heat treatment, such as the evaporation process - lack of thermal decomposition and release of gases,

reduced scale formation. Some of them can be separated from the water only by filtering. When wastewater is boiled, impurities will be completely released with concentrated sludge.

Group C3 – non-volatile impurities of organic plant origin. This includes insoluble dry matter in the form of macro particles such as fruit residues (pulp, seeds, bark), seeds, flowers, leaves, straws, roots, etc., residues of their derivatives (yeast, wort), paper particles, insoluble liquids such as vegetable fats, dissolved solids such as sugars (sucrose, glucose, fructose), starch, etc. Insoluble solids can be separated from wastewater by filtration. Chemically, these impurities are mainly carbohydrates - cellulose, fats, sugars, etc. As such, they are characterized by instability during longer storage and heat treatment. Processes of intensive development of microorganisms occur, leading to decomposition and release of gases, formation of scales, crystallization is observed.

Group C4 – non-volatile impurities of organic animal origin. Insoluble macro particles such as remains of animal tissues (muscles, skin, tendons, fur, feathers), bone particles, blood, fat, etc. are counted here. This type of impurities is characterized by a high content of proteins and fats. Macro particles can be separated from wastewater by filtration. Impurities from this subgroup are also characterized by instability during storage and heat treatment - intensive development of microorganisms with decomposition and release of gases, formation of scales, denaturation, saponification, etc.

Group C5 – non-volatile chemical impurities. Impurities such as bases (sodium, potassium), acids (nitric, citric), washing detergents, synthetic food additives and flavorings - dyes, preservatives, emulsifiers, anti-corrosion and oxygen-reducing inhibitors are included here. These impurities are relatively stable during storage and heat treatment.

Acidity of Wastewater

This indicator is directly related to composition of the impurities. Acidity of wastewater determines appropriate choice of construction materials and seals for equipment used in MVR heat pump system (Gurd et al., 2019; Valchev, 2014). According to acidity wastewater can be classified into the following groups:

Group D1 – neutral wastewater with an active pH value in range 6.5 – 7.5. They are obtained in absence of contact with fresh water with acidity-correcting substances. This wastewater is not aggressive compared to standard corrosion-resistant stainless-steel brands.

Group D2 – alkaline wastewater with a value of active reaction pH above 7.5. The presence of dissolved bases in wastewater is obtained (for example, from cleaning equipment). They are not aggressive to standard corrosion-resistant brands of stainless-steel brands.

Group D3 – acidic wastewater with a value of active reaction pH below 6.5. Acids dissolved in wastewater are present (for example, from cleaning equipment, from technological processes) and some of them are aggressive towards standard corrosion-resistant stainless-steel brands.

Cyclicity of Wastewater Generation

Observations on operating technological processes show that wastewater is released according to a different time schedule. This feature provides various possibilities of processing these waters within a day-simultaneously with their separation, with accumulation and processing through low electricity cost at night period, accumulation of clean condensate, etc. With this, cyclicity of wastewater separation affects energy costs incurred for their processing by MVR method (Brenan, 2006; Liang et al., 2013). According to cyclicity of wastewater generation wastewater can be classified into the following groups:

Group E1 – continuously generated wastewater. They are obtained from continuously operating technological processes and operations (evaporation, hydro transport, washing). Wastewater is characterized by a relatively constant mass flow over time for the entire working period of the enterprise.

Group E2 – periodically generated wastewater. They are obtained in periodic technological processes and operations (washing, rinsing). A certain mass flow of wastewater is released for a relatively short period compared to the entire working period of the enterprise.

Method

Samples of wastewater from various technological operations in production of: canned vegetables, beer, mayonnaise, baby food, oil, aromatic products, dairy products, meat preparations, were examined. A list of industrial wastewater samples studied is shown in Table 1. The density was determined by the weight method. A Gay-Lussac pycnometer with a capacity of 50 cm³, vessel with heater and thermostat VEB MLW Labortechnik Ilmenau/ GDR type MLW-WB2, Ne = 250 W, 220 V was used. The mass of wastewater was measured using an electronic balance KERN – PCB 250-3 with a maximum working range of 250 g. Dynamic viscosity was measured according to Höppler method using a viscometer with a falling ball type BH2. Electrical conductivity was measured using a WTW Inolab COND7110 Tetracon 325 sensor. pH was measured using a pH meter WTW INOLAB pH7110 pH electrode WTW SenTix 6L, pH 0-14 (0-100 °C) 3 kmol/l KCl. Optical transmission was measured using a Lovibond PFX880 V10 instrument.

Table 1. Studying industrial wastewater samples

Designation	Type
Sample 1	Wastewater from washing cucumbers /cold, fresh water/
Sample 2	Wastewater from washing pepper /cold, fresh water/
Sample 3	Wastewater from receiving tubs with pepper for transport and initial washing /cold, barometric water from evaporation system/
Sample 4	Wastewater from mayonnaise production /contains warm fresh water and degreaser/
Sample 5	Wastewater from rinsing PET bottles /contains 25-30 ppm peracetic acid and negligible impurities from expanded bottles/
Sample 6	Wastewater from poultry slaughterhouse /mix of wastewater for washing waterfowl birds with cold water 18 - 20 °C and washing equipment, floors, walls and alkaline warm water 60 °C, pH 13, wastewater contains fats, household waste, grit/
Sample 7	Wastewater from production of baby food (puree) /clean water 75 °C with 2% nitric acid, temperature 68 °C/
Sample 8	Wastewater from first step of “cleaning in place” (CIP) system in canning factory /pure water with 2% NaOH, temperature 87 °C/
Sample 9	Wastewater from saponification of free fatty acids with NaOH (23%) in extraction unit / temperature about 80 °C, wastewater contains soap, unreacted NaOH and organics.

Density and dynamic viscosity of wastewater were studied as a function of wastewater temperature. For this purpose, a classic one-factor experiment was used. All parameters were measured three times, and the obtained results are presented as an arithmetic mean value. In addition, the obtained values were evaluated statistically by determining variance and root mean square deviation of average result, as well as confidence error and dependence interval (Raichkov, 2001):

For mean score variance $S^2(\bar{x})$:

$$S^2(\bar{x}) = \frac{1}{m.(m-1)} \sum_{i=1}^m (x_i - \bar{x})^2$$

For root means square deviation of the mean score $S(\bar{x})$:

$$S(\bar{x}) = \sqrt{S^2(\bar{x})}$$

For confidence error $\varepsilon(\bar{x})$:

$$\varepsilon(\bar{x}) = t(p, m-1).S(\bar{x})$$

where $t(p, m-1)$ is Student's criterion for accepted confidence probability $p=0.95$ and number of repeated measurements $m-1=2$. A value of $t(0.95, 2) = 4.303$ is reported.

For confidence interval:

$$x = \bar{x} \pm \varepsilon(\bar{x})$$

Results

Wastewater density was studied for wastewater in its natural form as a function of temperature in range 25 °- 80 °C. The temperature factor variation levels are four and include values 25 °C, 40 °C, 60 °C and 80 °C. The results of measurements are presented in Table 2.

Table 2. Density of wastewater depending on temperature

Designation	Density at 25°C, kg/m ³	Density at 40°C, kg/m ³	Density at 60°C, kg/m ³	Density at 80°C, kg/m ³
Sample 1	998.5±1.1	994.0±1.1	983.7±0.8	973.3±0.9
Sample 2	998.5±0.9	994.2±1.0	984.9±0.9	971.9±1.0
Sample 3	998.2±1.9	994.2±0.7	984.7±1.5	973.1±1.4
Sample 4	1003.3±1.0	998.4±1.8	985.3±1.8	977.4±0.9
Sample 5	998.8±1.1	994.9±1.4	986.5±1.5	976.5±1.4
Sample 6	999.5±0.8	994.5±0.9	983.7±1.8	973.3±1.1
Sample 7	998.3±0.8	997.6±0.5	982.3±0.6	978.3±0.9
Sample 8	998.1±1.5	991.5±1.1	984.1±0.9	972.1±0.5
Sample 9	1005.1±1.4	1001.5±1.1	990.7±1.0	981.8±1.5
Distilled water	998.1	993.3	984.3	972.8

Wastewater dynamic viscosity was studied for wastewater in its natural form as a function of temperature in range 25 - 60 °C. The temperature factor variation levels are three and include values 25 °C, 40 °C, 60°C. The results of the measurements are presented in Table 3.

Table 3. Dynamic viscosity of wastewater depending on temperature

Designation	Dynamic viscosity at 25°C, cP	Dynamic viscosity at 40°C, cP	Dynamic viscosity at 60°C, cP
Sample 1	0.929±0.028	0.835±0.025	0.837±0.019
Sample 2	0.883±0.027	0.801±0.018	0.743±0.033
Sample 3	0.929±0.027	0.759±0.033	0.684±0.012
Sample 4	6.811±0.178	4.317±0.201	3.466±0.163
Sample 5	0.891±0.031	0.797±0.019	0.746±0.028
Sample 6	0.866±0.039	0.730±0.033	0.650±0.033
Sample 7	1.256±0.028	1.095±0.038	0.901±0.088
Sample 8	1.234±0.035	1.108±0.098	0.944±0.045
Sample 9	1.971±0.099	0.923±0.065	0.740±0.042
Distilled water	0.879	0.671	0.616

Electrical conductivity, active reaction and optical transmission of wastewater were investigated in natural form. The results of the measurements are presented in Table 4.

Table 4. Electrical conductivity, active reaction and optical transmission of wastewater

Designation	Electrical conductivity, µS/ cm ²	Active reaction (pH)	Optical transmission %
Sample 1	962.0±12.6	6.81±0.01	34.98±0.95
Sample 2	779.3±11.5	7.50±0.03	-
Sample 3	888.0±20.3	7.44±0.02	54.95±1.26
Sample 4	10.6±0.3	4.61±0.02	0.00±0.0
Sample 5	56.5±0.8	5.86±0.02	43.74±0.53
Sample 6	1128.3±22.9	6.68±0.03	13.33±0.22
Sample 7	-	4.24±0.00	-
Sample 8	-	12.67±0.06	-
Sample 9	-	12.46±0.04	-
Distilled water	3.0±0.2	-	-
Fresh water	622.0±12.4	-	-

The investigated wastewater samples, distributed by groups, are presented in Table 5.

Table 5. Classification of industrial wastewater by groups

Designation	Temperature, °C	Content of non-volatile impurities mg/dm ³	Cyclicalilty of wastewater generation	Group A	Group B	Group C	Group D	Group E
Sample 1	15 °C	0-200	continuously	A1	B1	C1	D1	E1
Sample 2	15 °C	0-200	continuously	A1	B1	C3	D1	E1
Sample 3	29 °C	0-200	continuously	A1	B1	C5	D1	E1
Sample 4	45 °C	>600	periodically	A2	B3	C5	D3	E2
Sample 5	42 °C	200-600	periodically	A2	B2	C5	D3	E2
Sample 6	43 °C	200-600	periodically	A2	B2	C4	D1	E2
Sample 7	75 °C	>600	periodically	A3	B3	C5	D3	E2
Sample 8	87 °C	>600	periodically	A3	B3	C5	D2	E2
Sample 9	80 °C	>600	periodically	A3	B3	C5	D2	E2

Conclusion

The obtained values for density and dynamic viscosity of wastewater show that for majority of samples values are higher than values of density and dynamic viscosity of distilled water for corresponding temperature. In general, due to low concentration of total dry matter in wastewater, these values are close to density and dynamic viscosity values of distilled water. Electrical conductivity values show that one group of wastewater has conductivity values close to the value of fresh water. Another group has an electrical conductivity value lower and third group has an electrical conductivity value higher than value of fresh water. than that of the drinking water due to the presence of organic substances in them. High values of electrical conductivity are dilated on presence of dissolved electrolytes - salts, acids and bases. Regarding to active reaction values, wastewater is divided into three groups – neutral (pH=7.0), with an acidic reaction (pH<7.0) and with a basic reaction (pH>7.0). Optical transmission values show that for wastewater with low dry matter concentration, optical transmittance values are high and vice versa. A classification system for industrial wastewater generated by enterprises of food and beverage industry in connection with their possibilities for recycling by evaporation method was created. On the basis, it can be concluded that a greater part of wastewater can be effectively purified and recycled with MVR heat pumps due to low values of dry matter in wastewater and close values of their thermophysical characteristics to values of distilled water.

Scientific Ethics Declaration

* The authors declare that the scientific ethical and legal responsibility of this article published in EPSTEM Journal belongs to the authors.

Conflict of Interest

* The authors declare that they have no conflicts of interest

Funding

* This study received no external funding.

Acknowledgements or Notes

* This article was presented as an oral presentation at the International Conference on Technology (www.icontechno.net) held in Trabzon/Türkiye on May 01-04, 2025.

References

Brennan, J.G. (2006). *Food processing handbook*. Weinheim, Germany: Wiley CRC Press.

- Gertsen, N., & Sonderby, L. (2009). *Water purification*. New York, NY: Nova Science Publishers.
- Ghimpusan, M., Nechifor, G., Nechifor, A. C., Dima, S. O., & Passeri, P. (2017). Case studies on the physical-chemical parameters' variation during three different purification approaches destined to treat wastewaters from food industry. *Journal of Environmental Management*, 203, 811-816,
- Gurd, G., Jefferson, B., & Villa, R. (2019). Characterisation of food service establishment wastewater and its implication for treatment. *Journal of Environmental Management*, 252, 109657,
- Liang, L., Han, D., Ma, R., Peng, T. (2013). Treatment of high-concentration wastewater using double-effect mechanical vapor recompression. *Desalination*, 314, 139-146.
- Muller, D., & Marechal, F. (2008). Energy management method in the food industry. *Handbook of water and energy management in food processing*. Woodhead Publishing.
- Ng, J.W. (2006). *Industrial wastewater treatment*. Imperial College Press.
- Raichkov, G. (2001). *Measurements and appliances in heat engineering*. Plovdiv, Bulgaria: Academic Publishing of University of food technology – Plovdiv.
- Ramalho, R.S. (1977). *Introduction to wastewater treatment processes*. Academic Press.
- Rilling, K. (2012). Treating oily wastewater from machining and casting operations. *Environmental Science & Engineering Magazine*, 24-29.
- Russell, D.L. (2006). *Practical wastewater treatment*. John Wiley & Sons Publication.
- Semerdzheva, A., Valchev, S., Atanasov, D., Dimitrov, A., Tasheva, S. (2024). Cohobation as a method for purification of distillation waters in manufacturing of essential oil. *Journal of Environmental Protection and Ecology*, 25(6), 1813-1819.
- Shrivastava, S., Ali, I., Marjub M. M., Rene, E.R., & Soto, A.M.F. (2022). Wastewater in the food industry: Treatment technologies and reuse potential. *Chemosphere*, 293, 133553,
- Smith, R. (2005). *Chemical process design and integration*. John Wiley & Sons.
- Stoyanova, S. (2011). Wastewater treatment from food industry. *Engineering Review*, 7, 96-98.
- Syed, S. (2006). Solid and liquid waste management. *Emirates Journal for Engineering Research*, 11(2), 19-36.
- Tabakov, D. (2004). Technologies for purification of fluids (wastewater and gases). In *General, and special part*. Bulgaria, Plovdiv.
- Valchev, S. (2014). Physic characteristics of industrial wastewater generated from firms in the food industry *Scientific Research of the Union of Scientists in Bulgaria-Plovdiv, Series C. Technics and Technologies*, 12, 88-94.
- Valchev, S., & Nenov, N. (2014). Pilot heat pump system for treatment of industrial wastewater (in Bulgarian). *Heat Engineering*, 2, 72-75.
- Valchev, S., Nenov, N., & Blazheva, D. (2016). Assessment of environmental impact of industrial wastewater treatment through heat pump system. Part II – Determination of basic physical and chemical indicators. (in Bulgarian). *Proceedings of National Scientific Conference with International Participation "Ecology and Health*.
- Waldron, K. W. (Ed.). (2007). *Handbook of waste management and co-product recovery in food processing* (Vol 1). Cambridge, UK: Elsevier.

Author(s) Information

Slav Valchev
University of Food Technology
26 Maritza Boulevard, Plovdiv, Bulgaria.
Contact e-mail: slavvalchev@uft-plovdiv.bg

Nenko Nenov
InnoSolv Ltd
Bulgaria

To cite this article:

Valchev, S., & Nenov, N. (2025). Classification of industrial wastewater generated by food and beverage industry. *The Eurasia Proceedings of Science, Technology, Engineering and Mathematics (EPSTEM)*, 33, 148-154.

The Eurasia Proceedings of Science, Technology, Engineering and Mathematics (EPSTEM), 2025

Volume 33, Pages 155-160

IConTech 2025: International Conference on Technology

Microhardness and Corrosion Resistance of AA1370 Aluminum Wire after Three ECAP-120° Passes

Youcef Hadj-Ali

Mouloud Mammeri University of Tizi-Ouzou

Fabienne Delaunois

University of Mons

Belkacem Koraichi

Mouloud Mammeri University of Tizi-Ouzou

Djedjigua Benabdesselam

Mouloud Mammeri University of Tizi-Ouzou

Nacer Zazi

Mouloud Mammeri University of Tizi-Ouzou

Abstract: This study contributes to exploring the impact of grain refinement and intermetallic particle fragmentation resulting from the Equal Channel Angular Pressing (ECAP) processing of AA1370 aluminum alloy wire. The samples underwent progressive deformation to three passes in the ECAP, with an intersection angle of $\Phi=120^\circ$ and a curvature radius of $\Psi=0^\circ$, following route A, at room temperature. Microstructural analysis was carried out using optical microscopy and scanning electron microscopy (SEM) before and after ECAP deformation. X-ray diffraction (XRD) analysis was conducted to examine texture and morphology. Corrosion behavior was assessed using open circuit potential (OCP) and polarization techniques before and after ECAP. Penetration resistance was studied using a microhardness tester. The results of the study indicate that intermetallic particle fragmentation and reduction in crystallite size are observed as early as the first pass. However, microhardness only increased after the third pass. Additionally, deformation caused by the ECAP process results in an increase in OCP values and shifts the corrosion potential towards less negative values.

Keywords: ECAP deformation, Aluminum wire AA1370, Corrosion, Hardness, Intermetallic particles

Introduction

The effect of ECAP (Equal Channel Angular Pressing) deformation on structurally hardening aluminum alloys is influenced by various factors and can have contradictory consequences on sample hardness and corrosion resistance. Understanding these complex mechanisms is essential for optimizing the properties of aluminum alloys and their performance in various applications (Lowe & Valiev, 2000; Valiev & Langdon, 2006, 1993).

During ECAP processing, the induced shear stress can impact sample hardness through modifications in the microstructure. This includes the fragmentation of intermetallic particles, dissolution, and/or precipitation of precipitates. These microstructural changes depend on several factors, such as the deformation rate (Chegini et al., 2015; Damavandi et al., 2019; Youcef Hadj Ali et al., 2021), deformation temperature, number of passes, deformation angle, and alloy composition (Nurislamova et al., 2008).

- This is an Open Access article distributed under the terms of the Creative Commons Attribution-Noncommercial 4.0 Unported License, permitting all non-commercial use, distribution, and reproduction in any medium, provided the original work is properly cited.

- Selection and peer-review under responsibility of the Organizing Committee of the Conference

© 2025 Published by ISRES Publishing: www.isres.org

Regarding the effect of ECAP deformation on the corrosion resistance of aluminum alloys, research results are variable. Some studies have suggested that grain refinement and increased dislocation density, resulting in a more homogeneous microstructure with fewer impurities and defects, can improve the corrosion resistance of different alloys (Abd El Aal & Sadawy, 2015; Divya et al., 2018). However, other research has found that while grain refinement can enhance the mechanical properties of alloys, it does not necessarily contribute to increased corrosion resistance (Gravina et al., 2017). Additionally, it has been observed that grain refinement through severe plastic deformation can lead to the formation of shear bands, which become preferential sites for localized corrosion such as pitting. Similarly, segregation of intermetallic particles can also result in intergranular corrosion, reducing corrosion resistance (Gravina et al., 2017; Ly et al., 2018). The figure represents the microstructure of the sample that has undergone one pass of deformation. The microstructure obtained reveals that the size and density of the intermetallic particles have decreased because of deformation.

Experimental procedure

The extruded samples are obtained from an aluminum wire of AA1370 grade, which has a diameter of 2 mm and commercial purity. Its chemical composition is represented in Table 1.

Table 1. The chemical composition of AA 1370 aluminum wire

Al %	Fe %max	Si %max	Cu %max	Zn %max	Ti %max	V %max	Ga %max	Mg %max	Mn %max	Cr %max	B %max
99.70	0.25	0.10	0.020	0.040	0.020	0.020	0.030	0.020	0.010	0.010	0.020

A mild steel, which is harder than the aluminum samples, is used to manufacture the ECAP die and compression piston. The die consists of two cylindrical channels with a diameter of 3 mm, forming an intersection angle of $\Phi=120^\circ$ and a curvature radius of $\Psi=0^\circ$. The specific details of the ECAP die are provided in Figure 1. The samples, cut for the extrusion of the aluminum wire, have a length of 20 mm.

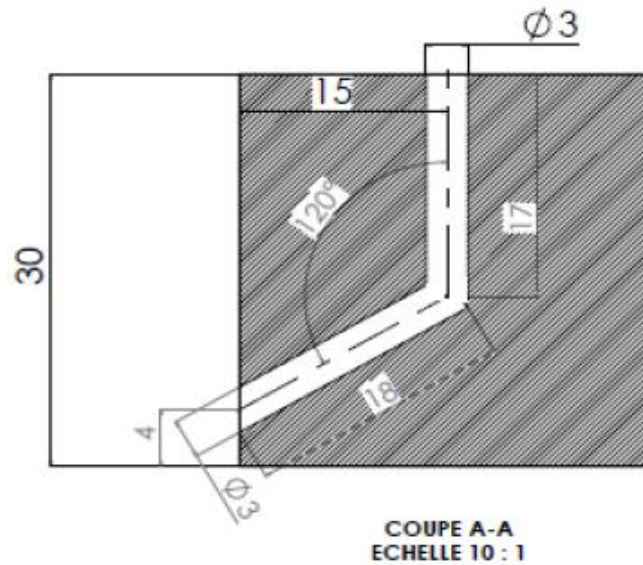


Figure 1. Parameters of the ECAP extrusion die

The studied surface is the cross-section of the AA1370 aluminum wire (sample P0) and the extruded samples, 1P120, 2P120, and 3P120, corresponding to the first, second, and third pass, respectively. The samples were cold-mounted, mechanically polished with abrasive paper of 2400 and 4000 grit, and then polished with OP-S (colloidal silica suspension) with a maximum particle size of 3 μm .

For the microstructural analysis, an optical microscope (OM) was used with a magnification of up to 5000X. A microhardness tester was employed to monitor the evolution of microhardness as a function of the number of passes. X-ray diffraction (XRD) was used to detect the diffraction peaks of aluminum, structural changes, and different phases after deformation. The study concluded with an analysis of corrosion behavior and morphology.

The potential was monitored for 48 hours of immersion in a 3% NaCl sodium chloride solution (by weight), using an Ag/AgCl reference electrode at room temperature. The polarization test was carried out under the same conditions after 24 hours of immersion, using two graphite auxiliary electrodes.

Results and Discussions

The microstructure in Figure 2. (P0) shows an aluminum matrix with the presence of two types of intermetallic particles, distributed heterogeneously and varying in size. SEM observations and EDS analyses confirm the microscopic observations and the presence of intermetallic particles in gray and light colors, with globular and/or irregular shapes and a heterogeneous distribution. The light-colored particles are rich in iron, whereas the dark-colored particles are rich in silicon.

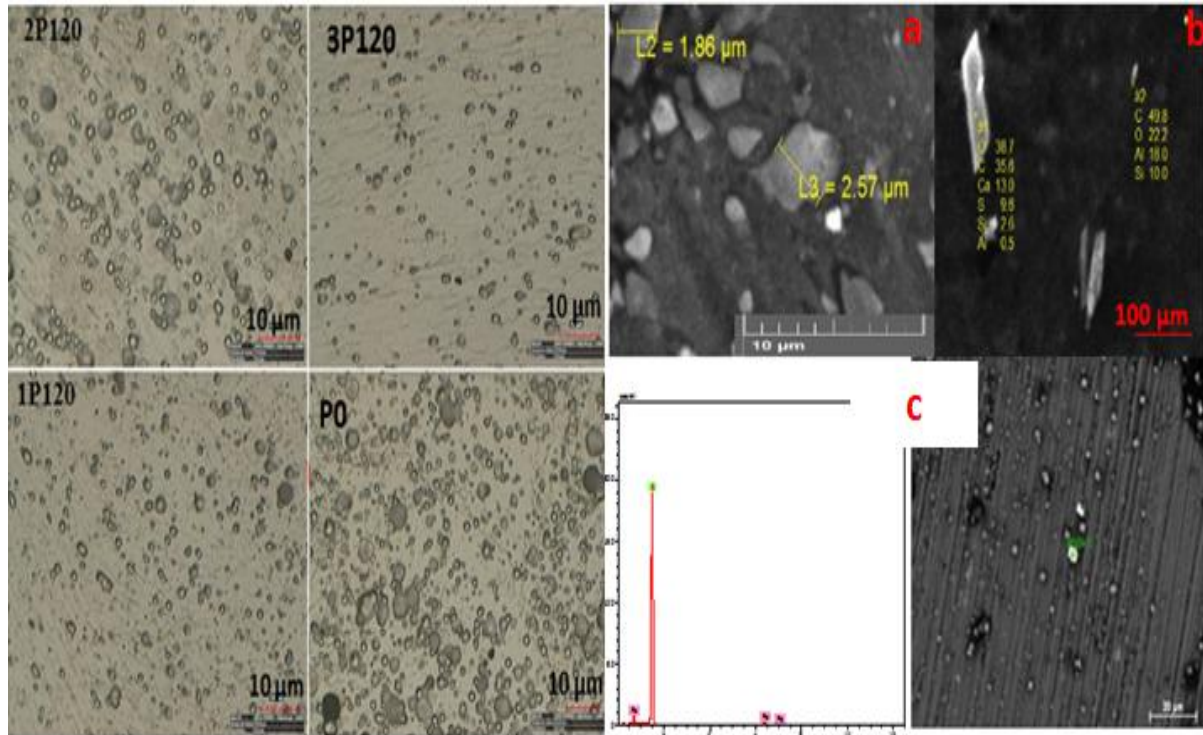


Figure 2. The microstructure before and after ECAP deformation

The figure shows that after the first pass, the intermetallic particles underwent fragmentation, resulting in reduced size and density. This fragmentation and shearing of the particles was further observed during the second pass. The third pass led to a decrease in the density of intermetallic particles. The results are in good agreement with the work of Gravina et al. (2017, 2018).

Figure 2. (1P120), represents the microstructure of the sample that has undergone one pass of deformation. The obtained microstructure reveals that the size and density of the intermetallic particles have decreased due to the effect of deformation. After the second and third passes of deformation, the intermetallic particles undergo further fragmentation, a reduction in density, and a preferential alignment in the direction of deformation figure 2. (2P120) and (3P120).

X-ray diffraction (XRD) analyses reveal the emergence of a new texture after the first deformation pass. A comparison of the diffraction spectra between the deformed and undeformed samples, using the ICDD for pure aluminum, shows the absence of peaks and a decrease in the intensity of existing peaks. X-ray diffraction (XRD) analyses reveal a structure with binary and ternary phases, rich in iron, aluminum, and silicon for the undeformed sample. After the first pass, a new iron phase appears under the crystallographic planes (111) and (200) (Figure 3).

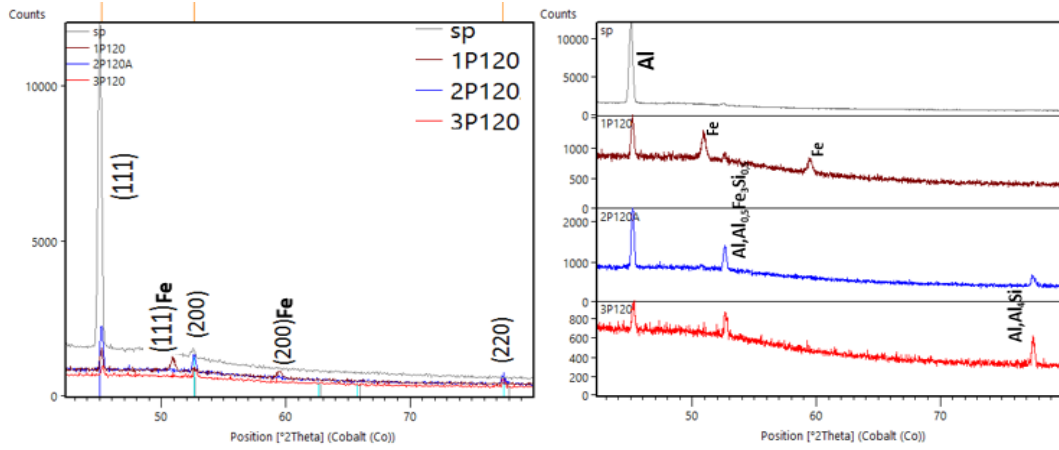


Figure 3. Comparison between the X-ray diffraction patterns of the AA1370 aluminum wire before and after deformation and phase identifications

The evolution of microhardness shows a non-linear trend throughout the different deformation stages. It decreases slightly after the first and second passes, followed by an increase after a third additional deformation. This initial decrease in microhardness could be related to a temporary softening due to local grain restructuring and partial annihilation of dislocations. The subsequent increase in hardness coincides with the reappearance of certain aluminum peaks in the diffractogram, particularly the (220) peak, suggesting a reorganization of the crystals and a new accumulation of defects in the crystal lattice. This microstructuring promotes hardening through dislocation density increase (Figure 4).

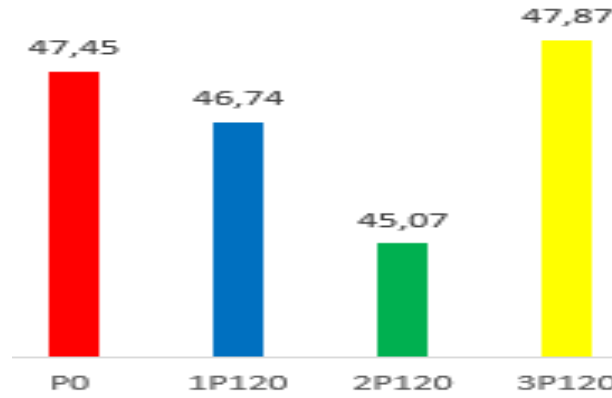


Figure 4. Comparison of microhardness between the undeformed sample and samples deformed with one, two, and three passes

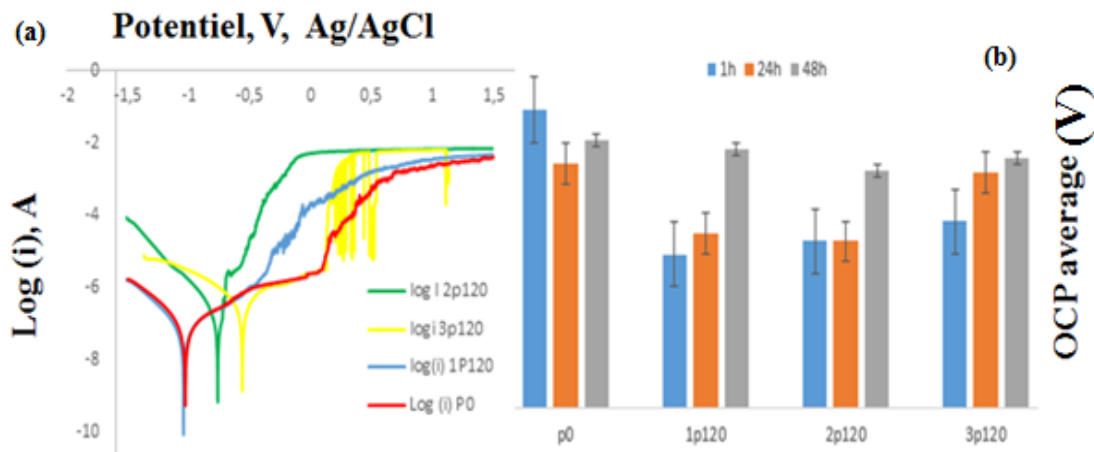


Figure 5. Electrochemical results. (a) Polarization curves and (b) OCP average, for the undeformed sample and samples deformed with one, two, and three passes

The evolution of electrochemical properties as a function of the number of deformation passes is presented in the attached figure. The polarization curves (a) and the open circuit potential (OCP) diagrams (b) reveal a general trend of improved corrosion resistance with increasing deformation. The corrosion potential (E_{corr}) becomes less negative, evolving with the increasing number of deformation passes. This evolution indicates a decrease in electrochemical activity, possibly linked to the progressive passivation of the surface. The average OCP follows the same trend, with less negative potentials as the number of passes increases. However, the increase in current density indicates an acceleration of corrosion processes, which limits the overall improvement in corrosion resistance despite the apparently more effective passivation. This improvement can be attributed to microstructural modifications such as grain size reduction, redistribution of intergranular phases, fragmentation of secondary particles, or a reduction in surface roughness.

Conclusion

The ECAP process induces significant microstructural and property changes in aluminum alloys. Fragmentation and alignment of intermetallic particles occur progressively with each deformation pass, contributing to a refined microstructure. XRD analysis confirms texture evolution and the emergence of new iron-rich phases after the first pass. Microhardness follows a nonlinear trend, with an initial decrease likely due to local softening, followed by an increase after the third pass, associated with dislocation accumulation and crystal reorganization.

Electrochemical measurements show improved corrosion resistance through enhanced passivation, reflected by less negative OCP and E_{corr} values. However, increased corrosion current density suggests a trade-off between passivation and corrosion kinetics. Overall, optimizing the number of ECAP passes is key to achieving a balance between mechanical strengthening and corrosion resistance.

Scientific Ethics Declaration

* The authors declare that the scientific ethical and legal responsibility of this article published in EPSTEM Journal belongs to the authors.

Conflict of Interest

* The authors declare that they have no conflicts of interest

Funding

* This study received no external funding.

Acknowledgements or Notes

* This article was presented as a poster presentation at the International Conference on Technology (www.icontechno.net) held in Trabzon/Türkiye on May 01-04, 2025.

* The authors would like to thank Mouloud Mammeri University of Tizi-Ouzou, the Mechanics, Structure and Energetics Laboratory (LMSE), and the Materials Research Institute for their technical and scientific support. The authors would like to sincerely thank all contributors for their valuable input in this work.

References

Abd El Aal, M. I., & Sadawy, M. M. (2015). Influence of ECAP as grain refinement technique on microstructure evolution, mechanical properties and corrosion behavior of pure aluminum. *Transactions of Nonferrous Metals Society of China*, 25(12), 3865-3876.

- Chegini, M., Fallahi, A., & Shaeri, M. H. (2015). Effect of equal channel angular pressing (ECAP) on wear behavior of Al-7075 alloy. *Procedia Materials Science*, 11, 95-100.
- Damavandi, E., Nourouzi, S., Rabiee, S. M., & Jamaati, R. (2019). Effect of ECAP on microstructure and tensile properties of A390 aluminum alloy. *Transactions of Nonferrous Metals Society of China*, 29(5), 931-940.
- Divya, S. P., Yoganandan, G., Balaraju, J. N., Srinivasan, S. A., Nagaraj, M., & Ravisankar, B. (2018). Investigation on wear and corrosion behavior of equal channel angular pressed aluminium 2014 alloy. *IOP Conference Series: Materials Science and Engineering*, 314, 012024.
- Gravina, R., Josse, C., Viguier, B., Laurino, A., Alexis, J., Hughes, A. E., & Blanc, C. (2018). Corrosion behaviour of AA 1370 strands for wires: Identification of the critical metallurgical parameters. *Corrosion Science*, 134, 112-121.
- Gravina, R., Pébère, N., Laurino, A., & Blanc, C. (2017). Corrosion behaviour of an assembly between an AA1370 cable and a pure copper connector for car manufacturing applications. *Corrosion Science*, 119, 79-90.
- Hadj-Ali, Y., Zazi, N., Durmus, H., & Chopart, J.-P. (2021). Effects of ECAP with one pass severe deformation on microhardness, texture, and corrosion behavior of AA1370 aluminum alloy wire. *Physics of Metals and Metallography*, 122(13), 1382-1390.
- Lowe, T. C., & Valiev, R. Z. (Eds.). (2000). *Investigations and applications of severe plastic deformation*. Netherlands: Springer.
- Ly, R., Hartwig, K. T., & Castaneda, H. (2018). Effects of strain localization on the corrosion behavior of ultra-fine grained aluminum alloy AA6061. *Corrosion Science*, 139, 47-57.
- Nurislamova, G., Sauvage, X., Murashkin, M., Islamgaliev, R., & Valiev, R. (2008). Nanostructure and related mechanical properties of an Al-Mg-Si alloy processed by severe plastic deformation. *Philosophical Magazine Letters*, 88(6), 459-466.
- Valiev, R. Z., & Langdon, T. G. (1993). An investigation of the role of intragranular dislocation strain in the superplastic Pb-62% Sn eutectic alloy. *Acta Metallurgica et Materialia*, 41(3), 949-954.
- Valiev, R. Z., & Langdon, T. G. (2006). Principles of equal-channel angular pressing as a processing tool for grain refinement. *Progress in Materials Science*, 51(7), 881-981.

Author(s) Information

Youcef Hadj-Ali

Mammeri University of Tizi-Ouzou, Faculty of Construction Engineering, Department of Mechanical Engineering, Mechanics, Structure and energetic laboratory (LMSE)
B.P.17 RP Tizi-Ouzou Algeria
Contact e-mail : youcef.hadj-ali@ummto.dz

Fabienne Delaunois

University of Mons, Metallurgy Department, Faculty of Engineering, Materials Research Institute
20, Place du Parc, Mons, Belgium

Belkacem Koraichi

Mouloud Mammeri University of Tizi-Ouzou, Faculty of Construction Engineering, Department of Mechanical Engineering, Mechanics, Structure and energetic laboratory (LMSE), B.P.17 RP Tizi-Ouzou Algeria

Djedjigua Benabdesselam

Mouloud Mouloud Mammeri University of Tizi-Ouzou, Faculty of Construction Engineering, Department of Mechanical Engineering, Mechanics, Structure and energetic laboratory (LMSE), B.P.17 RP Tizi-Ouzou Algeria

Nacer Zazi

Mouloud Mammeri University of Tizi-Ouzou, Faculty of Construction Engineering, Department of Mechanical Engineering, Mechanics, Structure and energetic laboratory (LMSE), B.P.17 RP Tizi-Ouzou Algeria

To cite this article:

Hadj-Ali, Y., Delaunois, F., Koraichi, B., Benabdesselam, D., & Zazi, N. (2025). Microhardness and corrosion resistance of AA1370 aluminum wire after three ECAP-120° passes. *The Eurasia Proceedings of Science, Technology, Engineering and Mathematics (EPSTEM)*, 33, 155-160.